I.R.Iran

ISSN:2423-5547
e-ISSN:2423-7469

# Journal of Renewable Energy and Environment

Volume 8, Number 3, Summer 2021

Materials and Energy Research Center

Iranian Association of Chemical Engineers

# CONTENTS

# AIMS AND SCOPE

*Journal of Renewable Energy and Environment (JREE)* publishes original papers, review articles, short communications and technical notes in the field of science and technology of renewable energies and environmental-related issues including:

- Generation
- Storage
- Conversion
- Distribution
- Management (economics, policies and planning)
- Environmental Sustainability

## INSTRUCTIONS FOR AUTHORS

Submission of manuscript represents that it had neither been published nor submitted for publication elsewhere and is result of research carried out by author(s). Only the extended and upgraded articles presented in a conference and/or appeared in a symposium proceedings could be evaluated for publication.
Authors are required to include a list describing all the symbols and abbreviations in the paper. Use of the international system of measurement units is mandatory.

- On-line submission of manuscripts results in faster publication process and is recommended. Instructions are given in the JREE web sites: www.jree.ir
- References should be numbered in brackets and appear in sequence through the text. List of references should be given at the end of the paper. All journal articles listed in the References section must follow with article doi.
- Figure captions are to be indicated under the illustrations. They should sufficiently explain the figures.
- Illustrations should appear in their appropriate places in the text.
- Tables and diagrams should be submitted in a form suitable for reproduction.
- Photographs should be of high quality saved as jpg files.
- Tables' illustrations, figures and diagrams will be normally printed in single column width (8 cm). Exceptionally large ones may be printed across two columns (17 cm).

Journal of Renewable Energy and Environment

Research Article

Journal Homepage: www.jree.ir

# Energy Consumption Management of Commercial Buildings by Optimizing the Angle of Solar Panels

Nima Amani *, Abdul Amir Reza Soroush

*Department of Civil Engineering, Chalous Branch, Islamic Azad University, P. O. Box: 46615-397, Chalous, Mazandaran, Iran.*

*PAPER INFO*

*Paper history:*
Received 30 July 2020
Accepted in revised form 24 January 2021

*Keywords*:
Optimal Angle,
Renewable Energy,
Photovoltaic Modules,
Energy Efficiency,
Energy Consumption Management

*ABSTRACT*

One of the main reasons of environmental pollution is energy consumption in buildings. Today, the use of renewable energy sources is increasing dramatically. Among these sources, solar energy has favorable costs for various applications. This study examined a commercial building in a hot and humid climate. The findings showed that choosing the optimal angle of solar panels with the goal of optimized energy consumption would yield reduced costs and less environmental pollutants with the least cost and maximum energy absorption. In this study, to calculate the energy requirements of the building, DesignBuilder software was used. To study the solar angles and estimate the energy produced by the solar panels, Polysun software was used after simulating the building energy. Energy simulation results showed that the whole building energy consumption was 26604 kWh/year. Finally, the evaluation results of solar panels showed that the energy produced by photovoltaic modules at an optimal angle of 31° would be equal to 26978 kWh/year, which is more than the energy required by the building. This system can prevent 14471 kg of carbon dioxide emissions annually. Sustainable energy criteria showed that for the studied building, photovoltaic modules could be used in energy production to reach a zero-energy system connected to the grid with an annual energy balance.

https://doi.org/10.30501/jree.2020.241836.1134

## 1. INTRODUCTION

Today, environmental threats have created a negative impact on construction fields due to urbanization and lack of energy in the public sector and professional organizations. Commercial buildings play an important role in saving energy. According to the Iran Department of Energy (2015), residential, commercial, and office buildings consume about 40 % of the total energy in the country [1, 2]. Due to the large share of final energy consumption in this sector, accurate analysis of the thermal and cooling loads of a building and the efforts to reduce energy losses in it are effective ways to reduce energy consumption [2]. Important decisions must be made by architects and engineers in the early stages of building design, regarding the final effects of building physics on the overall performance of the building [3]. As mentioned, one of the main reasons of environmental pollution is fuel consumption in commercial and residential buildings. This issue has captured the attention of many researchers and experts in recent years due to the need to optimize energy consumption in cities, especially the construction sector [4]. Amani and Reza Soroush (2020) examined effective parameters of energy consumption in the building. Their findings showed that each of the building components had a significant role in evaluating the energy performance of the building [2]. Today, the use of solar panels is increasing worldwide due to the importance of solar energy production [5]. Solar panels are one of the best renewable technologies for energizing buildings. For this purpose, knowledge of the optimum tilt angle is necessary for obtaining the highest possible annual or seasonal energy yield. The optimum tilt angle is dependent on many factors such as the latitude, weather conditions, and surroundings [6, 7]. To increase the efficiency of solar systems, it is suggested that necessary measures be considered from the initial phases of design to combine solar panels with the building facade [8]. For active solar systems such as solar collectors and PV panels, it is important to estimate the possible thermal or electrical energy production [9]. The availability of global irradiation data measurements is one of the most important factors in the assessment of the solar potential for the installation of photovoltaic panels [10]. For this purpose, the use of daily data for modeling is very important. Also, input data for the models and the data for validation should be assessed at the same station [9]. In some countries where it is not possible the use of numerical models has been proposed to estimate the monthly, seasonal, and annual solar radiation (global diffuse and direct solar radiation), especially on tilted surfaces [10]. Many solar panels are connected serially. As a result, the panels are often exposed to relatively high potential relative to the ground, resulting in High Voltage Pressure (HVS). The effect of this pressure was considered on the long-term stability of solar panels by NREL in 2005 [5]. One of the effective measures in the field of optimizing fuel consumption in commercial and residential buildings is the use of natural

*Corresponding Author's Email: nimaamani@iauc.ac.ir (N. Amani)
URL: http://www.jree.ir/article_124772.html

Please cite this article as: Amani, N. and Reza Soroush, A.A., "Energy consumption management of commercial buildings by optimizing the angle of solar panels", ***Journal of Renewable Energy and Environment (JREE)***, Vol. 8, No. 3, (2021), 1-7. (https://doi.org/10.30501/jree.2020.241836.1134).

energy in the climatic design of buildings based on the principles of architecture compatible with the climate of each region. Therefore, one of the main tasks of planning and design in Iran can be the revision of the construction laws due to the energy crisis and the necessity to save on energy consumption [11]. Ifaei et al. (2017) conducted a study on sustainable development in Iran using Technical-Economic-Socio-Environmental Multivariate Analysis (TESEMA) using renewable energy. The results showed that the current centralistic policies in Iran should be revised to achieve sustainable development [12]. Also, Karbasi et al. (2007) showed that increasing energy efficiency, including combined cycle power generation, was the most economical option for reducing greenhouse gas emissions in Iran. Therefore, price reform is the key policy in promoting energy savings and replacing fuel with renewable energy [13]. The most important factors that have challenged human beings in the past are climatic elements. Therefore, one of the issues that leads to the incompatibility of architecture with the regional climate is the lack of sufficient knowledge on recognizing the climatic conditions and their impact on architecture [11]. Since a large part of the country is located in a hot climate, the implementation of appropriate methods to reduce the cost of cooling the building is very important. Due to the climate of Ahvaz city, characterized by long and hot summers, it is necessary to apply the principles of energy optimization in the building [14]. On combined wind and solar systems, Ifaei et al. (2017) stated that Iran was mainly a solar country and had approximately 74 % solar energy fraction under optimum conditions [15]. Also, Karbassi et al. (2008) showed that solar water heating systems as a means of conventional energy substitution could reduce the use of electricity or fossil fuels by up to 80 % [16]. Due to the importance of reducing energy consumption to achieve sustainable development and reduce operating costs [17], the ways should be sought to reduce fossil fuel consumption. One of the building's energy management solutions is the use of new technologies to optimize and sustain energy. In other words, the use of new technologies in energy management is felt based on the cooling-heating needs of buildings in Iran. A comprehensive review of previous research has been done on the energy consumption of buildings using solar panels. These studies were adopted from such famous databases as Science Direct, Wiley, and Taylor & Francis. The issues relating to the building energy conservation and efficiency with solar panels through modeling and simulation have been discussed [18-29]. To perform energy analysis, DesignBuilder software was used. This software is one of the best building energy simulation and analysis software packages. The main reasons for choosing this software are its high accuracy in calculations as well as forecasting air temperature at any time of the year. Also, the application of advanced EnergyPlus engine may yield the results of energy analysis graphically and numerically. In this study, a 5-story commercial building in Ahvaz was simulated and it was finally showed that the use of solar panels to optimize energy consumption could reduce costs and environmental pollutants. It should be noted that the optimal angle of panels plays an important role in achieving this goal. It is a conceptual framework for implementing the principles of energy management and its application strategies in buildings with the perspective of the construction life cycle to contribute to sustainable development. This study intends to minimize the costs of using a solar panel system to optimally convert solar energy into electrical energy by selecting the suitable angle of solar panels using Polysun software.

## 2. METHODOLOGY

### 2.1. Software selection

In this study, DesignBuilder software was used to create the energy model. This software can be used to calculate cooling and heating loads based on such parameters as material structure, occupants, mechanical and electrical systems, and annual or hourly climate data to keep the temperature in the comfort range. Another feature of this software is predicting air temperature at different spaces of the building based on the mentioned parameters at any time of the year. After creating the energy model in DesignBuilder software, the annual energy requirement of the building was calculated. Then, to supply the required energy of the building using solar panels, Polysun software was used. According to the geographical location of the project, the angles of solar radiation were examined by Polysun software to select the most optimal annual angle. Fig. 1 shows the details of the composite roof layers in the DesignBuilder software.

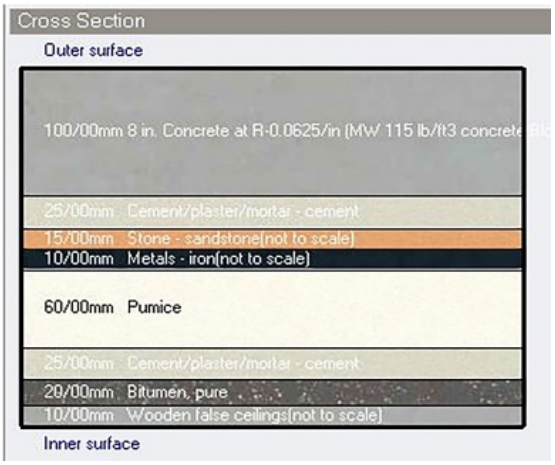


**Figure 1.** Details of the composite roof layers in DesignBuilder software

### 2.2. Case study

The case study building is a 5-story commercial building in Ahvaz with an area of 2200 $m^2$, which is located on an integrated concrete surface with a height of 30 cm. To calculate the amount of energy required to reach the comfort level, which is the supply of temperature and humidity in the standard range, the conditions of the spaces must be transient. For this purpose, the studied building was simulated using DesignBuilder software. This software provides the ability to energy simulation on an hourly basis throughout the year. Fig. 2 shows a three-dimensional view of the building in DesignBuilder software. The height of each floor is 3.5 m and the total height up to the rooftop is 17.5 m above the ground. The thickness of the exterior walls of the building was 20 cm and the roof material was the type of composite. All windows are double glazed with a 6 mm thickness middle air layer and have no shades. The window-to-wall ratio on the southern side of the building was 8 % and the eastern side of the building was 9 % on the floors. Also, the doors were made of unbreakable glass. The building lighting was supplied by fluorescent lamps with a light intensity of 600 Lux and a

brightness coefficient of 0.74. The average number of customers was considered 60 people per day.

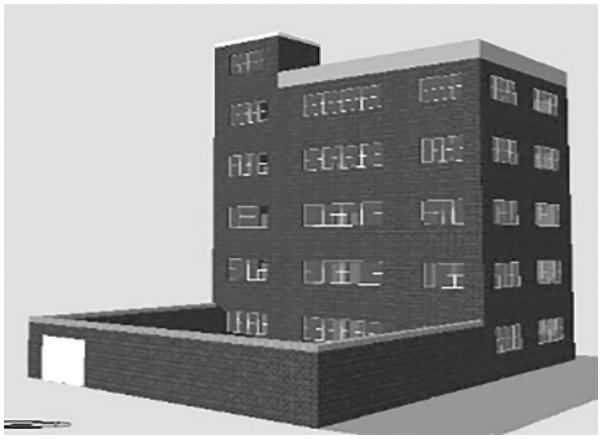

**Figure 2.** Three-dimensional view of the building in DesignBuilder software

## 2.3. Climate conditions

Ahvaz is characterized by particular climatic conditions due to its location in a special geographical location (topographic and climatic conditions of the region). One of the features of this climate is the high intensity of sunlight, which according to Article 19 of the National Building Regulations of Iran [30], is in the group of buildings with high energy consumption. Extreme heat causes many problems for people. Hence, the study of climatic conditions is an attempt to reduce relevant problems. For this purpose, synoptic meteorological data were employed to examine the climatic situation of Ahvaz. As shown in Table 1 [31], Ahvaz has hot and long summers and short and mild winters. The maximum temperature in July and August is higher than 50 °C and the maximum relative humidity in January is 60 %. The maximum rainfall in April is 40.8 mm. Also, the highest hours of sunshine in June are equal to 353 hours and the lowest hours of sunshine in January are equal to 167.5 hours.

## 2.4. Solar radiation analysis

Solar radiation modeling is a complex process that examines factors such as latitude, solar radiation interval, model height, surface orientation, surface reflectivity, and atmospheric phenomena. The results show that the lowest average monthly sunshine is in December, and its value varies from 2.83 to 3.46 kWh. Then, January and November have the least amount of sunshine. The maximum value of sunshine is in June with an average daily of 8.29 kWh/m$^2$. The average daily sunshine from April to September is higher than 5.78 kWh/m$^2$ (more than the average annual radiation). The average annual intensity of solar radiation is equal to 5.18 kWh/m$^2$/day, which is in a very suitable category according to the division of solar radiation by the US National Renewable Energy Laboratory. The highest amount of solar energy is in the hot months of the year, which coincides with the highest electricity consumption in Ahvaz. The high energy received during these months makes it possible to use it to supply part of the region's electricity and reduce the pressure on power transmission lines and, consequently, reduce the power outage. However, despite this massive potential, there is no photovoltaic power plant in Khuzestan province and solar energy production is negligible in the experimental and research stages. Fig. 3 shows the intensity of solar radiation based on the annual average [32].

**Table 1.** Meteorological information of Ahwaz station per month

| Month | Temperature (°C) | | | | |
|---|---|---|---|---|---|
| | Maximum average | Minimum average | Average | Highest maximum | lowest minimum |
| **January** | 20.5 | 9.2 | 14.9 | 25.9 | 9.2 |
| **February** | 19.2 | 7.1 | 13.2 | 25.2 | 7.1 |
| **March** | 25.4 | 11.3 | 18.3 | 30.5 | 11.3 |
| **April** | 29.5 | 16.0 | 22.7 | 35.6 | 16.0 |
| **May** | 39.7 | 23.8 | 31.8 | 45.8 | 23.8 |
| **June** | 42.3 | 26.4 | 34.4 | 47.8 | 26.4 |
| **July** | 47.3 | 30.7 | 39.0 | 50.4 | 30.7 |
| **August** | 47.4 | 29.9 | 38.6 | 50.4 | 29.9 |
| **September** | 45.0 | 27.4 | 36.2 | 49.1 | 27.4 |
| **October** | 38.2 | 20.0 | 29.1 | 43.5 | 20.0 |
| **November** | 31.6 | 15.5 | 23.6 | 36.6 | 15.5 |
| **December** | 20.8 | 9.0 | 14.9 | 25.6 | 9.0 |

| Month | Rainfall (mm) | Maximum rainfall in one day (mm) | Relative humidity (%) | Frosty day (s) | Dusty day (s) | Sunshine duration (h) | Wind speed (m/s) |
|---|---|---|---|---|---|---|---|
| **January** | 16.5 | 16.5 | 60.0 | 0.0 | 3.0 | 167.5 | 15.0 |
| **February** | 6.0 | 2.8 | 54.0 | 1.0 | 8.0 | 179.1 | 18.0 |
| **March** | 24.9 | 15.2 | 47.0 | 0.0 | 3.0 | 215.8 | 19.0 |
| **April** | 40.8 | 23.0 | 48.0 | 0.0 | 3.0 | 269.4 | 20.0 |
| **May** | 0.3 | 0.2 | 36.0 | 0.0 | 5.0 | 308.9 | 17.0 |
| **June** | 0.0 | 0.0 | 23.0 | 0.0 | 8.0 | 353.0 | 16.0 |
| **July** | 0.0 | 0.0 | 25.0 | 0.0 | 6.0 | 348.0 | 13.0 |
| **August** | 0.0 | 0.0 | 30.0 | 0.0 | 1.0 | 351.7 | 12.0 |
| **September** | 0.0 | 0.0 | 27.0 | 0.0 | 3.0 | 319.3 | 16.0 |
| **October** | 0.0 | 0.0 | 29.0 | 0.0 | 5.0 | 275.5 | 14.0 |
| **November** | 0.0 | 0.0 | 44.0 | 0.0 | 3.0 | 236.4 | 15.0 |
| **December** | 21.3 | 11.0 | 49.0 | 0.0 | 2.0 | 193.3 | 17.0 |

Solar radiation depends on the climate of the region and the different seasons of the year. The building orientation should be such that it receives the most solar radiation in cold months for maximum use of solar energy. Conversely, during hot months, the intensity of sunlight should be reduced on the surface of the building. However, according to the criteria of the region, the building location was considered to the south. The amount of solar energy received in different places varies based on latitude, altitude, atmospheric phenomena, and so on. Therefore, to receive information about solar radiation, the latitude and altitude of the region must be determined. In this case, the monthly and annual averages of solar radiation can be calculated for the desired location at all levels with different directions and slopes. In this study, the latitude is 31.3° and the altitude is 16 m. Fig. 4 shows the values of solar radiation in the building on an annual basis. These values have been extracted up to an acceptable level of 400 Lux, depending on the amount of energy received from the translucent walls. Also, all the spaces had enough light.

## 2.5. Surface coverage and location for solar panels

The use of solar panels reduces the cost of electricity in the building. These panels must be installed in the right place and at the right angle to achieve greater efficiency. The building roof has a high potential for using solar energy. Also, it is very important to determine the sunray angle to the desired surface. To install solar panels, much research has been done on the amount of usable roof area of buildings. One study in the United States shows that 32 % of the total roof area of houses can be used to install solar panels. This value will be 18 % for houses with sloping roofs and 65 % for flat roofs [33]. Another study shows that 60 % of flat roofs can be used in the tropical regions of the United States to install solar panels [34]. Another study showed that in places where there is no accurate information about its characteristics for the installation of solar panels, 50 % of the roof area can be considered [35]. Moreover, one study in Taiwan showed that 25 % of buildings' roofs for the installation of solar panels were considered [36]. In this study, the panel surfaces were determined by about 25 %. In order to increase the efficiency of solar panels, the angle of the panels should change according to the position of the sun in the sky. For this purpose, the angle of the sun must always be perpendicular to the surface of the panels. The angular altitude of the sun is indicated by SA and the latitude by L. Thus, the maximum and minimum values of the angle of radiation on the first days of summer and winter are calculated through Eqs. 1 and 2, respectively. On the first days of spring and autumn, the earth is in the middle of its orbital path between the two maximum and minimum values and the angle of deviation remains unaffected. Therefore, the average of the solar altitude angles is calculated through Eq. 3.

$$SA_{(Max)}=90\text{-}L+23.5=90\text{-}31.3+23.5=82.2 \quad (1)$$

$$SA_{(Min)}=90\text{-}L\text{-}23.5=90\text{-}31.3\text{-}23.5=35.2 \quad (2)$$

$$SA_{(Mid)}=90\text{-}L=90\text{-}31.3=58.7 \quad (3)$$

According to the above Equations, different approaches can be used to adjust the angle of the panels. Based on Rule no. 667 of the Ministry of Energy, the energy absorption efficiency rates in different modes of panels installation as the fixed panel, two-season constant, four-season constant, and two-axis tracker relative to the optimal annual angle of 23.7° for Ahvaz are equal to 71.1 %, 75.2 %, 75.7 %, and 100 %, respectively [37]. Energy simulation results show that the whole building energy consumption is 26604 kWh/year. Accordingly, the value of building energy consumption is 69.10 kWh/m$^2$/year. Due to the investment cost and the need for minimum energy in the building, which is the result of its architectural energy, it can be converted into a zero-energy building that is also economical. For this purpose, new energy production systems should be used. To achieve zero-energy standard, different ideas and methods are used. The use of active solar systems such as photovoltaic modules and solar water heater system is one of the most important solutions to produce the energy required by the building.

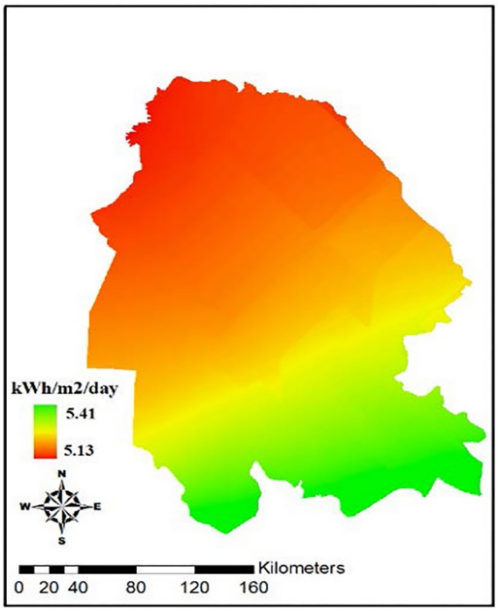


**Figure 3.** Average annual of daily solar radiation in Khuzestan province

Temperatures, Heat Gains and Energy Consumption - test, Building 1

EnergyPlus Output — 1 Jan - 31 Dec, Daily — Evaluation

Day

| | | | | | | | | | | |
|---|---|---|---|---|---|---|---|---|---|---|
| Air Temperature | 26/00 | 30/81 | 34/73 | 37/70 | 46/04 | 47/44 | 47/07 | 41/87 | 39/17 | 31/93 |
| Radiant Temperature | 27/61 | 31/82 | 35/47 | 39/00 | 46/87 | 48/10 | 47/73 | 43/24 | 40/48 | 33/67 |
| Operative Temperature | 26/81 | 31/31 | 35/10 | 38/35 | 46/46 | 47/77 | 47/40 | 42/55 | 39/82 | 32/80 |
| Outside Dry-Bulb Temperature | 14/46 | 20/51 | 26/55 | 29/42 | 36/48 | 39/23 | 38/79 | 31/28 | 26/53 | 16/31 |
| External Infiltration | -94/33 | -81/64 | -63/36 | -63/55 | -71/50 | -60/97 | -61/28 | -81/06 | -98/31 | -125/57 |
| General Lighting | 48/51 | 64/68 | 64/68 | 0/00 | 64/68 | 64/68 | 64/68 | 48/51 | 64/68 | 64/68 |
| Miscellaneous | 5/78 | 27/86 | 27/86 | 1/73 | 27/86 | 27/86 | 27/86 | 5/78 | 27/86 | 27/86 |
| Occupancy | 2/24 | 4/14 | 0/56 | 0/00 | 0/00 | 0/00 | 0/00 | 0/00 | 0/00 | 3/05 |
| Solar Gains Exterior Windows | 67/21 | 122/57 | 111/77 | 97/56 | 71/52 | 90/67 | 77/37 | 100/13 | 123/79 | 136/71 |
| Mech Vent + Nat Vent + Infiltration | 0/73 | 0/72 | 0/72 | 0/72 | 0/72 | 0/72 | 0/72 | 0/72 | 0/73 | 0/74 |

**Figure 4.** The values of solar radiation in the building using DesignBuilder software

### 2.6. Evaluation of photovoltaic modules in polysun software

In Polysun software, it is possible to simulate solar systems as well as facilities including heat pumps, geothermal energy, etc. to cover all or part of the building's energy needs. In this research, by specifying the project location in Polysun software, the required data were collected by the software. Table 2 shows the value of the energy generated by photovoltaic modules on an annual average. Also, for example, the value of energy production was calculated in August and February. The results showed that the average annual value of energy generated by 61 photovoltaic modules with a power of 350 watts and an angle of 31° was equal to 26978 kWh/year. This value will be higher than the whole building energy consumption. Also, the value of energy generated in August by 41 photovoltaic modules with a power of 350 watts and an angle of 5.3° is equal to 27572 kWh/year. This value of energy for February by 80 photovoltaic modules with a power of 350 watts and an angle of 42.3° will be equal to 26463 kWh/year. The surface coverage of panels in all cases was 99.5 $m^2$. Energy storage can be used based on the review in August and February to balance energy throughout the year. The angles provided based on the software analysis follow the minimum costs for installing solar panels to convert solar energy into electrical energy. Fig. 5 shows the value of energy generated by photovoltaic modules in general mode (annual average) in Polysun software. The results show that this system can prevent the emission of 14471 kg of carbon dioxide annually. Also, by using the solar water heater system, the release of environmental pollutants can be prevented as much as possible. At the national level, this amount can help preserve and sustain the environment and lead the country towards sustainable development.

**Table 2.** Energy generated by photovoltaic modules in Polysun software

| Component overview (annual values) | | | | |
|---|---|---|---|---|
| **Photovoltaics roof plan** | PV-Modul-350W | | | |
| | Unit | Annually | August | February |
| **Number of modules** | | 61 | 41 | 80 |
| **Total nominal power generator field** | kW | 21.35 | 21.35 | 21.35 |
| **Total gross area** | $M^2$ | 99.47 | 99.47 | 99.47 |
| **Tilt angle (hor.=0°, vert.=90°)** | ° | 31 | 5.3 | 42.3 |
| **Orientation (E=+90°, S=0°, W=-90°)** | ° | 0 | 0 | 0 |
| **Inverter 1: Name** | | Inverter 10500T | | |
| **Manufacturer** | | Anonymous | | |
| **Inverter 2: Name** | | Inverter 4000 | | |
| **Manufacturer** | | Anonymous | | |
| **Manufacturer** | | Anonymous | | |
| **Energy production AC [Qinv]** | kWh | 26978 | 27572 | 26463 |

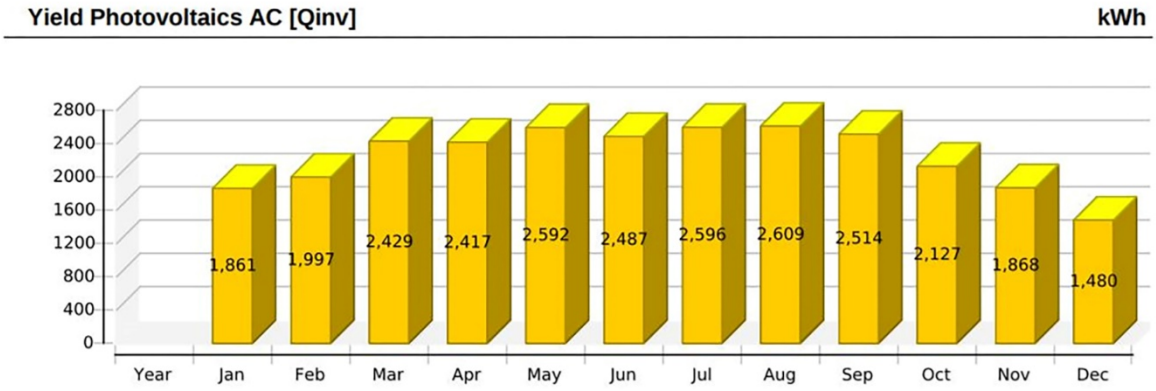


**Figure 5.** The energy produced by photovoltaic modules monthly

## 3. DISCUSSION

Increasing global warming and environmental pollutants has been on the minds of researchers for years to make a useful contribution to the future with the development of new energies. Solar energy is one of the clean and available energies. The solar panels are of great importance in this field due to the direct conversion of solar energy into electrical energy. The tilt angle of a solar energy system is one of the important parameters for achieving maximum solar radiation falling on the solar panels. This angle is site-specific which is dependent on the daily, monthly, and yearly path of the sun. The accurate determination of the optimum tilt angle is essential for maximum energy production by the system. Yadav and Chandel (2013) conducted a study on the relevance of the optimum tilt angle in energy production and reducing the cost of solar energy systems. Their findings showed that for maximum energy gain, the optimum tilt angle for solar systems must be determined accurately for each location. For this purpose, different anisotropic models and optimization techniques could be used. Also, for urban areas, the obstacles affecting solar radiation should be considered for computing optimum tilt angles [38]. In addition, Yadav and Chandel (2014) studied different isotropic and anisotropic diffused solar radiation models for determining optimum tilt angle in India. They found that the Liu and Jordan models showed the

lowest error among other models. Accordingly, the annual optimum tilt angle was determined to equal to 27.1° [39]. The thermal performance of a passive solar commercial building was evaluating by Chandel and Aggarwal (2008) in the Indian state of Himachal Pradesh. The results showed that the solar passive system features saved on the electricity required for space heating and the heat losses in the building are reduced by about 35 % [40]. Ben Othman et al. (2018) evaluated global solar radiation on tilted surfaces in Tunisia and found that the optimal annual angle in the north was equal to 37.5°and the northeast and south were equal to 36.6° [10]. This research simulated a commercial building in Ahvaz. Due to the high intensity of sunlight, Ahvaz is in a group of buildings with high energy consumption. This climate has a high potential for the optimal use of sunlight to produce energy. Solar radiation studies showed that the lowest average monthly solar radiation was in December and its value varied from 2.83 to 3.46 kWh. Also, the maximum value of sunshine was in June with an average daily rate of 8.29 kWh/m$^2$. The average daily sunshine from April to September is more than 5.78 kWh/m$^2$, which will be more than the average annual radiation. The optimum tilt angle of solar photovoltaic panels plays an important role in the optimum sizing of solar photovoltaic systems for a location. Hence, the capability of a solar module to maximize the incident radiation depends on monthly, seasonal, and yearly optimum tilt angles, which should be determined for the considered site to enhance the power generation of solar photovoltaic systems. In this study, the optimal tilt angle of the photovoltaic panels was determined to be 31°. Evaluation of photovoltaic modules showed that the angle of placement of panels affected the amount of energy produced and the number of modules. As a result, choosing the optimal angle of placement of panels will have a significant impact on cost optimization in the building life cycle. Sustainable energy criteria showed that the studied building could use photovoltaic modules in energy production to reach a zero-energy system connected to the grid with an annual energy balance. In designing zero-energy buildings, in addition to environmental aspects such as reducing energy consumption, economic and socio-cultural aspects should also be considered. The high potential of solar energy in Iran to diversify the energy basket and create a platform for the development and promotion of renewable energy provides the possibility of exploiting this endless resource.

## 4. CONCLUSIONS

The optimal annual angle for Ahvaz at 23.7° was set by Rule no. 667 of the Ministry of Energy. However, this study showed that determining the optimal angle of solar panels, based on the energy required by the building, would be the most important factor in reducing costs for optimal energy management. These results would minimize the cost of using solar panels to convert solar energy into electrical energy. Energy simulation results showed that the whole building energy consumption was 26604 kWh/year. Accordingly, the value of building energy consumption was equal to 69.10 kWh/m$^2$/year and to bring it to zero, the solar panels were used. Also, the results of photovoltaic modules evaluation in Polysun software showed that the energy generated by 61 photovoltaic modules with a power of 350 watts and surface coverage of 99.5 m$^2$ was 26978 kWh/year. This value was higher than the whole building energy consumption. By using this system, the emission of 14471 kg of carbon dioxide can be prevented annually. Finally, the comparison of different modes of energy consumption showed that the best method to achieve zero energy system was 61 photovoltaic modules with a power of 350 watts and an angle of 31° with a surface coverage of 99.5 m$^2$.

## 5. ACKNOWLEDGEMENT

This study was done at the Construction Management Group, Department of Civil Engineering, Islamic Azad University of Chalous in the years 2019-2020 as a research project.

## REFERENCES

1. Amani, N., "Building energy conservation in atrium spaces based on ECOTECT simulation software in hot summer and cold winter zone in Iran", ***International Journal of Energy Sector Management***, Vol. 122, (2018), 98-313. (https://doi.org/10.1108/IJESM-05-2016-0003).
2. Amani, N. and Reza Soroush, A.A., "Effective energy consumption parameters in residential buildings using Building Information Modeling", ***Global Journal of Environmental Science and Management (GJESM)***, Vol. 6, No. 4, (2020), 467-480. (https://doi.org/10.22034/gjesm.2020.04.04).
3. Halawa, E., Ghaffarianhoseini, A., Ghaffarianhoseini, A., Trombley, J., Hassan, N., Safiah, M., Yusoff., Y. and Ismail, M.A., "A review on energy conscious designs of building façades in hot and humid climates: Lessons for (and from) Kuala Lumpur and Darwin", ***Renewable and Sustainable Energy Reviews***, Vol. 82, (2018), 2147-2161. (https://doi.org/10.1016/j.rser.2017.08.061).
4. Omidi Avaj, M. and Bagheri, Z., "Use of new technologies in the management of building energy with an emphasis on solar energy", ***Proceedings of 1st Annual Conference on Architecture and Urban Planning in Iran***, (2015). (In Farsi). (https://www.civilica.com/Paper-AAUC01-AAUC01_095.html).
5. Hajizadeh, A. and Ijadi, H., "Maximum power point tracking of photovoltaic power generation system based on fuzzy approximation of operating point voltage with radiation intensity", ***Computational Intelligence in Electrical Engineering (Intelligent Systems in Electrical Engineering)***, Vol. 3, (2012), 73-86. (In Farsi). (https://www.sid.ir/fa/Journal/ViewPaper.aspx?ID=193671).
6. Gharakhani Siraki, A. and Pillay, P., "Study of optimum tilt angles for solar panels in different latitudes for urban applications", ***Solar Energy***, Vol. 86, (2012), 1920-1928. (https://doi.org/10.1016/j.solener.2012.02.030).
7. Schuster, C.S., "The quest for the optimum angular-tilt of terrestrial solar panels or their angle-resolved annual insolation", ***Renewable Energy***, Vol. 152, (2020), 1186-1191. (https://doi.org/10.1016/j.renene.2020.01.076).
8. Ahmed, M.M.S., Abel-Rahman, A.K. and Ali, A.H.H., "Development of intelligent façade based on outdoor environment and indoor thermal comfort", ***Procedia Technology***, Vol. 19, (2015), 742-749. (https://doi.org/10.1016/j.protcy.2015.02.105).
9. Horváth, M. and Csoknyai, T., "Evaluation of solar energy calculation methods for 45° inclined, south facing surface", ***Energy Procedia***, Vol. 78, (2015), 465-470. (https://doi.org/10.1016/j.egypro.2015.11.700).
10. Ben Othman, A., Belkilani, K. and Besbes, M., "Global solar radiation on tilted surfaces in Tunisia: Measurement, estimation and gained energy assessments", ***Energy Reports***, Vol. 4, (2018), 101-109. (https://doi.org/10.1016/j.egyr.2017.10.003).
11. Borna, R., "Study of climate conditions affecting the tourism Khuzestan Province using TCI", ***Quarterly of Geography (Regional Planning)***, Vol. 8, (2018), 107-118. (In Farsi). (http://www.jgeoqeshm.ir/article_61486.html).
12. Ifaei, P., Karbassi, A., Lee, S. and Yoo, C.K., "A renewable energies-assisted sustainable development plan for Iran using techno-econo-socio-environmental multivariate analysis and big data", ***Energy Conversion and Management***, Vol. 153, (2017), 257-277. (https://doi.org/10.1016/j.enconman.2017.10.014).
13. Karbassi, A.R., Abduli, M.A. and Mahin Abdollahzadeh, E., "Sustainability of energy production and use in Iran", ***Energy Policy***, Vol. 35, (2007), 5171-5180. (https://doi.org/10.1016/j.enpol.2007.04.031).
14. Saghafi, M.J. and Hajizadeh, M., "Thermal performance of common

clay blocks external wall system in Iran", ***Honar-Ha-Ye-Ziba Memari-Va-Shahrsazi,*** Vol. 17, (2012), 49–54. (In Farsi). (https://jfaup.ut.ac.ir/article_29696_6f7015b21e396f4a0be080fe670bf996.pdf).

15. Ifaei, P., Karbassi, A., Jacome, G. and Yoo, C.K., "A systematic approach of bottom-up assessment methodology for an optimal design of hybrid solar/wind energy resources–Case study at middle east region", ***Energy Conversion and Management***, Vol. 145, (2017), 138-157. (https://doi.org/10.1016/j.enconman.2017.04.097).
16. Karbassi, A.R., Abduli, M.A. and Neshastehriz, S., "Energy saving in Tehran international flower exhibition's building", ***International Journal of Environmental Research***, Vol. 2, (2008), 75-86. (https://doi.org/10.22059/IJER.2010.179).
17. Amani, N., "Energy simulation and management of the main building component materials using comparative analysis in a mild climate zone", ***Journal of Renewable Energy and Environment (JREE)***, Vol. 7, No. 3, (2020), 29-46. (https://doi.org/10.30501/JREE.2020.227079.1101).
18. Movahhed, Y., Safari, A., Motamedi, S. and Haghighi Khoshkhoo, R., "Simultaneous use of PV system and green roof: A techno-economic study on power generation and energy consumption", ***Energy Procedia***, Vol. 15, (2019), 478-483. (https://doi.org/10.1016/j.egypro.2018.12.037).
19. Wang, D., Qi, T., Liu, Y., Wang, Y., Fan, J. and Du, H., "A method for evaluating both shading and power generation effects of rooftop solar PV panels for different climate zones of China", ***Solar Energy***, Vol. 205, (2020), 432-445. (https://doi.org/10.1016/j.solener.2020.05.009).
20. Albadry, S., Tarabieh, Kh. and Sewilam, H., "Achieving net zero-energy buildings through retrofitting existing residential buildings using PV panels", ***Energy Procedia***, Vol. 115, (2017), 195-204. (https://doi.org/10.1016/j.egypro.2017.05.018).
21. Deltenre, Q., De Troyer, T. and Runacres., M.C., "Performance assessment of hybrid PV-wind systems on high-rise rooftops in the Brussels-Capital region", ***Energy and Buildings***, Vol. 224, (2020), 110137. (https://doi.org/10.1016/j.enbuild.2020.110137).
22. Pinamonti, M. and Baggio, P., "Energy and economic optimization of solar-assisted heat pump systems with storage technologies for heating and cooling in residential buildings", ***Renewable Energy,*** Vol. 157, (2020), 90-99. (https://doi.org/10.1016/j.renene.2020.04.121).
23. Sivaram, P.M., Mande, A.B., Premalatha, M. and Arunagiri, A., "Investigation on a building-integrated passive solar energy technology for air ventilation, clean water and power", ***Energy Conversion and Management***, Vol. 211, (2020), 112739. (https://doi.org/10.1016/j.enconman.2020.112739).
24. Fitriaty, P. and Shen, Z., "Predicting energy generation from residential building attached photovoltaic cells in a tropical area using 3D modeling analysis", ***Journal of Cleaner Production***, Vol. 195, (2018), 1422-1436. (https://doi.org/10.1016/j.jclepro.2018.02.133).
25. Thotakura, S., Kondamudi, S.C., Xavier, J.F., Quanjin, M., Reddy, G. R., Gangwar, P. and Davuluri, S.L., "Operational performance of megawatt-scale grid integrated rooftop solar PV system in tropical wet and dry climates of India", ***Case Studies in Thermal Engineering,*** Vol. 18, (2020), 100602. (https://doi.org/10.1016/j.csite.2020.100602).
26. Irshad, K., Habib, K., Saidur, R., Kareem, M.W. and Saha, B.B., "Study of thermoelectric and photovoltaic facade system for energy efficient building development: A review", ***Journal of Cleaner Production***, Vol. 209, (2019), 1376-1395. (https://doi.org/10.1016/j.jclepro.2018.09.245).
27. Toledo, C., López-Vicente, R., Abad, J. and Urbina, A., "Thermal performance of PV modules as building elements: Analysis under real operating conditions of different technologies", ***Energy and Buildings***, Vol. 223, (2020), 110087. (https://doi.org/10.1016/j.enbuild.2020.110087).
28. Mewes, D., Monsalve, P., Gustafsson, I., Hasan, B., Palén, J., Nakakido, R., Capobianchi, E. and Österlund, B., "Evaluation methods for photovoltaic installations on existing buildings at the KTH campus in Stockholm, Sweden", ***Energy Procedia***, Vol. 115, (2017), 409-422. (https://doi.org/10.1016/j.egypro.2017.05.038).
29. Couty, P., Lalou, M.J., Cuony, P., Cotture, S. and Saade, V., "Positive energy building with PV facade production and electrical storage designed by the Swiss team for the U.S. Department of Energy Solar Decathlon 2017", ***Energy Procedia***, Vol. 122, (2017), 919-924. (https://doi.org/10.1016/j.egypro.2017.07.410).
30. Office of National Building Regulations, "National building regulations of Iran, Energy saving", ***Article 19***, Iran Development Publishing, (2010), 70. (In Farsi). (http://inbr.ir/?page_id=2032).
31. Statistical Centre of Iran, "Iran statistical yearbook", ***Statistical yearbook of Khuzestan province, Chapter One, Land and climate***, Statistical Centre of Iran, (2016), 51. (In Farsi). (https://nnt.sci.org.ir/sites/Apps/yearbook/Lists/year_book_req/Item/newifs.aspx).
32. Asakereh, A., Ghadiryanfar, M. and Sheikhdavoodi, M., "The feasibility of electricity production by using rooftop solar panels in rural areas of Khuzestan Province", ***Quarterly of Geography and Development***, Vol. 14, (2016), 113-132. (In Farsi). (https://doi.org/10.22111/gdij.2016.2483).
33. Chaudhari, M., Frantzis, L. and Hoff, T.E., "PV grid connected market potential under a cost breakthrough scenario", ***Navigant Consulting Inc.***, No. 117373. (2004). (http://www.energycrisis.com/apollo2/photovoltaics/PVMktPotentialCostBreakthruNavigant200409.pdf).
34. Paidipati, J., Frantzis, L., Sawyer, H. and Kurrasch, A., "Rooftop photovoltaics market penetration scenarios", ***National Renewable Energy Laboratory (NREL)***, No. SR-581-42306, (2008). (https://www.nrel.gov/docs/fy08osti/42306.pdf).
35. La Gennusa, M., Lascari, G., Rizzo, G., Scaccianoce, G. and Sorrentino, G., "A model for predicting the potential diffusion of solar energy systems in complex urban environments", ***Energy Policy***, Vol. 39, (2011), 5335-5343. (https://doi.org/10.1016/j.enpol.2011.05.031).
36. Yue, C.D. and Wang, S.S., "GIS-based evaluation of multifarious local renewable energy sources: A case study of the Chigu area of southwestern Taiwan", ***Energy Policy***, Vol. 34, (2006), 730-742. (https://doi.org/10.1016/j.enpol.2004.07.003).
37. Management and Planning Organization, "Guide to designing photovoltaic systems to supply electrical energy divided by climate and application (Rule No. 667)", ***Technical System Affairs Department***, Vol. 101, (2014), 12. (In Farsi). (http://www.satba.gov.ir/suna_content/media/image/2015/09/3922_orig.pdf).
38. Yadav, A.K. and Chandel, S.S., "Tilt angle optimization to maximize incident solar radiation: A review", ***Renewable and Sustainable Energy Reviews***, Vol. 23, (2013), 503-513. (https://doi.org/10.1016/j.rser.2013.02.027).
39. Yadav, P. and Chandel, S.S., "Comparative analysis of diffused solar radiation models for optimum tilt angle determination for Indian locations", ***Applied Solar Energy***, Vol. 50, (2014), 53-59. (https://doi.org/10.3103/S0003701X14010137).
40. Chandel, S.S. and Aggarwal, R.K., "Performance evaluation of a passive solar building in Western Himalayas", ***Renewable Energy***, Vol. 33, (2008), 2166-2173. (https://doi.org/10.1016/j.renene.2008.01.008).

Journal of Renewable Energy and Environment

Research Article

Journal Homepage: www.jree.ir

# Simplex Centroid Mixture Design for Optimizing and Promoting the Anaerobic Co-Digestion Performance of Sheep Blood and Cheese Whey

Rasoul Aydram, Hossein Haj Agha Alizade *, Majid Rasouli, Behdad Shadidi

*Department of Biosystems Engineering, Faculty of Agriculture, Bu-Ali Sina University, Hamedan, Hamedan, Iran.*

*PAPER INFO*

*Paper history:*
Received 10 November 2020
Accepted in revised form 06 April 2021

*Keywords*:
Slaughterhouse Waste,
Biogas,
Biochemical Methane Potential Test,
Optimization,
Response Surface Methodology

*ABSTRACT*

Reduced emissions of greenhouse gases and global warming can be made possible by discovering alternative energies and reduced dependence on fossil fuels. Biogas is considered as one of the alternatives to fossil fuels. This study investigates anaerobic co-digestion for the development of biogas with sheep blood and cheese whey. Digested cow manure was used as inoculum. Using the Design Expert 10 program and within the context of mixture design, the experiments were designed. Then, 22 experimental digesters with a volume of 500 mL were considered for doing the experiments considering the design output provided by the software. Each one was filled with 300 mL of different compositions of three matters. The digesters were kept in the mesophilic temperature range (37 °C ) for 21 days. Biogas was measured using the BMP test on a daily basis. According to the experimental findings, the best composition included 35 % sheep blood, 35 % cheese whey, and 30 % inoculum. This biogas composition produced a biogas yield of 146.66 mL/g vs. The amount of methane production in this compound was 73.33 mL/g vs. After modeling, the Design Expert software predicted an optimal composition including 44 % sheep blood, 24 % cheese whey, and 32 % inoculum. Biogas yield of this prediction was 143 mL/g vs. The findings show that in order to overcome acidification in digestion of matters such as cheese whey, a composition of matters with higher pH stability can be used to increase the amount of biogas and methane produced in a particular period. Furthermore, using inoculum accelerates the digestion operations due to existence of many microorganisms and saves time and energy.

https://doi.org/10.30501/jree.2021.251583.1151

## 1. INTRODUCTION

Over the last few years, renewable energy resources received much attention [1]. Jungles, agricultural resources, urban and industrial organic sewage, urban solid waste, poultry manure, and livestock and biogas are among the major classifications for use. From a socio-economic perspective, biogas not only reduces the costs associated with destroying the wastes, but also has very low raw materials cost. Furthermore, the price of biogas is lower than diesel and gasoline. Generally, it refers to the gas obtained from anaerobic digestion units, a promising method for satisfying global energy needs and provides multiple environmental advantages [2].

Anaerobic digestion is an efficient and appropriate technology for managing organic matters. It involves several organisms with final effective environmental conditions. The type and composition of the substrate are effective in biogas production performance. Organic matters are mainly a mixture of proteins, fats, and carbohydrates that can be broken down into simpler compositions using microorganisms in an anaerobic environment during the following processes: hydrolysis, acidification, acetate production, and methanogenesis. The process of biogas production from different organic matters is mostly dependent on the substrate content, while the chemical compositions and their biodegradation are key factors in biogas and methane production [3].

Anaerobic co-digestion is anaerobic digestion of two or more substrates and is a promising method for overcoming the shortcomings of mono-digestion (involving one substrate) and improving economic satisfaction with anaerobic digestion units due to more methane production. Besides producing more biogas, this method has other advantages such as improved process stability, balance of nutrients, greater moisture in the digester feed, reduced greenhouse gases, contributory effects of microorganisms, increased load of biodegradable organic matter, and cost. Concurrent anaerobic digestion, compared to mono-digestion, will increase biogas yield from 25 to 400 percent [4].

Effective factors in anaerobic digestion include temperature regime, C / N proportion, pH, Organic Loading Rate (OLR), and Solid Retention Time (SRT) [5]. Anaerobic co-digestion of slaughterhouse waste has been considered as an applicable proposal to increase biogas production in the traditional digesters. Slaughterhouse wastes are characterized by high nitrogen contents. This effect adds an appropriate substrate for accomplishment of a composition with a balanced C/N ratio, which increases nitrogen concentration and biogas yield [6, 7]. Although nitrogen for anaerobic microorganisms is a

*Corresponding Author's Email: h-alizade@basu.ac.ir (H. Alizade)
URL: http://www.jree.ir/article_128825.html

Please cite this article as: Aydram, R., Haj Agha Alizade, H., Rasouli, M. and Shadidi, B., "Simplex centroid mixture design for optimizing and promoting the anaerobic co-digestion performance of sheep blood and cheese whey", ***Journal of Renewable Energy and Environment (JREE)***, Vol. 8, No. 3, (2021), 8-15. (https://doi.org/10.30501/jree.2021.251583.1151).

necessary nutrient, ammoniac concentration has been reported in digestion of wastes with high nitrogen content [8]. Nevertheless, recently, different mixtures of slaughterhouse waste and blood have been studied due to their high biochemical methane potential. Accordingly, Alvarez and Liden [9] examined digestion of a mixture of the contents of cow gut and that of pig and blood along with fruits and vegetable waste and fertilizer.

In addition to high Chemical Oxygen Demand (COD) and Biological Oxygen Demand (BOD), the cheese manufacturing industry produces a large volume of waste water with high durability [10]. Cheese whey is one of the peripheral products of cheese with a considerable amount of lactose (45-50 g/L), protein (6-8 g/L), carbohydrates (4-5 %), fat (4-5 g/L), and mineral salts (8-10 % of the dry extract). Cheese whey also includes a considerable amount of lactic acid, citric acid, and Vitamin Bs. Therefore, this substrate has the capacity for biological changes. High COD and the tendency toward quick acidification is very difficult [10].

Elena Cominoa [11] examined the biogas performance of the mixture of cow manure and cheese whey, methane yield, and the efficiency of chemical and biological oxygen demand removal at 35 °C. Production of sustainable biogas from volatile solids was 621 liters per kilogram within 42 days in a mixture containing 50 % fertilizer and 50 % cheese whey. Methane concentration in biogas was 55 %. Maximum Chemical Oxygen Demand (COD) removal rates were 82 % and 90 %, respectively. Rico et al. (2015) conducted another study with the purpose of creating a combinational process involving superioritys of co-digestion of cheese whey and fertilizer and short hydraulic retention time with high load. This process of co-digestion happened in an Up-flow anaerobic sludge blanket (UASB) reactor. In the constant hydraulic retention time of 2.2 days and by increasing the ratio of cheese whey in the feed, the system displayed stable operation up to a 75 % cheese whey deduction in the feed, with a practical organic loading rate of 19.4 kg COD $m^{-3}$ $d^{-1}$, obtaining a 94.7 % COD removal and a methane production rate of 6.4 $m^3$ $CH_4$ $m^{-3}$ $d^{-1}$.

Considering the fact that few studies have been conducted on digestion of blood waste for biogas production, the present study examined biogas production by co-digestion of sheep's blood and cheese whey and inoculum (cow manure) for the first time. The purpose of the present study was to achieve an optimal composition of inoculum (cow manure), sheep's blood, and cheese whey to maximize biogas and methane production. Therefore, the independent variable in the present study was different compositions of substrate and the dependent variables included biogas yield and the methane existing in it. The studies were developed using the software Design Expert and in the framework of mixture design. Co-digestion of these two matters in different proportions was analyzed and the best proportion in a mixture for maximizing production was identified.

## 2. EXPERIMENTAL

### 2.1. Preparing the substrate materials and inoculum for co-digestion

Inoculum was prepared from fresh cow manure. This manure was kept at a hydraulic retention time of 90 days in a separate reactor [12] and was then used in the experiments. Sheep blood was obtained from industrial slaughterhouse of Salehabad in Hamedan and then, was pasteurized at 70 °C for 60 minutes and used in digestion experiments [6]. cheese whey was obtained from a local dairy production workshop and used in the experiments instantly.

### 2.2. Analytical methods used for determining the substrate features

#### 2.2.1. Total solids

Measuring the level of solids was based on a standard method [13]. On this basis, the matters used in the experiments were kept in an oven for 24 hours at 105 °C. According to Equation 1 TS value was measured.

$$TS = (M_1 \times 100)/M_0 \quad (1)$$

where TS represents total solids, $M_0$ is the initial weight before drying, and $M_1$ denotes the final weight of the matter after drying.

#### 2.2.2. Volatile solids

The suspended solids were measured according to the standard method [13] based on the lost weight of the dry matter that included the same samples used in an oven for measuring TS. Accordingly, the matter extracted from the oven was put in a furnace at 550 °C for six hours and VS was measured through Equation 2.

$$VS = (M_1 - M_2) \times 100/M_1 \quad (2)$$

where VS represents the amount of suspended solids, $M_1$ shows the weight of the dry matter, and $M_2$ is the final weight after drying at 550 °C [14].

#### 2.2.3. pH

pH was measured using a pH meter model PH-230SD made in Taiwan. The obtained properties are presented in Table 1.

**Table 1.** Substrate properties used in the experiment

| Property | Inoculum | Sheep blood | Cheese whey |
|---|---|---|---|
| Total solids (TS %) | 13.7 | 10.7 | 7.4 |
| Volatile solids (VS %) | 89.9 | 94.2 | 90.5 |
| pH | 7 | 6.8 | 5.4 |

### 2.3. Experimental setup

#### 2.3.1. Biochemical methane potential test and biogas measurement

The potential test for biochemical methane is an anaerobic batch digestion process that is typically used to determine the quantity of biogas and methane derived from organic substrates.Two commonly used BMP test methods include volumetric and monomeric [15]. In the present study, the volumetric method was used. The substrate mixture was prepared according to Table 2 and put in 500-milliliter blue-capped glasses. From each mixture, 300 mL was put in each glass. The glasses were kept in water bath and at 37 °C for 21 days and the gas yield of the reactors was measured.

Each bottle had two taps, one as the produced gas outlet and one for sampling from the substrate. The gas coming out of the bottle entered the gas collector bottle. This bottle contained water and water came out of it as much as the gas inflow. pH of the reactors was measured once a day and if reduced, using 4 normal caustic soda (NaOH), it was brought back to the normal range (6.5-8.2).

### 2.3.2. Measuring methane percentage

In the anaerobic digestion process, most of the gases emitted include methane ($CH_4$) and $CO_2$. Methane content was measured using an apparatus called Einhorn. It is first filled with liquid sodium hydroxide (NaOH) and then, 5 mL of biogas was injected into it. The injected biogas passed through the sodium hydroxide content inside the apparatus and its $CO_2$ was absorbed. The remaining gas at the top of the apparatus shows the amount of methane in 5 mL of biogas [16].

## 2.4. Design of experiments (DOE)

Different percentages of the mixture were determined by the Design Expert software. For this purpose, the mixture design was used. The design of the mixture is a surface response design that allows the effect of changing the ratios between variables to be investigated. The domain is an ordered figure in this design with as many vertices as components, in a space of dimensionality equal to the number of components minus one. An equilateral triangle whose vertices correspond to combinations containing 100 percent of a single component is a mixture design of three components. A mixture that does not have one of the three components represents the sides of a triangle (Figure 1). Simplex designs are used to measure the effects of mixture components on the response variable, and simplex lattice or simplex centroid configuration may be chosen among them. The models used in the design of the mixture are different from the polynomials used for independent variables on the response surface. The well-known Scheffe polynominals that can be linear, quadratic, full-cubic and special cubic models are these models [17].

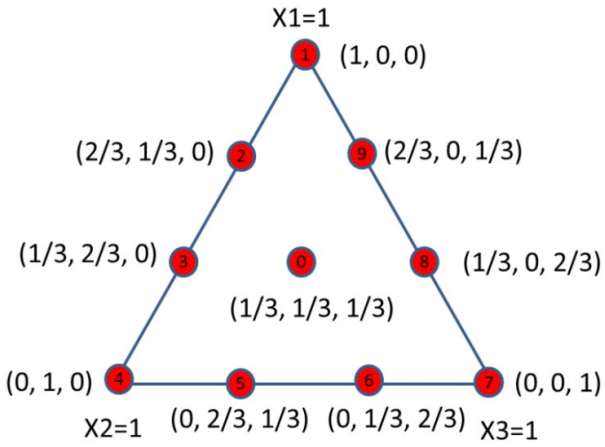


**Figure 1.** Augmented simplex centroid design plan used for experiments

Based on this design and according to the software output with a central point, four additional model points, five lack-of-fit points and three repetition points, 22 different compositions of substrate matters were loaded, as presented in Table 2. The experiment was carried out for 21 days. This retention time was obtained from pre-experiments.

To assess the effect of co-digestion on the output of biogas as a response variable, three components were used, which represented the percentage of each matter in the digester mixture. The amount of these components is 0-0.8 for sheep blood and cheese whey and 0.2-0.6 for inoculum. Accordingly, if "q" denotes the number of matters composing the system under study and xi represents the component of the mixture, the mixture in each reactor will be equal to:

$$\sum_{i=1}^{q} x_i = x_1 + x_2 + \ldots + x_q = 1.0 \quad x_i > 0 \quad i = 1, 2, 3, \ldots, q$$

**Table 2.** The order of different substrate mixtures based on the output from Design Expert software and responses

| Run | Build type | Space type | Component 1 | Component 2 | Component 3 | Response 1 | Response 2 |
|---|---|---|---|---|---|---|---|
| | | | A: blood | B: cheesse whey | C: inoculum | Biogas | $CH_4$ |
| | | | % | % | % | mL/g vs | mL/g vs |
| **1** | Replicate | Vertex | 80 | 0 | 20 | 122.92 | 38.11 |
| **2** | Model | AxialCB | 55 | 15 | 30 | 141.69 | 70.84 |
| **3** | Lack of fit | Interior | 35 | 35 | 30 | 146.66 | 73.33 |
| **4** | Model | CentEdge | 20 | 20 | 60 | 96.54 | 59.21 |
| **5** | Model | ThirdEdge | 0 | 66.6667 | 33.3333 | 111.51 | 65.04 |
| **6** | Lack of fit | CentEdge | 40 | 40 | 20 | 105.19 | 43.83 |
| **7** | Lack of fit | Center | 30 | 30 | 40 | 135.72 | 67.41 |
| **8** | Lack of fit | TripBlend | 40 | 13.3333 | 46.6667 | 113.00 | 47.83 |
| **9** | Model | ThirdEdge | 26.6667 | 53.3333 | 20 | 127.60 | 36.58 |
| **10** | Model | Vertex | 0 | 40 | 60 | 98.39 | 77.40 |
| **11** | Model | Vertex | 40 | 0 | 60 | 86.07 | 38.45 |
| **12** | Model | Vertex | 0 | 80 | 20 | 102.21 | 58.94 |
| **13** | Lack of fit | TripBlend | 13.3333 | 40 | 46.6667 | 112.18 | 49.36 |
| **14** | Model | ThirdEdge | 53.3333 | 26.6667 | 20 | 119.66 | 39.09 |
| **15** | Model | ThirdEdge | 0 | 53.3333 | 46.6667 | 108.88 | 71.86 |
| **16** | Model | Interior | 25 | 25 | 50 | 110.09 | 70.82 |
| **17** | Replicate | Vertex | 0 | 40 | 60 | 95.81 | 76.01 |
| **18** | Model | ThirdEdge | 53.3333 | 0 | 46.6667 | 95.75 | 54.89 |
| **19** | Replicate | Vertex | 0 | 80 | 20 | 110.73 | 57.94 |
| **20** | Model | ThirdEdge | 66.6667 | 0 | 33.3333 | 108.45 | 39.77 |
| **21** | Model | AxialCB | 15 | 55 | 30 | 110.68 | 44.64 |
| **22** | Model | Vertex | 80 | 0 | 20 | 118.24 | 31.92 |

## 3. RESULTS AND DISCUSSION

### 3.1. Cumulative biogas production analysis

Cumulative charts related to biogas production in different reactors are presented in Figures 2. According to Dareioti and Kornaros [18], care should be taken to ensure that alkalinity is high enough to prevent system instability as a result of likely accumulation of volatile fatty acids. Therefore, it can be concluded that Reactors 5, 10, 12, 17, and 19 had a biogas yield of less than 115 mL/g vs due to the lack of blood. These reactors, which had at least 40 % of cheese whey, faced a severe pH decline leading to reduced biogas production. Reactor 6 is of the same class, but had 40 % of blood in its mixture. However, due to the high cheese whey content (40 %), it had a similar performance to the previous reactors. Furthermore, in Reactors 4, 10, 11, and 17, the produced biogas was less than 100 mL/g vs due to the high amount of inoculum (60 %). The high amount of inoculum in the mixture causes insufficient supply of nutrients to the microorganisms reducing the biogas yield. Based on the findings of Dareioti and Kornaros [18], cheese whey has low levels of nitrogen, which increases the C/N proportion in this matter. The study by Cuetos, Gomez, Martinez, Fierro and Otero [19] also shows that considering the high nitrogen content in the blood, this matter had a high C/N proportion and could lead to system stability and optimized C/N proportion of the mixture. On this basis, Reactors 2 and 3 had 35 %-55 % blood and the amount of cheese whey was less than 40 %; this increased biogas production to more than 140 mL/g vs which was due to the pH stability of sheep blood and preventing acidification of the mixture. The highest performance of methane production was related to Reactors 10 and 17. These reactors were filled with a mixture of 60 % inoculum and 40 % cheese whey. The high amount of chesse whey caused the reactor to become unstable in terms of pH. As a result, they were ignored.

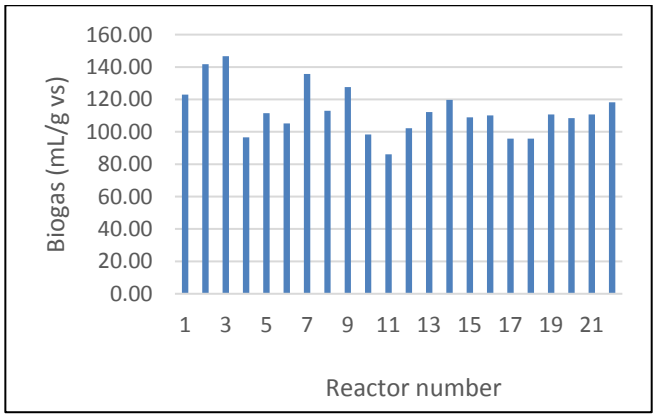


**Figure 2.** Cumulative chart related to biogas production

Whey presents a typical acidic pH value (5.4 ± 0.2) for these types of substrates, but is not suitable for the methanogenic step of AD. The organic fraction represented by VS/TS was 90.5 ± 4 %, indicating the high organic content of the substrate. C/N ratio was 15, indicating the high nitrogen content of the whey, but also the lactose content, which is an inherited characteristic of the substrate. It is worth mentioning that several authors have pointed out a higher cheese whey C/N ratio [20, 21].

The inoculum presented a pH of 7 ± 0.1, which is within the acceptable range reported in the literature for anaerobic digestion processes (6.6–7.9) [20, 22].

According to Vivekanand, Mulat, Eijsink, and Horn [21], biogas production potential of the three feedstocks fish ensilage, manure and whey was evaluated using Biochemical Methane Potential (BMP) tests. Since anaerobic digestion of single substrates may be inefficient due to imbalances in the carbon-nitrogen ratio, degree of biodegradability and/or due to lack of nutrients needed by the microbial community, co-digestion of these substrates was also assessed, revealing synergistic effects and a particularly good effect of combining manure with fish ensilage.

Cuetos et al. [23] showed that the addition of activated carbon for the digestion of residual blood significantly improved the digestion process. The adsorption capacity of ammonium, the protection this carrier may offer by limiting mass transfer of toxic compounds, and its toxic capacity as a conductive material may explain the successful digestion of residual blood as the sole substrate.

### 3.2. ANOVA analysis

#### 3.2.1. Fit summary

This table includes significant statistics for choosing the right starting point for the final model. Based on these statistics, the appropriate model(s) is selected. According to the output related to amount of biogas, the software presented a special Quartic vs Quadratic model (see Table 3).

#### 3.2.2. Coefficients in terms of coded factors

The calculation of the coefficient represents the predicted change in response per unit change in factor value if all the remaining variables are kept constant. The cut-off is the total average response of all the runs in an orthogonal design. Based on the factor settings, the coefficients are adaptations around that average. The VIFs are 1 when the variables are orthogonal; VIFs greater than 1 display multi-colinearity, the greater the VIF, the more extreme the association of factors. VIFs lower than 10 are tolerable as a rough norm (Table 4).

**Table 3.** Fit summary for the amount of biogas yield

| Source | Sequential p-value | Lack of fit p-value | Adjusted $R^2$ | Predicted $R^2$ | |
|---|---|---|---|---|---|
| Linear | 0.0354 | 0.0298 | 0.2225 | 0.1144 | |
| Quadratic | 0.0121 | 0.0578 | 0.5249 | 0.3847 | |
| Special cubic | 0.0871 | 0.0690 | 0.5858 | 0.4505 | |
| Cubic | 0.4918 | 0.0619 | 0.5732 | 0.0071 | |
| **Sp Quartic vs Quadratic** | **0.0059** | **0.1470** | **0.7687** | **0.6061** | **Suggested** |
| Quartic vs Cubic | 0.2909 | 0.0628 | 0.6515 | -0.8846 | |
| Quartic vs Sp Quartic | 0.9335 | 0.0628 | 0.6515 | -0.8846 | |

**Table 4.** Coefficients in terms of coded factors

| Component | Coefficient estimate | df | Standard error | 95 % CI Low | 95 % CI High | VIF |
|---|---|---|---|---|---|---|
| A: blood | 120.53 | 1 | 4.90 | 109.94 | 131.12 | 2.44 |
| B: cheesse whey | 107.44 | 1 | 4.91 | 96.84 | 118.04 | 2.56 |
| C: inoculum | 53.38 | 1 | 43.19 | -39.92 | 146.67 | 60.57 |
| AB | 14.51 | 1 | 23.96 | -37.25 | 66.27 | 2.96 |
| AC | -10.43 | 1 | 79.65 | -182.50 | 161.63 | 24.85 |
| BC | 74.74 | 1 | 82.96 | -104.49 | 253.97 | 34.95 |
| $A^2BC$ | 2481.59 | 1 | 599.77 | 1185.85 | 3777.32 | 5.48 |
| $AB^2C$ | 524.61 | 1 | 610.47 | -794.22 | 1843.45 | 5.68 |
| $ABC^2$ | -1545.33 | 1 | 677.32 | -3008.60 | -82.06 | 5.95 |

### 3.2.3. Final equation in terms of L-Pseudo components

In terms of coded variables, the equation can be used to make predictions about the answer to each factor's given levels. The high levels of the components of the mixture are coded by default as +1 and the low levels are coded as 0. By comparing the factor coefficients, the coded equation is helpful in identifying the relative influence of the factors.

$$\text{Biogas} = 120.53A + 107.44B + 53.38C + 14.51AB - 10.43AC + 74.74BC + 2481.59A^2BC + 524.61AB^2C - 1545.33ABC^2$$

## 3.3. Diagnostics plots

### 3.3.1. Normal plot

This plot demonstrates the distribution of residuals. If it follows a direct line, the residuals enjoy a good distribution and the model is desirable (see Figure 3).

### 3.3.2. Predicted vs actual plot

A graph of the response values is predicted against the actual response values. The objective is to find a value or a group of values that the model does not easily predict (see Figure 4).

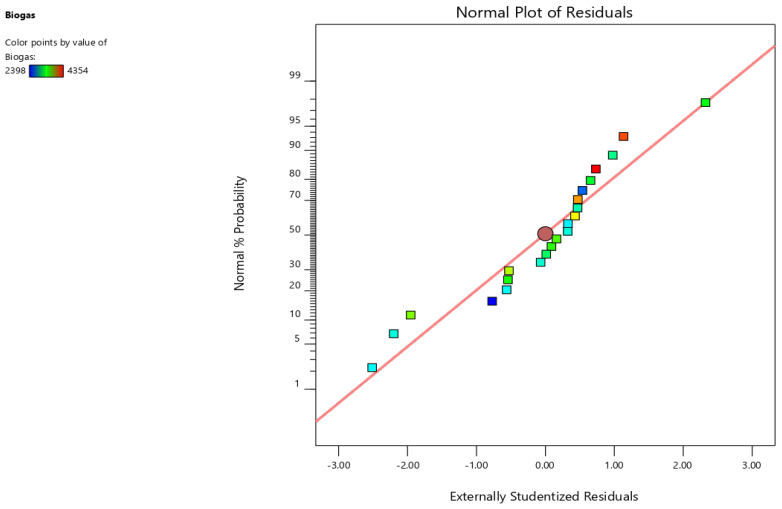


**Figure 3.** Standard plot of residuals for amount of biogas yield

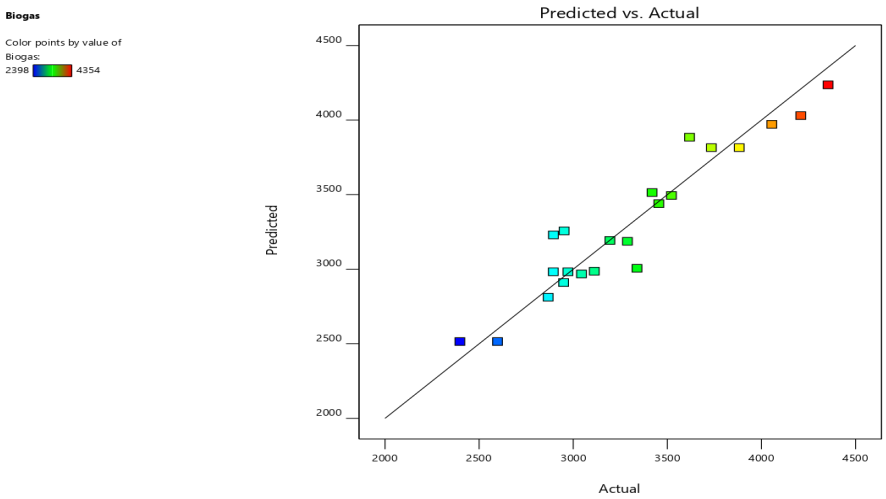


**Figure 4.** Predicted vs actual plots for amount of biogas yield

### 3.3.3. Box-Cox plot

Box-Cox plot helps identify the optimal power transfer function to be applied to the response. In the Box-Cox plot, the lowest point shows the amount of Lambda that contributes to the minimum residual number of squares in the transfer model. The current Lambda is within this range; according to Figure 5, there is no need for the transfer function to be added. The best Lambda value indicated by the plot, however, is -3.

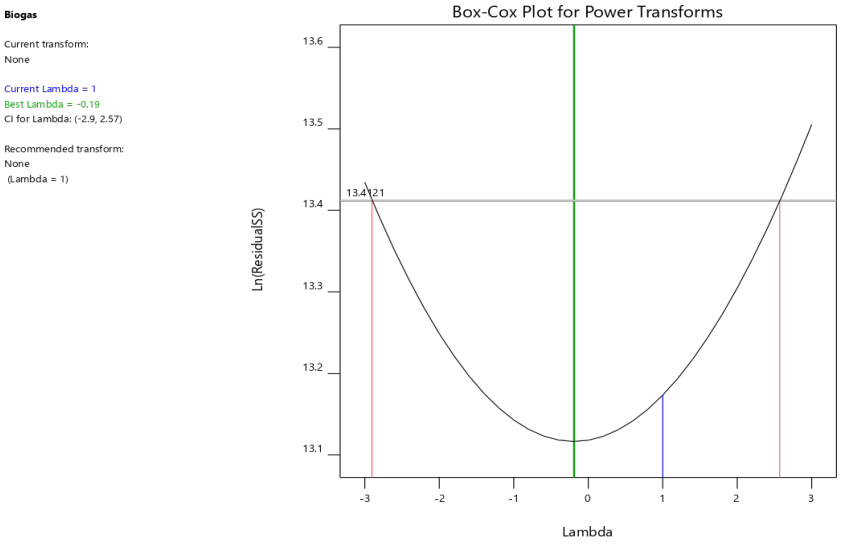


**Figure 5.** Box-Cox plot for biogas yield

## 3.4. Model graphs

### 3.4.1. Trace plot

For non-mixture designs, trace plots are identical to disturbance plots. They are used to compare the effects of all the components in the design space. To set the reference blend from which the traces are plotted, the factors tool is employed. The objective is to decide how sensitive the response near the reference blend is to deviation from the formulation. The reference blend is better defined by numerical optimization results, but defaults to the values of the centroid values (see Figure 6).

### 3.4.2. Contour plot and (3D) surface

This plot is a two-dimensional display of the response represented against the composition of the components of the mixture and illustrates the relationship between them. In this triangular graph, any of its vertices shows the maximum value for each matter, and as we move toward the side in front of each vertex, this value decreases. On the other hand, the color inside the triangle represents the response value. Accordingly, responses are determined from low to high using blue-red colors. The similar responses are linked together by a specified line. The responses that are in the red area of the graph demonstrate the optimal composition of the substrate matters, which are likely due to the optimal C/N proportion. Besides, low pH of cheese whey caused the red points in the graph to move toward compositions with more blood (see Figure 7). (3 D) Surface graph is the 3D contour plot with a slope and curve shape besides color (see Figure 8).

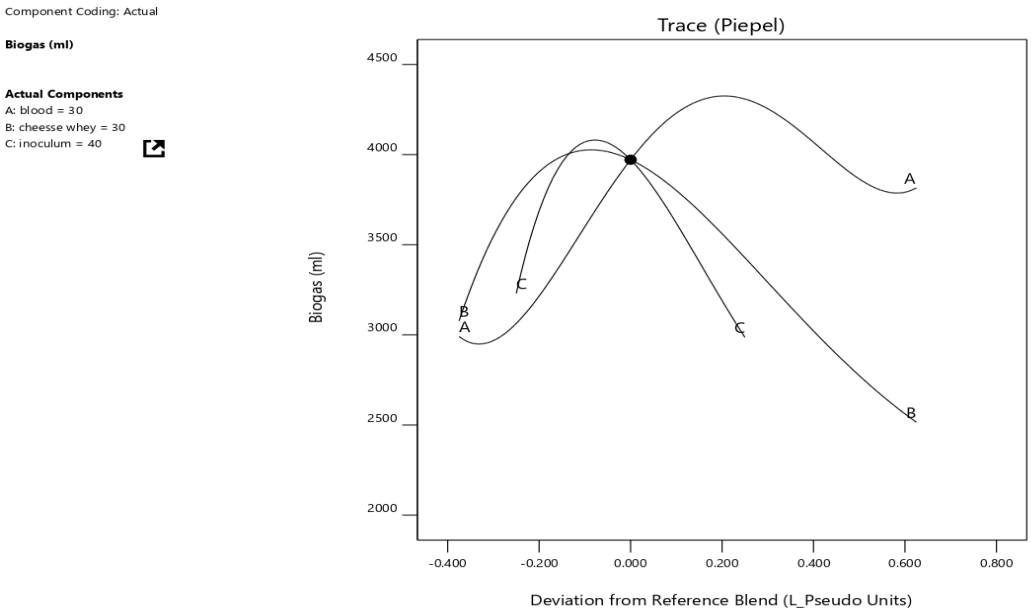


**Figure 6.** Trace plot for amount of biogas yield

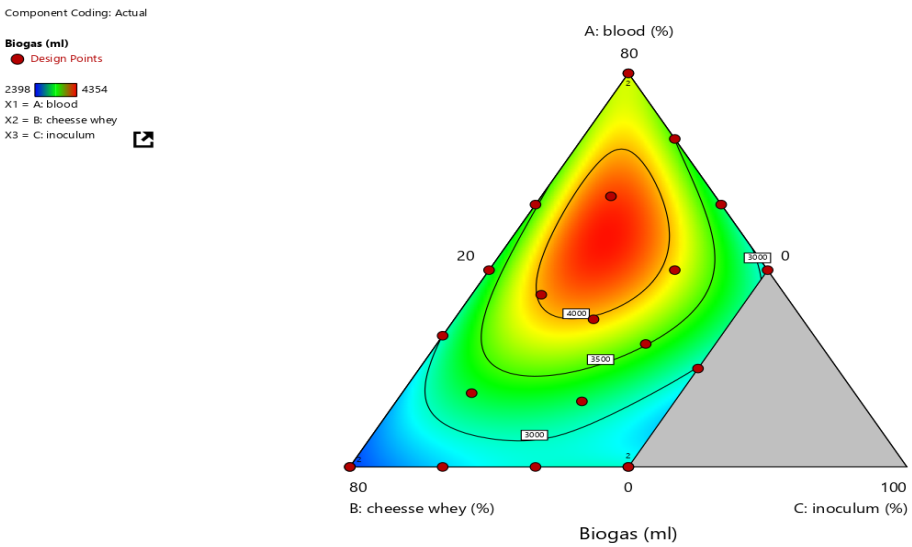


**Figure 7.** Contour plot for biogas yield

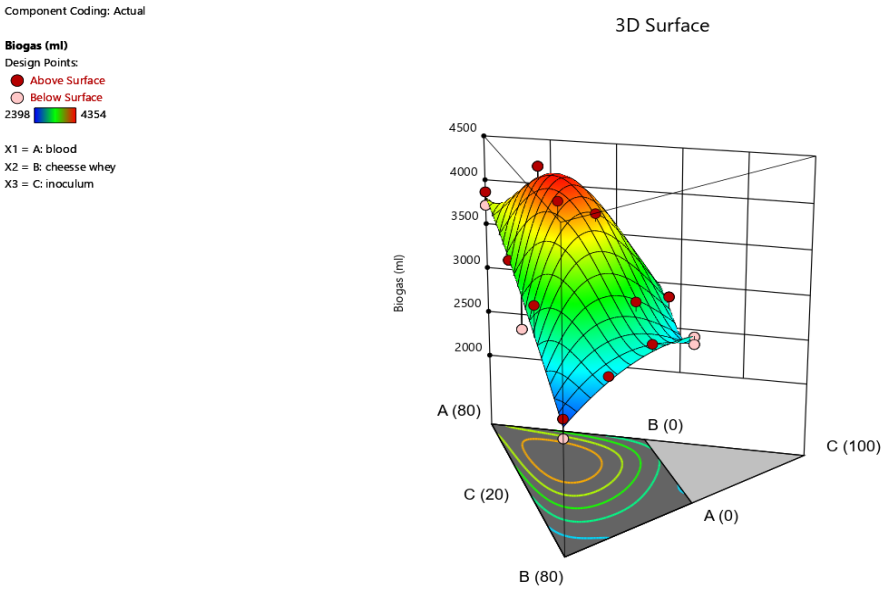


**Figure 8.** (3D) Surface graph for biogas yield

### 3.5. Optimization ramps

These ramps represent a graphical view of the optimal compositions. The optimal value for each independent variable are shown in red and those related to response (dependent variable) are in blue. According to the optimization, as shown in Figure 9, a composition consisting of 44 % sheep blood, 24 % cheese whey, and 32 % inoculum will produce the highest biogas possible, i.e., 143 mL/g vs of biogas.

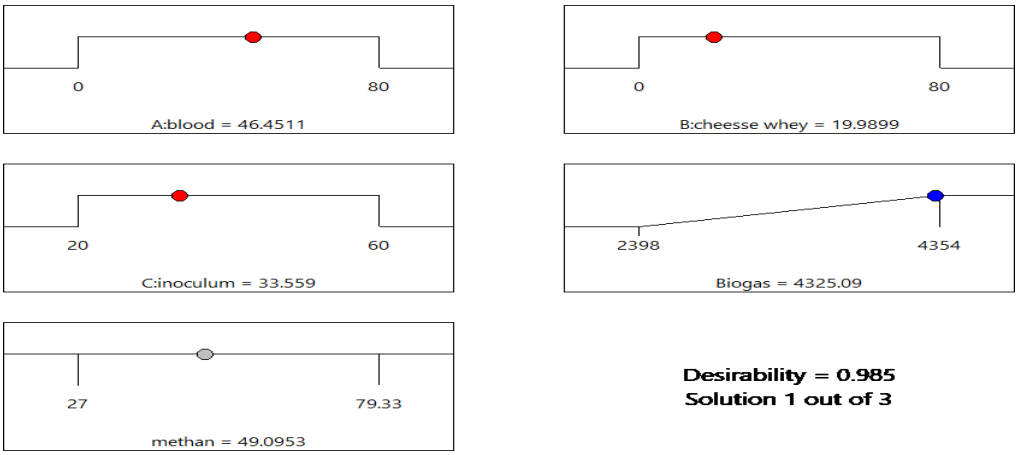


**Figure 9.** Optimization ramps for the highest biogas yield

## 4. CONCLUSIONS

Anaerobic co-digestion of three substances, including sheep blood, cheese whey, and inoculum, was investigated in the present study. The results can be summarized in the following. Design Expert software can be used as a practical program for designing experiments for the purpose of mixing different types of waste for biogas production. Using the mixture design enabled us to achieve optimal compositions of different matters for anaerobic co-digestion and measure these compositions together. In this study, the results related to anaerobic co-digestion of sheep blood, cheese whey, and inoculum showed that in the experimental phase, the optimal composition included 35 % sheep blood, 35 % cheese whey, and 30 % inoculum, which produced a biogas yield of 146.66 mL/g vs in a hydraulic retention time of 21 days. The obtained results were fed to the software for modeling and after modeling, the Design Expert software predicted an optimal composition that included 44 % sheep blood, 24 % cheese whey, and 32 % inoculum. The biogas yield in this prediction was 143 mL/g vs. Based on the findings, to overcome acidification in digestion of matters such as cheese whey, the composition of matters with higher constant pH can be used to increase the amount of the produced biogas and methane in a particular period. Furthermore, using inoculum accelerates the digestion operations due to abundant microorganisms and saves time and energy. Anaerobic digestion of wastes such as blood and cheese whey with a high COD can not only produce clear energies but also prevent environmental pollution to a considerable extent.

## 5. ACKNOWLEDGEMENT

This research was conducted in collaboration with the Faculty of Agriculture, Bu Ali Sina University.

## REFERENCES

1. Claassen, P.A.M., van Lier, J.B., Lopez Contreras A.M., van Niel E.W.J., Sijtsma, L., Stams, A.J.M.,de Vries, S.S. and Weusthuis, R.A., "Utilisation of biomass for the supply of energy carriers", ***Applied microbiology and biotechnology***, Vol. 52, (1999), 741-755. (https://link.springer.com/article/10.1007/s002530051586).
2. Mao, C., Feng, Y., Wang, X. and Ren, G., "Review on research achievements of biogas from anaerobic digestion", ***Renewable and Sustainable Energy Reviews,*** , Vol. 45, (2015), 540-555. (https://doi.org/10.1016/j.rser.2015.02.032).
3. Amon, T., Amon, B., Kryvoruchko, V., Zollitsch, W., Mayer, K. and Gruber, L., "Biogas production from maize and dairy cattle manure-Influence of biomass composition on the methane yield", ***Agriculture, Ecosystems & Environment***, Vol. 118, No. 1, (2007), 173-182. (https://doi.org/10.1016/j.agee.2006.05.007).
4. Hagos, K., Zong, J., Li, D., Liu, C. and Lu, X., "Anaerobic co-digestion process for biogas production: Progress, challenges and perspectives", ***Renewable and Sustainable Energy Reviews***, Vol. 76, (2017), 1485-1496. (https://doi.org/10.1016/j.rser.2016.11.184).
5. Rasouli, M., Mousavi, S.M., Azargoshasb, H., Jamialahmadi, O. and Ajabshirchi, Y., "CFD simulation of fluid flow in a novel prototype radial mixed plug-flow reactor", ***Journal of Industrial and Engineering Chemistry***, Vol. 64, (2018), 124-133. (https://doi.org/10.1016/j.jiec.2018.03.008).
6. Cuetos, M.J., Moran, A., Otero, M. and Gomez, X., "Anaerobic co-digestion of poultry blood with OFMSW: FTIR and TG-DTG study of process stabilization", ***Environmental Technology***, Vol. 30, No. 6, (2009), 571-582. (https://doi.org/10.1080/09593330902835730).
7. Lehtomäki, A., Huttunen, S. and Rintala, J.A., "Laboratory investigations on co-digestion of energy crops and crop residues with cow manure for methane production: Effect of crop to manure ratio", ***Resources, Conservation and Recycling***, Vol. 51, No. 3, (2007), 591-609. (https://doi.org/10.1016/j.resconrec.2006.11.004).
8. Salminen, E., Rintala, J., Lokshina, L.Y. and Vavilin, V.A., "Anaerobic batch degradation of solid poultry slaughterhouse waste", ***Water Science and Technology***, Vol. 10, No. 3, (2000), 33-41. (https://doi.org/10.2166/wst.2000.0053).
9. Alvarez, R. and Liden, G., "Semi-continuous co-digestion of solid slaughterhouse waste, manure, and fruit and vegetable waste", ***Renewable Energy***, Vol. 33, No. 4, (2008), 726-734. (https://doi.org/10.1016/j.renene.2007.05.001).
10. Prazeres, A.R., Carvalho, F. and Rivas, J., "Cheese whey management: A review", ***Journal of Environmental Management***, Vol. 110, (2012), 48-68. (https://doi.org/10.1016/j.jenvman.2012.05.018).
11. Comino, E., Riggio, V.A. and Rosso, M., "Biogas production by anaerobic co-digestion of cattle slurry and cheese whey", ***Bioresource Technology***, Vol. 114, (2013), 46-53. (https://doi.org/10.1016/j.biortech.2012.02.090).
12. Rasouli, M., Ajabshirchi, Y., Mousavi, S.M., Nosrati, M. and Yaghmaei, S., "Process optimization and modeling of anaerobic digestion of cow manure for enhanced biogas yield in a mixed plug-flow reactor using response surface methodology", ***Biosciences, Biotechnology Research Asia***, Vol. 12, (2015), 2333-2344. (https://doi.org/10.13005/bbra/1909).
13. Standard methods for the examination of water and wastewater, 20th edition, American Public Health Association/American Water Works Association/Water Environment Federation, Washington DC, USA, (1998). (http://srjcstaff.santarosa.edu/~oraola/Assets/APHA_SM_20.pdf).
14. Elasri, O. and El amin Afilal, M., "Potential for biogas production from the anaerobic digestion of chicken droppings in Morocco", ***International Journal of Recycling of Organic Waste in Agriculture***, Vol. 5, No. 3, (2016), 195-204. (https://link.springer.com/article/10.1007/s40093-016-0128-4#citeas).
15. Valero, D., Montes, J.A., Rico, J.L. and Rico, C., "Influence of headspace pressure on methane production in Biochemical Methane Potential (BMP) tests", ***Waste Management***, Vol. 48, (2016), 193-198. (https://doi.org/10.1016/j.wasman.2015.11.012).
16. Stoddard, I., "Communal polyethylene biogas systems: Experiences from on-farm research in rural West Java", Student Thesis, (2010). (http://urn.kb.se/resolve?urn=urn:nbn:se:uu:diva-131203).
17. Candioti, L.V., De Zan, M.M., Camara, M.S. and Goicoechea, H.C., "Experimental design and multiple response optimization: Using the desirability function in analytical methods development", ***Talanta***, Vol. 124, (2014), 123-138. (https://doi.org/10.1016/j.talanta.2014.01.034).
18. Dareioti, M.A. and Kornaros, M., "Anaerobic mesophilic co-digestion of ensiled sorghum, cheese whey and liquid cow manure in a two-stage CSTR system: Effect of hydraulic retention time", ***Bioresource Technology***, Vol. 175, (2015), 553-562. (https://doi.org/10.1016/j.biortech.2014.10.102).
19. Cuetos, M.J., Gomez, X., Martinez, E.J., Fierro, J. and Otero, M., "Feasibility of anaerobic co-digestion of poultry blood with maize residues", ***Bioresource Technology***, Vol. 144, (2013), 513-520. (https://doi.org/10.1016/j.biortech.2013.06.129).
20. Fernández-Rodríguez. M.J., Puntano, N.F., Mancilla-Leytón, J.M. and Borja, R., "Batch mesophilic anaerobic co-digestion of spent goat batch mesophilic anaerobic co-digestion of spent goat straw bedding and goat cheese whey: Comparison with the mono-digestion of the two sole substrates", ***Journal of Environmental Management***, (2020). 111733. (https://doi.org/10.1016/j.jenvman.2020.111733).
21. Vivekanand, V., Mulat, D.G., Eijsink, V.G.H. and Horn, S.J., "Synergistic effects of anaerobic co-digestion of whey, manure and fish ensilage", ***Bioresource Technology,*** Vol. 249, (2018), 35-41. (https://doi.org/10.1016/j.biortech.2017.09.169).
22. Carvalho, A., Fragoso, R., Gominho, J. and Duarte, E., "Effect of minimizing d-limonene compound on anaerobic co-digestion feeding mixtures to improve methane yield", ***Waste and Biomass Valorization,*** Vol. 10, (2019), 75-83. (https://doi:10.1007/s12649-017-0048-1).
23. Cuetos, M.J., Martinez, E.J., Moreno, R., Gonzalez, R., Otero, M. and Gomez, X., "Enhancing anaerobic digestion of poultry blood using activated carbon", ***Journal of Advanced Research,*** Vol. 8, (2017), 297-307. (https://doi.org/10.1016/j.jare.2016.12.004).

JREE: Vol. 8, No. 3, (Summer 2021) 16-25

Journal of Renewable Energy and Environment

Research Article

Journal Homepage: www.jree.ir

# Evaluation of the Effective Factors in Locating a Photovoltaic Solar Power Plant Using Fuzzy Multi-Criteria Decision-Making Method

Aychar Khajavi Pour [a], Mohammad Reza Shahraki [a*], Faranak Hosseinzadeh Saljooghi [b]

[a] *Department of Industrial Engineering, School of Engineering, University of Sistan and Baluchestan, Zahedan, Sistan and Baluchestan, Iran.*
[b] *Department of Mathematics, School of Mathematics, University of Sistan and Baluchestan, Zahedan, Sistan and Baluchestan, Iran.*

*PAPER INFO*

*Paper history:*
Received 21 September 2020
Accepted in revised form 25 April 2021

*Keywords*:
Locating,
Photovoltaic Solar Power Plant,
Fuzzy Hierarchical Method

*ABSTRACT*

The energy of processes is mainly supplied by fossil fuels. Short life of fossil energy sources and increasing environmental pollution caused by fossil fuels and increasing demand have made researchers introduce new solutions for supply of energy. Energy production in a photovoltaic solar power plant is cost-effective due to being clean and renewable. The power generation of these plants is affected by their site due to climate conditions, effective radiation periods, and the rate of solar radiation absorption. Therefore, finding the optimal location to establish a solar power plant is important. Identifying effective location criteria and the importance of these criteria is effective in choosing the optimal location.In this research, in the first phase, the effective criteria in locating a photovoltaic solar power plant were investigated based on the Delphi method. Then, in the second phase, based on the criteria identified in the first phase, fuzzy hierarchy method was used to compare the criteria with each other and determine the importance of each of them. The results of the study showed that the rate of solar radiation and average temperature were the most important criteria in locating photovoltaic solar power plant. Moreover, the criteria of slope, distance to main roads, distance to power lines, and land use were of highest importance in locating a photovoltaic solar power plant.

https://doi.org/10.30501/jree.2020.247756.1145

## 1. INTRODUCTION

Almost all processes are performed through using energy [1]. Fossil fuels are sources for supply of energy, but they cause environmental pollution in proportion to their use. In addition, increasing growth of population and increasing energy demand have made energy suppliers seek alternative energy sources [2]. Solar energy is a clean and renewable source that is suitable for meeting global energy needs. As energy production affects all aspects of the social, economic, and environmental aspects [3], the criteria for selecting the optimal site for the construction of a photovoltaic solar power plant should be in accordance with these aspects. Identifying and investigating the role (and its extent) of the influential criteria in locating a photovoltaic solar power plant is essential for more and better energy absorption [4]. Fuzzy multi-criteria decision-making methods are used to examine different aspects of locating in the uncertainty state. Thus, they can help managers achieve optimal site.

One of the multi-criteria decision-making methods is the hierarchical method. Some of the advantages of using the hierarchical method can be mentioned in the following:

1) Breaking the problem into different levels that lead to more precise and better decision-making.
2) More accurate recognition of the level relationship of criteria related to the problem [5].

Many studies have been conducted on the location of solar power plants using decision-making techniques. Some of these studies are listed in Table 1.

In this research, in the first phase, the effective criteria in locating a photovoltaic solar power plant were identified using Delphi methods. In order to recognize the criteria, a questionnaire proportionate for the studies mentioned in Table 1 was designed and distributed among the experts of solar power plants. The following questionnaires were designed and distributed according to the consensus of experts. Eventually, the effective criteria for the location of photovoltaic solar power plants were determined and collected. Then, in the second phase, the problem was broken into three levels by the fuzzy hierarchy method and investigated. Aim of the problem, group, and criteria were placed in the first, second, and third levels, respectively. In this phase, the experts were asked to perform the paired comparisons among the criteria. By adding the data to the Super Decision software using a hierarchical method, the calculations were done using hierarchical method. Finally, the importance of these criteria over each other was determined.

## 2. LITERATURE REVIEW AND BACKGROUND OF THE STUDY

*Corresponding Author's Email: mr.shahraki@eng.usb.ac.ir (M.R. Shahraki)
URL: http://www.jree.ir/article_129570.html

Please cite this article as: Khajavi Pour, A., Shahraki, M.R. and Hosseinzadeh Saljooghi, F., "Evaluation of the effective factors in locating a photovoltaic solar power plant using fuzzy multi-criteria decision-making method", ***Journal of Renewable Energy and Environment (JREE)***, Vol. 8, No. 3, (2021), 16-25. (https://doi.org/10.30501/jree.2020.247756.1145).

Locating is the optimal selection of sites for a specific purpose based on certain criteria. Selecting a suitable site for a photovoltaic solar power plant reduces the cost of energy production and transfer [5]. One of the technologies for using solar energy is photovoltaic systems. Photovoltaic systems consist of semiconducting devices that absorb the sunlight and store energy through the battery [1]. As there are some criteria with a varying degree of importance in locating a photovoltaic solar power plant, examining the importance of each of these criteria is necessary. A fuzzy hierarchical method can be used to determine the importance of the criteria involved in locating a photovoltaic solar power plant and comparing these criteria. A fuzzy hierarchical method is one of the multi-criteria decision-making methods [30].

**Table 1.** Applications of multi-criteria decision-making techniques in different studies

| Method | RES | Location | Reference |
|---|---|---|---|
| AHP & GIS | GPPPs | Southern Spain | [6] |
| GIS | Solar PV and wind | Colorado | [7] |
| GIS | PV | Oman | [8] |
| GIS & AHP | PV | Konya/Turkey | [3] |
| GIS & MCDM | PV | Cartagena/Southeast Spain | [9] |
| GIS & Fuzzy | Solar PV and wind | Turkey | [10] |
| AHP | PV | Egypt | [11] |
| GIS & Electere3 | PV | Murcia/Southeast Spain | [12] |
| MCDM | Solar PV and wind | Southern England | [13] |
| GIS & MCDM | PV | Southeast of Spain | [14] |
| GIS | PV | Nigeria | [15] |
| GIS | PV | Morocco | [5] |
| GIS | PV | United Arab Emirates | [16] |
| GIS & AHP | PV | Spain | [17] |
| GIS & MCDM | Solar PV and wind | Afghanistan | [18] |
| AHP & FTOPSIS | PV | India | [19] |
| GCP | PV | Northwest China | [20] |
| GIS & MCDM | PV & CSP | Africa | [21] |
| GIS | PV | Malaysia | [22] |
| GIS & AHP | PV | Saudi Arabia | [23] |
| FAHP | PV | Iran | [24] |
| Gray Number | PV | Global | [25] |
| GIS & MCDM | PV & CSP | West Africa | [26] |
| DEA | PV | Iran | [27] |
| GIS & MCDM | PV | Mauritius | [28] |
| GIS & MCAM | PV | The State of Arizona | [29] |

Several studies have been conducted to identify the effective factors in locating a photovoltaic solar power plant. Suitable criteria for locating a photovoltaic solar power plant were distance from the river, population density, and distance from the main roads, slope, flood, earthquake, and solar radiation. Ref. [10] considered distance from power lines, distance from urban areas, and slope and direction as suitable criteria for locating a photovoltaic solar power plant. In Ref. [12], land use, distance from river, distance from villages, distance from power lines, distance from transporting stations, distance from urban areas, and distance from main roads, slope, slope direction and average temperature were effective criteria for locating a photovoltaic solar power plant. In Ref. [16], the slope, the direction of slope, the distance from the main road, and the average temperature were considered as effective criteria for locating photovoltaic solar power plant. Ref. [23] considered land use, distances from power lines, distance from urban areas, distance from main lines, slope, solar radiation, and average temperatures as effective criteria in locating a photovoltaic solar power plant. Ref. [25] considered the criteria of land use, distance from river, distance from stations, flood, storm, earthquake, and solar radiation as suitable criteria for locating a photovoltaic solar power plant. In Ref. [31], the criteria for locating a photovoltaic solar power plant were reported to be distance from river, distance from power lines, distance from main roads, the slope, and the rate of solar radiation. In Ref. [28], the distance from main lines, slope, rate of solar radiation, average temperature, and humidity were effective criteria for locating the photovoltaic solar power plant. In Ref. [29], land use, distance from river, distance from main lines, flood, storm, and earthquake were considered as effective criteria for locating the photovoltaic solar power plant.

A review of previous research papers in this field indicates that they have only dealt with the location of solar power plants using decision methods and GIS software; however, the present study first employs the Delphi method, comprehensive criteria, and appropriate water conditions. Then, the climate of the study area is considered. In addition, the location of the solar power plant and the importance of these criteria are examined.

## 3. METHOD

### 3.1. Methodology

This study was conducted in two phases. First, effective criteria for locating a photovoltaic solar power plant were identified based on the conducted studies and the views of

experts in this area using the Delphi method. Then, in the second phase, using the fuzzy hierarchical method, the importance of each criterion was examined. Additionally, the criteria were compared with each other. Figure 1 illustrates the phases of the research method.

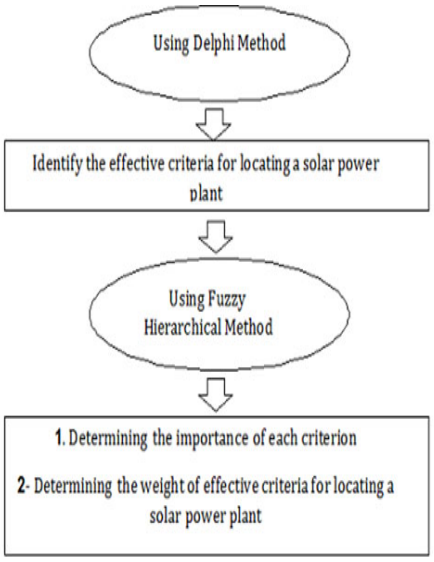


**Figure 1.** Research phases

### 3.1.1. Delphi method

The Delphi method is one of the methods used for gaining group knowledge. It is applied to making decision in qualitative issues. The Delphi method is used to collect experts' views to reach a consensus on the importance of decision making criteria for locating a photovoltaic solar power plant. The steps in the Delphi method are as follows [32]:

**Step 1:** Identification of criteria for locating a photovoltaic solar power plant.

At this step, the criteria related to locating solar power plant are identified using a comprehensive review of the theoretical principles of criteria, previous studies, and the views of the experts.

**Step 2:** Selection of the number of decision-makers.

The views of the experts participating in the Delphi method play a central role in identifying efficient criteria for locating a photovoltaic solar power plant. The participants comprised 60 experts in the area of distribution, generation, operation, and installation of photovoltaic solar power plants.

**Step 3:** Distribution of questionnaire.

First, a questionnaire containing the criteria extracted from previous studies and experts' views was prepared. In distributing the questionnaire, the experts were asked to express their views on the importance and quality of the criteria for locating the photovoltaic solar power plant and to add new criteria, if needed. Then, the next modified questionnaire based on the information extracted from the total responses to the first questionnaire was designed and re-distributed among experts. The number of repetitions of the distribution of the questionnaire to determine the criteria depends on Kendall's coefficient of concordance, calculated at each step.

**Step 4:** Determining the level of consensus.

At this step, using Kendall's coefficient of concordance derived from Equation (1), the level of consensus among decision-makers is determined. As the value of this coefficient gets closer to 1, it would indicate high consensus among the decision-makers and thus, the final questionnaire and the criteria in the final questionnaire could be identified as selection criteria. Moreover, Delphi method would stop when the value of the Kendall's coefficient of concordance be at least 0.95.

$$W = \frac{12s}{m^2(n^2-n)} \quad (1)$$

where W indicates the Kendall's coefficient of concordance, s is the sum of the total deviations squared, n is the number of ranked criteria, and m is the number of ranked groups.

### 3.1.2. Fuzzy analytic hierarchy process

In multi-criteria decision-making methods, multiple criteria are used rather than one criterion for decision making [33]. Multi-criteria decision-making methods reduce decision-making costs and increase decision-making accuracy and provide a good framework for solving problems [34]. Fuzzy Analytic Hierarchy Process is one of the multi-criteria decision-making methods based on experts' views. In the Fuzzy Analytic Hierarchy Process, it is possible to define problem criteria as a hierarchical structure and determine the importance of each criterion by making a paired comparison between the criteria [30].

The steps of the fuzzy hierarchy process are as follows [35]:

**Step 1:** Drawing a hierarchical chart.

At this step, the objective is considered at Level 1 and the criterion is placed at Level 2 of the chart. Figure 2 illustrates the hierarchy of the objective as well as the structure of the hierarchy of criteria and sub-criteria.

In multi-criteria decision-making methods, multiple criteria are used rather than one criterion for decision making [33]. Multi-criteria decision-making methods reduce decision-making costs and increase decision-making accuracy and provide a good framework for solving problems [34]. Fuzzy Analytic Hierarchy Process is one of the multi-criteria decision-making methods based on experts' views. In the Fuzzy Analytic Hierarchy Process, it is possible to define problem criteria as a hierarchical structure and determine the importance of each criterion by making a paired comparison between the criteria [30].

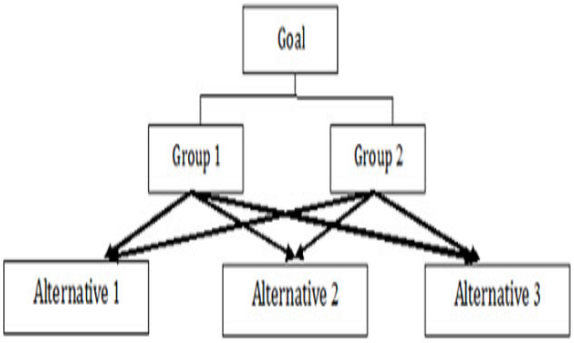


**Figure 2.** Hierarchical chart

**Step 2:** Defining fuzzy numbers.

At this step, the pairwise comparisons of sub-criteria expressed as linguistic variables based on experts' views are expressed as fuzzy numbers for mathematical calculations. The theory of fuzzy sets has been proposed to solve the non-accurate issues that exist in real world. A triangular fuzzy number is denoted by $\widetilde{M} = (l, m, u)$. The membership function $\mu_{\widetilde{M}}(x)$ is also in the form of Equation (2).

$$\mu_{\widetilde{M}}(x) = \begin{cases} \frac{x-l}{m-l} & l \le x \le m \\ \frac{u-x}{u-m} & m \le x \le u \\ 0 & \text{otherwise} \end{cases} \quad (2)$$

L is lower limit, m is the part that has the maximum membership degree, and u is also the upper limit of the fuzzy number $\widetilde{M}$ [36].

If a ($a_1$, $a_2$, $a_3$) and b ($b_1$, $b_2$, $b_3$) are two triangular fuzzy numbers, a = b is when $a_1=b_1$, a = b, $a_3=b_3$. The mathematical relations between fuzzy numbers are shown in Equations (3) and (4) [37].

$$A + B = (a_1 + b_1, a_2 + b_2, a_3 + b_3) \quad (3)$$

$$a \times b = (a_1b_1, a_2b_2, a_3b_3) \qquad \text{if } a_1, b_1 \ge 0 \quad (4)$$

Table 2 indicates the linguistic variables used to evaluate the importance of the criteria in the pairwise comparison.

**Table 2.** Linguistic variables for evaluating the importance of criteria [38]

| Fuzzy number | Importance |
|---|---|
| (0.1,0.1,0.2) | Very low |
| (0.1,0.3,0.5) | Low |
| (0.2,0.5,0.8) | Moderate |
| (0.5,0.7,1) | High |
| (0.7,1,1) | Very high |

**Step 3:** Formation of a pairwise comparison matrix.

The pairwise comparison matrix of the criteria is formed using the fuzzy numbers of Table 1. The pairwise comparison matrix was in the form of Equation (5).

$$\widetilde{A} = \begin{bmatrix} 1 & \tilde{a}_{12} & \cdots & \tilde{a}_{1n} \\ \tilde{a}_{21} & 1 & \cdots & \tilde{a}_{2n} \\ \vdots & \vdots & \ddots & \vdots \\ \tilde{a}_{n1} & \tilde{a}_{n2} & \cdots & 1 \end{bmatrix} \quad (5)$$

One of the most important features of a paired comparison matrix is as follows:

$$\tilde{a}_{ji} = \frac{1}{\tilde{a}_{ij}} \quad (6)$$

where $\tilde{a}_{ij}$ represents the importance of the $i^{th}$ criterion rather than $j^{th}$ criterion.

**Step 4:** Calculating the value of each alternative compared to each criteria.

For each row of the pairwise comparison matrix, the value of $S_i$ has been calculated by Equation (10).

$$\sum_{j=1}^{m} M_{gi}^{j} = \left(\sum_{j=1}^{m} l_j , \sum_{j=1}^{m} m_j , \sum_{j=1}^{m} u_j\right) \quad (7)$$

$$\sum_{i=1}^{n}\sum_{j=1}^{m} M_{gi}^{j} = \left(\sum_{i=1}^{n} l_i , \sum_{i=1}^{n} m_i , \sum_{i=1}^{n} u_i\right) \quad (8)$$

$$\left[\sum_{i=1}^{n}\sum_{j=1}^{m} M_{gi}^{j}\right]^{-1} = \left(\frac{1}{\sum_{i=1}^{n} u_i} , \frac{1}{\sum_{i=1}^{n} m_i}, \frac{1}{\sum_{i=1}^{n} l_i}\right) \quad (9)$$

$$S_i = \sum_{j=1}^{m} M_{gi}^{j} \times \left[\sum_{i=1}^{n}\sum_{j=1}^{m} M_{gi}^{j}\right]^{-1} \quad (10)$$

where $M_i = (l_i, m_i, u_i)$ is a triangular fuzzy number inside the pairwise comparisons matrix; $u_i$, $m_i$, and $l_i$ are the upper, middle, and upper triangular fuzzy numbers of $M_i$, respectively. In computing the matrix S, each of the components of the fuzzy number is summed up and multiplied by the inverse fuzzy of the sum total.

**Step 5:** Ranking.

At this step, if $S_1 = (l_1, m_1, u_1)$ and $S_2 = (l_2, m_2, u_2)$ are two triangular fuzzy numbers, the degree of $S_1$ versus $S_2$ can be calculated as in Equation (11).

$$V(S_1 \ge S_2) = \begin{cases} 1 & \text{if } m_1 \ge m_2 \\ 0 & \text{if } l_2 \ge u_1 \\ \frac{l_2 - u_1}{(m_1 - u_1) - (m_2 - l_2)} & \text{otherwise} \end{cases} \quad (11)$$

**Step 6:** Calculating the weight of the criteria in the pairwise comparisons matrix.

At this step, the weight of the criteria is calculated using Equation (12) and the non-normalized weight is obtained.

$$d'(A_i) = \text{Min } V(S_i \ge S_k) \qquad k = 1, 2, \ldots, n \qquad k \ne i \quad (12)$$

**Step 7:** Calculating the final weight vector.

The final weight vector of each criterion was derived by dividing the non-normalized weight of each criterion by the sum of non-normalized weights of the total criteria.

## 4. ANALYSIS OF THE RESULTS

In this research, three types of questionnaires were used to collect the data. First, the first questionnaire was developed based on theoretical foundations and previous research on locating the solar photovoltaic power plant. Table 3 presents a number of photovoltaic solar power plant locating studies along with locating criteria.

**Table 3.** Solar PV site suitability criteria

| References | Criteria | Group |
|---|---|---|
| **Climatology** | Solar irradiation | [6, 7, 8, 23, 24, 25, 26, 27,28,31, 39] |
| | Average temperature | [3, 8, 9,12,14, 16, 17, 23, 28,40,41] |
| | Wetland | [28] |
| **Topography** | Orientation slope | [3, 6, 9, 10, 11, 12, 16, 42] |
| | Slope | [3, 6, 9,10,11,12,14,16, 17, 23, 28, 31] |
| **Economic-Social** | Distance to main roads | [5,6, 7, 8, 9, 12,13,14,15,17, 22, 23, 24, 26, 28, 29,31] |
| | Distance to urban | [3,6, 7, 9,10, 11, 12,13,17,23] |
| | Population density | [8,22,26,27,43] |
| | Transformer substation | [12] |
| **Electrical issue** | Distance to substations | [9, 12, 14, 17, 25] |
| | Distance to power line | [3, 5,6, 7, 8, 9, 10, 11, 12, 13,14,15,17, 22,23, 6, 40,44,45] |
| | Distance to village | [12] |
| **Environment** | Distance to river | [12,25,29,31] |
| | Land use & cover | [3,6,7,12,22,23,24,25,29,42,43] |

A questionnaire was distributed among 60 experts in the solar power plant location and they were asked to classify the criteria and express their views on the importance and quality of the criteria. After collecting the questionnaire and entering the data in SPSS software, Kendall's coefficient of concordance was calculated 0.68. Then, another questionnaire was designed according to the information extracted from the first questionnaire and distributed among the experts. In the second questionnaire, the criteria increased and changed. The value of Kendall's coefficient of concordance of the second questionnaire was calculated as 0.87. The third questionnaire was designed and distributed according to the views of experts. The Kendall's coefficient of concordance was calculated as 0.95; therefore, the Delphi method stopped. Accordingly, the criteria were classified into five groups of topography, environment, climatological, socioeconomic, power distribution lines. The information derived from the third questionnaire is presented in Table 4.

**Table 4.** Effective criteria for locating a photovoltaic solar power plant

| Group | Climatology | Environment | Electrical issues | Economic-Social | Topography |
|---|---|---|---|---|---|
| **Criteria** | Average temperature | Distance to river | Distance to power posts | Distance to main roads | Fault |
| | Solar irradiation | | | Distance to urban | Slope |
| | Wetland | Land use | Distance to power line | Distance to village | Height |
| | Evaporation | | | | |

After identifying the criteria using the Delphi method, in the second phase, the importance of each of the criteria has been determined using the fuzzy hierarchical analysis method. The reason for the importance of each criterion is presented in Table 5.

**Table 5.** The type of the effect of criteria on locating a photovoltaic solar power plant

| Group | Criteria | Type of effect in locating |
|---|---|---|
| **Economic-Social** | Distance to main roads | The proximity of solar power plant to main roads will reduce the cost |
| | Distance to urban | It can be used to supply power and human resource |
| | Distance to village | It can be used to supply power and human resource |
| **Climatology** | Solar irradiation | More solar radiation will generate more electrical energy |
| | Average temperature | As average temperature of environment increases, the power of solar panels decreases |
| | Evaporation | Increasing evaporation reduces the power of solar panels. |
| | Wetland | Increasing the humidity reduces the power of solar panels |
| **Electrical issues** | Distance to power line | Proximity of power plant to power transmission lines reduces the cost |
| | Distance to power posts | Proximity of power plant to power transmission posts reduces the cost. |
| **Environment** | Land use | It reduces the environmental damages |
| | Distance to river | As the distance of power plant to river increases, future costs will decrease |
| **Topography** | Fault | As the distance of power plant to fault increases, future costs will decrease |
| | Slope | As slope is lower, the power of solar panels will be higher |
| | Height | By increasing the height, the power of solar panels will increase |

Based on the factors and criteria identified in the Delphi method, the hierarchical chart for determining the importance of criteria for locating photovoltaic solar power plants was plotted at three levels. The first level was related to the goal of

the problem, the second level to the group, and the third level to criteria. Figure 3 represents the hierarchical chart of these three levels. The identified criteria for locating a photovoltaic solar power plant included five groups of socioeconomic, climatological, topographic, environment, and electrical energy related issues such as distance to village (C1), distance to electricity posts (C2), distance to urban areas (C3), distance to river (C4), height (C5), fault (C6), evaporation (C7), humidity (C8), distance to power lines (C9), land use (C10) distance to main roads (C11), mean temperature (C12), rate of solar radiation (C13), and slope (C14).

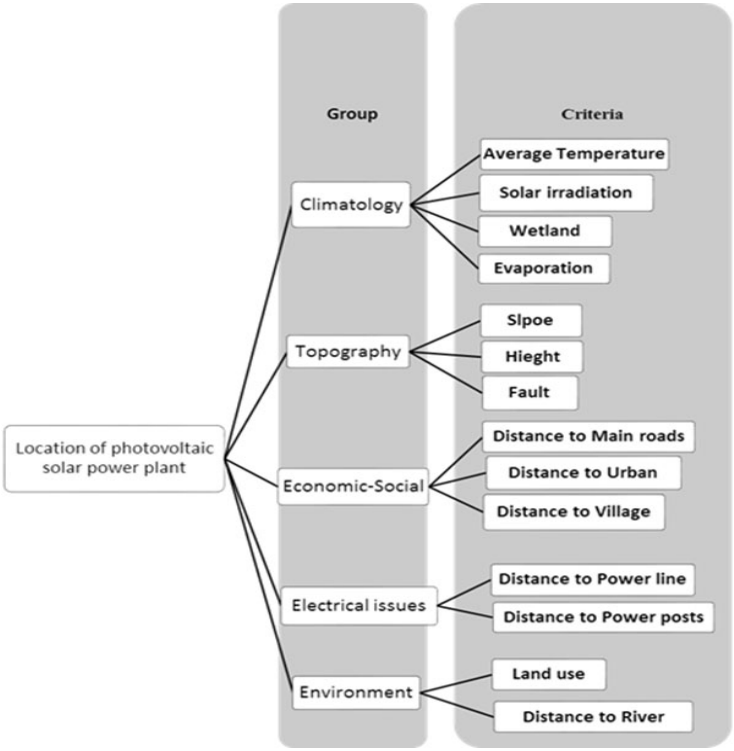


**Figure 3.** Hierarchical chart of locating a photovoltaic solar power plant

After plotting the hierarchical chart, decision-makers were asked to compare the criteria with each other and to express the relative importance of the elements using the linguistic variables of Table 2. By adding data to the Super Decision software, the weight of each criterion was extracted and the results are presented in Table 6.

**Table 6.** The matrix of pairwise comparisons of sub-criteria

| | $C_1$ | $C_2$ | $C_3$ | $C_4$ | $C_5$ | $C_6$ | $C_7$ | $C_8$ | $C_9$ | $C_{10}$ | $C_{11}$ | $C_{12}$ | $C_{13}$ | $C_{14}$ |
|---|---|---|---|---|---|---|---|---|---|---|---|---|---|---|
| $C_1$ | (1,1,1) | (5,10,10) | (1,1,1.4) | (5,10,10) | (1,1.4,2) | (2,3.3,10) | (1,1,1.4) | (1,1.4,2) | (1,1,1.4) | (1,1.4,2) | (2,3.3,10) | (5,10,10) | (5,10,10) | (2,3.3,10) |
| $C_2$ | (0.1,0.1,0.2) | (1,1,1) | (2,3.3,10) | (1,1,1.4) | (1.25,2,5) | (1,1.4,2) | (2,3.3,10) | (1.25,2,3.3) | (2,3.3,10) | (1.25,2,5) | (1,1.4,2) | (1,1,1.4) | (1,1,1.4) | (1,1.4,2) |
| $C_3$ | (0.7,1,1) | (0.1,0.3,0.5) | (1,1,1) | (5,10,10) | (1.25,2,5) | (2,3.3,10) | (1,1.4,2) | (1.25,2,3.3) | (1,1.4,2) | (1.25,2,3.3) | (2,3.3,10) | (5,10,10) | (5,10,10) | (2,3.3,10) |
| $C_4$ | (0.1,0.1,0.2) | (0.7,1,1) | (0.1,0.1,0.2) | (1,1,1) | (1.25,2,5) | (1,1.4,2) | (2,3.3,10) | (1.25,2,5) | (2,3.3,10) | (1.25,2,5) | (1,1.4,2) | (1,1,1.4) | (1,1,1.4) | (1,1.4,2) |
| $C_5$ | (0.5,0.7,1) | (0.2,0.5,0.8) | (0.2,0.5,0.8) | (0.2,0.5,0.8) | (1,1,1) | (1,1.4,2) | (2,3.3,10) | (1.25,2,5) | (2,3.3,10) | (1.25,2,5) | (1,1.4,2) | (1,1,1.4) | (1,1,1.4) | (1,1.4,2) |
| $C_6$ | (0.1,0.3,0.5) | (0.5,0.7,1) | (0.1,0.3,0.5) | (0.5,0.7,1) | (0.5,0.7,1) | (1,1,1) | (2,3.3,10) | (1.25,2,5) | (2,3.3,10) | (1.25,2,5) | (1,1.4,2) | (1,1,1.4) | (1,1,1.4) | (1,1.4,2) |
| $C_7$ | (0.7,1,1) | (0.1,0.3,0.5) | (0.5,0.7,1) | (0.1,0.3,0.5) | (0.1,0.3,0.5) | (0.1,0.3,0.5) | (1,1,1) | (1.25,2,5) | (1,1.4,2) | (1.25,2,5) | (2,3.3,10) | (5,10,10) | (5,10,10) | (2,3.3,10) |
| $C_8$ | (0.5,0.7,1) | (0.2,0.5,0.8) | (0.2,0.5,0.8) | (0.2,0.5,0.8) | (0.2,0.5,0.8) | (0.2,0.5,0.8) | (0.2,0.5,0.8) | (1,1,1) | (2,3.3,10) | (1.25,2,5) | (1,1.4,2) | (1,1,1.4) | (1,1,1.4) | (1,1.4,2) |
| $C_9$ | (0.7,1,1) | (0.1,0.3,0.5) | (0.5,0.7,1) | (0.1,0.3,0.5) | (0.1,0.3,0.5) | (0.1,0.3,0.5) | (0.5,0.7,1) | (0.1,0.3,0.5) | (1,1,1) | (1.25,2,5) | (2,3.3,10) | (5,10,10) | (5,10,10) | (2,3.3,10) |
| $C_{10}$ | (0.5,0.7,1) | (0.2,0.5,0.8) | (0.2,0.5,0.8) | (0.2,0.5,0.8) | (0.2,0.5,0.8) | (0.2,0.5,0.8) | (0.2,0.5,0.8) | (0.2,0.5,0.8) | (0.2,0.5,0.8) | (1,1,1) | (1,1.4,2) | (1,1,1.4) | (1,1,1.4) | (1,1.4,2) |
| $C_{11}$ | (0.1,0.3,0.5) | (0.5,0.7,1) | (0.1,0.3,0.5) | (0.5,0.7,1) | (0.5,0.7,1) | (0.5,0.7,1) | (0.1,0.3,0.5) | (0.5,0.7,1) | (0.1,0.3,0.5) | (0.5,0.7,1) | (1,1,1) | (1,1,1.4) | (1,1,1.4) | (1,1.4,2) |
| $C_{12}$ | (0.1,0.1,0.2) | (0.7,1,1) | (0.1,0.1,0.2) | (0.7,1,1) | (0.7,1,1) | (0.7,1,1) | (0.1,0.1,0.2) | (0.7,1,1) | (0.1,0.3,0.5) | (0.7,1,1) | (0.7,1,1) | (1,1,1) | (1,1,1.4) | (1,1.4,2) |
| $C_{13}$ | (0.1,0.1,0.2) | (0.7,1,1) | (0.1,0.1,0.2) | (0.7,1,1) | (0.7,1,1) | (0.7,1,1) | (0.1,0.1,0.2) | (0.7,1,1) | (0.1,0.1,0.2) | (0.7,1,1) | (0.7,1,1) | (0.7,1,1) | (1,1,1) | (1,1.4,2) |
| $C_{14}$ | (0.1,0.3,0.5) | (0.5,0.7,1) | (0.1,0.3,0.5) | (0.5,0.7,1) | (0.5,0.7,1) | (0.5,0.7,1) | (0.1,0.3,0.5) | (0.5,0.7,1) | (0.1,0.3,0.5)) | (0.5,0.7,1) | (0.5,0.7,1) | (0.5,0.7,1) | (0.5,0.7,1) | (1,1,1) |

According to Equations (7) to (10), the value of $S_i$ was calculated for each row of the pairwise comparison matrix. The general results of calculations are given in Table 7.

$$\sum_{i=1}^{14}\sum_{j=1}^{14} M_{gi}^{j} = (205.25, 331.1, 547.3)$$

$$\left[\sum_{i=1}^{14}\sum_{j=1}^{14} M_{gi}^{j}\right]^{-1} = (0.0018, 0.003, 0.0048)$$

**Table 7.** Mean value of each criterion

| $S_1$ | $S_2$ | $S_3$ | $S_4$ | $S_5$ | $S_6$ | $S_7$ |
|---|---|---|---|---|---|---|
| (0.0096,0.022,0.045) | (0.019,0.055,0.101) | (0.011,0.028,0.092) | (0.028,0.085,0.15) | (0.016,0.042,0.12) | (0.02,0.061,0.16) | (0.022,0.057,0.23) |
| | | | | | | |
| $S_8$ | $S_9$ | $S_{10}$ | $S_{11}$ | $S_{12}$ | $S_{13}$ | $S_{14}$ |
| (0.022,0.056,0.17) | (0.026,0.067,0.28) | (0.026,0.065,0.22) | (0.03,0.075,0.27) | (0.053,0.15,0.25) | (0.053,0.15,0.25) | (0.032,0.08,0.28) |

At this step, according to Equation (11), for each criterion, the degree of preference of Si over Sk was obtained and the results are presented in Table 8.

According to the values given in Table 8, each of the ratios was calculated for each row according to Equation (12). The weights presented in Table 8 were normalized by dividing each weight by the total weights. The results of calculation are given in Table 9.

**Table 8.** Comparison of the mean value of each criterion

| | | | | | | | | | | | | | |
|---|---|---|---|---|---|---|---|---|---|---|---|---|---|
| $S_1>S_2$ | 0.43 | $S_2>S_1$ | 1 | $S_3>S_1$ | 1 | $S_4>S_1$ | 1 | $S_5>S_1$ | 1 | $S_6>S_1$ | 1 | $S_7>S_1$ | 1 |
| $S_1>S_3$ | 0.85 | $S_2>S_3$ | 1 | $S_3>S_2$ | 0.72 | $S_4>S_2$ | 1 | $S_5>S_2$ | 0.89 | $S_6>S_2$ | 1 | $S_7>S_2$ | 1 |
| $S_1>S_4$ | 0.21 | $S_2>S_4$ | 0.76 | $S_3>S_4$ | 0.53 | $S_4>S_3$ | 1 | $S_5>S_3$ | 1 | $S_6>S_3$ | 1 | $S_7>S_3$ | 1 |
| $S_1>S_5$ | 0.57 | $S_2>S_5$ | 1 | $S_3>S_5$ | 0.83 | $S_4>S_5$ | 1 | $S_5>S_4$ | 0.7 | $S_6>S_4$ | 0.84 | $S_7>S_4$ | 0.85 |
| $S_1>S_6$ | 0.39 | $S_2>S_6$ | 1.03 | $S_3>S_6$ | 0.69 | $S_4>S_6$ | 1 | $S_5>S_6$ | 0.86 | $S_6>S_5$ | 1 | $S_7>S_5$ | 1 |
| $S_1>S_7$ | 0.47 | $S_2>S_7$ | 1 | $S_3>S_7$ | 0.76 | $S_4>S_7$ | 1 | $S_5>S_7$ | 0.94 | $S_6>S_7$ | 1 | $S_7>S_6$ | 0.95 |
| $S_1>S_8$ | 0.39 | $S_2>S_8$ | 1.08 | $S_3>S_8$ | 0.7 | $S_4>S_8$ | 1 | $S_5>S_8$ | 0.77 | $S_6>S_8$ | 1 | $S_7>S_8$ | 1.43 |
| $S_1>S_9$ | 0.29 | $S_2>S_9$ | 0.93 | $S_3>S_9$ | 0.62 | $S_4>S_9$ | 1 | $S_5>S_9$ | 0.8 | $S_6>S_9$ | 0.94 | $S_7>S_9$ | 1.47 |
| $S_1>S_{10}$ | 0.29 | $S_2>S_{10}$ | 0.96 | $S_3>S_{10}$ | 0.63 | $S_4>S_{10}$ | 1 | $S_5>S_{10}$ | 0.82 | $S_6>S_{10}$ | 0.95 | $S_7>S_{10}$ | 1.43 |
| $S_1>S_{11}$ | 0.2 | $S_2>S_{11}$ | 0.85 | $S_3>S_{11}$ | 0.56 | $S_4>S_{11}$ | 1 | $S_5>S_{11}$ | 0.75 | $S_6>S_{11}$ | 0.89 | $S_7>S_{11}$ | 1.46 |
| $S_1>S_{12}$ | 1 | $S_2>S_{12}$ | 0.35 | $S_3>S_{12}$ | 0.24 | $S_4>S_{12}$ | 0.59 | **$S_5>S_{12}$** | **0.42** | $S_6>S_{12}$ | 0.54 | **$S_7>S_{12}$** | **0.63** |
| $S_1>S_{13}$ | 1 | **$S_2>S_{13}$** | **0.34** | **$S_3>S_{13}$** | **0.23** | **$S_4>S_{13}$** | **0.58** | $S_5>S_{13}$ | 0.42 | **$S_6>S_{13}$** | **0.54** | $S_7>S_{13}$ | 0.64 |
| **$S_1>S_{14}$** | **0.17** | $S_2>S_{14}$ | 0.61 | $S_3>S_{14}$ | 0.53 | $S_4>S_{14}$ | 1 | $S_5>S_{14}$ | 0.72 | $S_6>S_{14}$ | 0.86 | $S_7>S_{14}$ | 0.86 |
| | | | | | | | | | | | | | |
| $S_8>S_1$ | 1 | $S_9>S_1$ | 1 | $S_{10}>S_1$ | 1 | $S_{11}>S_1$ | 1 | $S_{12}>S_1$ | 1 | $S_{13}>S_1$ | 1 | $S_{14}>S_1$ | 1 |
| $S_8>S_2$ | 1 | $S_9>S_2$ | 1 | $S_{10}>S_2$ | 1 | $S_{11}>S_2$ | 1 | $S_{12}>S_2$ | 1 | $S_{13}>S_2$ | 1 | $S_{14}>S_2$ | 1 |
| $S_8>S_3$ | 1 | $S_9>S_3$ | 1 | $S_{10}>S_3$ | 1 | $S_{11}>S_3$ | 1 | $S_{12}>S_3$ | 1 | $S_{13}>S_3$ | 1 | $S_{14}>S_3$ | 1 |
| $S_8>S_4$ | 0.79 | $S_9>S_4$ | 0.94 | $S_{10}>S_4$ | 0.9 | $S_{11}>S_4$ | 0.96 | $S_{12}>S_4$ | 1 | $S_{13}>S_4$ | 1 | $S_{14}>S_4$ | 0.98 |
| $S_8>S_5$ | 1 | $S_9>S_5$ | 1 | $S_{10}>S_5$ | 1 | $S_{11}>S_5$ | 1 | $S_{12}>S_5$ | 1 | $S_{13}>S_5$ | 1 | $S_{14}>S_5$ | 1 |
| $S_8>S_6$ | 0.98 | $S_9>S_6$ | 1 | $S_{10}>S_6$ | 1 | $S_{11}>S_6$ | 1 | $S_{12}>S_6$ | 1 | $S_{13}>S_6$ | 1 | $S_{14}>S_6$ | 1 |
| $S_8>S_7$ | 1 | $S_9>S_7$ | 1 | $S_{10}>S_7$ | 1 | $S_{11}>S_7$ | 1 | $S_{12}>S_7$ | 1 | $S_{13}>S_7$ | 1 | $S_{14}>S_7$ | 1 |
| $S_8>S_9$ | 0.93 | $S_9>S_8$ | 1 | $S_{10}>S_8$ | 1 | $S_{11}>S_8$ | 1 | $S_{12}>S_8$ | 1 | $S_{13}>S_8$ | 1 | $S_{14}>S_8$ | 1 |
| $S_8>S_{10}$ | 0.94 | $S_9>S_{10}$ | 1 | $S_{10}>S_9$ | 0.98 | $S_{11}>S_9$ | 1 | $S_{12}>S_9$ | 1 | $S_{13}>S_9$ | 1 | $S_{14}>S_9$ | 1 |
| $S_8>S_{11}$ | 0.88 | $S_9>S_{11}$ | 0.97 | $S_{10}>S_{11}$ | 0.95 | $S_{11}>S_{10}$ | 1 | $S_{12}>S_{10}$ | 1 | $S_{13}>S_{10}$ | 1 | $S_{14}>S_{10}$ | 1 |
| $S_8>S_{12}$ | 0.56 | **$S_9>S_{12}$** | **0.73** | **$S_{10}>S_{12}$** | **0.66** | **$S_{11}>S_{12}$** | **0.74** | $S_{12}>S_{11}$ | 1 | $S_{13}>S_{11}$ | 1 | $S_{14}>S_{11}$ | 0.77 |
| **$S_8>S_{13}$** | **0.55** | $S_9>S_{13}$ | 0.73 | $S_{10}>S_{13}$ | 0.66 | $S_{11}>S_{13}$ | 0.74 | **$S_{12}>S_{13}$** | **1** | **$S_{13}>S_{12}$** | **1** | **$S_{14}>S_{12}$** | **0.77** |
| $S_8>S_{14}$ | 0.85 | $S_9>S_{14}$ | 0.95 | $S_{10}>S_{14}$ | 0.93 | $S_{11}>S_{14}$ | 0.95 | $S_{12}>S_{14}$ | 1 | $S_{13}>S_{14}$ | 1 | $S_{14}>S_{13}$ | 1 |

**Table 9.** Normalized weight of criteria

| | Criteria | Normalized weight | Ranking |
|---|---|---|---|
| $C_1$ | Distance to village | 0.02 | 13 |
| $C_2$ | Distance to power posts | 0.04 | 11 |
| $C_3$ | Distance to urban | 0.027 | 12 |
| $C_4$ | Distance to rives | 0.07 | 7 |
| $C_5$ | Height | 0.05 | 10 |
| $C_6$ | Fault | 0.064 | 9 |
| $C_7$ | Evaporation | 0.075 | 6 |
| $C_8$ | Wetland | 0.065 | 8 |
| $C_9$ | Distance to power line | 0.087 | 4 |
| $C_{10}$ | Land use | 0.078 | 5 |
| $C_{11}$ | Distance to main roads | 0.088 | 3 |
| $C_{12}$ | Average temperature | 0.12 | 1 |
| $C_{13}$ | Solar irradiation | 0.12 | 1 |
| $C_{14}$ | Slope | 0.091 | 2 |

Based on Table 9, the rates of solar radiation and average temperature were the most important criteria for locating the photovoltaic solar power plant. Moreover, the criteria of slope, distance to main roads, distance to power lines, and land use were of the highest importance in locating a photovoltaic solar power plant. Sunny hours represented the

total monthly sunny hours of the regions and the rate of energy received from sunlight. As the power of photovoltaic solar panels depended on ambient temperature and solar radiation, the average temperature and sunny hours were of great importance in the establishment of photovoltaic solar power plants. Previous studies suggested that the criteria identified in this research for locating solar power plants were very consistent and similar to previous studies (12 and 23), some of which are given in Table 10.

**Table 10.** Similar studies

| Reference | Environment | | Electrical issues | | | Economic-Social | | | | Topography | | Climatology | | |
|---|---|---|---|---|---|---|---|---|---|---|---|---|---|---|
| | Land use & cover | River | Distance to village | Distance to power line | Distance to substations | Transformer substation | Population density | Distance to urban | Distance to main roads | Slope | Orientation slope | Solar irradiation | Average temperature | Wetland |
| [6] | ✦ | | | ✦ | | | | ✦ | ✦ | ✦ | ✦ | ✦ | | |
| [7] | ✦ | | | ✦ | | | ✦ | ✦ | ✦ | | | ✦ | | |
| [43] | | ✦ | | | | | ✦ | | ✦ | ✦ | | ✦ | | |
| [3] | ✦ | | | ✦ | | | | ✦ | | ✦ | ✦ | | | |
| [9] | | | | ✦ | ✦ | | | ✦ | ✦ | ✦ | ✦ | | ✦ | |
| [11] | | | | ✦ | | | | ✦ | ✦ | ✦ | ✦ | | | |
| [12] | ✦ | ✦ | ✦ | ✦ | ✦ | ✦ | | ✦ | ✦ | ✦ | ✦ | | ✦ | |
| [14] | | | | ✦ | ✦ | | | ✦ | ✦ | ✦ | | | ✦ | |
| [17] | | | | ✦ | ✦ | | | ✦ | ✦ | ✦ | | | ✦ | |
| [23] | ✦ | | | ✦ | | | | ✦ | ✦ | ✦ | | ✦ | ✦ | |
| [25] | ✦ | ✦ | | | ✦ | | | | | | | ✦ | | |
| [26] | | | | ✦ | | | ✦ | | ✦ | | | ✦ | | |
| [31] | | ✦ | | ✦ | | | | | ✦ | ✦ | | ✦ | | |
| [28] | | | | | | | | | ✦ | ✦ | | ✦ | ✦ | ✦ |
| [29] | ✦ | ✦ | | | | | | | ✦ | | | | | |

## 5. CONCLUSIONS

Fossil fuels are the main source of energy. Environmental pollutions caused by fossil fuels and increasing energy demand have forced energy suppliers seek other sources. Solar energy is one of the sources of clean energy. Solar energy is available to humans without any restriction. The establishment of a photovoltaic solar power plant is an essential. Selecting a suitable site increases the absorption of more sunlight leading to storage of more solar energy. Thus, it is important to identify effective criteria for locating a solar photovoltaic power plant. In this research, two types of questionnaires were used to collect the data. The first questionnaire was developed based on the theoretical foundations of the subject and the previous studies as well as the views of the experts on locating the photovoltaic solar

power plant. This questionnaire assesses the importance of effective factors in locating the power plant. These factors were presented in five topographic, environment, climatologic, socio-economic, and power distribution lines groups. Data derived from the first questionnaire were collected and classified through the Delphi method. Then, in the second phase, the criteria identified in the first phase were evaluated to determine the importance of the criteria using the hierarchical method.

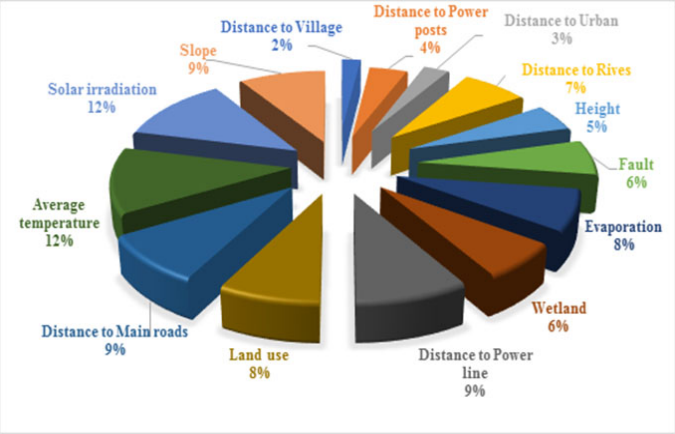


**Figure 4.** The importance of criteria to each other

According to Figure 4, the importance of average temperature and solar radiation is 13 %. Therefore, these two criteria are of greater importance than other criteria in constructing the solar power plant. More solar radiation and more solar absorption will be on photovoltaic panels. The average temperature is very important for panels. Establishing temperature balance in panels improves the efficiency of panels in solar radiation.

Based on the results of this research, it is recommended that other effective criteria according to the climate conditions of each region, other decision making methods, and GIS software be considered in locating a photovoltaic solar power plant.

## 6. ACKNOWLEDGEMENT

The first author, Mohammadreza Shahraki, likes to acknowledge Financial Assistance under scholarship programs received from the University of Sistan and Baluchestan of Iran to conduct this research.

## REFERENCES

1. Smets, A., Jäger, K., Isabella, O., van Swaaij, R. and Zeman, M., Solar energy: The physics and engineering of photovoltaic conversion technologies and systems, UIT Cambridge Ltd., Cambridge, (2016). (https://www.amazon.com/Solar-Energy-Engineering-Photovoltaic-Technologies/dp/1906860327).
2. Dehghani, E., Jabalameli, M.S. and Jabbarzadeh, A., "Robust design and optimization of solar photovoltaic supply chain in an uncertain environment", ***Energy***, Vol. 142, (2018), 139-156. (In Farsi). (https://doi.org/10.1016/j.energy.2017.10.004).
3. Uyan, M., "GIS-based solar farms site selection using analytic hierarchy process (AHP) in Karapinar region, Konya/Turkey", ***Renewable and Sustainable Energy Reviews***, Vol. 28, (2013), 11-17. (https://doi.org/10.1016/j.rser.2013.07.042).
4. Boxwell, M., The solar electricity handbook-2017 Edition: A simple, practical guide to solar energy–designing and installing solar photovoltaic systems. Greenstream Publishing, (2017). (https://www.amazon.com/Solar-Electricity-Handbook-installing-photovoltaic/dp/1907670653).
5. Merrouni, A.A., Mezrhab, A. and Mezrhab, A., "PV sites suitability analysis in the eastern region of Morocco", ***Sustainable Energy Technologies and Assessments***, Vol. 18, (2016), 6-15. (https://doi.org/10.1016/j.seta.2016.09.006).
6. Carrion, J.A., Espin Estrella, A., Aznar Dols, F. and Ramos Ridao, A., "The electricity production capacity of photovoltaic power plants and the selection of solar energy sites in Andalusia (Spain)", ***Renewable Energy***, Vol. 33, (2008), 545-552. (https://doi.org/10.1016/j.renene.2007.05.041).
7. Janke, J.R., "Multicriteria GIS modeling of wind and solar farms in Colorado", ***Renewable Energy***, Vol. 35, (2010), 2228-2234. (https://doi.org/10.1016/j.renene.2010.03.014).
8. Charabi, Y. and Gastli, A., "PV site suitability analysis, using GIS based spatial fuzzy multi-criteria evaluation", ***Renewable Energy***, Vol. 36, (2011), 2554-2561. (https://doi.org/10.1016/j.renene.2010.10.037).
9. Sanchez-Lozano, J.M., Teruel-Solano, J., Soto-Elvira, P.L., Garcia-Cascales, M.S. and Socorro, M., "Geographical information systems and multi-criteria decision making methods for the evaluation of solar farms locations: Case study in south-eastern Spain", ***Renewable and Sustainable Energy Reviews***, Vol. 24, (2013), 544-556. (https://doi.org/10.1142/S0219622016500218).
10. Aydin, N.Y., Kentel, E. and Sebnem Duzgun, H., "GIS-based site selection methodology for hybrid renewable energy systems: A case study from western Turkey", ***Energy Conversion and Management***, Vol. 70, (2013), 90-106. (https://doi.org/10.1016/j.enconman.2013.02.004).
11. Effat, H.A., "Selection of potential sites for solar energy farms in Ismailia Governorate, Egypt using SRTM and multicriteria analysis", ***Cloud Publications, International Journal of Advanced Remote Sensing and GIS***, Vol. 2, (2013), 205-220. (technical.cloud journals.com/index.php/IJARSG/article/view/Tech-125).
12. Sanchez-Lozano, J.M., Henggeler Antunes, C., Garcia-Cascales, M.S. and Dias, L.C., "GIS-based photovoltaic solar farms site selection using ELECTRE-TRI: Evaluating the case for Torre Pacheco, Murcia, southeast of Spain", ***Renewable Energy***, Vol. 66, (2014), 478-494. (https://doi.org/10.1016/j.renene.2013.12.038).
13. Watson, J.J. and Hudson, M.D., "Regional scale wind farm and solar farm suitability assessment using GIS-assisted multi-criteria evaluation", ***Landscape and Urban Planning***, Vol. 138, (2015), 20-31. (https://doi.org/10.1016/j.landurbplan.2015.02.001).
14. Sanchez-Lozano, J.M., Garcia-Cascales, M.S. and Lamata, M.T., "Evaluation of suitable locations for the installation of solar thermoelectric power plants", ***Computers & Industrial Engineering***, Vol. 87, (2015), 343-355. (https://doi.org/10.1016/j.cie.2015.05.028).
15. Mentis, D., Welsch, M., Fuso Nerini, F., Broad, O., Howells, M., Bazilian, M. and Rogner., H., "A GIS-based approach for electrification planning—A case study on Nigeria", ***Energy for Sustainable Development***, Vol. 29, (2015), 142-150. (https://doi.org/10.1016/j.esd.2015.09.007).
16. Gherboudj, I. and Ghedira, H., "Assessment of solar energy potential over the United Arab Emirates using remote sensing and weather forecast data", ***Renewable and Sustainable Energy Reviews***, Vol. 55, (2016), 1210-1224. (https://doi.org/10.1016/j.rser.2015.03.099).
17. Sanchez-Lozano, J.M., Garcia-Cascales, M.S. and Lamata, M.T., "Comparative TOPSIS-ELECTRE TRI methods for optimal sites for photovoltaic solar farms: Case study in Spain", ***Journal of Cleaner Production***, Vol. 127, (2016), 387-398. (https://doi.org/10.1016/j.jclepro.2016.04.005).
18. Anwarzai, M.A. and Nagasaka, K., "Utility-scale implementable potential of wind and solar energies for Afghanistan using GIS multi-criteria decision analysis", ***Renewable and Sustainable Energy Reviews***, Vol. 71, (2017), 150-160. (https://doi.org/10.1016/j.rser.2016.12.048).
19. Sindhu, S., Nehra, V. and Luthra, S., "Investigation of feasibility study of solar farms deployment using hybrid AHP-TOPSIS analysis: Case study of India", ***Renewable and Sustainable Energy Reviews***, Vol. 73, (2017), 496-511. (https://doi.org/10.1016/j.rser.2017.01.135).
20. Liu, J., Xu, F. and Lin, S., "Site selection of photovoltaic power plants in a value chain based on grey cumulative prospect theory for sustainability: A case study in northwest China", ***Journal of Cleaner Production***, Vol. 148, (2017), 386-397. (https://doi.org/10.1016/j.jclepro.2017.02.012).
21. Aly, A., Jensen, S.S. and Pedersen, A.B., "Solar power potential of Tanzania: Identifying CSP and PV hot spots through a GIS multicriteria

decision making analysis", ***Renewable Energy***, Vol. 113, (2017), 159-175. (https://doi.org/10.1016/j.renene.2017.05.077).

22. Sabo, M.L., Mariun, N., Hizam, H., Mohd Radzi, M.A. and Zakaria, A., "Spatial matching of large-scale grid-connected photovoltaic power generation with utility demand in Peninsular Malaysia", ***Apllied Energy***, Vol. 191, (2017), 663-688. (https://doi.org/10.1016/j.apenergy.2017.01.087).
23. Garni, H.Z.A. and Awasthi, A., "Solar PV power plant site selection using a GIS-AHP based approach with application in Saudi Arabia", ***Applied Energy***, Vol. 206, (2017), 1225-1240. (https://doi.org/10.1016/j.apenergy.2017.10.024).
24. Tavana, M., Arteaga, F.J.S., Mohammadi, S. and Alimohammadi, M., "A fuzzy multi-criteria spatial deision support system for solar farm location planning", ***Energy Strategy Reviews***, Vol. 18, (2017), 93-105. (https://doi.org/10.1016/j.esr.2017.09.003).
25. Saracoglu, B.O., Ohunakin, O.S., Adelekan, D.S., Gill, J., Atiba, O.E., Okokpujie, I.P. and Atayero, A.A., "A framework for selecting the location of very large photovoltaic solar power plants on a global/supergrid", ***Energy Reports***, Vol. 4, (2018), 586-602. (https://doi.org/10.1016/j.egyr.2018.09.002).
26. Yushchenko, A., Bono, A., Chatenoux, B., Patel, M.K. and Ray, N., "GIS-based assessment of photovoltaic (PV) and concentrated solar power (CSP) generation potential in West Africa", ***Renewable and Sustainable Energy Reviews***, Vol. 81, (2018), 2088-2103. (https://doi.org/10.1016/j.rser.2017.06.021).
27. Dehghani, E., Jabalameli, M.S., Pishvaee, M.S. and Jabarzadeh, A., "Integrating information of the efficient and anti-efficient frontiers in DEA analysis to assess location of solar plants: A case study in Iran", ***Journal of Industrial and Systems Engineering***, Vol. 11, No. 1, (2018), 163-179. (In Farsi). (www.jise.ir/article_50883.html).
28. Doorga, J.R.S., Rughooputh, S.D.D.V. and Boojhawon, R., "Multi-criteria GIS-based modelling technique for identifying potential solar farm sites: A case study in Mauritius", ***Renewable Energy***, Vol. 133, (2019), 1201-1219. (https://doi.org/10.1016/j.renene.2018.08.105).
29. Majumdar, D. and Pasqualetti, M.J., "Analysis of land availability for utility-scale power plants and assessment of solar photovoltaic development in the state of Arizona, USA", ***Renewable Energy***, Vol. 134, (2019), 1213-1231. (https://doi.org/10.1016/j.renene.2018.08.064).
30. Altuzarra, A., Gargallo, P., Moreno-Jiménez, J.M. and Salvador, M., "Influence, relevance and discordance of criteria in AHP-Global Bayesian prioritization", ***International Journal of Information Technology & Decision Making***, Vol. 12, No. 04, (2013), 837-861. (https://www.worldscientific.com/doi/abs/10.1142/S0219622013500314).
31. Merrouni, A.A., Elalaoui, F.E., Mezrhab, A., Mezrhab, A. and Ghennioui, A., "Large scale PV sites selection by combining GIS and Analytical Hierarchy Process, Case study: Eastern Morocco", ***Renewable Energy***, Vol. 119, (2018), 863-873. (https://doi.org/10.1016/j.renene.2017.10.044).
32. Habibi. A., Sarfarazi, R. and Izadyar, S., "Delphi technique theoretical framework in qualitative research", ***The International Journal Of Engineering And Science (IJES)***, Vol. 3, No. 4, (2014), 8-13. (In Farsi). (https://doi.org/v3-i4/Version-4/B03404008013).
33. Beck, P. and Hofmann, E., "Multiple criteria decision making in supply chain management: Currently available methods and possibilities for future research", ***Die Unternehmung***, Nomos Verlagsgesellschaft, Vol. 66, No. 2, (2012), 182-217. (https://www.alexandria.unisg.ch/publications/211721).
34. Triantaphyllou, E., Multi-criteria decision making methods: A comparative study, Springer, Boston, (2000), 5-21. (https://doi.org/10.1007/978-1-4757-3157-6).
35. Chang, D.Y., "Applications of the extent analysis method on fuzzy AHP", ***European Journal of Operational Research***, Vol. 95, No. 3, (1996), 649-655. (https://doi.org/10.1016/0377-2217(95)00300-2).
36. Dawal, S.Z.M., Yusoff, N., Nguyen, H.T. and Aoyama, H., "Multi-attribute decision-making for CNC machine tool selection in FMC based on the integration of the improved consistent fuzzy AHP and TOPSIS", ***ASEAN Engineering Journal Part A***, Vol. 3, No. 2, (2013), 15-31. (http://www.aseanengineering.net/aej/issue/2013-v3-2/15-31%20MULTI-ATTRIBUTE%20DECISION-MAKING%20FOR%20CNC%20MACHINE%20TOOL%20SELECTION%20IN%20....pdf).
37. Hatami-Marbini, A., Tavana, M., Emrouznejad, A. and Saati, S., "Efficiency measurement in fuzzy additive data envelopment analysis", ***Industrial and Systems Engineering***, Vol. 10, (2017), 1-20. (In Farsi). (https://doi.org/10.1504/IJISE.2012.044041).
38. Skalna, I., Rębiasz, B., Gaweł, B., Basiura, B., Duda, J., Opiła, J. and Pełech-Pilichowski, T., Advances in fuzzy decision making, Springer, Vol. 333, (2015), 1-162. (https://www.springer.com/gp/book/9783319264929).
39. Dawson, L. and Schlyter, P., "Less is more: Strategic scale site suitability for concentrated solar thermal power in western Australia", ***Energy Policy***, Vol. 47, (2012), 91-101. (https://doi.org/10.1016/j.enpol.2012.04.025).
40. Borgogno Mondino, E., Fabrizio, E. and Chiabrando, R., "Site selection of large ground-mounted photovoltaic plants: A GIS decision support system and an application to Italy", ***International Journal of Green Energy***, Vol. 12, No. 5, (2015), 515-525. (https://doi.org/10.1080/15435075.2013.858047).
41. Lee, A., Kang, H.Y., Lin, C.Y. and Shen, K.C., "An integrated decision-making model for the location of a PV solar plant", ***Sustainability***, Vol. 7, No. 10, (2015), 13522-13541. (https://doi.org/10.3390/su71013522).
42. Wang, Q., M'Ikiugu, M. and Kinoshita, I., "A GIS-based approach in support of spatial planning for renewable energy: A case study of Fukushima, Japan", ***Sustainability***, Vol. 6, No. 4, (2014), 2087-2117. (https://doi.org/10.3390/su6042087).
43. Massimo, A., Dell'Isola, M., Frattolillo, A. and Ficco, G., "Development of a Geographical Information System (GIS) for the integration of solar energy in the energy planning of a wide area", ***Sustainability***, Vol. 6, No. 9, (2014), 5730-5744. (https://doi.org/10.3390/su6095730).
44. Yunna, W. and Geng, S., "Multi-criteria decision making on selection of solar–wind hybrid power station location: A case of China", ***Energy Conversion and Management***, Vol. 81, (2014), 527-533. (https://doi.org/10.1016/j.enconman.2014.02.056).
45. Olufemi, A., Omitaomu, K., Brandon, R., Blevins, C., Gary, T., Stanton, W., Hadley, J., Harrison, J., Budhendra, L. and Amy, N., "Adapting a GIS based multicriteria decision analysis approach for evaluating new power generating sites", ***Applied Energy***, Vol. 96, (2012), 292-301. (https://doi.org/10.1016/j.apenergy.2011.11.087).

Journal of Renewable Energy and Environment

Research Article

Journal Homepage: www.jree.ir

# The Assessment of Effect of Fatty Acid Profile on the Physical Properties and Emission Characteristics of New Feedstocks Used for Biodiesel

Farid Jafarihaghighi [a], Hassanali Bahrami [b], Mehdi Ardjmand [a*], Mehrdad Mirzajanzadeh [a]

[a] *Department of Chemical Engineering, South Tehran Branch, Islamic Azad University, Tehran, Tehran, Iran.*
[b] *Department of Mechatronics, Arak University, Arak, Markazi, Iran.*

*PAPER INFO*

*Paper history:*
Received 15 November 2020
Accepted in revised form 26 April 2021

*Keywords*:
Physical Properties,
Chemical Properties,
Three Different Biodiesel Generation,
Emissions

*ABSTRACT*

The present study uses three generations of biodiesels and studies their effects on physical properties and exhaust gases. They are comprised of *Palmaria palmate* oil (third generation), *Eucheuma spinosum* oil (third generation), *Eucheuma cottonii* oil (third generation), *Common wormwood* oil (second generation), *Marjoram* oil (second generation), *Peganum harmala* oil (second generation), *Zingiber officinale* oil (first generation), *Anethum graveolens* oil (first generation), and *Cacao bean* oil (first generation). Results show that first-generation oils gain a higher level of Calorific value around 41.16 MJ/kg than other generations. The longest carbon chain is observed by the first generation with higher unsaturated fatty acids than other generations (94.11 %). The first generation gains a higher level of density around 882 kg/m$^3$ than other generations. Also, the first generation gains a higher level of flash point around 193 ˚C than other generations. The third generation gains a high level of cetane number at about 69, compared to other generations. The first generation gains a minimum level of cloud and pour point around -3 ˚C and -2 ˚C compared to other generations. Moreover, the third generation gains the lowest level of viscosity about 2.51 CSt compared to the first generation. The third generation gains the lowest level of $NO_x$ around 371 ppm compared to other generations. Finally, the third generation gains the lowest level of soot, CO, and HC around 0.47 Vol. %, 0.018 Vol. %, and 4.82 ppm, compared to other generations.

https://doi.org/10.30501/jree.2021.257527.1161

## 1. INTRODUCTION

Fossil fuels face many problems today, the most important of which are price changes and their environmental problems. Furthermore, lack of sufficient resources and their proper distribution among countries have caused various crises. Therefore, the growing human need for alternative fuels is of utmost importance. Biofuels represent a good option with their benefits over fossil fuels. They are characterized by being highly biodegradable and renewable, being environmentally friendly, low toxicity, low combustion emission, high engine performance, advanced rural economic potential, combinable with diesel fuel at any ratio, and so on [1, 2].

The feedstock is a noteworthy cause for biodiesel production, as the production value should be cost effective. Biodiesels are now divided into four generations. The first generation is comprised of mint oil, colza oil, etc. They are considered as edible oils. The next generation encompasses jatropha oil, mahua oil, cottonseed oil, etc. They are considered as non-edible oils. The third generation is considered as microalgae oil, animal fat, and waste cooking oil. The last generation of biofuels is derived from genetically modified crops. This group is fixated on amalgamating feedstock biology, Carbon Capture Storage (CCS) processes, and producing high-quality biofuels and supreme performance efficiencies with zero carbon emission [3, 4].

The physical properties of biodiesels are displayed by the structural characteristics of fatty acids. Some of their physical characteristics are exhaust gas emissions, ignition quality, the heat of combustion, viscosity, density and lubricity, cold flow, and oxidative stability. The created biodiesel properties should meet the European standard specification (EN) 14214 or American Society for Testing and Materials (ASTM) D6751. Approaches that survey biodiesel properties include gas chromatography-mass spectroscopy (GC/MS), Fourier Transforms Infrared spectroscopy (FTIR), Nuclear Magnetic Resonance spectroscopy (NMR), and High-Performance Liquid Chromatography (HPLC) [5]. Numerous studies have shown that physical properties have an enormous effect on emission and combustion. Flashpoint, kinematic viscosity, boiling point, Cetane Number (CN), pour point, cloud point, heating value, and oxidative stability are the most significant physical properties affecting emission and combustion [6]. The fuel autoignition and CN are influenced by each other. The growth of CN triggers an effect on ignition quality [7]. Additionally, CN impacts the diesel combustion method by reducing the ignition delay. Thus, it lessens premixed combustion and also weakens the sudden spike at an

*Corresponding Author's Email: m_arjmand@azad.ac.ir (M. Ardjmand)
URL: http://www.jree.ir/article_129680.html

Please cite this article as: Jafarihaghighi, F., Bahrami, H.A., Ardjmand, M. and Mirzajanzadeh, M., "The assessment of effect of fatty acid profile on the physical properties and emission characteristics of new feedstocks used for biodiesel", ***Journal of Renewable Energy and Environment (JREE)***, Vol. 8, No. 3, (2021), 26-35. (https://doi.org/10.30501/jree.2021.257527.1161).

in-cylinder temperature, which is responsible for enhancing the predisposition of thermal NO [8]. Hence, improving the CN triggers lessening the NO concentration. Folayan et al. indicated that palm kernel and coconut oil had upper pour and cloud point, low-temperature filterability, and cold filter plugging point and examination point compared to linoleic and oleic oils, which caused poor cold flow conduct. This is because these properties are considerably enhanced with a greater degree of unsaturation, longer carbon chain, and higher degrees of branching. Saponification number dropped with molecular weight and chain length. The iodine value rises as the mark of unsaturation rises, but drops with chain length. They also indicated the effect of fatty acids on CN, heating value, and density [9]. Marlina et al. worked on fatty acids and their results showed that polar fatty acids were further reactive because of electric charge. Bent and long polar fatty acids were more reactive than the straight and short polar ones, as the former had durable higher and polarity electron mobility. The uppermost electron mobility caused molecules to be less tight; therefore, evaporation level increased. The presence of more than one double bond in polyunsaturated oil partly inhibited electron mobility. Quicker evaporation level caused ignition temperature to decrease, meanwhile heat energy was altered in latent heat for stage change over evaporation [10]. Jafarihaghighi et al. used several samples and showed that the physical properties affected emissions. They showed that the structure of fatty acids decreased or increased physical properties and had a direct effect on exhaust emissions [11].

In this paper, the main objective is to show the physical properties and exhaust gases of three different generations of biodiesel under the same conditions to demonstrate which generation will have better efficiency and better outcomes. All the oils used are new to give a new perspective and eliminate the exclusivity of certain groups. In this path, the length of chains, ratio of hydrogen to carbon, oxygen to carbon, saturated acids, and unsaturated acids of the three generations are examined and compared. One of the most important reasons for choosing different generations in this report is that they have the ability to grow in harsh conditions in the Middle East and Iran, and that an attempt is made to show which future generation is better for use.

## 2. MATERIALS AND METHODS

Nine different oils from three different generations were considered. They include *Palmaria palmata* oil (third generation), *Eucheuma spinosum* oil (third generation), *Eucheuma cottonii* oil (third generation), *Common wormwood* oil (second generation), *Marjoram* oil (second generation), *Peganum harmala* oil (second generation), *Zingiber officinale* oil (first generation), *Anethum graveolens* oil (first generation), and *Cacao bean* oil (first generation). The methanol (99 %) and KOH (99 %) were supplied by Aldrich Chemical Co. (USA).

The transesterification technique was applied to the samples. Biodiesel samples were created through the KOH-catalyzed transesterification reaction at a level of 1 to 3 (v/v) for methanol-to-oil. Therefore, they were completed in the presence of KOH as the acid catalyst for around 1 h at 55-60 ˚C. Between one to two hours was adequate to separate the solution for eliminating methanol-water at the top stage. Then, in the bottom stage, the value of the acid level was calculated. The yields of biodiesel produced for first, second, and third generations of biodiesel were around 85-90 %, 89-95 %, and 93-95 %, respectively. All biodiesels were composed by a combination of 20 % net biofuel with 80 % diesel [1].

The flashpoint was calculated according to ASTM standard D93. The level of viscosity and value of density were determined with Stabinger Viscometer, Anton Paar, SVM3000 model (Anton Paar Co., Austria). The viscosity was also assessed by ASTM-D445. The flashpoint was calculated with the Constantly Close Cup Flash Point (CCCFP) tester applying the Grabner FLPH Miniflash Tester (Grabner, Austria). The level of cloud point was assessed by the s/500 (Italian) model, compliant with the ASTM standard D2500. Sediment and water measurements were completed by Karl Fischer setup, metrohm, 794 Basic Titrino model. Biodiesel mixtures, which were created with transesterification, were specified by Gas Chromatography (GC, Claus 580 GC model, Perkin Elmer Co., USA). The level of CN was shown by the Octan-IM device.

In this research, a 3LD 510 model was used for a 12-horsepower single-cylinder diesel engine manufactured by the Italian Lombardy Company. Its specifications are shown in Table 1. The dynamometer Eddy Current WE400 model from Pars Andish Innovative Company (MPA) was employed to measure the torque, rotational speed, and power of the 3LD 510 Diesel Engine. Specifications of the MAHA-MGT5 analyzer used in the test are shown in Table 2. The test was carried out at 2000 rpm and full load.

**Table 1.** The engine parameters

| Specification | Explanations |
|---|---|
| Model | 3LD510 |
| Number of cylinders | 1 |
| Bore and stroke (mm) | 85 × 90 |
| Displacement ($cm^3$) | 510 |
| Aspiration | Naturally aspirated |
| Cycle | 4 stroke |
| Combustion system | Direct Injection |
| Rotation | Counter-clockwise (view from main PTO side) |
| Cooling system | Air |
| Fuel tank capacity (l) | 5.3 |
| Oil sump capacity (l) | 1.75 |
| Length (mm) | 466 |
| Width (mm) | 422 |
| Height (mm) | 568 |
| Dry weight (kg) | 60 |
| Cylinder course (mm) | 90 |
| Cylinder diameter (mm) | 85 |
| Cylinder volume ($cm^3$) | 510 |
| Maximum power hp (3000 rpm) | 12.2 |
| Maximum torque 1800rpm (Nm) | 33 |
| Compression ratio | 17.5:1 |

**Table 2.** Qualifications of the MAHA-MGT5 analyzer used in the test

| Specification | Explanations |
|---|---|
| Measurable gases | HC, CO, $CO_2$, $O_2$, NO (Option) |
| Measuring principle Infrared spectrometry | HC, CO, $CO_2$ |
| Measuring principle electrochemical detection | $O_2$, NO |
| Warm-up time | 480 s |
| Flow | 3.5 l/min |
| Working pressure | 0.75 bar–1.1 bar |
| Accuracy class | O (OIML) |
| On-board voltage | 12 V/42 V |
| Power supply | 1/N/PE 85 V/285 V 50 Hz |
| Dimensions total (L × W × H) | 240 mm × 560 mm × 300 mm |
| Weight | 10 kg |
| CO - Measurement range / Measured value resolution (max.) | 0-15 Vol. %/0.01 |
| $CO_2$ - Measurement range / Measured value resolution (max.) | 0-20 Vol. %/0.01 |
| HC - Measurement range / Measured value resolution (max.) | 0-9999 ppm/0.1 (Hexan) 0-20000 ppm/1 (Propan) |
| $O_2$ - Measurement range / Measured value resolution (max.) | 0-25 Vol. %/0.01 |
| Lambda (calculated) | 0.5–9.99/0.01 |
| NO (Option) - Measurement range / Measured value resolution (max.) | 0-5000 ppm/1 |

## 3. RESULTS AND DISCUSSION

### 3.1. Physical properties

#### 3.1.1. Structure of fatty acids

Fatty acids play an important role in the structure and emission of biodiesel. The carbon chain of different biodiesels ranged from C14 to C24. According to Table 3, the highest saturated acids for *Common wormwood* oil were Palmitic acids and also the highest unsaturated acids were Linoleic acids. The highest saturated acids for *Marjoram* oil were Palmitic acids and also the highest unsaturated acids were Oleic acids. The highest saturated acids for *Peganum harmala* oil were Palmitic acids and also the highest unsaturated acids were Oleic acids. The highest saturated acids for *Palmaria palmata* oil were Palmitic acids and also the highest unsaturated acids were Oleic acids. The highest saturated acids for *Eucheuma spinosum* oil were Palmitic acids and also the highest unsaturated acids were Linoleic acids. The highest saturated acids for *Eucheuma cottonii* algae oil were Palmitic acids and also the highest unsaturated acids were Oleic acids. The highest saturated acids for *Zingiber officinale* oil were Palmitic acids and also the highest unsaturated acids were Oleic acids. The highest saturated acids for *Anethum graveolens* oil were Palmitic acids and also the highest unsaturated acids were Oleic acids. The highest saturated acids for *Cacao bean* oil were Palmitic acids and also the highest unsaturated acids were Oleic acids.

Obviously, in Fig. 1, the longest carbon chain presented to *Anethum graveolens* biodiesel (C18-C24) was around 94.11 %. *Common wormwood* displayed a long carbon chain (C18-C22) around 93.35 %. Next, *Peganum harmala* displayed a long carbon chain (C18-C22) around 88.93 %. *Cacao bean* oil displayed a long carbon chain (C18-C20) around 88.47 %. Subsequently, *Marjoram* oil displayed a long carbon chain (C18-C22) around 86.73 %. *Zingiber officinale* oil displayed a long carbon chain (C18-C20) around 84.52 %. *Palmaria palmata* oil displayed a long carbon chain (C18-C22) around 80.19 %. *Eucheuma spinosum* oil displayed a long carbon chain (C18-C22) around 70.60 %. Finally, *Eucheuma cottonii* algae oil displayed a long carbon chain (C18-C20) around 58.40 %.

The presence of fatty acids in biodiesel can affect the rate of oxygen to carbon (O/C) and hydrogen to carbon (H/C). Vividly, the enhancement of fatty acids affects the amount of oxygen in the process. On the other hand, the amount of hydrogen can be altered by fatty acids. Therefore, the growth of saturated acids triggers the increase of hydrogen in the process. Hence, the maximum saturated acids, O/C, and H/C were gained by *Eucheuma cottonii*, *Eucheuma spinosum*, *Palmaria palmata*, *Zingiber officinale*, *Marjoram*, *Cacao bean*, *Peganum harmala, Common wormwood*, and *Anethum graveolens* biodiesels [2, 3].

**Table 3.** The result of physical and chemical properties of biodiesel sources

| Fatty acid | *Common wormwood* % Wt | *Marjoram* % Wt | *Peganum harmala* % Wt | *Palmaria palmata* % Wt | *Eucheuma spinosum* % Wt | *Eucheuma cottonii* % Wt | *Zingiber officinale* % Wt | *Anethum graveolens* % Wt | *Cacao bean* % Wt |
|---|---|---|---|---|---|---|---|---|---|
| Caprylic (C8:0) | - | - | - | - | - | - | - | - | - |
| Capric (C10:0) | - | - | - | - | - | - | - | - | - |
| Lauric (C12:0) | - | - | - | - | - | - | - | - | - |
| Myristic (C14:0) | - | - | - | - | - | - | - | - | - |
| Myristoleic (C14:1) | - | - | - | - | - | - | - | - | - |
| Pentadecanoic (C15:0) | - | - | - | - | - | - | - | - | 1.28 |

| | | | | | | | | | |
|---|---|---|---|---|---|---|---|---|---|
| Palmitic (C16:0) | 7.78 | 13.13 | 10.92 | 15.92 | 23.75 | 37.41 | 11.71 | 5.89 | 9.77 |
| Palmitoleic (C16:1) | - | - | 0.19 | 2.96 | 2.97 | - | - | - | 2.55 |
| Heptadecanoate (C17:0) | - | - | - | - | - | - | 2.40 | - | - |
| Stearic (C18:0) | 2.35 | 3.20 | 5.16 | 3.60 | 5.01 | 4.70 | 9.31 | 1.09 | 1.35 |
| Oleic (C18:1) | 30.30 | 16.32 | 56.40 | 60.48 | 23.05 | 29.09 | 50.09 | 45.60 | 47.03 |
| Linoleic (C18:2) | 59.14 | 24.11 | 14.50 | 10.60 | 35.16 | 21.34 | 22.80 | 22.16 | 35.83 |
| Linolenic (C18:3) | 0.41 | 41.17 | 9.00 | 2.80 | 6.07 | 2.25 | 0.31 | 7.38 | 1.30 |
| Arachidic (C20:0) | 0.49 | 0 | 1.89 | 1.77 | 3.72 | 1.02 | 2.01 | 2.51 | 0.96 |
| Gondoic (C20:1) | - | 0.56 | 1.10 | - | - | - | - | - | - |
| Behenic (C22:0) | 0.66 | 1.30 | 0.88 | - | - | - | - | 2.82 | |
| Erocic (C22:1) | - | 0.21 | - | 0.94 | - | - | - | - | - |
| Lignoceric (C24:0) | - | - | - | - | - | - | - | 4.02 | - |
| Nervonic (C24:1) | - | - | - | - | - | - | - | 8.53 | - |
| Total | 100 | 100 | 100 | 100 | 100 | 100 | 100 | 100 | 100 |

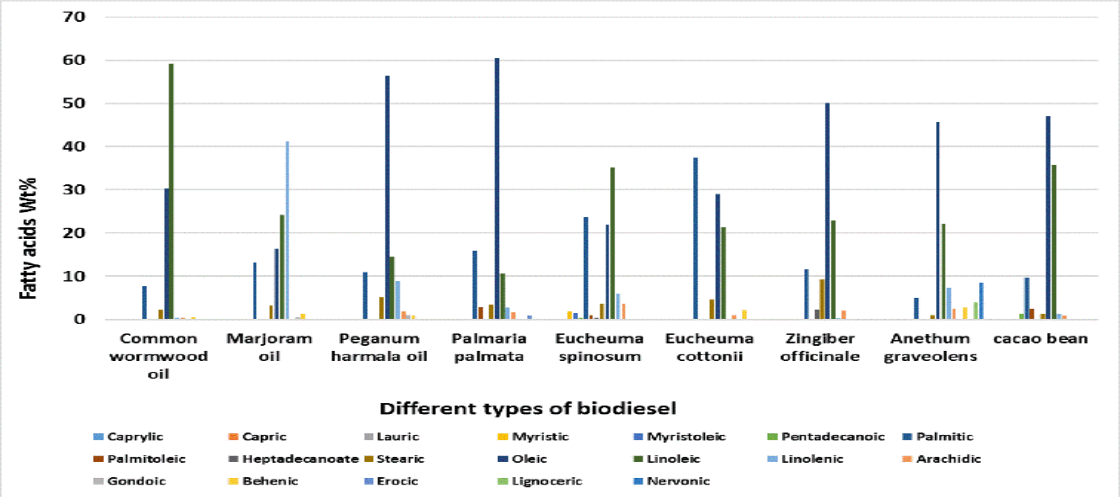


**Figure 1.** The highest amount of fatty acids in various biodiesel sources

### 3.1.2. Calorific value (CV)

The heat of combustion (CV) of fuels is a noteworthy measurable parameter, as it can represent the quantity of heat liberated with fuels in the engine that empowers the engines to prepare the work. Fig. 2 displays that greater CV is obtained by *Anethum graveolens* biodiesel around 43.21 MJ/kg. *Common wormwood* biodiesel acquired the second place and it was around 41.16 MJ/kg. The least level of CV was revealed by *Eucheuma cottonii* biodiesel close to 34.97 MJ/kg. The list was continued with *Peganum harmala*, *Cacao bean*, *Marjoram*, *Zingiber officinale*, *Palmaria palmata*, and *Eucheuma spinosum* biodiesel around approximately 37.58, 37.02, 36.12, 36, 35.19, and 35.07 MJ/kg, respectively. According to Fig. 2, the third generation of biodiesel gained the lowest amount of CV; however, the difference between them was low. The first generation of biodiesel showed better results than the second and third generations. Regarding Figure 1, the longest carbon chain is revealed by *Anethum graveolens* biodiesel; consequently, the supreme CV level was observed by it. However, the shortest carbon chain was demonstrated by *Eucheuma cottonii* biodiesel, which had the lowest CV among all biodiesels [4, 5]. The carbon chain had a direct effect on CV and triggered the growth of CV of biodiesels. In fact, the increase of carbon chain could enhance the amount of molecular mass, increasing CV. Ogbu et al. used *Cucurbita pepo*, *Afzelia africana*, and *Hura crepitans* oil and achieved the same results, indicating that CV and carbon chain were interconnected [6].

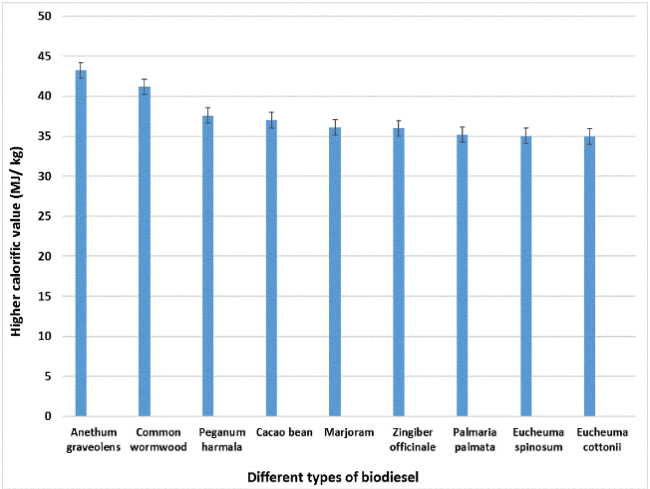


**Figure 2.** The upper calorific value in numerous biodiesel sources

### 3.1.3. Density

Density is considered as momentous fuel characteristic, as injection systems, pumps, and injectors must convey the quantity of fuel precisely adjusted to provide precise combustion. Therefore, one of the parameters that contributes to the advancement in biodiesel source density is their molecular weight. The level of density of fuel has an impact on the engine act properties. The superior density will escalate the diameter of fuel droplets. Thus, fuels with slighter density will enhance the efficiency of air-fuel combination formation and atomization. Consequently, *Anethum graveolens* biodiesel had the highest level of density around 882 kg/m$^3$ (Fig. 3). However, the least density was seen by *Eucheuma cottonii* biodiesel, which was roughly 850 kg/m$^3$. The list was continued with *Common wormwood*, *Peganum harmala*, *Cacao bean*, *Marjoram*, *Zingiber officinale*, *Palmaria palmata*, and *Eucheuma spinosum* biodiesel, with approximate levels of 880, 876, 871, 869, 863, 857, and 855 kg/m$^3$, respectively. As shown in Fig. 1, the longest carbon chain and double bond number affected density and enhanced this parameter. *Anethum graveolens* biodiesel had the longest and greatest number of double bonds (94.11 Wt %), which had the highest density level among all the biodiesel samples in contrast to *Eucheuma cottonii* biodiesel (58.40 Wt %). Therefore, the third generation of biodiesel had the lowest amount of density; however, the difference among them was low. Almost, the first generation of biodiesel showed better results than the second and third generations [2]. The fatty acids influenced the density; thus, the growth of the carbon chain and double bonds boosted the level of these characteristics. Mer et al. applied Karanja and Palm oil in their study, showing that carbon chain and double bonds could affect the density level, which complied with the results of this study [7].

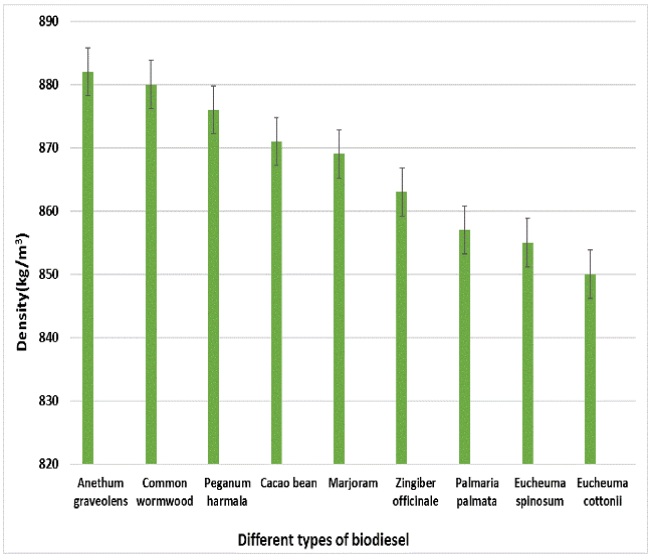


**Figure 3.** The density level in various biodiesel sources

### 3.1.4. Flash point

The flashpoint is considered as a temperature at which the fuel commences to burn while it comes to contact with fire. It is vitally important with regard to fuel handling, transportation, and storage. Biodiesels normally have a higher flash point than diesel fuels. There are some parameters such as the number of double bonds, residual alcohol content, and number of carbon atoms that could influence flashpoint. Similar results were found in the study of Mer et al. and Ogbu et al., indicating the impact of double bonds and carbon atoms [6, 7]. Among the oils used in this study, *Anethum graveolens* biodiesel had the highest level of flashpoint around 193 ˚C (Fig. 4), whereas the least flashpoint level was seen in *Eucheuma cottonii* biodiesel, which was roughly 174.6 ˚C. The list continued with *Common wormwood*, *Peganum harmala*, *Cacao bean*, *Marjoram*, *Zingiber officinale*, *Palmaria palmata*, and *Eucheuma spinosum* biodiesel with approximate flashpoint levels of 190.1, 188.7, 185.9, 181.5, 179.2, 177.7, and 175.6 ˚C, respectively. *Anethum graveolens* biodiesel had the longest double bonds and carbon chain among other samples, which was around 94.11 Wt%. Among all the samples, *Eucheuma cottonii* biodiesel had the shortest carbon chain length and double bonds, being 58.40 Wt % (Fig. 1). Therefore, the third generation of biodiesel had the lowest amount of flashpoint. The first generation of biodiesel showed better results than the second and third generations.

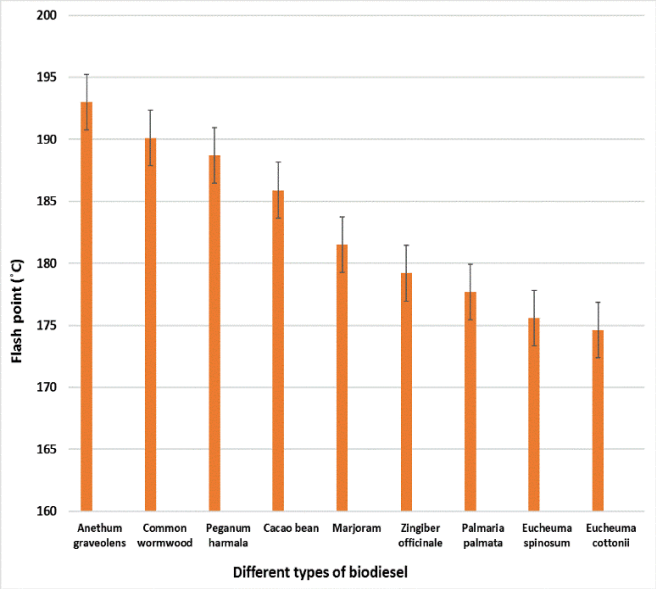


**Figure 4.** The flash point quantity in different biodiesel sources

### 3.1.5. Cetane number (CN)

CN is a reverse function of a fuel's ignition delay and it is the period between the ignition start and the first identifiable pressure rise over fuel combustion. In a specific diesel engine, upper CN had a shorter ignition delay period than the lower CN. In this regard, *Eucheuma cottonii* biodiesel had the highest level of CN around 69 (Fig. 5), whereas the least of the CN was observed in *Anethum graveolens* biodiesel that was roughly 55. The list continued with *Eucheuma spinosum*, *Palmaria palmata*, *Zingiber officinale*, *Marjoram*, *Cacao bean*, *Peganum harmala*, and *Common wormwood* biodiesel with approximate CN levels of 67, 67, 65, 64, 62, 60, and 59, respectively. The growth of carbon chain length and unsaturated acids affected CN development [8]. However, our results showed that the effect of unsaturated acids was greater than the chain length, which led to greater CN changes. The results of this study are in line with the study of Ogbu et al. [3, 6]. Moreover, the highest amount of saturated acids was obtained by *Anethum graveolens* and the minimum was achieved by *Eucheuma cottonii* biodiesel. Consequently, the third generation of biodiesel gained the highest amount of CN. Almost, the first generation of biodiesel showed less significant results than the second and third generations.

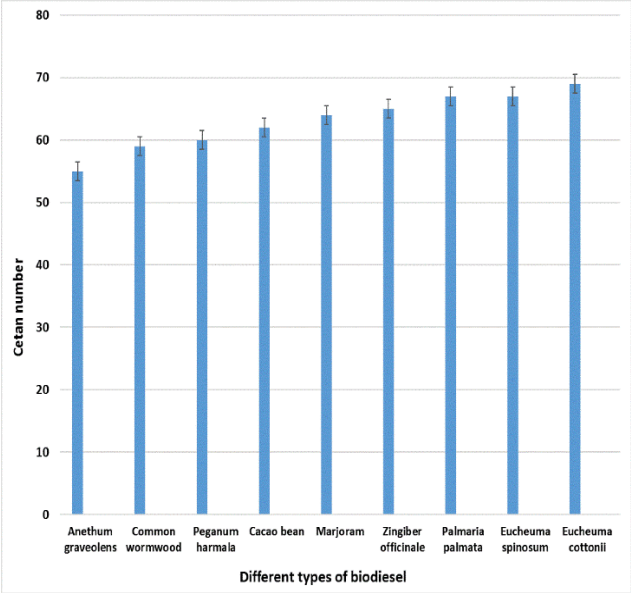


**Figure. 5.** The CN value in different biodiesel sources

### 3.1.6. Cloud and pour point

Pour point is identified as the lowest temperature that fuels can flow. Also, cloud point is renowned for the bottommost temperature where the cloud of wax crystals is formed while cooled. Both parameters in biodiesel are at a higher level than diesel fuels because of a higher level of saturated fatty acids, making it difficult in cold climate circumstances. Biodiesels with a notable level of saturated fatty compounds had a higher pour point and cloud point. In some studies, it has been reported that the chain length increase affects these points, being consistent with the current results because increasing the chain length increases the amount of unsaturated acids, thus changing these points [9, 10]. In this regard, *Anethum graveolens* biodiesel had the lowest level of cloud point around -3 ˚C (Fig. 6), whereas the highest cloud point was exposed by *Eucheuma cottonii* biodiesel that was roughly 6 ˚C. The list continued with *Common wormwood*, *Peganum harmala*, *Cacao bean*, *Marjoram*, *Zingiber officinale*, *Palmaria palmata*, and *Eucheuma spinosum* biodiesel with approximate cloud points of -2, -1, 1, 2, 3, 3, and 4 ˚C, respectively. *Anethum graveolens* biodiesel had the lowest level of pour point around -2 ˚C (Fig. 6), whereas the highest pour point was exposed by *Eucheuma cottonii* biodiesel that was roughly 8 ˚C. The list continued with *Common wormwood*, *Peganum harmala*, *Cacao bean*, *Marjoram*, *Zingiber officinale*, *Palmaria palmata*, and *Eucheuma spinosum* biodiesel with approximate pour points of 1, 1, 3, 5, 5, 6, and 6 ˚C, respectively. *Eucheuma cottonii* biodiesel had the highest level of saturated acids (more than 46 %), thus improving both parameters. Therefore, the third generation of biodiesel gained the highest level of pour and cloud points. The first generation of biodiesel showed better results than the second and third generations.

### 3.1.7. Viscosity

The enhancement of the level of viscosity caused several issues in the engine. Some of them are poor atomization, excess penetration, and poor mixing with air. The level of viscosity can be lessened via pre-heating the oil through a transesterification method. In this regard, *Anethum graveolens* biodiesel had the highest level of viscosity around 3.11 CSt (Fig. 7). However, the lowest viscosity level was observed by *Eucheuma cottonii* biodiesel that was roughly 2.51 CSt. The list continued with *Common wormwood*, *Peganum harmala*, *Cacao bean*, *Marjoram*, *Zingiber officinale*, *Palmaria palmata*, and *Eucheuma spinosum* biodiesel with approximate viscosity levels of 3.13, 3.04, 3, 2.94, 2.88, 2.73, and 2.69 CSt, respectively. Furthermore, the viscosity advanced with the ester chain and *Anethum graveolens* biodiesel had the longest carbon chain among all the samples in contrast to *Eucheuma cottonii* biodiesel [11, 12]. Numerous reports indicated that chain length had the highest effect on viscosity [10, 13]. However, in a recent study, it was shown that the amount of saturated and unsaturated acids could also have a direct effect on viscosity, which contradicted the results of previous reports that point to the low effect of this factor [6]. Therefore, the third generation of biodiesel had the lowest amount of viscosity. Almost, the first generation of biodiesel showed better results than the second and third generations.

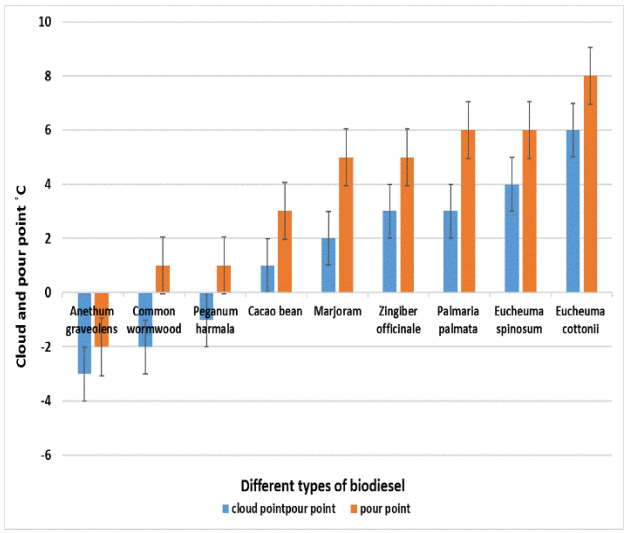


**Figure 6.** The cloud and pour rate in different biodiesel sources

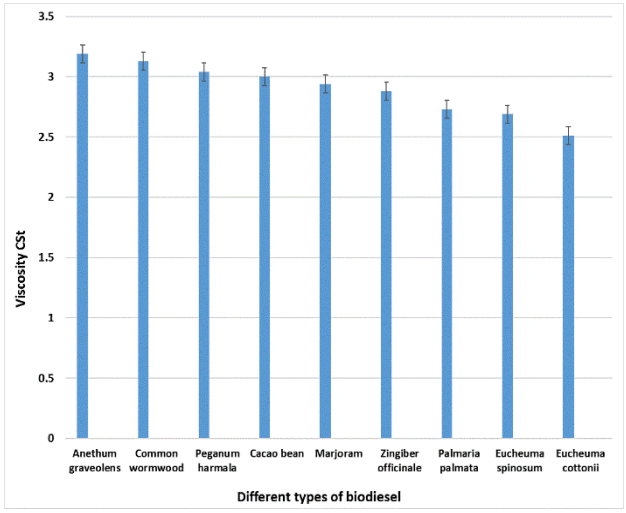


**Figure 7.** The viscosity level in different biodiesel sources

## 3.2. EMISSIONS

### 3.2.1. $NO_x$ emission

The ignition quality is normally connected to CN and the great CN level demonstrates short ignition delay. So, it implies

minimum fuel energy in the premixed phase that triggers lower $NO_x$ emissions through the premixed phase. Therefore, in Table 4, the *Anethum graveolens* showed maximum $NO_x$ emission at around 470 ppm, with the bottommost CN among all the samples. The bottommost $NO_x$ emission was related to *Eucheuma cottonii* biodiesel that had the highest level of CN among the samples. The list continued with *Common wormwood*, *Peganum harmala*, *Cacao bean*, *Marjoram*, *Zingiber officinale*, *Palmaria palmata*, and *Eucheuma spinosum* biodiesel, respectively. The results showed that lessening CN level affected the progress of $NO_x$ [14-16]. Furthermore, $NO_x$ construction is subject to combustion duration, exclusive temperature, and volumetric efficiency arising from great activation energy connected to the reactions involved. Also, the influence of carbon chain and unsaturated acids on $NO_x$ emissions is shown [17, 18]. Therefore, according to Fig. 8, the maximum level of unsaturated acids and the minimum level of CN were observed by *Anethum graveolens* biodiesel in contrast to *Eucheuma cottonii* biodiesel; therefore, the highest amount of $NO_x$ was emitted by this biodiesel due to the enhanced ignition delay and amount of premixed combustion [3]. Increased O/C level improved $NO_x$ emission in biodiesels. The burning reaction stoichiometry and the thermal $NO_x$ formation mechanisms exhibited that enlarged oxygen rate improved $NO_x$ emissions. With reference to the O/C level and $NO_x$ emissions, the escalation of the O/C ratio indicated shorter chains and further oxygen in the procedure that assisted generating more $NO_x$ output. Consequently, the *Eucheuma cottonii* biodiesel with the greatest quantity of unsaturated acids had the bottommost O/C ratio. Moreover, the lowest oxygen content decreased $NO_x$ emissions [19]. Therefore, the third generation of biodiesel caused the lowest amount of $NO_x$ emission. The first generation of biodiesel showed almost higher results than the second and third generations.

**Table 4.** The amount of $NO_x$ in different sources

| Biodiesels | Exhaust emission |
|---|---|
| | $NO_x$ ppm |
| *Anethum graveolens* | 470 |
| *Common wormwood* | 467 |
| *Peganum harmala* | 443 |
| *Cacao bean* | 438 |
| *Marjoram* | 415 |
| *Zingiber officinale* | 396 |
| *Palmaria palmata* | 382 |
| *Eucheuma spinosum* | 377 |
| *Eucheuma cottonii* | 371 |

### 3.2.2. Soot emission

Table 5 shows soot emissions of several biodiesel sources. The *Anethum graveolens* showed maximum soot emission around 0.83 Vol. %. The bottommost soot emission is related to *Eucheuma cottonii* biodiesel. The list continued with *Common wormwood*, *Peganum harmala*, *Cacao bean*, *Marjoram*, *Zingiber officinale*, *Palmaria palmata*, and *Eucheuma spinosum* biodiesel, respectively.

Some parameters, such as the rise of the carbon chain, affect soot emission. Therefore, the longest chain was seen in *Anethum graveolens* biodiesel around 94.11 %. In fact, the upsurge of *Anethum graveolens* carbon chain improved the soot level that touched 0.83 Vol. %. The *Common wormwood* biodiesel was in the second place with a carbon chain of about 93.35 % and soot level of virtually 0.78 Vol. %. *Eucheuma cottonii* biodiesel had the shortest carbon chain that was only 58.40 % in the array of C18 – C24. Consequently, this caused a decline in soot emission levels. Results do not comply with those of the former study which indicated that the upsurge of carbon chain did not increase the soot levels [24, 20]. This occurred due to the oxygen content in biodiesels, which was reduced with the upsurge of the carbon chain. Higher oxygen content reduced soot level. The results demonstrated that the highest oxygen content was seen in *Eucheuma cottonii* biodiesel. The level of O/C belonged to *Eucheuma cottonii* biodiesel. *Anethum graveolens* biodiesel had the bottommost O/C level, which had improved soot emissions [3, 21].

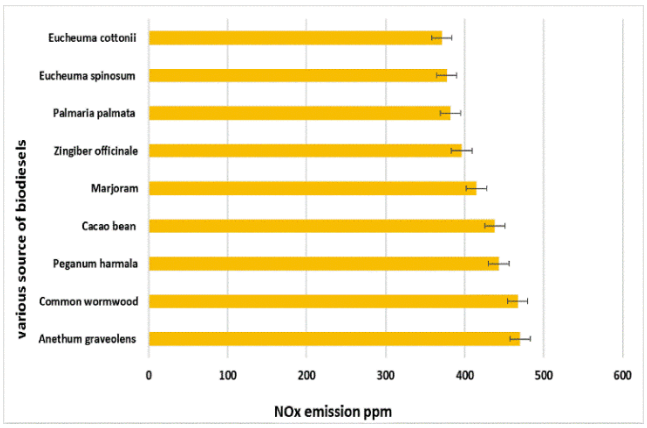


**Figure 8.** The level of $NO_x$ emissions in different biodiesel sources

The greatest quantity of unsaturated acids was seen in *Anethum graveolens* biodiesel (94.11 %) and the minimum was observed in *Eucheuma cottonii* biodiesel. In the experiments conducted in this study, a direct link was observed between the improvement of unsaturated acid number and the soot level. As the number of unsaturated acids improved, the rate of soot level enhanced. The lowest quantity of unsaturated acids was linked to *Eucheuma cottonii* biodiesel (58.40 %), which caused the bottommost soot level. Increasing the number of unsaturated acids in the models boosted the number of the binary bonds, elevating the quantity of soot yield [22, 23]. The H/C ratio exhibited the level of saturated acids. The improvement of this level had an indirect effect on soot outputs since soot emission declines while the fuel burns well. Therefore, the third generation of biodiesel had the lowest amount of soot emission. The first generation of biodiesel showed almost better results than the second and third generations.

**Table 5.** The amount of soot in different sources

| Biodiesels | Exhaust emission |
|---|---|
| | Soot Vol. % |
| *Anethum graveolens* | 0.83 |
| *Common wormwood* | 0.78 |
| *Peganum harmala* | 0.74 |
| *Cacao bean* | 0.69 |
| *Marjoram* | 0.66 |
| *Zingiber officinale* | 0.63 |
| *Palmaria palmata* | 0.57 |
| *Eucheuma spinosum* | 0.52 |
| *Eucheuma cottonii* | 0.47 |

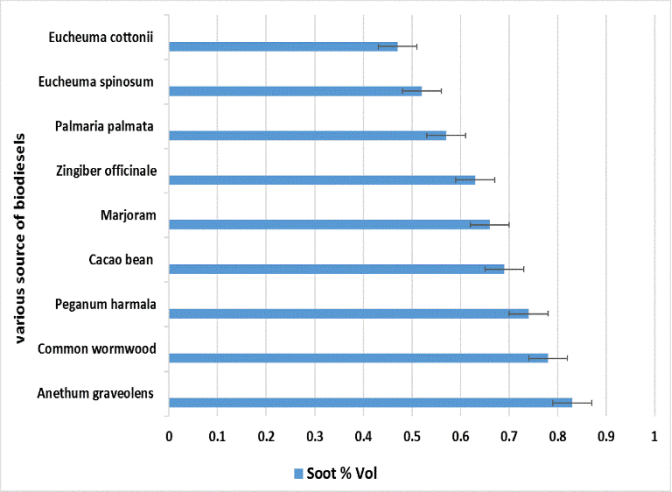


**Figure 9.** Soot emission levels in different biodiesel sources

### 3.2.2. CO emissions

The quantity of CO emissions of various biodiesel sources is shown in Fig. 10. The *Anethum graveolens* showed the highest CO emission around 0.038 Vol. %. The lowest HC emission was linked to *Eucheuma cottonii* biodiesel. The list continued with *Common wormwood*, *Peganum harmala*, *Cacao bean*, *Marjoram*, *Zingiber officinale*, *Palmaria palmata*, and *Eucheuma spinosum* biodiesel, respectively.

The lessening of CO emissions perhaps occurred due to the oxygen, leading to easier burning at upper temperatures in cylinders. This is demonstrated by the greater oxygen content in the shorter carbon chain that resulted in cleaner and further complete combustion. Besides, there were methyl esters in longer chains that had upper melting and boiling points, which were less probable to be entirely vaporized and burnt, thus promoting CO level. According to Table 6, the longest chain as well as the lowest O/C among all samples were seen in *Anethum graveolens* biodiesel (94.11 %), contributing to an opposite link between O/C and CO [24, 25]. Therefore, the third generation of biodiesel had the lowest amount of CO emission. The first generation of biodiesel showed almost better results than the second and third generations.

**Table 6.** CO emission for biodiesel sources

| Biodiesels | Exhaust emission |
|---|---|
| | CO emissions (% Vol) |
| *Anethum graveolens* | 0.038 |
| *Common wormwood* | 0.036 |
| *Peganum harmala* | 0.035 |
| *Cacao bean* | 0.032 |
| *Marjoram* | 0.028 |
| *Zingiber officinale* | 0.025 |
| *Palmaria palmate* | 0.024 |
| *Eucheuma spinosum* | 0.022 |
| *Eucheuma cottonii* | 0.018 |

### 3.2.3. HC emissions

The quantity of HC emissions of samples is shown in Fig. 11. The *Anethum graveolens* had the highest HC emission around 6.23 ppm. The lowest HC emission was seen in *Eucheuma cottonii* biodiesel. The list continued with *Common wormwood*, *Peganum harmala*, *Cacao bean*, *Marjoram*, *Zingiber officinale*, Palmaria palmata, and *Eucheuma spinosum* biodiesel, respectively. According to Table 3, carbon-chain improved HC level due to the extended chain length and greater boiling point. This improvement is the reason for the lessening of O/C rate and an upsurge of HC amount due to inferior oxygen content [3, 26]. Therefore, the third generation of biodiesel had the lowest amount of HC emission. The first generation of biodiesel showed almost better results than second and third generations.

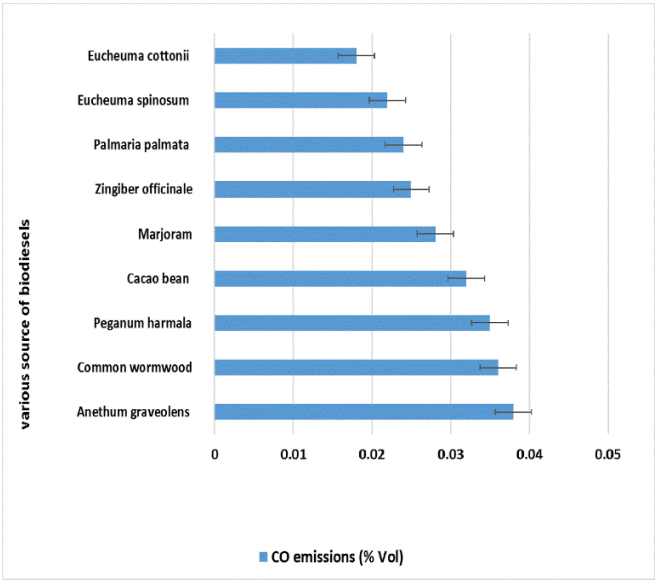


**Figure 10.** CO emission levels in different biodiesel sources

**Table 7.** HC emission for biodiesel sources

| Biodiesels | Exhaust emission |
|---|---|
| | HC emissions (ppm) |
| *Anethum graveolens* | 6.23 |
| *Common wormwood* | 6.10 |
| *Peganum harmala* | 5.85 |
| *Cacao bean* | 5.46 |
| *Marjoram* | 5.33 |
| *Zingiber officinale* | 5.07 |
| *Palmaria palmata* | 4.97 |
| *Eucheuma spinosum* | 4.86 |
| *Eucheuma cottonii* | 4.82 |

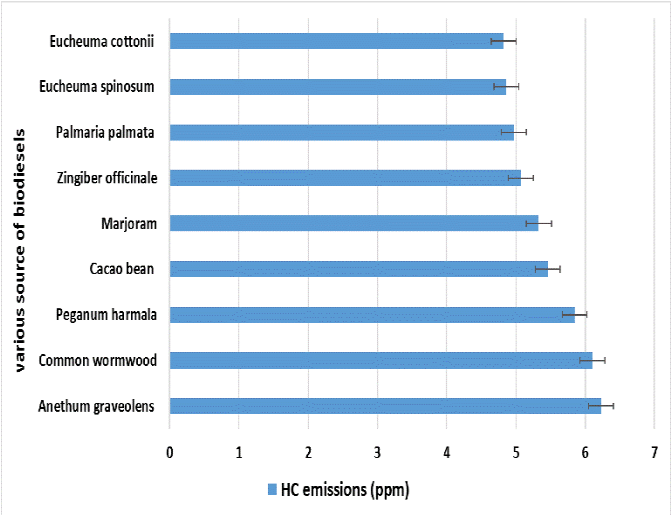


**Figure 11.** The HC emission levels in different biodiesel sources

## 4. CONCLUSIONS

In this study, we studied nine different types of biodiesels. These biodiesel types are of different generations, making it possible to show a complete view of the differences between the first and third generations. The main research objective was to investigate fatty acids, their physical properties as well as exhaust gases to compare the three generations. The results are given below:

- Nine different oils from three generations of biodiesels were examined. All species are capable of growing in most parts of the world and are able to grow in harsh climates.
- The longest carbon chains belonged to the first and second generations of biodiesel, while the third generation had more saturated acids and shorter carbon chains than the other generations.
- The third generation of biodiesel had the lowest quantity of CV. The first generation of biodiesel had better results than the second and third generations. Besides, the carbon chain could affect the CV level.
- The third generation of biodiesel had the lowest amount of density; almost the first generation of biodiesel showed better results than the second and third generations. Also, the carbon chain and double bonds could affect the level of density.
- The third generation of biodiesel had the lowest amount of flashpoint; almost, the first generation of biodiesel showed better results than the second and third generations. In addition, the carbon chain and double bonds could affect the level of flashpoint.
- The third generation of biodiesel had the highest amount of CN. The first generation of biodiesel showed lower results than the second and third generations. In addition, the carbon chain and saturated acids could affect the level of CN.
- The third generation of biodiesel had the highest level of pour and cloud points. The first generation of biodiesel showed better results compared to the second and third generations. In addition, the saturated acids could affect the level of pour and cloud points.
- The third generation of biodiesel had the lowest amount of viscosity. The first generation of biodiesel showed better results than the second and third generation. In addition, the carbon chain could affect the level of viscosity.
- The third generation of biodiesel had the lowest amount of $NO_x$ emission. The first generation of biodiesel showed better results than the second and third generations. Also, some factors such as O/C ratio, carbon-chain, and CN can manipulate the level of $NO_x$ emission.
- The third generation of biodiesel had the lowest amount of soot emission. The first generation of biodiesel showed better results than the second and third generations. Besides, some factors, such as O/C ratio, carbon-chain, H/C ratio, and saturated and unsaturated acids could change the level of $NO_x$ emission.
- The third generation of biodiesel had the lowest amount of CO emission. The first generation of biodiesel showed higher results than the second and third generations. There are some parameters that could alter the level of CO, such as O/C ratio, carbon-chain, and oxygen content.
- The third generation of biodiesel had the lowest amount of HC emission. The first generation of biodiesel showed better results than the second and third generations. There are some parameters that could alter the level of HC such as O/C ratio, carbon-chain, and oxygen content.

## 5. ACKNOWLEDGEMENT

This research did not receive any specific grant from funding agencies in the public, commercial, or not-for-profit sectors.

## NOMENCLATURE

| | |
|---|---|
| $NO_x$ | Nitrogen oxides |
| KOH | Potassium hydroxide |
| ASTM | American Society for Testing and Materials |
| EN | European standard |
| CN | Cetane number |
| O/C | Oxygen to carbon |
| H/C | Hydrogen to carbon |
| HC | Unburned hydrocarbons |
| CO | Carbon monoxide |

## REFERENCES

1. Ardjmand, M., Jafarihaghighi, F. and Mirzajanzadeh, M., "Combustion and emission analysis of *Cyclamen Persicum* and *Fritillariapersica* biodiesel biotechnology", ***Unite Prime Publication***, Vol. 1, No. 1, (2020), 1-10. (https://www.untdprimepub.com/ebooks-articles/bio-technology.php).
2. Jafarihaghighi, F., Ardjmand, M., Salar Hassani, M., Mirzajanzadeh, M. and Bahrami, H., "Effect of fatty acid profiles and molecular structures of nine new source of biodiesel on combustion and emission", ***ACS Omega***, Vol. 5, No. 26, (2020), 16053-16063. (https://pubs.acs.org/doi/10.1021/acsomega.0c01526).
3. Pinzi, S., Rounce, P., Herreros, J., Tsolakis, A. and Dorado, M., "The effect of biodiesel fatty acid composition on combustion and diesel engine exhaust emissions", ***Fuel***, Vol. 104, (2013), 170-182. (https://doi.org/10.1016/j.fuel.2012.08.056).
4. Knothe, G., "Biodiesel and renewable diesel: A comparison", ***Progress in Energy and Combustion Science***, Vol 36, No. 3, (2010), 364-373. (https://doi.org/10.1016/j.pecs.2009.11.004).
5. Ardjmand, M., Jafarihaghighi, F., Salar Hassani, M., Bazel, N. and Bahrami, H., Advances in biotechnology, ***openaccessebook.com***, Vol. 5, No. 3, (2020), 1-41. (https://openaccessebooks.com/advances-in-biotechnology-volume-5.html).
6. Ogbu, I. and Ajiwe, V., "Fuel properties and their correlations with fatty acids structures of methyl-and butyl-esters of *Afzelia africana*, *Cucurbita pepo* and *Hura crepitans* seed oils", ***Waste and Biomass Valorization***, Vol. 7, (2016), 373-81. (https://doi.org/10.1007/s12649-015-9446-4).
7. Mer, N.G., Rathod, N.P. and Sorthiya, N.S., "To evaluate the performance and emission characteristics of hybrid (dual) biodiesel diesel blend on single cylinder diesel engine", ***International Journal of Engineering Development and Research***, (2016), 852-859. (https://www.semanticscholar.org/paper/To-evaluate-the-performance-and-emission-of-Hybrid-Mer-Rathod/baf4e610e66f6cd807fa713071aca62be661d1a7).
8. Scragg, A.H., Biofuels: production, application and development, CABI Publishing, (2009). (https://books.google.com/books?hl=en&lr=&id=e2OLEkGWg3EC&oi=fnd&pg=PR5&dq=Biofuels:+production,+application+and+development&ots=z2gY579bLL&sig=WOcpwytP7YzWxmaN2IUVsK7dl14#v=onepage&q=Biofuels%3A%20production%2C%20application%20and%20development&f=false).
9. Wu, M., Wu, G., Han, L. and Wang. L., "Low-temperature fluidity of bio-diesel fuel prepared from edible vegetable oil", ***Pet Process Petrochem***, (2005), 57-60. (https://www.researchgate.net/publication/279567550_Low-temperature_fluidity_of_bio-diesel_fuel_prepared_from_edible_vegetable_oil).

10. Jesús Ramos, M., María Fernández, C., Casas, A., Rodríguez, L. and Pérez, A., "Influence of fatty acid composition of raw materials on biodiesel properties", ***Bioresource Technology***, Vol. 100, No. 1, (2009), 261-268. (https://doi.org/10.1016/j.biortech.2008.06.039).
11. Jorge Pratas, M., Freitas, S., Oliveira, M.B., Monteiro, S.C., Lima, A.S. and Coutinho, J.A.P., "Densities and viscosities of fatty acid methyl and ethyl esters", ***Journal of Chemical & Engineering Data***, Vol. 55, No. 9, (2010), 3983-3990. (https://doi.org/10.1021/je100042c).
12. Knothe, G. and Steidley, K.R., "Kinematic viscosity of biodiesel fuel components and related compounds. Influence of compound structure and comparison to petrodiesel fuel components", ***Fuel***, Vol. 84, No. 9, (2005), 1059-1065. (https://doi.org/10.1016/j.fuel.2005.01.016).
13. Knothe, G., "Dependence of biodiesel fuel properties on the structure of fatty acid alkyl esters", ***Fuel Processing Technology***, Vol. 86, No. 10, (2005), 1059-1070. (https://doi.org/10.1016/j.fuproc.2004.11.002).
14. Kidoguchi, Y., Yang, C., Kato, R. and Miwa. K., "Effects of fuel cetane number and aromatics on combustion process and emissions of a direct-injection diesel engine", ***JSAE Review***, Vol. 21, No. 4, (2000), 469-475. (https://doi.org/10.1016/S0389-4304(00)00075-8).
15. Schönborn, A., Ladommatos, N., Williams, J., Allan, R. and Rogerson, J., "The influence of molecular structure of fatty acid monoalkyl esters on diesel combustion", ***Combustion and Flame***, Vol. 156, No. 7, (2009), 1396-1412. (https://doi.org/10.1016/j.combustflame.2009.03.011).
16. Mueller, C.J., Boehman, A.L. and Martin, G.C., "An experimental investigation of the origin of increased $NO_x$ emissions when fueling a heavy-duty compression-ignition engine with soy biodiesel", ***SAE International Journal of Fuels and Lubricants***, Vol. 2, No. 1, (2009), 789-816. (https://www.jstor.org/stable/26273427).
17. Devarajan, Y., Mahalingam, A., Munuswamy, D. and Arunkumar, T., "Combustion, performance, and emission study of a research diesel engine fueled with palm oil biodiesel and its additive", ***Energy & Fuels***, Vol. 32, No. 8, (2018), 8447-8452. (https://doi.org/10.1021/acs.energyfuels.8b01125).
18. Buyukkaya, E., "Effects of biodiesel on a DI diesel engine performance, emission and combustion characteristics", ***Fuel***, Vol. 89, No. 10, (2010), 3099-3105. (https://doi.org/10.1016/j.fuel.2010.05.034).
19. Schmidt, K. and Van Gerpen, J., "The effect of biodiesel fuel composition on diesel combustion and emissions", ***SAE International***, (1996). (https://doi.org/10.4271/961086).
20. Jafarihaghighi, F., Ardjmand, M., Bahrami, H., Mirzajanzadeh, M. and Salar Hassani, M., "The effect of three new biodiesel feedstocks (second-generation) on the performance and emissions of diesel engines", ***Energy Sources, Part A: Recovery, Utilization, and Environmental Effects***, (2020), 1-13. (https://doi.org/10.1080/15567036.2020.1806412).
21. Zhu, L., Cheung, C. and Huang, Z., "Impact of chemical structure of individual fatty acid esters on combustion and emission characteristics of diesel engine", ***Energy***, Vol. 107, (2016), 305-320. (https://doi.org/10.1016/j.energy.2016.04.030).
22. Kathrotia, T. and Riedel, U., "Predicting the soot emission tendency of real fuels–A relative assessment based on an empirical formula", ***Fuel***, Vol. 261, (2020), 116482. (https://doi.org/10.1016/j.fuel.2019.116482).
23. Wang, Z., Li, L., Wang, J. and Reitz, R., "Effect of biodiesel saturation on soot formation in diesel engines", ***Fuel***, Vol. 175, (2016), 240-248. (https://doi.org/10.1016/j.fuel.2016.02.048).
24. Mer, N.G., Rathod, N.P. and Sorthiya, N.S., "To evaluate the performance and emission characteristics of hybrid (dual) biodiesel diesel blend on single cylinder diesel engine", ***International Journal of Engineering Development and Research (IJEDR)***, (2016), 852-859. (https://www.semanticscholar.org/paper/To-evaluate-the-performance-and-emission-of-Hybrid-Mer-Rathod/baf4e610e66f6cd807fa713071aca62be661d1a7).
25. Hellier, P., Talibi, M., Eveleigh, A. and Ladommatos, N., "An overview of the effects of fuel molecular structure on the combustion and emissions characteristics of compression ignition engines", ***Proceedings of the Institution of Mechanical Engineers, Part D: Journal of Automobile Engineering***, (2018), 90-105. (https://doi.org/10.1177/0954407016687453).
26. Lapuerta, M., Armas, O. and Rodriguez-Fernandez, J., "Effect of biodiesel fuels on diesel engine emissions", ***Progress in Energy and Combustion Science***, Vol. 28, No. 2, (2008), 198-223. (https://doi.org/10.1016/j.ejpe.2019.03.001).

Journal of Renewable Energy and Environment

Research Article

Journal Homepage: www.jree.ir

# Determining Optimal Locations for Biogas Plants: Case Study of Tehran Province for Utilization of Bovine and Aviculture Wastes

Maryam Nosratinia [a], Ali Asghar Tofigh [b], Mehrdad Adl [a*]

[a] *Department of Energy, Materials and Energy Research Center (MERC), P. O. Box: 3177983634, MeshkinDasht, Alborz, Iran.*
[b] *Department of Industrial Engineering, Amirkabir University of Technology, P. O. Box: 159163-4311, Tehran, Tehran, Iran.*

*PAPER INFO*

*Paper history:*
Received 13 October 2020
Accepted in revised form 17 May 2021

*Keywords*:
Location,
Biogas,
Geographical Information System (GIS),
Fuzzy Logic

*ABSTRACT*

Given the world's growing population and energy demand, modern methods are developed to contribute to generating alternative energies. They aim to maintain the renewability of the supplied energy and decrease environmental contaminations. Biogas is a renewable energy carrier that has recently been under consideration in Iran. One objective of such plans is to find proper locations for installing and running the existing potentials and infrastructures. In this paper, Tehran, Iran is selected as the study area which is ranked the 1st in population density and proper infrastructures available here are accessible. According to the widespread poultry and cow-breading farms in this province, bovine and aviculture excreta are considered as raw materials in producing biogas. An inference network was established in this research for evaluating the process taking into account the infrastructural parameters, geomorphological constraints, resource availability factors, and limiting parameters such as protected/prohibited areas.In this paper, the fuzzy method was used to standardize the data and the fuzzy-analytical hierarchy process method was employed to weight the locating criteria in the geographical information system. The evaluation outcomes suggested certain zones in southern parts of the province in which the industrial livestock farms become frequently widespread and the suburb areas of smaller cities on the eastern part of the province are the most proper areas for this purpose.

https://doi.org/10.30501/jree.2021.251191.1149

## 1. INTRODUCTION

The location of proper places for constructing power plants is among important issues for energy decision-makers. Access to primary energy resources, nearness to necessary infrastructures like electricity network, transportation roads, water resources, and no interference to prohibited areas such as environmental protected areas or military zones are the most noted factors that should be considered in selecting proper places for constructing power plants. For power plants that exploit renewable energy resources, besides the above considerations, considering the proper potential of and access to the renewable energy resources is of great importance. From the viewpoint of location and potential evaluation of different types of renewable energies, a large number ofstudies have been carried out in Iran and other parts of the world. For instance, one can point to the studies of Segheli et al. [1], Kiani & Veisinezhad [2], and Azadeh et al. [3] concerning the location selection for wind power plants and Nooshad et al. [4], Torabi et al. [5], and Ghadimi et al. [6] regarding small hydroelectric power plants. Similarly, several studies have been done in Iran and the world regarding the location of bioenergy-based power plants, among which the research by Omarni et al. [7] for solid waste incinerator power plants or Duarte et al. [8] for biofuels production facilities as well as the work of Franco et al. [9] for locating biogas plants might be mentioned.

Site selection of renewable energy generation plants is a sophisticated process that should take several influential parameters including limiting factors and criteria into account. One key step of this process is weighting various criteria in order to make a justified comparison and evaluate the importance of each criterion. Among the methods for weighting the criteria, Analytical Hierarchy Process (AHP), Equal Weighting, and Analytic Network Process (ANP) are more frequently applied.

One of the very powerful tools for locating various project plans (i.e., power plants, garbage disposal sites, or industrial complexes) is Geographical Information System (GIS) that is capable of combining criteria weighting tools and provides wide abilities of multi-layer spatial data processing. To establish energy plants, GIS is utilized for different purposes, as suggested in the studies of Klassen et al.[10] and Delaney et al. [11], for selecting proper locations for wind turbine power plants and as suggested in the study of Martin and Hannah [12] for locating conventional power plants, and Voets et al. [13] for determining the location of biomass power plants. Few studies including Ghazi and Omrani [14] have considered determing proper location for biogas power plants in Iran and surveyed the potentials of biogas in Iran's provinces using GIS software.

*Corresponding Author's Email: adl.mehrdad@gmail.com (M. Adl)
URL: http://www.jree.ir/article_130673.html

Please cite this article as: Nosratinia, M., Tofigh, A.A. and Adl M., "Determining optimal locations for biogas plants: Case study of Tehran province for utilization of bovine and aviculture wastes", ***Journal of Renewable Energy and Environment (JREE)***, Vol. 8, No. 3, (2021), 36-44. (https://doi.org/10.30501/jree.2021.251191.1149).

On the other hand, eliminating environmental contaminations caused by livestock excreta release represents another motivation for simultaneous production of energy and sanitary organic fertilizer using anaerobic digestion process out of these sources [15-17]. Wahyudi et al. studied the applicability of the concept of biogas production to industrial dairy farms in Indonesia in terms of sustainability [18]. The role of biogas technology in solving the Peri-urban sanitation problems was also investigated by Sibanda et al. [19]. Of note, using biogas technology in medium- and large-scale plants for the purpose of energy generation and electricity sale to the national power grid has increasingly drawn much attention over the last decades in Iran. As a sub-activity of the current research, the talented regions of Iran for biogas production were appraised and consequently, Tehran province was identified as one of the appropriate areas due to the high potential of biodegradable resources and abundance of energy consumer entities and suitable infrastructures. One significant category of biomass resources in Tehran province is livestock wastes resulting from many animal breeding activities in suburb and rural areas. In terms of the logistics management of raw materials, the industrial cattle and poultry farms are more preferred than traditional counterparts due to their centrality and automated tools. In terms of proper site selection, it is important to identify the most appropriate locations for establishing biogas generation facilities taking into account various parameters and restricting issues. Therefore, this paper aims at employing GIS system along with multi-objective criteria evaluation for the purpose of presenting the most proper and talented areas for industrial biogas installation feeding by aviculture and bovine wastes on the provincial scale.

## 2. EXPERIMENTAL

In this research, the bovine and aviculture's excreta of industrial livestock farms were considered as the source of bioenergy and Tehran province was considered as the surveyed area. The importance of the selected bioenergy source is described in brief in Sub-section 2.1. Afterwards, important factors in determining the proper location for establishing biogas plants and effectiveness of each factor were further determined. With respect to the nature and the extent of the studied area and also incompleteness of required information in each of existing map scales, it is necessary to perform the process of location planning in a hierarchal manner in different stages. In this way, initial locations were determined ona smaller scale; then, a more precise study was done ona broader scale and proper locations were selected. To this end, the scale of 1:25000 was adopted to be surveyed following the appraisal of different types of provincial maps and information layers.

### 2.1. Short description of the study area

Tehran city as the capital is located between 34 to 36.5 degrees of northern latitude and 50 to 53 degree of eastern longitude and its surface area is about 12,981 km$^2$ [20].This province, as shown in Fig. 1, is confined to Mazandaran province from north, to Qom province from south, Markazi province from south west, to Alborz province from west, and to Semnan province from east. The city is home to 13 million population as of the latest sensus 2016 which composes 19 percent of the total Iran's population. It should be noted that 12,252,000 out of the province population (94 %) live in urban areas, while 1,161,000 individuals reside in rural residents [20]. This research generally covers the Tehran province and marginal parts of the neighboring provinces. According to the auxiliary survey in this research, there is a potential of more than 73 million cubic meters per year biogas production from bovine and aviculture wastes in this province, implying a figure of 5,620 cubic meter per sq. km per year biogas production density. Tehran province stands as one of the highly ranked provinces in Iran in this regard.

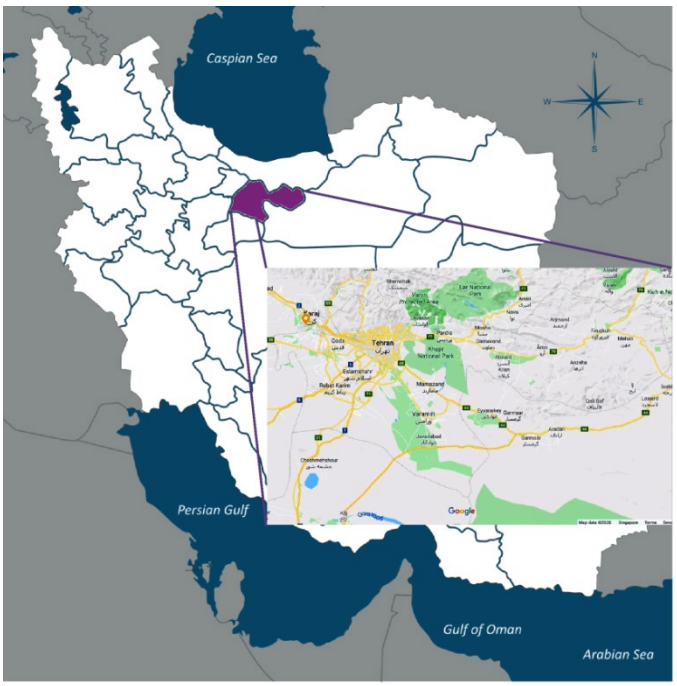


**Figure 1.** The location of the study area on the national map (source: Google maps)

## 3. METHOD

### 3.1. Methodology

The research method is implemented as follows; first, effective factors in determining the location of installing anaerobic digestion were specified and then, Boolean and fuzzy models were selected to combine the information. The objectives of selecting these models is to specify and eliminate the constrained areas for construction of anaerobic digestion using Boolean logic and binary maps and to determine the better remaining areas (allowed areas) for constructing anaerobic digestion plants.

### 3.2. The survey of effective factors and selection criteria

Determining aproper location for installing the anaerobic digestion greatly depends on complete and accurate knowledge of effective factors and the way of selecting them. The technical, economic, social, and environmental factors are determined by consulting the experts on anaerobic digestion and studying the relevant literature. Then, the factors with possibility of providing relevant data and modeling were selected. In fact, providing location layers for some factors and preparing them for the decision model can bedifficult, or even impossible.

Effective factors in determining the location of anaerobic digestion, the reason for their effectiveness, and the type of

their effectiveness are given in Table 1. It should be noted that some factors may be eliminated or added depending on circumstances. The selection of factors in this research was mainly done following the method that had been employed by Rezaeisabzevar et al. [21] as well as by Cheng and Thompson [22]. Closure to the industrial units of cattle breeding or poultry farms as the sources of raw biomass is one of the most important factors in biogas plants; hence, the distance of no more than 10 km to the sources was adopted as a positive factor [19]. Regarding the availability of water resources, the distribution of legal underground water extraction wells or surface water transfer channels was taken into account for evaluating the process of site selection. Since access to the transportation network is another influential factor, the distance of less than 200 m to the asphalt roads or no more than 500 m from gravel roads was considered a positive parameter [22]. A buffer distance of minimum 200 m to the protected or prohibited areas or natural water bodies and a buffer distance of 75 m from the roads' axes were taken into account for biogas plant sites. Furthermore, experts' judgments and existing data from Tehran province were also employed in this procedure.

**Table 1.** Site selection criteria [21-23]

| Criterion | Sub criteria | Importance reason | Criterion type | Standardization function | (f1, f2) |
|---|---|---|---|---|---|
| Raw materials | Water resources ranges | Water requirement for anaerobic digestion | Same distance | Fuzzy small | (200, 5) |
| Raw materials | Range of livestock | Reduction of shipment costs of raw material to anaerobic digestion | Density | Fuzzy small | (1000, 5) |
| Infrastructure | Asphalt roads, gravel roads, Foot routs | Ease of transportation | Same distance | Fuzzy small | (2000, 5) |
| Infrastructure | Power and gas transfer lines | Possibility of connecting the produced electricity or gas to the electricity or gas network | Same distance | Fuzzy small | (200, 5) |
| Population areas | Urban, rural | Nearness to the consumer | Density | Fuzzy large | (2000, 5) |
| Earth form | Slope, altitude | Possibility of construction | DEM | Fuzzy small | (10, 5) |
| Earth form | Flood way, fault | Possibility of construction | Same distance | Fuzzy large | (500, 5) |
| Constraint | Protected and prohibited areas | Possibility of establishment | Boolean | Real | Zero: prohibited area, 1: allowed area |
| Constraint | Forest | Possibility of establishment | Boolean | Real | Zero: prohibited area, 1: allowed area |
| Constraint | Mine | Possibility of establishment | Boolean | Real | Zero: prohibited area, 1: allowed area |
| f1 and f2 are middle point and dispersion values of fuzzy parameters, respectively. | | | | | |

### 3.3. The studied combination model

Simultaneous attention to effective factors in determining the location of anaerobic digestion requires combining the related information layers. In this research, the Boolean and fuzzy models were used to combine the information and modeling in the GIS environment. ArcGIS was employed as a powerful software product along with ModelBuilder as one of its applied tools for this purpose. The steps of this combined model are given below [23]:

a) Determining the required locative and descriptive information;
b) Creating the required layers in ArcGIS;
c) Defining the proper factors for each information layer;
d) Preparing the factor map and re-categorizing them;
e) Determining the weights of the factor maps that affects the location;
f) Combining the factor maps and determining the optimal location;
g) Evaluating the results and drawing the suggestions.

#### 3.3.1. Boolean logic

In the Boolean logic, membership of an element in a set is stated as zero (no-membership) or one (membership) [24]. In order to use the Boolean model in location, an input map is first prepared for each factor in the binary form. In this way, the value of one for each pixel unit represents the properness, while value of zero represents the improperness of location of that pixel. For example, the value of zero is assigned to protected areas in location of anaerobic digestion, while value of one is assigned to other areas. Then, the input maps are combined by Boolean operators AND/OR and create an output binary map. If the combination of maps is done using AND operator, then the pixels with the value of one represent locations where all criteria are satisfied. If the combination of maps is done using OR operator, then the pixels with the value of one represent locations where one or several criteria are satisfied [22].

Following this method, for instance, value of one is assigned to proper locations for building the anaerobic digestion facility in the output map, while the value of zero is assigned to improper locations in the output map.

1) All of the input factors are of the same value. In practice, it is not usually proper to consider equal importance for all location criteria. The weight of factors should be determined with respect to their relative importance.
2) The location units of each factor map that have the same value with that factor lie in one of the zero/one classes. For example, the value of one is assigned to all points that are

in a specific range of the roads in the map of connection roads, whereas those points are at different distances of the roads.

3) In the output map, the selected areas cannot be prioritized with respect to their properness with the related activity. In other words, the selected areas would have the same value in this model.

### 3.3.2. The fuzzy logic

The main characteristic of fuzzy logic compared to the classic logic is that it is able to state knowledge and experience of the human in the mathematical form. With respect to the fuzzy theory, membership of members in a set may not be complete, such that each member has a membership degree of one to zero. Unlike the Boolean (classic) logic, there is no certainty in fuzzy logic to consider an area fully proper or fully improper. The fuzzy sets are versus classic sets[25].

The OR operator is defined through Equation (1):

$$\mu c = \max\{\mu_1(x), \mu_2(x), ..., \mu_n(x)\} \quad (1)$$

where μA, μB, and μC represent the membership values of the pixel in the related layer.

This operator represents the union of the sets such that it extracts the maximum membership degree of the members and has not much accuracy in location. This operator uses the maximum function in combination and is equivalent to union. When using this operator for two membership functions, the maximum value of membership function is selected.

The AND operator is defined as Equation (2):

$$\mu c(x) = \min\{\mu_1(x), \mu_2(x), ..., \mu_n(x)\} \quad (2)$$

This operator represents the intersection of the sets such that it extracts aminimum membership degree of the members, i.e., it extracts the minimum value (weight) of each pixel among all information layers and applies it to the final map. This operator uses the minimum function in overlap and is defined as equivalent as intersect.

In independent parameters and when two or more parts of evidences necessary to prove the hypothesis must exist, using the AND operator is proper. The fuzzy multiplication operator is defined as relation (3):

$$\mu_{prod.} = \prod_{i=1}^{n} \mu_i \quad (3)$$

where μi represents the membership value of the pixel in the related layer of factor i.

In this operator, all of the information layers are multiplied. Due to the nature of zero and one numbers, which are the membership degrees in the fuzzy set, this operator causes the numbers to become smaller and tend to be zero in the output map. Therefore, fewer pixels would be in a very good class. For this reason, this operator is high sensitive concerning location. The fuzzy sum operator is defined in the equation:

$$\mu_{sum} = 1 - \prod_{i=1}^{n} (1 - \mu_i) \quad (4)$$

where μi represents the membership value of the pixel in the related layer of factor i.

In this operator, the complement of multiplication of complement of sets is calculated. For this reason, the values of pixels in the output map tend to one, unlike the algebraic multiplication operator. Therefore, more pixels would be placed in a very good class and the values of the final map would be greater. In other words, the strength of the factors with respect to each other and combination of maps would have incremental effect. For this reason, this operator applies very low sensitivity to the location.

The fuzzy gamma operator is defined as multiplication of fuzzy multiplication and fuzzy sum operators, as stated in Equation (5).

$$\mu_g = (\mu_{sum})^{\gamma} \times (\mu_{prod.})^{1-\gamma} \quad (5)$$

where the operators are described in Equations (3) and (4). The value of gamma (γ) is a number between zero and one by which a certain limit of gamma makes the mean value of μ>0.5; otherwise, the amount of gamma provides a normal distribution for the value of μ [26]. The accurate and informed selection of gamma creates the output values that represent flexible consistency between the decreasing tendencies of fuzzy multiplication and the increasing tendencies of fuzzy sum [27]. The data are gathered from various sources by different producers such that the method and procedures of data gathering and standardization are different. After preparing the data, the information layers are converted to raster and the pixel's dimensions are considered on the scale of 1:25000 and 30*30 meters. Then, the maps are standardized.

### 3.4. The maps of the Boolean model

The purpose of these maps is to specify and eliminate the areas with no possibility of constructing anaerobic digestion. These maps were created for geographical features such as lakes, mines, etc. If there are such features in a place, severe constraints would be imposed on constructing anaerobic digestion in that place or even ata specified distance to it. Therefore, maintaining a specified distance from geographical features is necessary. It should be noted that the objective of Boolean maps is only elimination of constrained areas and it is not necessary to rank the eliminated areas [22].In the raster mode, a binary constraint map is prepared for each constraining factor in which the value of zero is assigned to constrained areas for constructing anaerobic digestion and value of one is assigned to other areas. The factors for which the binary maps are prepared include protected areas, forests, and mines.

### 3.5. The maps of the fuzzy model

In the fuzzy maps, each feature is prepared such that the value of each location unit represents the properness of that location for constructing the anaerobic digestion. Being successful in using the fuzzy mathematics in different applications depends greatly on the definitions of proper membership functions. With respect to the effects of different factors in location of the anaerobic digestion and status of existing relevant data, small fuzzy and large fuzzy membership functions are used to fuzzify them [21].

Small fuzzy: f1 and f2 represent the middle point and the dispersion, respectively. The dispersion is stated as a number between 1 and 10. Equation (6) represents the related function in which the changes are depicted in Figure 2. As can be seen in this figure, the smaller the dispersion, the smoother the curve.

$$\mu(x)=\frac{1}{1+\left(\frac{x}{f_2}\right)^{f1}} \quad (6)$$

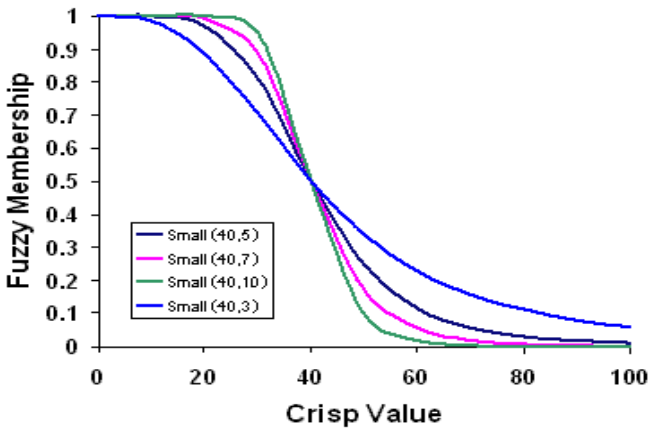


**Figure 2.** The small fuzzy chart

Big fuzzy: f1 represents the middle point and f2 represents the dispersion. The dispersion is a number between 1 and 10. Equation (7) represents the relation in whichits changes are given in Figure 3 and it is evident that the larger the dispersion value, the wider the fuzzy membership.

$$\mu(x)=\frac{1}{1+\left(\frac{x}{f_2}\right)^{-f1}} \quad (7)$$

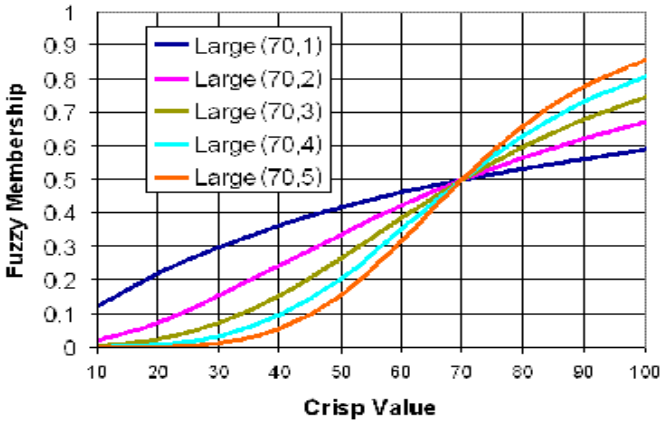


**Figure 3.** The big fuzzy chart

## 4. RESULTS AND DISCUSSION

### 4.1. The standardized fuzzy maps

In the following, some of the maps that are standardized with fuzzy method are given. The fuzzy map of rural population is depicted in Figures 4 as rural residents are influential population according to their employment in biomass production practices such as agriculture and animal husbandary, and they are potential consumers of anaerobic digestion products including energy carriers (biogas, electricity, heat) and digestate [17]. Figure 5 shows the fuzzy map of the roads. As mentioned before, road accessability is quite important for the projects that handle wastes such as landfills, solid waste recycling plants, and large biogas facilities. In this manner, a range of distances with lower and upper limits is significantly influential since the minimum distance to the roads is mandatory according to their legal buffer zones as well as some environmental concerns such as odor emission or landscape downgrading [21]. On the other hand, economical aspects of feedstock transportation impose an upper limit of economic distance from the roads, as emphasized by Franco et al, for locating biogas plants for a certain district in Denmark [9]. The areas marked by blue in Figure 5 are of high suitability in terms of access to the transportation network. These areas comply with the residential and industrial areas, but do not necessarily represent the suitable areas for biogas facility installations. The fuzzy map of rivers is combined with the maps of groundwater extraction wells and water transmission channels in order to form the fuzzy map of water resources, as shown in Figure 9.

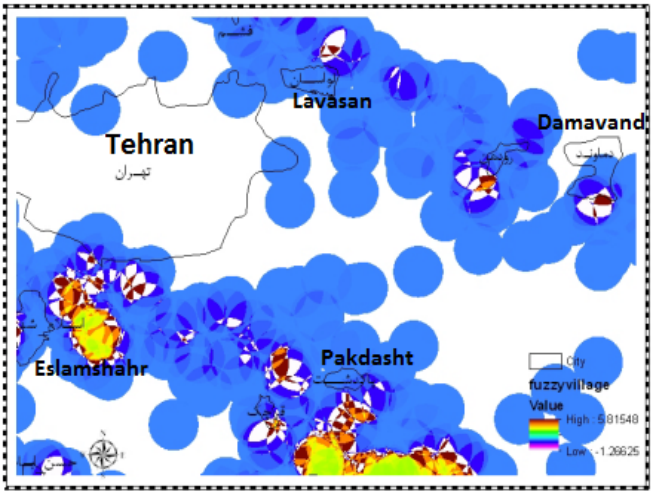


**Figure 4.** The fuzzy map of rural population

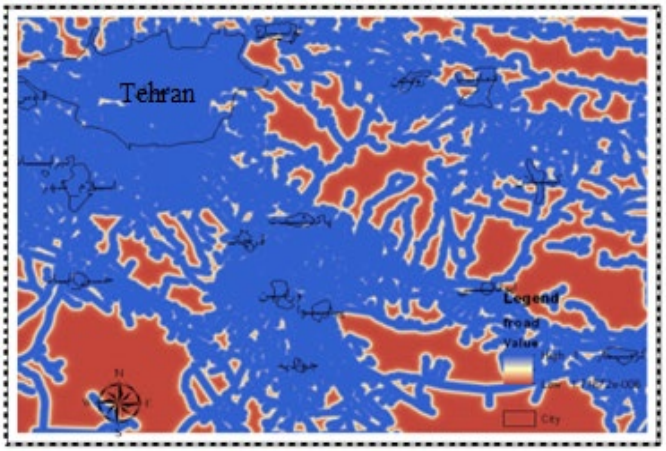


**Figure 5.** The fuzzy map of roads

### 4.2. Weighting the factors

In order to determine the relative importance of different factors of location, a weight is considered for each. In the location of anaerobic digestion plant, the weights of factors are determined using the AHP method based on the published relevant articles as well as experts' judgments [22]. In the AHP method, the decision-maker is asked to state a number from 1 to 7 for the relative importance of each criterion with respect to other criteria [24, 28]. Number 1 represents very low relative importance and Number 7 very high relative importance. However, in real world, it is very difficult to extract precise data pertaining to measurement factors since all human preferences are subject toa degree of uncertainty.

For this reason, fuzzy AHP methods effectively resemble human thoughts and perceptions. The weight of each factor is specified by fuzzy weighted averaging. The application of experts' opinion in the weighting procedure was also employed by Franco et al. for biogas plants locations [9]. A consistency ratio of 0.5 was allocated to acceptance in this research since the values below 0.1 were considered as acceptable, according to Saaty [28]. As a result of judgement amounts, the weights of criteria are givenin Table 2.

**Table 2.** Weighting the criteria [22, 26]

| Main criterion | Weight of main criterion | Sub criterion | Weight of sub criterion |
|---|---|---|---|
| infrastructure | 0.40 | Asphalt road | **0.8** |
| | | Gravel road | **0.2** |
| | | Foot rout | **0.1** |
| Consumer | 0.35 | Town | **0.76** |
| | | Village | **0.24** |
| Earth form | 0.12 | slope | **0.33** |
| | | Altitude | **0.23** |
| | | Flood | **0.24** |
| | | Fault | **0.20** |
| Raw materials | 0.13 | Water | **0.4** |
| | | Raw manure availability | **0.6** |

### 4.3. Combining the maps and designing the network

After developing the factor maps of Boolean and fuzzy models, these maps are to be combined using operators of each model. The proper locations are identified by combining the maps obtained by Boolean and fuzzy models through a similar procedure examined by Cheng and Thompson [22].

The maps of Boolean model were combined using AND operator. In the obtained output map, the location units with value of one in all maps of constraining factors were assigned value of one. Likewise, the location units with value of zero in at least one map were assigned value of zero. In terms of the convinence, performance speed, and also its conceptual consistency to the maps of constraining factors, the Boolean model is the best model to combine these maps [22]. In these maps as shown in Figure 6, the objective is the complete elimination of constrained areas. The dark-pink colored areas in this map might be considered for biogas plants establishment; nevertheless, other factors should also be taken into account in order to filterize the inappropriate zones accordingly. Therefore, it is not necessary to considerthe weight value of factor or a specific class of a factor.

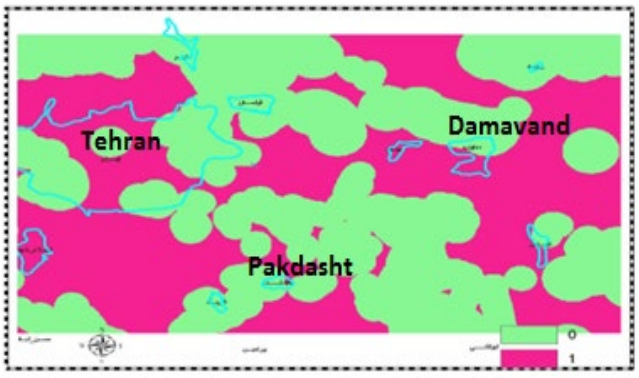


**Figure 6.** The map derived from combining the Boolean maps

### 4.4. Combining the fuzzy maps

After preparing maps of the fuzzy model, it is necessary to combine the maps using fuzzy operators. Selection of a proper fuzzy operator to combine different layers is done with respect to the relations and interactions of factors of those layers [21]. Usually, it is not possible to combine all required layers of an application only with one operator. Therefore, different operators are often used to combine different information layers instead of a single network operator. In this research, the designed inference network is depicted in Figure 7.

In the designed inference networks, instead of combining all factor maps in one stage, the factors are classed based on experts' knowledge, their nature and role in determining the proper location, and their relationships. The pertaining information layers are combined in different stages. For example, factors such as the earth slope and application, both of which are relevant to the physical form and morphology of the earth, can be considered in a class and combined from a certain viewpoint. It should be noted that selection of the fuzzy operators can be different according to different logics. If the role of water resources in the location is confined to only supplying the required water, no difference is considered between the surface water and underground water, and only one water resource is enough for supplying the required water; then, the water layers can be combined using OR operator.In this way, the pixels' values of the output map are determined with the value of one of input layers with the highest value in that pixel and the weighted values of two other factors are interfered in the output value. In other words, closeness to two or three water resources does not make any substantial advantage compared to closeness to only one water resource. Figure 8 depicts the obtained map.

In the combined fuzzy map of the connection roads, three information layers are used for the roads that include asphalt roads, gravel roads, and foot routs. With respect to the importance of each road type, the weight of asphalt road is considered as 0.8, the weight of gravel road is considered as 0.2, and the weight of foot rout is considered as 0.1 following the suggestions made by Rezayisabzevar et al. [21]. It is notable that the weight of crierion for transportation roads was adopted within a range of 0.286 to 0.499 as lower and upper limits by Franco et al. [9]. Figure 9 depicts the output fuzzy map. This map proposes many locations mostly in suburb areas and around the transportation roads with significant traffic.

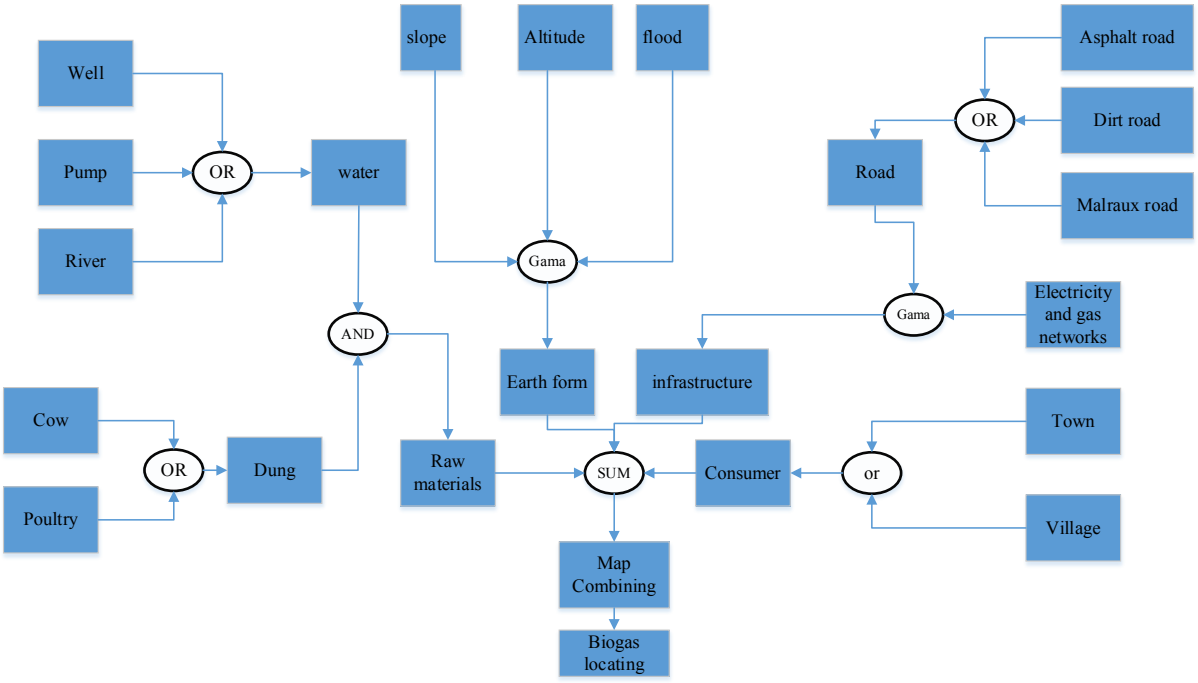


**Figure 7.** The inference network model

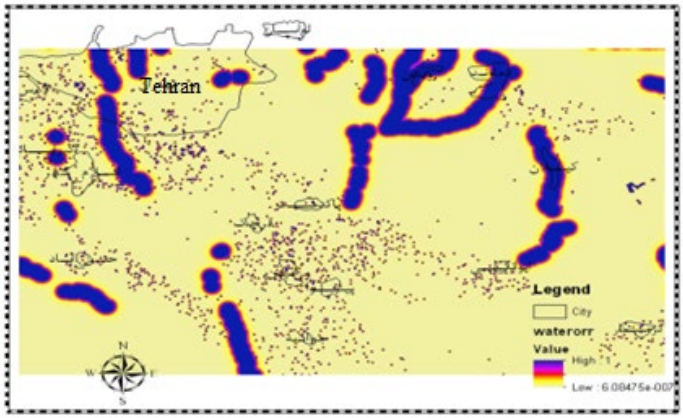


**Figure 8.** The combined fuzzy map of water resources

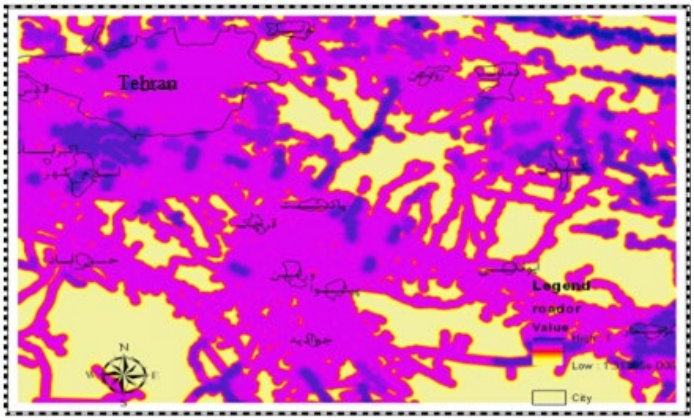


**Figure 9.** The combined fuzzy map of connection roads

By considering gamma equal to 0.8, the infrastructures map, which is obtained by combining information layers of electricity fuzzy network and connection roads, is depicted in Figure 10 which shows highly ranked zones for biogas plants as a function of closure to the transportation roads as well as to the power transmission lines.

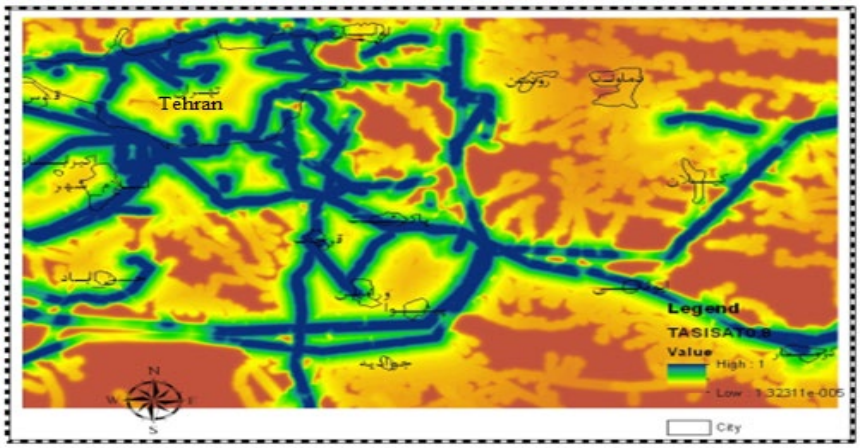


**Figure 10.** The fuzzy map of infrastructures

According to Figure 11, obtained by fuzzy combination of all layers, the dark blue areas are the most proper locations for constructing biogas power plants. In addition, the yellow-white areas are the least proper locations for this

purpose. The areas marked by dark-blue color in southern parts of Tehran province certainly comply with the locations of abundant cattle farms and poultry farms such as the suburb of Eslamshahr. Furthermore, three other zones have been realized as appropriate locations for such purposes in the northern suburb of Lavasn, southern suburb of Rudehen, and southern part of Damavand county. The evidence of industrial livestock farms in the aforementioned locations along with the essential infrastructures complies with the outcomes of location evaluating process in this research.

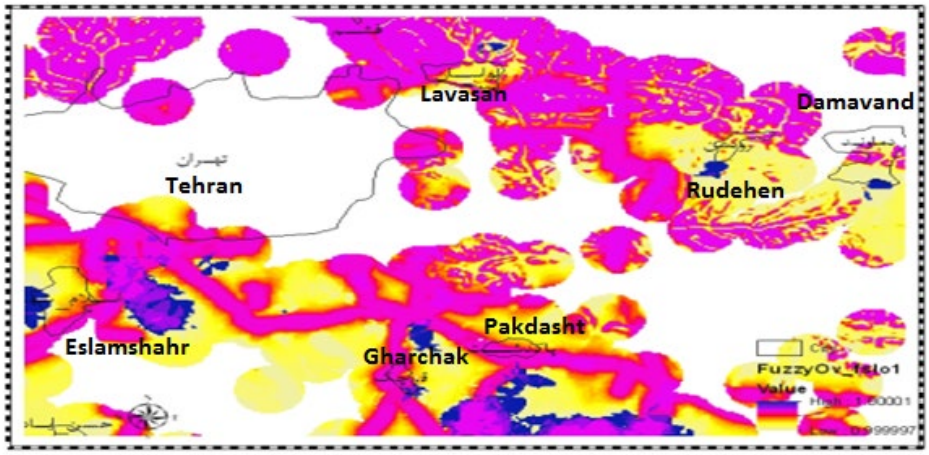


**Figure 11.** Ranking of proper locations for installation of industrial biogas plants

## 5. CONCLUSIONS

Utilization of fuzzy analysis method has many advantages including continuity of numbers in the map and greater closeness to the real world, which can guide managers and decision-makers to the right choices and greatly assist them in identifying proper locations for establishment of biogas plants. The final map shows that although there are proper areas in north Lavasan, Rudehen, and southern Damavand county for constructing such biogas plants, there are more proper areas in the southern part of Tehran province in the margin of Eslamshahr, Gharchak, and Pakdasht.

## 6. ACKNOWLEDGEMENT

The authors should warmly appreciate the contributions made by Mr. Pourfathi for training of geographical information system software and for helping to providet he required data for this research work. This research was conducted under the Ph. D. scheme No. 381392057 supported by the Materials and Energy Research Center (MERC).

## NOMENCLATURE

| | |
|---|---|
| AHP | Analytical Hierarchy Process |
| ANP | Analytic Network Process |
| DEM | Digital Elevation Model |
| GIS | Geographical Information System |
| **Greek letters** | |
| $\mu$ | Fuzzy logic operator |
| $\mu_{prod}$ | Fuzzy multiplication operator |
| $\mu_{sum}$ | Fuzzy sum operator |
| **Subscripts** | |
| f1 | The middle point of fuzzy value |
| f2 | Dispersion of fuzzy value |

## REFERENCES

1. Segheli, K., Nikookar, J. and Ebrahimi, A., "The technical and economical evaluation of hybrid wind-solar power plants: A case study of Minoodasht county, Golestan province", ***Proceedings of the 1st National Conference on Alternative and Clean Energies***, Tehran, Iran, (2013). (In Farsi). (https://civilica.com/doc/210064/).
2. Kiani, A. and Veisinezhad, A., "Evaluation of using wind energy in urban development of Iran, case study: Zabol city", ***Proceedings of the 1st National Conference on Alternative and Clean Energies***, Tehran, Iran, (2013). (In Farsi). (https://civilica.com/doc/209974/).
3. Azadeh, A., Ghaderi, S.F. and Nasrollahi, M.R.,"Location optimization of wind plants in Iran by an integrated hierarchical Data Envelopment Analysis", ***Renewable Energy***, Vol. 36, No. 5, (2011), 1621-1631. (https://doi.org/10.1016/j.renene.2010.11.004).
4. Nooshad, B., Seifi, H. and Hosseini, S.H., "The feasibility study of construction of pumped-storage power plants using the forward dynamic plan for Iran's overall electricity network", ***Proceedings of 13th International Power System Conference***, Tehran, Iran, (2005). (In Farsi). (https://civilica.com/doc/41964/).
5. Torabi, G., Khoshnavaz, M., Safari Karchani, A. and Ghadimi, A.A., "Identification of talented points for installing micro hydro power plants in Lorestan province", ***Proceedings of 24th International Power System Conference***, Niroo Rresearch Institute, Tehran, Iran, (2009). (In Farsi). (https://civilica.com/doc/89322).
6. Ghadimi, A.A., Razavi, F. and Mohammadian, B., "Determining optimum location and capacity for micro hydropower plants in Lorestan province in Iran", ***Renewable and Sustainable Energy Reviews***, Vol. 15, No. 8, (2011), 4125-4131. (https://doi.org/10.1016/j.rser.2011.07.003).
7. Omrani, G.A., Atabai, F., Barzegar, K. and Rahimi, S., "The environmental, technical, and economical feasibility study of constructing incinerator power plants in Amol city", ***Proceedings of the 6th National Conference on Environmental Engineering***, Tehran, Iran, (2012). (In Farsi). (https://civilica.com/doc/169837/).
8. Duarte, A.E., Sarache, W.A. and Costa, Y.J., "A facility-location model for biofuel plants: Applications in the Colombian context", ***Energy***, Vol. 72, (2014), 476-483. (https://doi.org/10.1016/j.energy.2014.05.069).
9. Franco, C., Bojesen, M., Hougaard, J.L. and Nielsen, K., "A fuzzy approach to a multiple criteria and Geographical Information System for decision support on suitable locations for biogas plants", ***Applied Energy***, Vol. 140, (2015), 304-315. (https://doi.org/10.1016/j.apenergy.2014.11.060).
10. Klassen, K. and Marjerrison, A., "Sitting a wind turbine farm in Pipestone County, Minnesota using a GIS framework", (2002). (http://www.uoguelph.ca/geography/filetran/geog4480w2002/Group04/index.html).
11. Delaney, K. and Lachapelle, A., "A GIS approach to sitting a coal fired power plant in Franklin County, Illinois", (2003). (http://www.uoguelph.ca/geography/research/geog4480_w2003/group21/index.html).
12. Martin, P.C. and Hannah, I.W., Modern power station practice (3rd edition), Volume A: Station planning and design, British Electricity International, (1992). (https://doi.org/10.1016/B978-0-08-040735-7.50009-0).

13. Voets, T., Neven, A., Thewys, T. and Kuppens, T., "GIS-BASED location optimization of a biomass conversion plant on contaminated willow in the Campine region (Belgium)", ***Biomass and Bioenergy***, Vol. 55, (2013), 339-349. (https://doi.org/10.1016/j.biombioe.2013.02.037).

14. Ghazi, S. and Omrani, G.A., "Evaluating potential of proper places for constructing biogas units; An step to energy sustainable development", ***Proceedings of 6th National Conference of Iran's Association of Environmental Experts***, Tehran, Iran, (2006). (In Farsi). (https://civilica.com/doc/13994/).

15. Alemayehu, Y.A., "Enhancement and optimization mechanisms of biogas production for rural household energy in developing countries: A review", ***International Journal of Renewable Energy Development***, Vol. 4, No. 3, (2015), 189-196. (https://doi.org/10.14710/ijred.4.3.189-196).

16. Wellinger, A., Murphy, J.D. and Baxter, D., The biogas handbook: Science, production and applications, Elsevier, (2013). (https://www.elsevier.com/books/the-biogas-handbook/wellinger/978-0-85709-498-8).

17. Tsachidou, B., Scheuren, M., Gennen, J., Debbaut, V., Toussaint, B., Hissler, C., George, I. and Delfosse, P., "Biogas residues in substitution for chemical fertilizers: A comparative study on a grassland in the Walloon Region", ***Science of the Total Environment***., Vol. 666, (2019), 212-225. (https://doi.org/10.1016/j.scitotenv.2019.02.238).

18. Wahyudi, J., Kurnani, B.A. and Clancy, J., "Biogas production in dairy farming in Indonesia: A challenge for sustainability", ***International Journal of Renewable Energy Development***, Vol. 4, No. 3, (2015), 219-226. (https://doi.org/10.14710/ijred.6.3.235-240).

19. Sibanda, G., Musademba, D., Chihobo, H. and Zanamwe, L., "A feasibility study of biogas technology to solving peri-urban sanitation problems in developing countries, A case for Harare, Zimbabwe", ***International Journal of Renewable Energy Development***, Vol. 2, No. 2, (2013), 97-104. (https://doi.org/10.14710/ijred.2.2.97-104).

20. Iran Statistical Yearbook 2018, Iranian National Organization of Statistics, (June 2019). (www.amar.org.ir).

21. Rezaeisabzevar, Y., Bazargan A. and Zohourian, B., "Landfill site selection using multi criteria decision making: Influential factors for comparing locations", ***Journal of Environmental Sciences***, Vol. 93, (2020), 170-184. (https://doi.org/10.1016/j.jes.2020.02.030).

22. Cheng, C. and Thompson, R.G., "Application of Boolean logic and GIS for determining suitable locations for Temporary Disaster Waste Management Sites", ***International Journal of Disaster Risk Reduction***, Vol. 20, (2016), 78-92. (https://doi.org/10.1016/j.ijdrr.2016.10.011).

23. Beheshtifar, S., Saadi-Mesgari, M., Valadanzoej, M.J. and Karimi, M., "Using the fuzzy logic in GIS environment to determine locations for gas power plants", ***Journal of Civil and Surveying Engineering***, Vol. 44, No. 4, (2011), 583-595. (In Farsi with English Abstract). (https://jcse.ut.ac.ir/article_21765.html).

24. Asgharpour, M.J., The multiple criteria decision making, 8th edition, University of Tehran, Tehran, Iran, (2010). (In Farsi). (https://www.gisoom.com/book/1952783/%DA%A9%D8%AA%D8%A7%D8%A8-%D8%AA%D8%B5%D9%85%DB%8C%D9%85-%DA%AF%DB%8C%D8%B1%DB%8C-%D9%87%D8%A7%DB%8C-%DA%86%D9%86%D8%AF-%D9%85%D8%B9%DB%8C%D8%A7%D8%B1%D9%87/).

25. Azar, A. and Faraji, H., The fuzzy management science, 4th edition, Ketab-e-Mehraban Publications, Tehran, Iran, (2010). (In Farsi). (https://www.gisoom.com/book/11222066/%DA%A9%D8%AA%D8%A7%D8%A8-%D8%B9%D9%84%D9%85-%D9%85%D8%AF%DB%8C%D8%B1%DB%8C%D8%AA-%D9%81%D8%A7%D8%B2%DB%8C/).

26. Liu, X.P., Zhang, J.Q., Cai, W.Y. and Tong, Z.J., "Assessing maize drought hazard for agricultural areas based on fuzzy gamma model", ***Journal of Integrative Agriculture***, Vol. 12, No. 3, (2013), 532-540. (https://doi.org/10.1016/S2095-3119(13)60254-3).

27. Yousefi, H., Noorollahi, Y., Soltanmohammadi, M. and Arjmandi, R., "Using fuzzy logic and fuzzy TOPSIS for sake site selection of solar power plant by GIS,(Case Study, Tehran)", ***Iranian Journal of Energy***, Vol. 15, No. 4, (2013). (In Farsi with English Abstract). (http://necjournals.ir/article-1-447-en.html).

28. Saaty, T., The analytic hierarchy process, McGraw Hill, USA, (1980).

JREE: Vol. 8, No. 3, (Summer 2021) 45-53

Journal of Renewable Energy and Environment

Research Article

Journal Homepage: www.jree.ir

# Effects of PCM Mass on Heat Dynamics and Thermal Performance of Solar Air Heaters: A Numerical and Analytical Study

Ehsan Hasan Zaim [a], Hadi Farzan [b*]

[a] Department of Mechanical Engineering, School of Engineering, Sirjan University of Technology, P. O. Box: 78137-33385, Sirjan, Kerman, Iran.
[b] Department of Mechanical Engineering, School of Engineering, Higher Education Complex of Bam, P. O. Box: 76615-314, Bam, Kerman, Iran.

PAPER INFO

*Paper history:*
Received 04 December 2020
Accepted in revised form 18 May 2021

*Keywords*:
Solar Air Heater,
Phase Change Material,
Analytical Study,
Thermal Performance,
Heat Dynamics

ABSTRACT

Utilizing thermal storage units such as Phase Change Materials (PCMs) is a suitable approach to improving Solar Air Heaters (SAHs). The present study tries to assess the effects of PCM mass values on the heat dynamics and thermal performance of SAHs. To this aim, an analytical thermodynamic model was developed and validated by available experimental data. This model provides a robust numerical framework to model the phase change phenomenon and analyze the heat dynamics and thermal performance of SAH using various PCM masses. Four scenarios were considered using the developed analytical model including SAHs using 0, 30, 60, 90 kg PCM. The obtained results illustrated that the maximum outlet temperature was reduced, approximately near 20 %, by increasing the PCM mass between 0 and 90 kg; however, heating time was extended to periods when solar energy availability was inadequate. The thermal performance improved by nearly 14.5 % in the SAH using 90 kg PCM mass compared to the SAH without using PCM. The thermal performance of the SAH with 90 kg PCM was slightly higher than the SAH using 30 kg of PCM; hence, a significant portion of stored thermal energy was lost during nighttime through heat exchange with ambient surroundings. The obtained results also showed that despite available latent thermal energy, the outlet air temperature profiles for the SAHs using different PCM mass were close after sunset due to the low thermal conductivity of paraffin.

https://doi.org/10.30501/jree.2021.259570.1169

## 1. INTRODUCTION

Besides environmental pollution concerns, sustainable growth urges many countries to substitute fossil fuels with renewable and clean energy resources [1]. Solar energy attracts many researchers, engineers, and investors among available renewable energy sources due to its inexhaustibility and pollution-free nature. However, solar energy is not available at night and on cloudy or rainy days. Solar Air Heaters (SAHs) with integrated PCM blocks offer a feasible and inexpensive alternative to collect solar energy, store excess energy, and release it when required. These collectors operate based on extracting thermal energy from hot absorber plates, charging PCM blocks during daytime hours, and delivering stored thermal energy at nighttime hours.

Due to the simplicity and vast applications, numerous studies extensively paid attention to solar heaters and investigated the heat dynamics and thermal performance of these collectors [2-5]. Charvat et al. [6] carried out a numerical and experimental study of PCMs usage as thermal storage units in air-based solar thermal systems to shave peak demand. Shalaby et al. [7] summarized methods used to enhance PCM thermal conductivity, particularly paraffin waxes. Bouadila et al. [8] and Salih et al. [9] experimentally investigated the effects of mass flow rate on absorbed and recovered heat in a solar air heater with integrated capsulated PCMs. Navarro et al. [10] conducted a research study using latent heat storage to reduce energy consumption for heating purposes in domestic applications. The importance of using PCM on the heat dynamics and thermal performance of SAH was experimentally investigated using two SAHs without and with using thermal storage units [11]. Jain and Tewari [12] investigated the effects of using PCM in a solar crop dryer to keep drying continuity and improve the color and flavor of dried herbs. The energy and exergy efficiency of a single-pass double-glazed solar air heater with packed bed paraffin waxes were investigated at two different mass flow rates [13, 14]. The results illustrated that the daily energy and exergy efficiency varied in ranges from 20.7 % to 26.8 % and from 10.7 % to 19.5 %. In a review study, Khan et al. [15] represented the classification of various PCMs to obtain the long-term durability of latent storage systems. Moradi et al. [16] developed a numerical transient model to investigate the effects of paraffin's thermal conductivity, paraffin's mass, and air mass flow rate on thermal performance. The heat dynamics and performance of a solar air heater using a two-packed bed absorber were investigated by comparing operating time and hot outlet temperature. This study reported that the daily thermal efficiency reached around 47 % [17]. A solar heater using PCMs with honeycomb structure in the PCM panels was

*Corresponding Author's Email: hadi.farzan@bam.ac.ir (H. Farzan)
URL: http://www.jree.ir/article_130708.html

Please cite this article as: Hasan Zaim, E. and Farzan, H., "Effects of PCM mass on heat dynamics and thermal performance of solar air heaters: A numerical and analytical study", ***Journal of Renewable Energy and Environment (JREE)***, Vol. 8, No. 3, (2021), 45-53. (https://doi.org/10.30501/jree.2021.259570.1169).

compared with conventional SAHs using PCM to investigate the introduced honeycomb impacts on the thermal performance of SAHs [18, 19]. The acquired experimental results showed that the honeycomb structure reduced charge/discharge time but slightly decreased the average daily performance. Raj et al. [20] investigated a double-pass SAH using encapsulated PCMs and examined the role of geometries of capsules in SAH's heat dynamics of SAH and the charge/discharge process. Jawad et al. [21] suggested adding aluminum chips and tubes with nano-silicon carbide into paraffin wax used in solar heaters to improve their thermophysical properties. Different configurations of absorber plates with embedded capsulated paraffin wax were studied to optimize the thermal performance of SAHs integrated with PCMs [22]. Reddy et al. [23] developed a validated numerical model to study the phase change characteristics and charge/discharge operation in SAHs using PCM blocks.

Phase change modeling in investigating the heat dynamics of SAHs using PCMs is a crucial factor in performing an accurate and precise analysis. Reddy et al. [23] used the enthalpy-porosity technique, while Charvat et al. [24] employed the effective heat capacity method to consider various PCM phases. Summer et al. [25] utilized a lumped parameter model to achieve the temperatures and heat fluxes in a solar collector using PCM. Some studies only used a simple model to obtain the stored thermal energy in PCM [13, 14]. Moradi et al. [16] and Salih et al. [9] used the enthalpy method to model the phase change problem in SAHs with integrated PCMs. All these models are characterized by certain pros and cons and an accurate framework to model the phase change problem with different computational costs. However, these models were tested under extensively different input parameters.

As illustrated in the literature review, early and recent studies have mainly investigated improving SAHs' thermal performance by using phase change materials and compared the heat dynamics of conventional SAHs with SAHs utilizing PCM blocks. These studies assessed the thermal performance of SAHs by concentrating on the technical specifications such as different absorber configurations, using PCMs' thermal conductivity enhancement, or operational conditions such as charge/discharge durations, air mass flow rate, and inlet air temperature. The current study attempts to assess a crucial technical factor as PCM mass affects SAHs' heat dynamics, such as outlet air temperature, charge/discharge process, and operating duration after sunset. The phase change problem was solved based on a model introduced by Leoni and Amon [26]. This model is an accurate and robust approach to simulating the phase change phenomenon in latent thermal storage units considering the computational cost.

An analytical model was then developed and validated by experimental results, to this aim. The used experimental data were based on an experimental study reported in [11]. Four scenarios were considered using the validated analytical model as a robust framework including SAH without using PCM, SAHs using 30 kg, 60 kg, and 90 kg PCM. The acquired results were analyzed and compared to assess the effects of used PCM mass on the heat dynamics and thermal performance of SAHs.

## 2. ANALYTICAL MODEL

The experimental approach is an expensive and time-consuming method and, in some cases, needs technical changes in experimental setups. The analytical model provides this opportunity to assess the effects of PCM mass value on the heat dynamics and thermal performance of the collector under study. Experimental data then validated the developed analytical model to examine its accuracy and robustness. The experimental runs were carried out at Tunisia (Longitude 10°25' E, Latitude 36°43' N) during August 27$^{th}$ and 28$^{th}$. The experiments began from 6:00 to 18:00 (local time) and continued throughout the night from 18:00 to 6:00 (next day). The air mass flow rate was 0.018 kg/s, and the calculated Reynolds number implied that the airflow regime was laminar. The SAH studied in [11] used 60 kg paraffin as latent heat storage. Figure 1 shows the schematic of the modeled SAH.

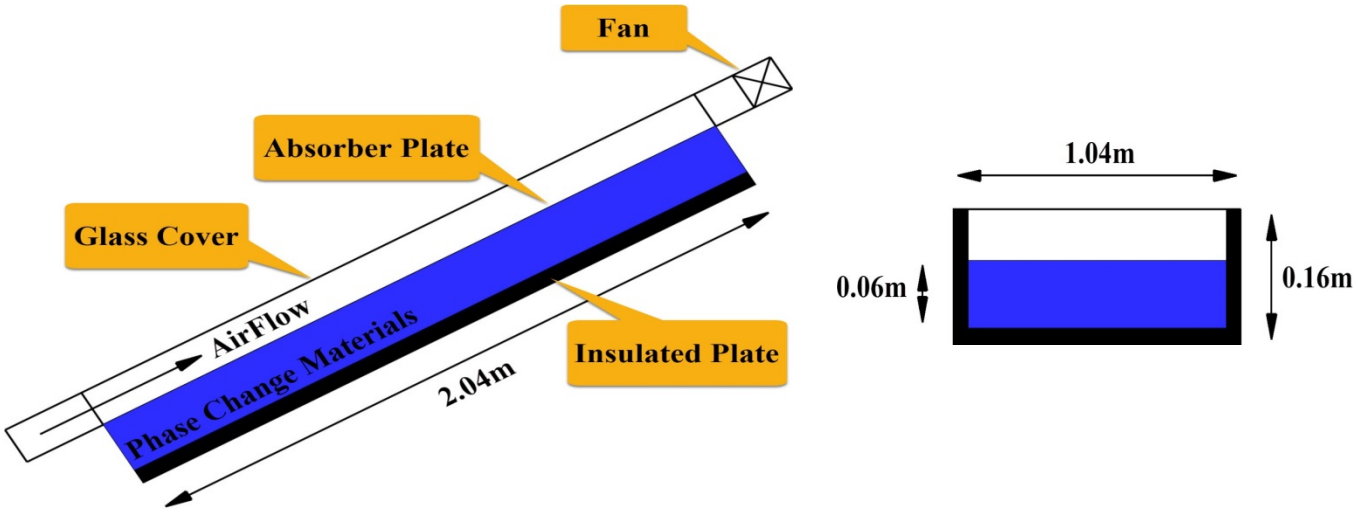


**Figure 1.** Schematic of solar air heater under study

To simplify the analytical model, the following assumptions were considered:

- The system is operating under quasi-steady-state conditions.
- The airflow regime inside the collector is laminar based on the reported experimental data.
- The inlet air temperature is equal to the ambient air temperature.

- The temperature distribution through the absorber plate and glass cover is considered uniform.
- The collector has heat exchange with its surroundings only through its top surface.
- The phase change problem is one dimensional and occurs in the PCM thickness direction.
- The thermophysical properties of PCMs are constant and do not depend on temperature.

The total collector heat gain is the amount of heat extracted by the collector exposed to solar irradiation. The energy balance can be utilized to obtain total heat gain and it indicates the distribution of incident solar energy into useful energy gain, thermal energy storage, thermal losses, and optical losses. By using energy balance, total energy gain can be written as follows:

$$Q_{total} = A_c [S - U_L (T_{pm} - T_a)] \quad (1)$$

where $Q_{total}$ and $U_L$ are the total energy gain and heat transfer coefficient, respectively, while $A_c$ is the collector surface area. $T_{pm}$ and $T_a$ represent the mean absorber plate temperature and ambient temperature. S indicates the solar radiation absorbed by a collector per unit area of the absorber and obtains as follow:

$$S = I (\tau\alpha) \quad (2)$$

Here, I is the solar irradiation measured by the installed pyranometer. τα is the transmittance-absorptance product and comprehensively discussed in [27]. All collector surfaces were insulated, and only the top one had heat exchange with the surrounding. Hence, $U_L$ can be assumed to equal $U_t$ in which $U_t$ is the top heat loss coefficient. Using thermal network (from ambient air to absorber plate), the top heat loss coefficient, $U_t$, is obtained as:

$$U_t = \left[\frac{1}{h_{c,abs-g} - h_{r,abs-g}} + \frac{1}{h_w - h_{r,g-a}}\right]^{-1} \quad (3)$$

The used thermal network and its associated thermal resistances are shown in Figure 2.

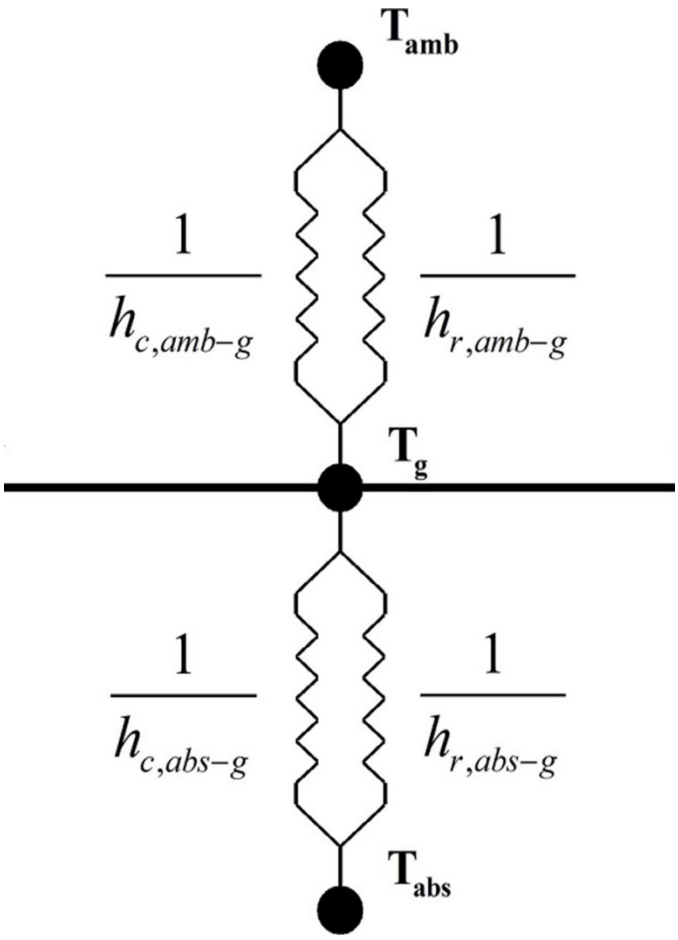


**Figure 2.** Thermal network of SAH

The reported heat transfer coefficients in Eq. (3) are comprehensively discussed in Table 1.

**Table 1.** Heat transfer coefficients and calculation formulas

| Heat transfer coefficient | Definition | Calculation formula |
|---|---|---|
| $h_{c,abs-g}$ | Convective heat transfer coefficient between the absorber plate and glass cover | $Nu_{abs-g}\frac{L}{k_a}$ |
| $h_{r,abs-g}$ | Radiant heat transfer coefficient between the absorber plate and glass cover | $\frac{\sigma(T_{abs}^2 + T_g^2)(T_{abs} + T_{g)}}{\frac{1}{\varepsilon_{abs}} + \frac{1}{\varepsilon_g} - 1}$ |
| $h_{c,g-amb}$ | Convective heat transfer coefficient between the glass cover and ambient air [28] | $5.67 + 3.8\, v_a$ |
| $h_{r,g-amb}$ | Radiant heat transfer coefficient between the glass cover and ambient air | $\varepsilon_g\sigma(T_{sky}^2 + T_g^2)(T_{sky} + T_{g)})$ |

The sky temperature is given as follows [28]:

$$T_{sky} = 0.0552\, T_a^{1.5} \quad (4)$$

Using the energy balance, Eq. (1), the total heat gain was calculated. The total heat gain consists of two main parts given as:

$$Q_{total} = Q_u + Q_{st} \quad (5)$$

where $Q_u$ and $Q_{st}$ denote the useful energy gain and thermal energy stored in PCM blocks. The useful collector heat gain is the amount of heat extracted by the flowing air and given as:

$$Q_u = \dot{m}_a c_{p,a} (T_{a,out} - T_{a,in}) \quad (6)$$

Figure 3 represents the energy flow between all elements of the solar heater under study. As shown in Figure 3, the flowing air exchanges heat with the glass cover and absorber plate. By using the energy balance, the useful energy gain by the flowing air can be rewritten as follows:

$$Q_u = h_{c,g\text{-}a} A_c (T_g - T_{a,m}) + h_{c,abs\text{-}a} A_c (T_{abs} - T_{a,m}) \quad (7)$$

Here, $T_g$ and $T_{a,m}$ are the glass cover temperature and mean flowing air temperature, respectively. The mean flowing air temperature, $T_{a,m}$, inside the collector is obtained as:

$$T_{a,m} = \frac{T_{a,in} - T_{a,out}}{2} \quad (8)$$

where $h_{c,g\text{-}a}$ and $h_{c,abs\text{-}a}$ are the convective heat transfer coefficients between the flowing air, glass and absorber plate, respectively. To simplify calculations, the heat transfer coefficients between the flowing air, glass cover, and absorber plate are considered equal as given by Eq. (4) in the following:

$$h_c = \frac{N_u \times k_f}{D_k} \quad (9)$$

Here, $k_f$ is the thermal conductivity of flowing air. The Nusselt number for laminar forced convection flow, $N_u$, can be obtained as [28]:

$$Nu = 4.9 + \frac{0.0606(\frac{RePrD_h}{L})^{1.2}}{1 + 0.0909(\frac{RePrD_h}{L})^{0.7} Pr^{0.17}} \quad (10)$$

$$D_h = \frac{4 \text{ (Flow Area)}}{\text{Wetted Perimeter}} \quad (11)$$

where Re is the Reynolds number, and Pr denotes the Prandtl number. $D_h$ is the hydraulic diameter. Flow area and wetted perimeter are the area and perimeter of the flowing cross-section, respectively.

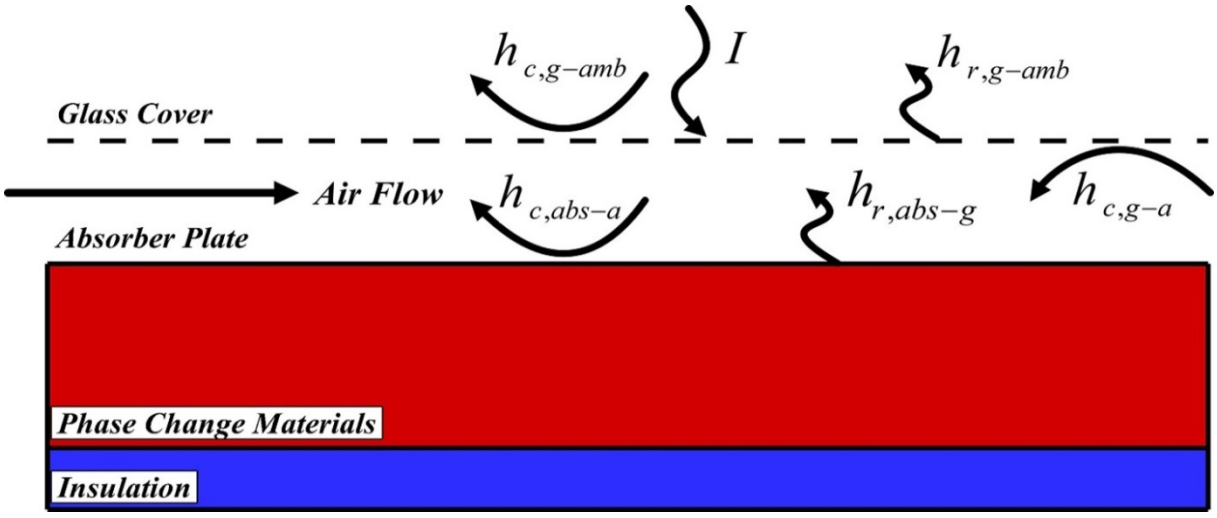


**Figure 3.** Schematic diagram of energy flow between collector elements

### 2.1. Phase change modeling

The analytical model used 60 kg paraffin as the latent heat storage unit based on the experimental setup. PCM energy content includes two main parts, including sensible and latent heat contents as follows:

$$E_{PCM} = E_{PCM,\,Sensible} + E_{PCM,\,Latent} \quad (12)$$

The latent heat content changes to the sensible heat content and vice versa in the charge/discharge process. Phase change modeling in the current study is based on the transient one-dimensional heat transfer equation that includes an internal heat source, given below [24]:

$$\rho_{PCM} c_{p,PCM} \frac{\partial T_{PCM}}{\partial t} = \frac{\partial}{\partial x}\left(k_{PCM} \frac{\partial T_{PCM}}{\partial x}\right) - \dot{Q} \quad (13)$$

Here, $\rho_{PCM}$,$c_{p,PCM}$ and $k_{PCM}$ denote the density, specific heat capacity, and thermal conductivity of phase change materials, respectively. $\dot{Q}$ is the internal heat source given below [24]:

$$\dot{Q} = \rho_{PCM} L_{f,PCM} \frac{\partial f_{PCM}}{\partial t} \quad (14)$$

where $L_{f,PCM}$ denotes the PCM latent heat and f is the molten mass fraction. By solving the phase change problem, the PCM molten mass fraction and temperature distribution in PCM were calculated at each time interval. The mathematical procedure to solve the phase change problem was comprehensively discussed in [24]. The thermophysical properties of PCM (paraffin wax) are represented in Table 2.

**Table 2.** Thermophysical properties of PCM [29]

| Material | Melting temperature (°C) | Latent heat (J/kg) | Thermal conductivity (W/m K) | Specific heat (J/kg K) | | Density (kg/m$^3$) | |
|---|---|---|---|---|---|---|---|
| Paraffin | 60 | 214400 | 0.21 | Liquid | Solid | Liquid | Solid |
| | | | | 3890 | 2940 | 775 | 850 |

The energy balance equations for the solar air heater and flowing air inside the collector in conjunction with the phase change problem were simultaneously solved by EES software in a trial and error procedure. Figure 4 shows the schematic diagram of the phase change problem and the associated boundary conditions. Using heat balance analysis for each element in the computational domain, we have:

$$q_{PCM,i} - q_{PCM,i+1} = \frac{dU_{PCM,i}}{dt} \qquad \text{for } i = 1,2,\dots,n-1 \qquad (15a)$$

$$q_{PCM,i} = k_{PCM} A_{PCM} \frac{(T_{PCM,i} - T_{PCM,i+1})}{l} \qquad (15b)$$

$$BC \begin{cases} Q_{st} = k_{PCM} A_{PCM} \dfrac{(T_{abs} - T_{PCM,1})}{l/2} \\ q_{PCM,n} = 0 \end{cases} \qquad (15c)$$

Here, U defines PCM internal energy. $k_{PCM}$ and $A_{PCM}$ are the thermal conductivity and surface area of the integrated PCM. q is the heat exchange rate at two adjacent node interfaces and l denotes the distance between two adjacent nodes. The initial temperature distribution through the PCM was assumed 30 °C. Here, $\frac{dU_{PCM,i}}{d_t}$ shows the thermal energy variation and is equal to:

$$\frac{dU_{PCM,i}}{dt} = m_{PCM} c_{p,s} \frac{dT_{PCM}}{dt} = m_{PCM} c_{p,s} (T^{t+1}_{PCM,i} - T^{t}_{PCM,i}) \qquad f = 0, \text{ for } T^{t}_{PCM,i} < T_m \qquad (16a)$$

$$\frac{dU_{PCM,i}}{dt} = m_{PCM} L_{PCM,f} \frac{df}{dt} = m_{PCM} L_{PCM,f} (f_i^{t+1} - f_i^{t}) \qquad 0 < f < 1, \text{ for } T^{t}_{PCM,i} = T_m \qquad (16b)$$

$$\frac{dU_{PCM,i}}{dt} = m_{PCM} c_{p,l} \frac{dT_{PCM}}{dt} = m_{PCM} c_{p,l} (T^{t+1}_{PCM,i} - T^{t}_{PCM,i}) \qquad f = 1, \text{ for } T^{t}_{PCM,i} > T_m \qquad (16c)$$

where $c_{p,s}$ and $c_{p,l}$ are the liquid and solid specific heat capacities of PCM, respectively. The PCM temperature in the ith node, $T_{PCM,i}$, was obtained at each time step based on its calculated heat content. It is worth noting that after and before the melting process, there was a linear relationship between the PCM temperature and its heat content for each node (Eqs. 16a and 16c). However, in the phase change process, the PCM temperature remained constant until the molten mass fraction reached one (16b). Equations (15) to (16) were simultaneously solved to obtain the PCM temperature and molten mass fraction. By solving the governing equations, outlet air and absorber plate temperatures, useful heat gain, and molten mass fraction were obtained.

Since the change in the PCM mass resulted in variations in the storage unit volume, only the PCM thickness would be altered to handle this problem, while the other two dimensions were constant. This issue caused the hydraulic and technical features of the modeled SAH such as absorber surface area and air channel cross-section which did not change in the different considered scenarios.

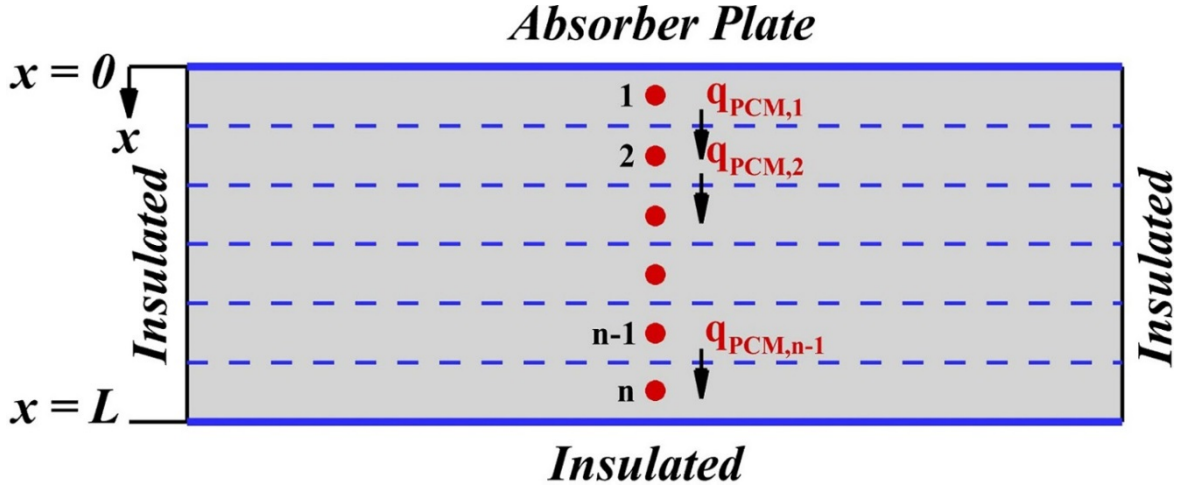


**Figure 4.** Schematic diagram of the phase change problem and the associated boundary conditions

## 2.2. Analytical model validation

Figure 5 shows a comparison of the measured and experimental data reported in [11] with the obtained analytical data by the developed model. As seen in Figure 5, there is good agreement between the experimental and analytical data. The percentage mean absolute error (PAME) was used to ensure the accuracy and validity of the analytical method. The PAME is described as follows [30]:

$$PAME = \frac{100}{n} \sum_{i=100}^{n} \left| \frac{T_{Analyt,i} - T_{Exp,i}}{T_{Exp,i}} \right| \qquad (17)$$

where $T_{Analyt,i}$ and $T_{Exp,i}$ are the $i^{th}$ analytical and experimental temperature values, while n denotes temperature values. The PAME is obtained 3.52 % for the set of measured and calculated outlet temperatures that illustrates the accuracy and preciseness of the obtained analytical data.

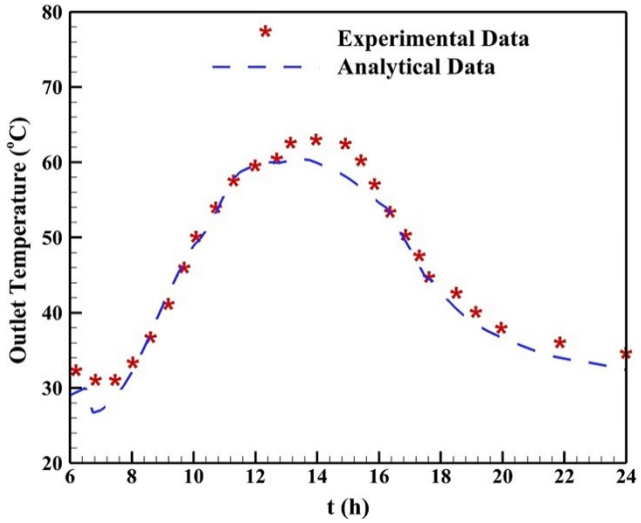


**Figure 5.** Comparison of available experimental data and obtained analytical data [11]

## 3. RESULTS AND DISCUSSION

The current study attempts to investigate the effects of PCM mass values on the heat dynamics and thermal performance of SAH using PCM blocks as thermal storage units. To this aim, an analytical model was then developed and validated using available experimental data to assess the effects of PCM mass vales on the thermal dynamics of the contracted SAHs. Since the change in the PCM mass resulted in the change in the storage unit volume, only the PCM thickness was altered to handle this problem, while the other two dimensions remained constant. This issue is the reason why the hydraulic and technical features of the modeled SAH, such as absorber surface area and air channel cross-section, did not change in the different considered scenarios.

Environmental conditions such as ambient air temperature and solar intensity can significantly affect the thermal performance of SAHs. Hence, these parameters were monitored and recorded during the experimental runs reported in [11]. Figure 6 represents these measured ambient factors. According to Fig. 6, the ambient air temperature was close to 12 °C at 6:00 and increased to 34 °C until 11:30. The air temperature then began to decrease to approximately 26 °C at 24:00. In the same trend, the solar intensity was zero W/m$^2$ at 6:00, increased to near 750 W/m$^2$ at 13:00, and then reduced to zero at 19:00.

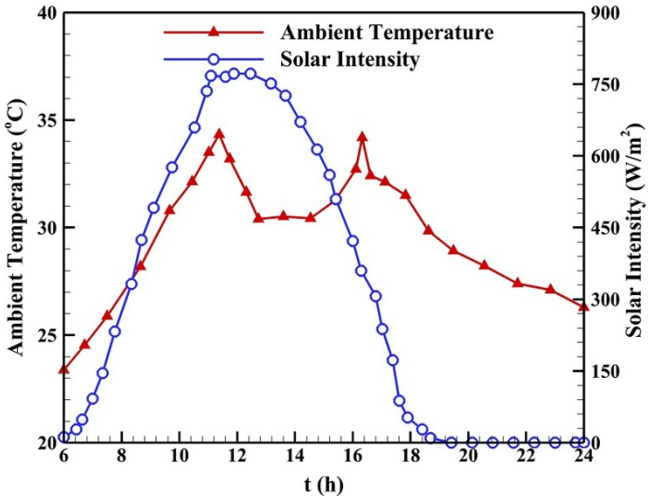


**Figure 6.** Measured ambient parameters during experimental runs [11]

The outlet temperature is a critical factor that determines the capability of the constructed collector to harvest solar energy. Simply put, the higher the outlet temperature, the higher the SAHs' thermal performance. The developed analytical model was utilized to obtain the heat dynamics and outlet temperature of the constructed SAH using different PCM masses. Figure 7 represents the outlet air temperature using the developed analytical model. As seen in Figure 7, by increasing the PCM mass, the maximum outlet temperature reduced, showing greater thermal energy stored in the PCM blocks instead of heating the flowing air. The maximum reduction in outlet temperature was near 20 °C as the PCM mass varied between 0 kg and 90 kg and occurred in the charging process at around 11:00.

When solar energy availability was not adequate to heat the flowing air, the PCM blocks started to discharge. Figure 7 shows that the SAH containing a higher mass of PCM had higher outlet air temperatures after the sunset. In better words, due to the higher mass of PCM, more thermal energy was stored and then, released during the periods when solar energy was absent. This issue helps the collector with a higher mass of PCM work for longer periods and extends the heating duration. However, Figure 7 shows that the outlet air temperature profiles for the SAHs using different PCM masses were close at the final hours. It is required to mention that a portion of stored thermal energy heated the flowing air, and the remaining portion was lost to ambient surroundings through convective/radiant heat exchange. The outlet temperature started to reduce in a steeper gradient by discharging the PCM blocks at the late operative time.

Comparison of the outlet air temperature profiles shows that in the SAHs with integrated PCMs, the discharging process began at 16:00 and continued until midnight. The temperature profile for the SAH without the storage unit had a steeper gradient after 16:00 when solar irradiation approached zero; therefore, input thermal energy was inadequate to heating the flowing air. The difference of maximum outlet temperature between the SAH with and without integrated PCMs reached up to near 12 °C. This issue shows the importance of using storage units during the periods when solar irradiation is insufficient.

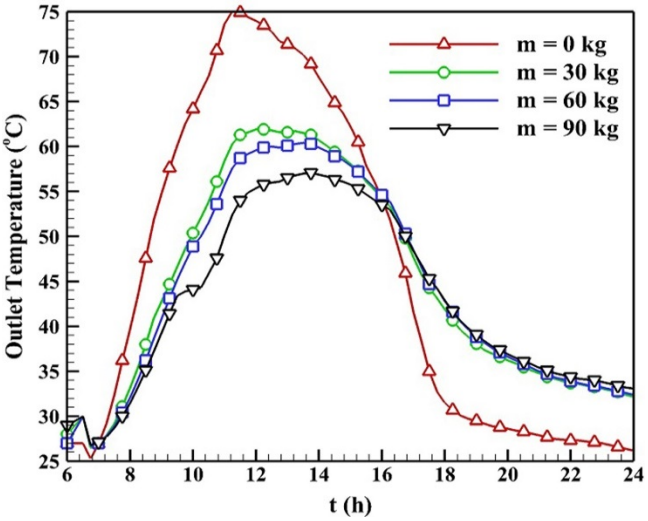


**Figure 7.** Comparison of outlet air temperature in different considered scenarios

Figure 8 provides an insight into the melting/solidification processes in different considered scenarios using molten mass fraction profiles. As shown in Figure 8, the melting process started at around 9:00 and continued until 18:00; then, the solidification process began. Due to the low thermal diffusivity of paraffin, the heat penetrated slowly into paraffin long after solar intensity peak. Therefore, the melting process continued until 18:00, when solar intensity was negligible. Before 9:00, the input solar energy increased the sensible heat content of the integrated PCM.

Although increasing the PCM mass reduced the mass fraction that melted in the charging process, it improved stored thermal energy. All PCM mass melted in the scenario using 30 kg and this value increased to near 85 kg in the scenario using 90 kg paraffin. In other words, increasing the PCM mass improves the thermal storage capability; this strategy extends the duration that SAHs can perform.

The large amount of PCM was still in the liquid phase at 24:00 according to Figure 8, especially in the SAHs with high PCM amounts, which implied that a large amount of energy

was still stored in PCM. Paraffin's low thermal conductivity resulted in the stored latent energy, which slowly heated the flowing air. This issue is shown in the outlet air temperature profiles. In fact, despite available stored latent energy, the outlet air temperatures in the SAHs using different amounts of PCM masses were so close in the last hours of experimental runs.

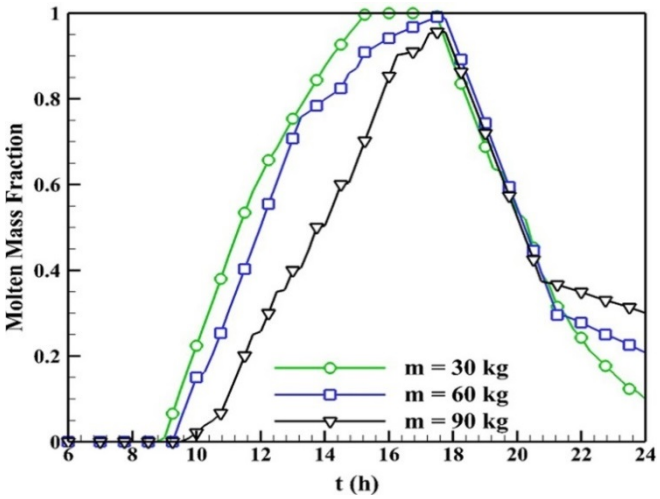


**Figure 8.** Comparison of charge/discharge process in different considered scenarios

Figure 9 represents the absorber temperature in the different considered scenarios. According to Figure 9, increasing the amount of PCM mass reduced the absorber plate temperature. By increasing the amount of PCM mass, higher absorbed thermal energy was consumed to melt PCM; hence, the absorber plate temperature decreased. This issue had an inherent advantage such as reducing the absorber plate temperature which in turn reduced heat losses in ambient environments.

After 18:00, the absorber plate temperature was reduced to 60 ºC, the PCM melting temperature. Therefore, the melting process stopped at 18:00, and the solidification process began. This crucial issue is illustrated in Figure 8, representing the melting/solidification process by the molten mass fraction profile.

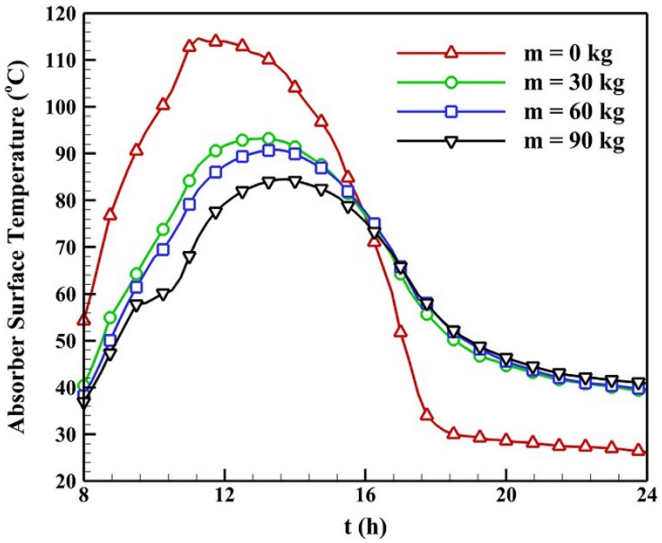


**Figure 9.** Comparison of absorber temperatures in different considered scenarios

Figure 10 represents the accumulated heat gains in different considered scenarios at each of two hours interval. As represented in Figure 10, heat gains in the SAHs with higher PCM masses are lower than those with lower PCM mass during the daytime. However, during the night, the SAH with the higher mass of PCM represents higher heat gains. This issue proves that the higher amount of PCM mass, the higher the stored energy. The stored energy released during the night and improved the thermal performance of SAHs. It is worth noting that a portion of stored thermal energy was lost due to convective/radiant heat exchange with ambient surroundings. The heat gains data are plotted at every time intervals (two hours).

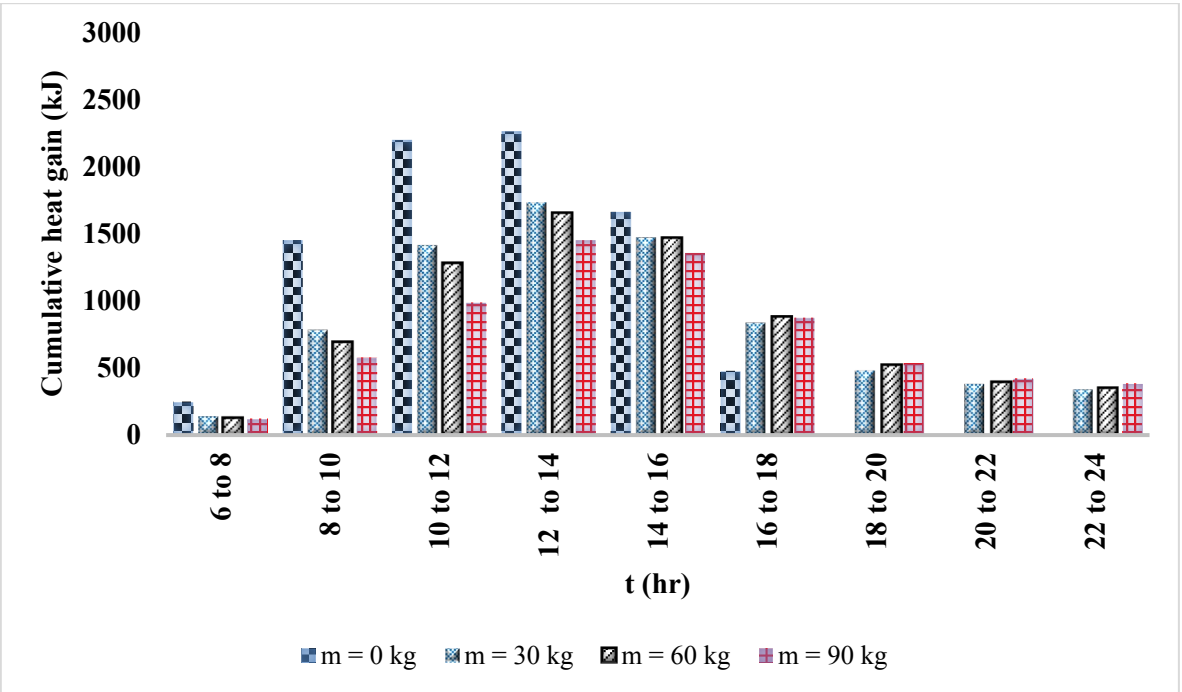


**Figure 10.** Comparison of accumulated heat gains in different considered scenarios at each of two hours interval

Assessing the daily thermal performance of an energy system is a feasible and useful approach to optimizing the crucial factor affecting the system's performance. In solar thermal systems, the daily thermal performance, $\eta_{Daily}$, is defined as the ratio of useful energy gain to received solar energy and given as:

$$\eta_{Daily} = \frac{\dot{m}c_p \int_{t_1}^{t_2} (T_{a,out} - T_{a,in}) dt}{A_t \int_{t_1}^{t_2} I dt} \quad (18)$$

Table 3 shows the daily thermal performance of the SAHs using different PCM masses. As represented in Table 3, the maximum daily thermal performance belongs to the SAH using 90 kg of PCM and the SAH without using PCM has the lowest thermal performance. By increasing the amount of integrated PCM mass, the SAH's thermal performance slightly improved. Indeed, increasing the PCM increased the stored thermal energy. However, a portion of this stored energy was lost by the absorber plate, SAH framework, and convective/radiant heat exchange with the surroundings. Therefore, the remaining part of the stored energy was consumed to heat the flowing air after the sunset.

**Table 3.** Daily thermal performance of SAH using different masses of PCM

| Scenario | Thermal performance |
|---|---|
| SAH without using | 19.16 % |
| SAH using 30 kg of PCM | 27. 01 % |
| SAH using 60 kg of PCM | 28.77 % |
| SAH using 90 kg of PCM | 33.65 % |

## 4. CONCLUSIONS

SAHs with integrated PCMs have been extensively in domestic and industrial applications due to their simple technical structure, low-cost operation and maintenance, and acceptable performance. The current study investigates the effects of PCM mass value on the heat dynamics and thermal performance of SAHs. An analytical model was developed to this aim and validated by available experimental data. The obtained results illustrate that by increasing the PCM mass from zero to 90 kg, the stored thermal energy increased. The stored thermal energy released during nighttime hours and extended the heating process. However, by increasing the PCM mass, the maximum obtained outlet air and absorber plate temperatures were reduced by near 20 ºC and 35 ºC, respectively. Indeed, the thermal energy that could heat the flowing air was consumed to increase the PCM heat content. Interestingly, the thermal performance improved by increasing the PCM mass from zero to 90 kg by almost 14.5 %. The obtained results showed that despite available latent thermal energy at 24:00, the outlet air temperature profiles for the SAHs using PCM were close due to the low thermal conductivity of paraffin.

## 5. ACKNOWLEDGEMENT

The authors would like to thank the Sirjan University of Technology and the Higher Education Complex of Bam for their supports.

## NOMENCLATURE

| | |
|---|---|
| $A_c$ | Collector surface area ($m^2$) |
| $c_p$ | Specific heat (J/kg.K) |
| E | Energy (J) |
| h | Enthalpy (J) |
| $h_w$ | Wind velocity (m/s) |
| I | Solar irradiation heat flux ($W/m^2$) |
| l | Distance between two adjacent nodes (m) |
| $N_g$ | Glass number |
| $\dot{m}$ | Mass flow rate (kg/s) |
| PAME | Percentage mean absolute errors |
| q | Heat exchange rate at two adjacent node interfaces (W) |
| $Q_u$ | Useful energy gain (W) |
| r | Equivalent thermal energy |
| S | Absorbed solar intensity ($W/m^2$) |
| T | Temperature (ºC) |
| U | Internal energy (J) |
| $U_L$ | Heat loss coefficient ($W/m^2.K$) |
| $U_t$ | Top heat loss coefficient ($W/m^2$) |
| V | Wind velocity (m/s) |
| w | Uncertainty |
| **Greek letters** | |
| β | Tilt angle |
| ε | Emissivity |
| η | Efficiency |
| τα | Transmittance-absorptance product |
| **Superscripts** | |
| t | Time step |
| **Subscripts** | |
| a | Air |
| abs | Absorber plate |
| Analyt | Analytical |
| cv | Control volume |
| Exp | Experimental |
| in | Inlet |
| out | Outlet |

## REFERENCES

1. Bayati, N., Baghaee, H.R., Hajizadeh, A. and Soltani, M., "Localized protection of radial DC microgrids with high penetration of constant power loads", ***IEEE Systems Journal***, (2020), 1-12. (https://doi.org/10.1109/JSYST.2020.2998059).
2. Daghigh, R. and Shafieian, A., "Thermal performance of a double-pass solar air heater", ***Journal of Renewable Energy and Environment (JREE)***, Vol. 3, No. 2, (2016), 35-46. (https://doi.org/10.30501/jree.2016.70083).
3. Kabeel, A. and Abdelgaied, M., "Solar energy assisted desiccant air conditioning system with PCM as a thermal storage medium", ***Renewable Energy***, Vol. 122, (2018), 632-642. (https://doi.org/10.1016/j.renene.2018.02.020).
4. Patel, J., Shukla, D., Raval, H. and Mudgal, A., "Experimental evaluation of the performance of latent heat storage unit integrated with solar air heater", ***International Journal of Ambient Energy***, (2019), 1-9. (https://doi.org/10.1080/01430750.2019.1636862).
5. SunilRaj, B. and Eswaramoorthy, M., "Experimental study on hybrid natural circulation type solar air heater with paraffin wax based thermal storage", ***Materials Today: Proceedings***, Vol. 23, (2020), 49-52. (https://doi.org/10.1016/j.matpr.2019.06.381).
6. Charvát, P., Klimeš, L. and Ostrý, M., "Numerical and experimental investigation of a PCM-based thermal storage unit for solar air systems", ***Energy Buildings***, Vol. 68, (2014), 488-497. (https://doi.org/10.1016/j.enbuild.2013.10.011).

7. Shalaby, S., Bek, M. and El-Sebaii, A., "Solar dryers with PCM as energy storage medium: A review", ***Renewable Sustainable Energy Reviews***, Vol. 33, (2014), 110-116. (https://doi.org/10.1016/j.rser.2014.01.073).
8. Bouadila, S., Lazaar, M., Skouri, S., Kooli, S. and Farhat, A., "Energy and exergy analysis of a new solar air heater with latent storage energy", ***International Journal of Hydrogen Energy***, Vol. 39, (2014), 15266-15274. (https://doi.org/10.1016/j.ijhydene.2014.04.074).
9. Salih, S.M., Jalil, J.M. and Najim, S.E., "Experimental and numerical analysis of double-pass solar air heater utilizing multiple capsules PCM", ***Renewable Energy***, Vol. 143, (2019), 1053-1066. (https://doi.org/10.1016/j.renene.2019.05.050).
10. Navarro, L., de Gracia, A., Castell, A. and Cabeza, L.F., "Experimental study of an active slab with PCM coupled to a solar air collector for heating purposes", ***Energy Buildings***, Vol. 128, (2016), 12-21. (https://doi.org/10.1016/j.enbuild.2016.06.069).
11. El Khadraoui, A., Bouadila, S., Kooli, S., Guizani, A. and Farhat, A., "Solar air heater with phase change material: An energy analysis and a comparative study", ***Applied Thermal Engineering***, Vol. 107, (2016), 1057-1064. (https://doi.org/10.1016/j.applthermaleng.2016.07.004).
12. Jain, D. and Tewari, P., "Performance of indirect through pass natural convective solar crop dryer with phase change thermal energy storage", ***Renewable Energy***, Vol. 80, (2015), 244-250. (https://doi.org/10.1016/j.renene.2015.02.012).
13. Ghiami, A., Kianifar, A., Aryana, K. and Edalatpour, M., "Energy and exergy analysis of a single-pass sequenced array baffled solar air heater with packed bed latent storage unit for nocturnal use", ***Heat Transfer-Asian Research***, Vol. 46, (2017), 546-568. (https://doi.org/10.1002/htj.21230).
14. Ghiami, A. and Ghiami, S., "Comparative study based on energy and exergy analyses of a baffled solar air heater with latent storage collector", ***Applied Thermal Engineering***, Vol. 133, (2018), 797-808. (https://doi.org/10.1016/j.applthermaleng.2017.11.111).
15. Khan, Z., Khan, Z. and Ghafoor, A., "A review of performance enhancement of PCM based latent heat storage system within the context of materials, thermal stability and compatibility", ***Energy Conversion Management***, Vol. 115, (2016), 132-158. (https://doi.org/10.1016/j.enconman.2016.02.045).
16. Moradi, R., Kianifar, A. and Wongwises, S., "Optimization of a solar air heater with phase change materials: Experimental and numerical study", ***Experimental Thermal Fluid Science***, Vol. 89, (2017), 41-49. (https://doi.org/10.1016/j.expthermflusci.2017.07.011).
17. Arfaoui, N., Bouadila, S. and Guizani, A., "A highly efficient solution of off-sunshine solar air heating using two packed beds of latent storage energy", ***Solar Energy***, Vol. 155, (2017), 1243-1253. (https://doi.org/10.1016/j.solener.2017.07.075).
18. Abuşka, M., Şevik, S. and Kayapunar, A., "Experimental analysis of solar air collector with PCM-honeycomb combination under the natural convection", ***Solar Energy Materials Solar Cells***, Vol. 195, (2019), 299-308. (https://doi.org/10.1016/j.solmat.2019.02.040).
19. Abuşka, M., Şevik, S. and Kayapunar, A., "A comparative investigation of the effect of honeycomb core on the latent heat storage with PCM in solar air heater", ***Applied Thermal Engineering***, Vol. 148, (2019), 684-693. (https://doi.org/10.1016/j.applthermaleng.2018.11.056).
20. Raj, A., Srinivas, M. and Jayaraj, S., "A cost-effective method to improve the performance of solar air heaters using discrete macro-encapsulated PCM capsules for drying applications", ***Applied Thermal Engineering***, Vol. 146, (2019), 910-920. (https://doi.org/10.1016/j.applthermaleng.2018.10.055).
21. Jawad, Q.A., Mahdy, A.M., Khuder, A.H. and Chaichan, M.T., "Improve the performance of a solar air heater by adding aluminum chip, paraffin wax, and nano-SiC", ***Case Studies in Thermal Engineering***, (2020), 100622. (https://doi.org/10.1016/j.csite.2020.100622).
22. Sudhakar, P. and Cheralathan, M., "Encapsulated PCM based double pass solar air heater: A comparative experimental study", ***Chemical Engineering Communications***, (2019), 1-13. (https://doi.org/10.1080/00986445.2019.1641701).
23. Reddy, S.S., Soni, V. and Kumar, A., "Diurnal thermal performance characterization of a solar air heater at local and global scales integrated with thermal battery", ***Energy***, Vol. 177, (2019), 144-157. (https://doi.org/10.1016/j.energy.2019.04.017).
24. Charvát, P., Klimeš, L. and Ostrý, M., "Numerical and experimental investigation of a PCM-based thermal storage unit for solar air systems", ***Energy and Buildings***, Vol. 68, (2014), 488-497. (https://doi.org/10.1016/j.enbuild.2013.10.011).
25. Summers, E.K. and Antar, M.A., "Design and optimization of an air heating solar collector with integrated phase change material energy storage for use in humidification–dehumidification desalination", ***Solar Energy***, Vol. 86, (2012), 3417-3429. (https://doi.org/10.1016/j.solener.2012.07.017).
26. Leoni, N. and Amon, C., "Thermal design for transient operation of the TIA wearable computer", ***Proceedings of ASME InterPack***, Vol. 2, (1997), 2151-2161.
27. Kalogirou, S.A., Solar energy engineering: Processes and systems, Academic Press, (2013). (https://www.elsevier.com/books/solar-energy-engineering/kalogirou/978-0-12-397270-5).
28. Duffie, J.A. and Beckman, W.A., Solar engineering of thermal processes, fourth edition, John Wiley & Sons, (2013). (https://www.sku.ac.ir/Datafiles/BookLibrary/45/John%20A.%20Duffie,%20William%20A.%20Beckman(auth.)-Solar%20Engineering%20of%20Thermal%20Processes,%20Fourth%20Edition%20(2013).pdf).
29. Enibe, S., "Thermal analysis of a natural circulation solar air heater with phase change material energy storage", ***Renewable Energy***, Vol. 28, (2003), 2269-2299. (https://doi.org/10.1016/S0960-1481(03)00071-5).
30. O'Hegarty, R., Kinnane, O. and McCormack, S.J., "Concrete solar collectors for façade integration: An experimental and numerical investigation", ***Applied Energy***, Vol. 206, (2017), 1040-1061. (https://doi.org/10.1016/j.apenergy.2017.08.239).

JREE: Vol. 8, No. 3, (Summer 2021) 54-67

Journal of Renewable Energy and Environment

Journal Homepage: www.jree.ir

Research Article

# Assessment of Optimum Renewable Energy System for the Somalia–Turkish Training and Research Hospital in Mogadishu

Sibel Dursun [a], Ercan Aykut [b], Bahtiyar Dursun [c*]

[a] *Branch of Physics, Capa Final Anatolian High School, P. O. Box: 34093, Istanbul, Turkey.*
[b] *Department of Electrics, Gelisim Vocational School, Istanbul Gelisim University, P. O. Box: 34310, Istanbul, Turkey.*
[c] *Department of Electrical-Electronics Engineering, Fatih Sultan Mehmet Vakif University, P. O. Box: 34421, Istanbul, Turkey.*

*PAPER INFO*

*Paper history:*
Received 20 October 2020
Accepted in revised form 19 May 2021

*Keywords*:
Somalia,
Renewable Power Generating System,
Hospital,
Environmental Assessment,
Hybrid Systems,
Renewable Energy

*ABSTRACT*

Somalia–Turkish Training and Research Hospital in Mogadishu, is only powered by diesel generator currently. In this paper, the energy demand of this hospital is utilized by determining the optimum hybrid renewable energy generating system. By HOMER, a sensitivity analysis has been made with emphasis on three significant variables such as average wind speed, present diesel price, and solar radiation. From the results, it can be said that an optimum system is the standalone wind-diesel-battery storage Hybrid Renewable Energy System (HRES) with the configuration of 1,000 kW wind turbine, 350 kW diesel generator, 250 kW power converters, and 300 batteries. Additionally, the net present cost of the optimum system is calculated to be $5,056,700 and its cost of energy is estimated to be 0.191 $/kWh. The present cost of energy for Somalia is 0.5 $/kWh. This shows that the energy cost for the proposed HRES is cheaper than the conventional one. Lastly, according to the results, it is clear that the wind–diesel–battery storage HRES seems more environment friendly than other HRESs.

https://doi.org/10.30501/jree.2021.245232.1140

## 1. INTRODUCTION

Somalia is an African country in the east of Africa neighboring Kenya, Ethiopia, and the Republic of Djibouti. Somalia's weather is mostly warm and dry over the year. According to the energy statistics, it is the most advantageous country among other African countries by means of both conventional and renewable energy potentials. These potentials can be exploited through coordination with and regulations by Somalian government. Since Somalia has abundant renewable energy sources like solar energy, wind energy, and biomass energy, these sources can be used in both residential and industrial applications. Besides, it has a high potential for geothermal and wave energy sources. Although Juba and Shebelle rivers have the potential for hydropower production, nowadays, they are not being used efficiently. Wind, biomass, and solar-based renewable energy sources can be utilized by means of tolerable capital investment with current technology [1]. By expanding the use of grid-supplied hybrid consisting of both conventional and renewable energy sources and transmitting them to rural areas, welfare, productivity, and security will ensue [2]. Many companies supply their energy needs by either grid or diesel generators in Mogadishu, capital of Somalia. Diesel generators have intensively been used, especially for companies, hospitals, schools, etc. because grid is more expensive than diesel. The intensive use of diesel generators has emitted harmful gases into the atmosphere and increasingly polluted the environment and caused climate change in Mogadishu. Difficulties caused by environmental pollution and climate change can diminish employing renewable and alternative power generating systems such as fuel cells and hydrogen instead of diesel generators [3-5]. Nowadays, using renewable energy resources as a power supplier in an energy system instead of conventional ones has been more popular. The system including at least two or more power supplier is defined as a hybrid energy system. Such systems not only produce less harmful emission gases and are less dependent on fossil fuels but also need no grid connection like the conventional ones [6]. They are rather useful alternative ways to supply electricity demand to the remote and isolated places from city center when extending the gridline, which is comparatively more expensive. Besides, they can be used in the system to generate all or any given portion of the electricity demand depending on location, regional renewable energy potential, and green structure of the hybrid system. Hybrid systems must be applied with the support of an auxiliary power supplier such as a diesel generator because of their instable and discontinuous nature. Usually, diesel generators are used in the electrification of the isolated or remote consumers. As an alternative solution, hybrid energy systems can be proposed for diesel generators.

*Corresponding Author's Email: bdursun@fsm.edu.tr (B. Dursun)
URL: http://www.jree.ir/article_130748.html

Please cite this article as: Dursun, S., Aykut, E. and Dursun, B., "Assessment of optimum renewable energy system for the Somalia–Turkish training and research hospital in Mogadishu", ***Journal of Renewable Energy and Environment (JREE)***, Vol. 8, No. 3, (2021), 54-67. (https://doi.org/10.30501/jree.2021.245232.1140).

HRESs should be preferred over diesel generators in isolated places. There are many studies in the literature related to the renewable HRES applications and their design, optimization, and parametric analysis. However, although there are many studies about HRESs, there are only few on Africa. Some of the conducted studies on Africa are summarized below. Pemndje et al. determined and compared the cost of energy of various hybrid systems for several off-grid facilities in North and Far North regions of Cameroon by integrating renewable sources and/or storage with diesel generators [7]. Orosz et al. evaluated health and education by means of techno-economic aspect for Sub-Saharan Africa. Using the meteorological data supplied by NASA, they compared conventional PV and diesel systems with micro-concentrating solar power and other related technology [8]. Malik presented a research to determine the renewable energy potential of Brunei Darussalam. He put forth the existence of renewable energy sources that could be applied in Brunei [9]. Ajao et al. evaluated off-grid and grid-connected HRES options for University of Ilorin in Nigeria using HOMER software [10]. Moreover, Himri et al. assessed techno-economic aspect of non-grid hybrid energy generation systems for a location in south west of Algeria. In that study, they evaluated the energy production, life-cycle costs, and greenhouse gas emission reduction using HOMER software [11]. Gholami et al. investigated the feasibility of renewable energy harvesting to meet the energy need of a dairy farm in Shahroud, Iran. HOMER software was used to determine the optimum system configuration. It was shown that although there was wind potential within the farm site, the most economical system would be a system consisting of a 100 kW biomass power plant and a 169 kW PV plant [12]. Nfah suggested the optimal photovoltaic hybrid systems for remote villages in Far North Cameroon using a recent iterative optimization method based on the desired annual number of generator working hours and the net present value technique [13]. Similarly, using HOMER software, Nfah et al. modeled solar/diesel/battery HRES for the electrification of typical rural households and schools in remote areas of the far north province of Cameroon [14]. Olatomiwa et al. studied the feasibility of different power generation configurations for different locations within the geo-political zones of Nigeria [15]. Lastly, Olatomiwa determined the optimal configurations of the HRES for rural health clinic application in three grid-unconnected rural villages in Nigeria [16]. Somalia–Turkish Training and Research Hospital in Mogadishu is currently only powered by diesel generator. In this paper, the energy demand of this hospital is supplied by determining the optimum hybrid power renewable generating system. Therefore, numerous HRESs in different configurations of wind turbines, PV panels, diesel generators, and battery banks are taken into account. Moreover, considering the significant data such as solar irradiation, wind speed, and diesel price, sensitivity analysis is conducted. Then, the optimum HRES is determined and at last, the optimum system is also investigated by means of its emitting gases such as $CO_2$, CO, $NO_x$, $CH_4$ and $SO_x$. These are air polluting and threatening gases. Finally, a hospital, presently fed by only diesel generators, is analyzed by means of techno-economical-environmental parameters if the energy is replaced by the hybrid renewable sources. This is the first attempt to use renewable energy for hospitals in Africa.

## 2. DESCRIPTION OF SOMALIA–TURKISH TRAINING AND RESEARCH HOSPITAL IN MOGADISHU

### 2.1. Location and population

Mogadishu is the capital of Somalia and it is the largest city with a population of 2,425,000. Somalia–Turkish Training and Research Hospital in Mogadishu has a 200-bed capacity. It is characterized by 2º 2" North latitude and 45º 18" East longitudes. The hospital has an approximate area of 13,500 $m^2$ with an indoor space that includes 12 intensive care beds, 14 newborn intensive care beds, 20 incubators, four operating rooms, a delivery room, as well as radiology and laboratory units. It is in service for the Somalian people since 2015. The location of the Somalia–Turkish Training and Research Hospital in Mogadishu is shown in Figure 1 [17].


**Figure 1.** The location of the Somalia–Turkish Training and Research Hospital in Mogadishu [18]

### 2.2. Energy demand of the hospital and electrification

Energy demand of the hospital is presently met by diesel generators. The average hourly load profile data are measured by technical department of the hospital. The load data are used in this paper after arranging the collected data into the monthly category for a whole year period (2017-2018). The electrical load demand is obtained from Somalia–Turkish Training and Research Hospital in Mogadishu [17]. Total energy demand of the hospital is provided by four diesel generators with a capacity of three 800 kVA and one 1,100 kVA systems. For the load data, the average daily energy demand of the hospital is around 8,000 kWh. The minimum demand load of the hospital is consumed between 22:00 and 08:00. The minimum load demand is about 200 kWh, whereas the maximum load demand is about 550 kWh. Since the climate of Mogadishu is dry, the load demand has increased by about 15 % because of air conditioning in winter. Load profile of the hospital is given in Figure 2. While the minimum load demand is about 140 kWh between June and August, maximum load demand is about 480 kWh. The data chart of the load demand is shown in Figure 3. In the figure, the breakdown of the yearly data series can be seen and accordingly, day-to-day change rate is 4 %. The 5 % time-step randomness shows variation in electric energy consumption of the hospital.

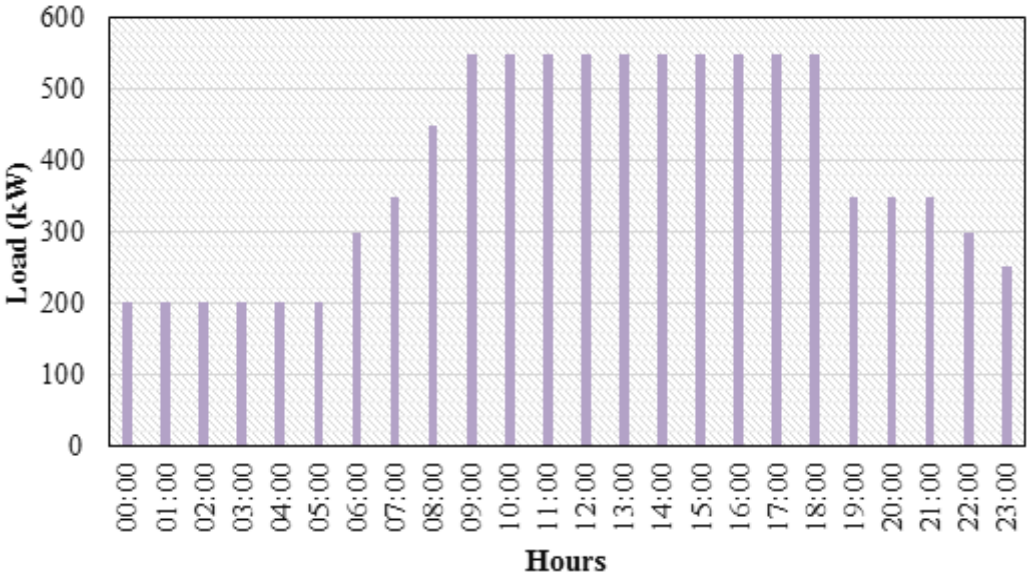


**Figure 2.** Load profile of the Hospital [17]

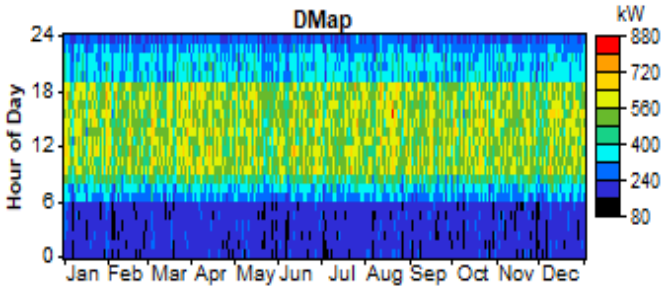


**Figure 3.** Data chart of electrical load of the hospital [17]

### 2.3. Available renewable energy resources assessment

#### 2.3.1. Wind speed

The wind speed data for Somalia–Turkish Training and Research Hospital in Mogadishu is evaluated. The average hourly wind speed data between the years 2015 and 2017 was measured at 10 m, 30 m, and 50 m higher than the surface of sea level, as shown in Figure 4 [19].

$$V_{ave} = \left( \frac{\sum_{i=1}^{n} f_i V_i}{\sum_{i=1}^{n} f_i} \right) \quad (1)$$

where $V_{ave}$ is the average wind speed (m/s), $f_i$ is frequency, and $V_i$ is mean wind speed m/s. According to Equation (1), the average wind speed is calculated at 5.63 m/s. Taking the wind speed data into account, it can be mentioned that the distribution of wind speed changes between 3.58 m/s and 7.26 m/s as the average wind speed of the region is about 5.63 m/s. While the highest wind speed occurs in July, the least wind speed appears in April. The parameter weibull k is calculated as 1.71.

#### 2.3.2. Solar radiation

In Figure 5, Somalia's solar irradiation map is presented which shows the average yearly solar energy per square meter [20].

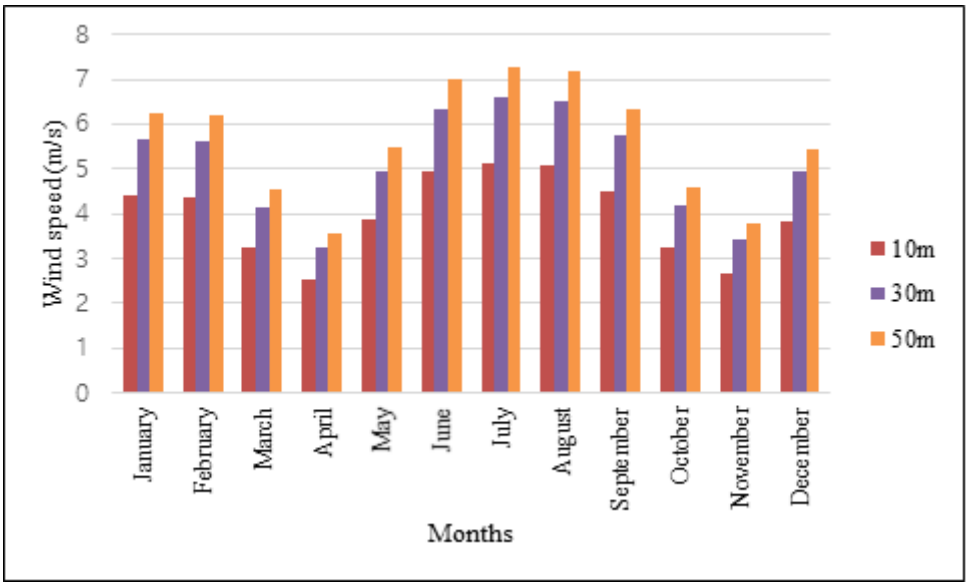


**Figure 4.** The monthly wind speed data in Mogadishu, Somalia [19]

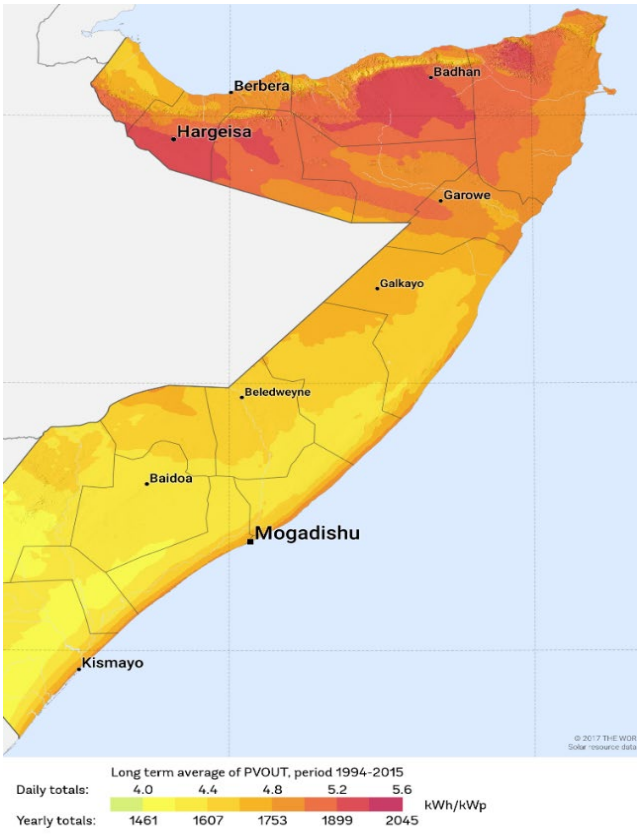


**Figure 5.** Global Horizontal Irradiation (GHI) of Somalia (kWh/m$^2$) [20]

In the figure, the area shown with red corresponds to high solar irradiation values. It means it has the highest solar energy potential. Since most of the locations of Somalia are exposed to high solar irradiation level, they are appropriate for generating electricity from solar energy. Sunlight radiation data of the location are achieved by HOMER from the database of NASA Surface Meteorology and Solar Energy [19]. For coordinates in HOMER, 2º 2˝ North latitude and 45º 18" East longitudes are used. These are the coordinates of Somalia–Turkish Training and Research Hospital in Mogadishu. Sunlight radiation data are synthesized for each 8,760 hours of the whole year by means of Graham algorithm, as a result of which hourly data are generated. The algorithm is very simple to use since it needs monthly averages and latitudes. The processed data show the realized day-to-day and hour-to-hour models. Monthly average solar radiation value is given in Figure 6. The annual average sunlight radiation value and the average clearness index are calculated as 5.645 kWh/m$^2$/d and 0.565, respectively. As shown in Figure 6, the monthly average daily solar radiation ranges from 3.26 to 7.61 kWh/m$^2$/d [21].

### 2.3.3. Diesel

Diesel price is about 1 $/kWh in Mogadishu–Somalia. Somalia government plans to cancel the support on type of

petrol and diesel, meaning that the price of diesel may fluctuate intensively between 0.75 $/l and 1.3 $/l in the last six months of 2017. Therefore, diesel prices vary between 0.75 $/l and 2.5 $/l with an increment of 0.5 in the HOMER simulation to evaluate its effect on the system cost.

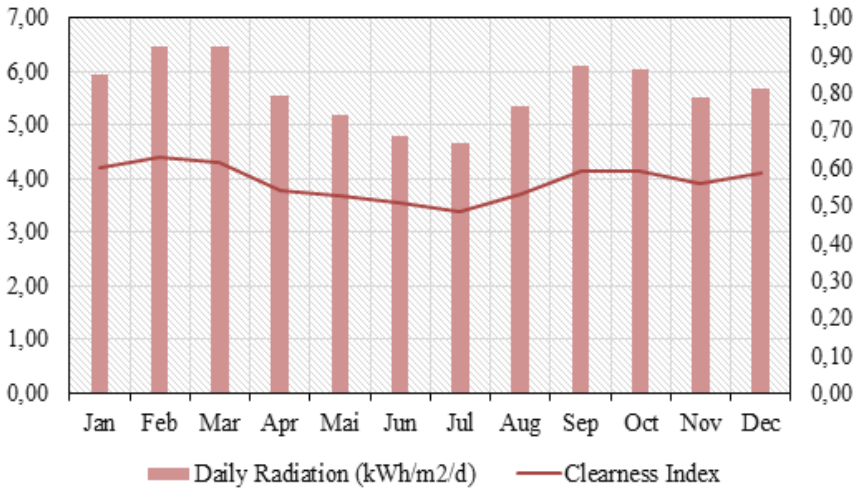


**Figure 6.** Monthly average solar radiation value of the hospital [21]

## 3. TECHNO-ECONOMIC ANALYSIS

### 3.1. Estimation of the annual real interest rate for Somalia

Annual real interest rate is a significant input parameter of HOMER in techno-economic analysis. The relation between annual real interest rate and nominal interest rate is shown in Equation (2):

$$i=\frac{i_0-f}{1+f} \tag{2}$$

where i corresponds to the real interest rate, $i_0$ the nominal interest rate which means the rate at which one can get a loan, and f the annual inflation rate. According to the previous year data, annual inflation rates $i_0$ = 6.09 % and f=3.22 % are used for Somalia. The real interest rate is estimated at 44.8 % using Equation (3) [22-24].

$$i=\frac{i_0-f}{1+f}=0.448 \qquad i=44.8\% \tag{3}$$

In the simulation process, the real interest rate is calculated at 44.8%.

### 3.2. Levelized Cost of Energy (CoE)

The average cost per energy of the generated energy is defined as CoE and can be estimated by Equation (4).

$$CoE=\frac{C_{a,t}}{E_{p,AC}+E_{p,DC}+E_{g,s}} \tag{4}$$

Total annual cost is defined as the summation of the cost of each system components and other yearly costs. It is used in the estimation of both levelized CoE and total NPC. Therefore, this parameter is very momentous [23, 24].

### 3.3. Net Present Cost (NPC)

NPC is the essential economic indicator of the HOMER software. It is defined as the current value of the cost of establishing and running any power system within the life cycle of the project, called as the life cycle cost. In this paper, the proposed life cycle of the project is assumed to be 20 years. For the calculation of NPC, all the systems are sorted and in order to find the NPC, all of other economic outputs are estimated. NPC can be calculated by Equation (5) [23].

$$NPC=\frac{C_{a,t}}{CRF(i,R_p)} \tag{5}$$

CRF is defined as the ratio used for the estimation of the current value of an annuity and presented in Equation (6).

$$CRF(i,N)=\frac{i(1+i)^N}{(1+i)^N-1} \tag{6}$$

As mentioned before, the lifecycle of the project is assumed to be 20 years. The annual real interest rate is 3.22 % for Somalia. It must be taken into account that Somalia government does not promote the installation energy [22]. Details of cost and technical information of the essential components of HRES are presented below.

## 4. COMPONENTS OF THE HYBRID SYSTEM AND ITS COMPONENTS

The energy demand of the hospital has been supplied by diesel generators with a total power capacity of 3,500 kVA since the hospital started serving Somalia's people. As an alternative solution to this situation, a HRES consisting mainly of PV panels, wind turbines, diesel generator, batteries, and converter is proposed. All components of both only diesel generator and proposed HRES are shown in Figures 7(a) and 7(b). Some parameters such as size, capital cost, quantity, replacement cost, operation, and maintenance cost for the hybrid system are determined according to the references and presented in detail in Table 1.

Table 1 shows technical and economic parameters for components of the suggested HRES. The replacement cost is the cost of renewing a component after it breaks down. This cost may be different from the starting cost since not all of the components require renewing at the end of their lifetime period.

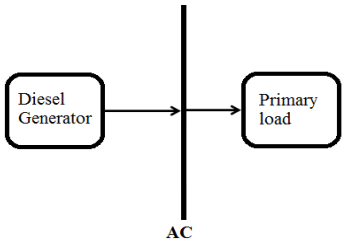


(a) Diesel power generating system

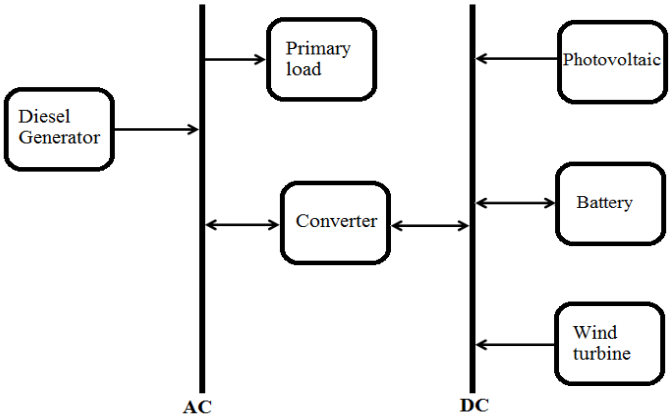


(b) HRES

**Figure 7.** Descriptions of HRES and Diesel energy system

**Table 1.** Technical and economic parameters for components of the suggested HRES

| Descriptions | Specifications |
|---|---|
| **PV Panel** | |
| PV model | Sonali Solar S-300W PV panel [25] |
| Power (kW peak) | 750 kWp |
| Starting cost | 7,000 $/kW |
| Replacement cost | 6,000 $/kW |
| Operational and maintenance cost | 15 $/year |
| Lifetime | 25 years |
| **Wind turbine** | |
| Wind turbine model | Fuhrlander 250 kW |
| Rated power | 250 kW |
| Starting cost | $480,000 |
| Replacement cost | $480,000 |
| Operational and maintenance cost | 480 $/year |
| Lifetime | 25 years |
| **Diesel generator** | |
| Turbine model | AKSA AC 350 Diesel Generator [26] |
| Rated power | 350 kW |
| Starting cost | $30,260 or 116,500 TL |
| Replacement cost | $24,208 or 92,716 TL |
| Operational and maintenance cost | 0.030 $/h |
| Lifetime | 15,000 operating hours |
| **Inverter** | |
| Inverter model | Solectria SGI 250 [27] |
| Rated power | 250 kW |
| Starting cost | 655 $/kW |
| Replacement cost | 655 $/kW |
| Operational and maintenance cost | 10 $/year |
| Lifetime | 15 years |
| Efficiency | 95 % |
| **Battery bank** | |
| Battery model | Surrette 6CS25P [28] |
| Starting cost | $400 |
| Replacement cost | $300 |
| Operational and maintenance cost | 10 $/year |
| Lifetime | 15 |

### 4.1. PV panel

The peak power demand of the hospital is about 656 kWp and the sizing of PV panel is determined at 20 % more than the peak power demand. Therefore, the sizing of the PV panel is selected as 750 kWp in case it supplies the demand load of the hospital. If the demand is met by the PV panel, then the rest of its energy is stored in the battery bank. Since the proposed hybrid system is a combination of PV panels, wind turbines, and diesel generators, the size of the PV panel changes from 250 kWp to 1,500 kWp with an increment of 250 kWp to determine the effect of the economic cost of the HRES. The proposed PV panel is a 72-cell polycrystalline whose output power is 300 Wp. The model of PV panel is Sonali Solar S-300W. There are 2,500 PV panels connected in series to generate 750 kWp. Costs and other technical information data of the PV panels can be found in Table 1 in detail [25-29].

### 4.2. Wind turbine

In Mogadishu–Somalia, another significant energy source is wind energy. Therefore, it is one of the essential load suppliers of the proposed system. Wind energy is mainly converted to other energy types by means of wind turbines. In the proposed system, wind turbines with 250 kW power will be used. Among the five different brand and model wind turbines with the same output power, the optimum one will be chosen and used in the proposed system [30-34]. Power charts of the different model wind turbines can be seen in Figures 8-12.

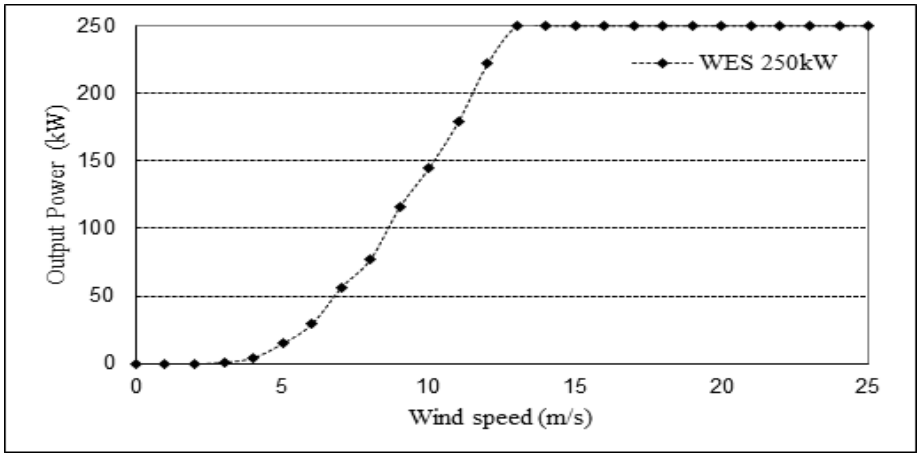


**Figure 8.** Power charts of WES 250 kW wind turbine [30]

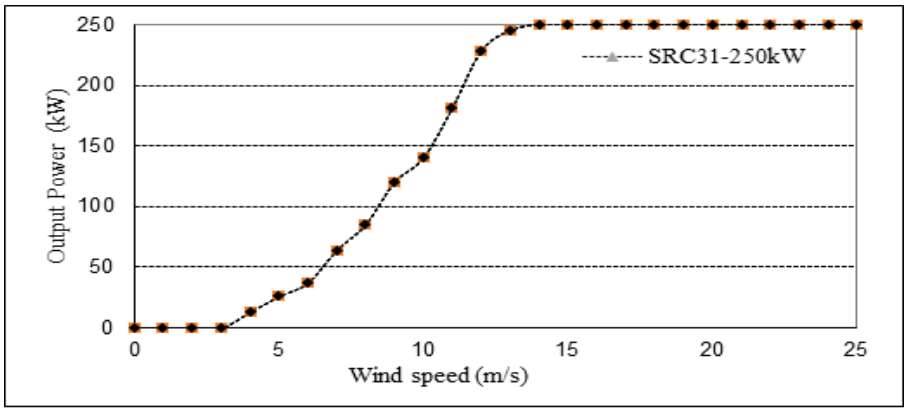


**Figure 9.** Power charts of SRC31-250 kW wind turbine [31]

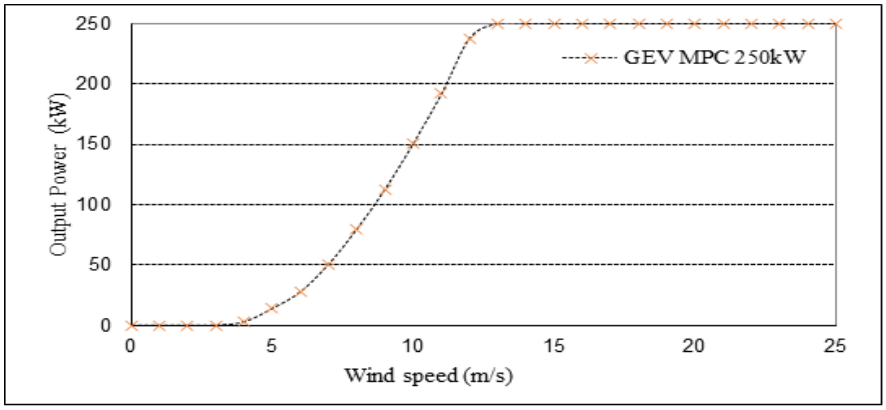


**Figure 10.** Power charts of GEV MPC 250 kW wind turbine [32]

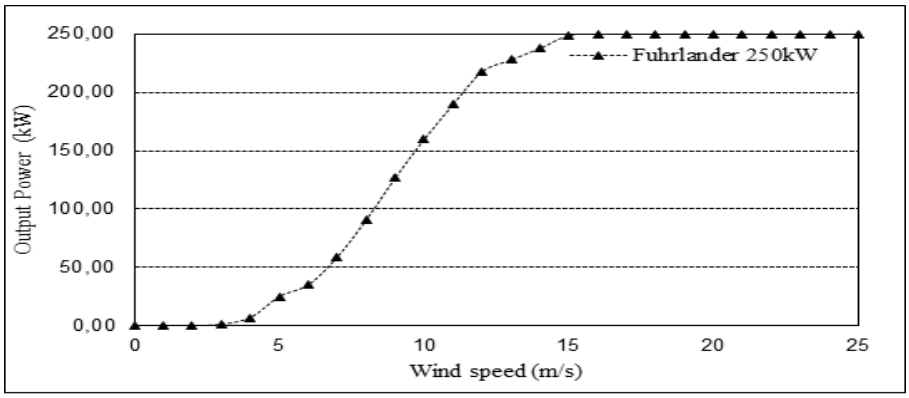


**Figure 11.** Power charts of Fuhrlander 250 kW wind turbine [33]

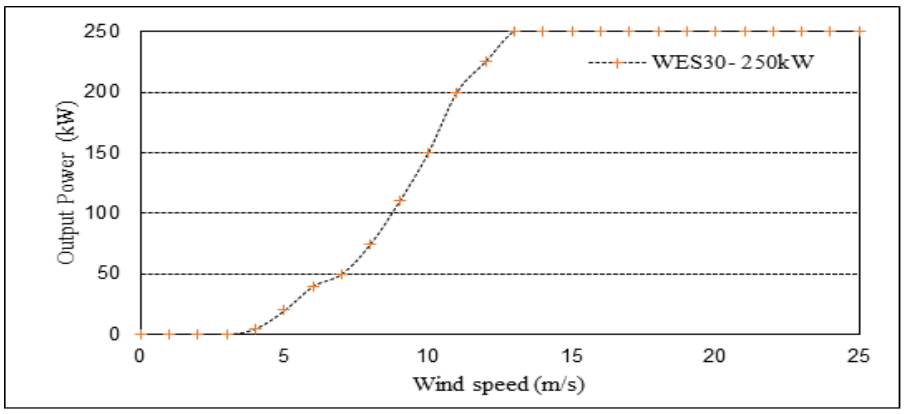


**Figure 12.** Power charts of WES30-250 kW wind turbine [34]

By using Equation 7 which is implemented in various research articles, the electrical output power of a wind turbine model can be calculated.

$$P_e = \begin{cases} 0 & v < v_c \\ P_{eR}\dfrac{v - v_c}{v_R - v_c} & v_c \le v \le v_R \\ P_{eR} & v_R \le v \le v_F \\ 0 & v > v_F \end{cases} \quad (7)$$

The capacity factor can be estimated by Equation 8 [35, 36].

$$CP = \frac{\sum_{i=1}^{17520} P_{e_i}}{17520.P_{eR}} \quad (8)$$

The total power produced by each wind turbine is estimated by the use of wind speed data from the years 2015 to 2017 for Somalia–Turkish Training and Research Hospital in Mogadishu. The total power produced by the wind turbines and their capacity factors are given in Table 2 [30-34].

**Table 2.** The overall power production of the wind turbines and their capacity factors

| Model of wind turbine | WES 250 kW [30] | SRC31-250 kW [31] | GEV MPC 250 kW [32] | Fuhrlander 250 kW [33] | WES30-250 kW [34] |
|---|---|---|---|---|---|
| **Total generated power (kWh)** | 1,017,603 | 1,031,744 | 1,024,715 | **1,076,790** | 1,011,915 |
| **Output power x 17520 (kWh)** | 4,380,000 | 4,380,000 | 4,380,000 | **4,380,000** | 4,380,000 |
| **Capacity factor** | 23 % | 23 % | 23 % | **25 %** | 23 % |

In the comparison of the wind turbines with the same output power, the one producing the highest energy and having the biggest capacity factor should be chosen as the optimum wind turbine. In this sense, it is notable that Fuhrlander 250 kW is the most appropriate wind turbine for Somalia–Turkish Training and Research Hospital in Mogadishu. The wind turbine has about 250 kW output power and its hub height is 41 m. It has a life cycle of 25 years. It has a rotor diameter of 29.5 m and is equipped with 3 blades. It has Cut-in speed of 2.5 m/s, rated speed of 12 m/s, and cut-out wind speed of 25 m/s. It has capital cost of $48,000, replacement cost of $480,000, and annual operational and maintenance costs of $480. In HOMER, the quantity of the wind turbines changes from 0 to 4 and the optimum type and model of wind turbine used in the HRES is decided by the techno-economic analysis. Costs and some other detailed technical properties of the wind turbines are shown in Table 1 [37].

### 4.3. Diesel generator

The output power of the diesel generator used in the proposed system is about 350 kW. Generally, the price of diesel generators used in the industry may vay between 250 $/kW and 500 $/kW. The cost per power is lower for high-powered units and similarly, the cost per power is higher for

low-powered units [38]. Diesel generator is AKSA AC350 in model. In the simulation, the number of diesel generators varies between 0 (no diesel generator) and 3 [26].

### 4.4. Inverter

The power converter has a rated power of 250 kW and it can thoroughly meet both PV power and residual power of the wind turbine after meeting the load demand. Moreover, the power converter has a conversion efficiency of 95 %. The model of the inverter is Solectria SGI 250. The starting and replacement cost and other specifications of the inverter are shown in Table 1 [27].

### 4.5. Batteries

The quantity of batteries used in the HOMER changes between 12 and 144 pieces. One battery bank consists of 12 batteries and, therefore, the quantity is a multiple of 12. In the proposed HRES Surrette 6CS25P model batteries are used whose nominal capacity is 1,156 Ah and nominal voltage is 12 V. Each battery can store energy about 6.94 kWh. Battery bank is designed to be six rows and two columns. Finally, Nominal bus voltage of the battery bank including 12 pieces of batteries, is 12 V. According to the datasheet information provided by HOMER, the batteries have 80 % round trip efficiency and they have minimum state of charge level of 40 %. The starting cost, replacement cost, and operational and maintenance cost of the batteries are shown in Table 1 [28].

## 5. OPERATION STRATEGIES

The proposed HRES intends to work with the load following dispatch strategy, which means that the energy produced by PV panels will be stored in the batteries and diesel generator and wind turbines will generate energy only for meeting the energy demand of the hospital. Mainly, load following dispatch strategy seems to be the optimum one for systems with multiple renewable energy sources. The most important significance of the strategy may be its contribution to optimizing the total NPC of the system and to decrease the excessive power production [39]. The operating reserve is the excessive operating capacity ensuring secure power supply although the load instantly goes up or renewable power output instantly goes down. Operating reserve can be estimated by Equation (9) [40].

$$\text{Operating reserve}=\left(\%_{L}\times E_{L}\right)+\left(\%_{PV}\times E_{PV}\right)+\left(\%_{WT}\times E_{WT}\right) \quad (9)$$

## 6. RESULTS AND DISCUSSION

Renewable energy systems must be analyzed in the techno-economic terms to determine its efficiency and economic feasibility. Since the system includes multiple generation systems, the analysis may be very complex. Moreover, the optimum design of the energy production system is related to the load demand and the use of renewable energy sources, which is hard to analyze completely in detail. The capacity of the designed system must be in accordance with operation planning to prevent excessive energy. Future load demand and predicted energy production must be planned [41, 42]. All configurations of HRES with the present parameters, average wind speed value of 5.61 m/s, average solar radiation of 5.63 kWh/m$^2$/d, and diesel fuel price of 0.75 $/l are examined in the next sections.

### 6.1. Standalone diesel power generating system

The standalone diesel power generating system is the expensive system among the studied hybrid configurations. The total NPC is about $9,608,750 and CoE is calculated at 0.360 $/kWh. Renewable fraction is about 0 %. The energy demand of the hospital is supplied by only two diesel generators with an output power of 350 kW. The annual average primary AC load of the hospital is estimated at 2,436,836 kWh/year. In this hybrid system, the standalone diesel power generating system could generate 2,662,261 kWh/year with the excess electricity of 159,453 kWh/year.

### 6.2. Standalone wind/diesel without battery storage HRES

The standalone wind/diesel without battery storage HRES comes after the standalone wind/diesel/battery storage HRES by means of the least NPC. The total NPC of this system is about $5,663,186. The CoE is calculated to be 0.213 $/kWh and results from the combination of 750 kW wind turbine and 350 kW diesel generator. Renewable fraction of the system is about 56 %. AC primary load of the hospital is estimated to be 2,436,836 kWh/year. In this hybrid system, while diesel generator is able to generate 1,508,223 kWh/year, the wind turbine generates 1,016,096 kWh/year. The diesel generator has operated 8,245 hours throughout the year.

### 6.3. Standalone wind/diesel/battery storage HRES

The standalone wind/diesel/battery storage HRES is the best configuration by means of net present cost and cost of energy.

When the total NPC of the system is about $5,418,316, CoE is 0.208 $/kWh. The system configuration comprises 350 kW diesel generator, 330 kW wind turbine, 200 kW inverter, and 300 batteries. Renewable fraction is about 34 %. In this hybrid system, when diesel generator could generate 1,657,635 kWh/year, the rest of it generates from wind turbine. The diesel generator has operated 7,372 hours throughout the year. The use of the battery storage has decreased by about 10 % of the operation hours of the diesel generator.

### 6.4. Standalone PV/diesel without battery storage HRES

The standalone PV/diesel without battery storage HRES consists of 350 kW diesel generator, 250 kW PV panel, and 200 kW inverter. When the total NPC is about $7,989,642, the CoE is calculated at 0.308 $/kWh. Renewable fraction is about 16 %. In this hybrid system, when diesel generator could generate 1,997,114 kWh/year, the rest of it is produced from PV panel. The diesel generator has operated 8,057 hours throughout the year.

### 6.5. Standalone PV/wind/diesel without battery storage HRES

The standalone PV/wind/diesel without battery storage HRES consists of 250 kW PV panel, 350 kW diesel generator, 330 kW wind turbine, and 200 kW inverter. When the total NPC is about $6,836,281, CoE is calculated 0.258 $/kWh. Renewable fraction is about 45 %. In this hybrid system, AC primary load of the hospital is estimated at 2,436,836 kWh/year which comprises 16 % of PV, 35 % wind turbine, and the rest of diesel generator. The diesel generator has operated 8,100 hours throughout the year.

### 6.6. Standalone wind-PV-diesel-battery storage HRES

The standalone wind-PV-diesel-battery storage HRES comes after the standalone wind/diesel without battery storage HRES by means of the least NPC. The system configuration consists of 250 kW PV panel, 350 kW diesel generator, 330 kW wind turbine, 200 kW inverter, and 300 batteries. When the total NPC is about $6,302,950, CoE is calculated 0.238 $/kWh. Renewable fraction is about 49 %. In this hybrid system, AC primary load of the hospital is estimated 2,436,836 kWh/year, which comprises 464,481 kWh/year of PV, 1,016,096 kWh/year of wind turbine, 1,171,352 kWh/year of diesel generator, and rest of batteries. The diesel generator has operated 6,934 hours throughout the year. The excess energy of the standalone PV/wind/diesel/battery storage HRES is 101,958 kWh/year. The payback period is calculated to be about 5 years. The cost of energy is about 0.5 $/kWh for Somalia and the daily Load is 8,000 kWh. Now that the NPC of the system is $5,056,700, the payback is assumed to be about 5 years.

## 7. ENVIRONMENTAL ASSESSMENT OF THE HRESs

With the aim of reducing the $CO_2$ emission, several optimization attempts have been made for the hospital. When all power system configurations are examined by means of greenhouse gas emissions such as $CO_2$, CO, $SO_x$ etc., the most appropriate and least $CO_2$ emission value of HRES belongs to PV/wind/diesel/battery storage system, which can be seen in Table 3. Moreover, Table 3 shows all pollutants and emission values of all HRES. As Table 3 is studied in detail, the diesel power generating system produced the greatest $CO_2$ emissions, while the lowest emission value belonged to PV/wind/diesel/battery HRES.

**Table 3.** All emission values for hybrid renewable power generating systems

| Pollutant | Only Diesel (kg/yr) | Wind/Diesel (kg/yr) | Wind/Diesel/Battery (kg/yr) | PV/Diesel (kg/yr) | PV/Wind/Diesel (kg/yr) | PV/WindDiesel/Battery (kg/yr) |
|---|---|---|---|---|---|---|
| Carbon dioxide | 3,044,463 | 1,699,208 | 1,536,476 | 1,960,666 | 1,513,318 | 1,282,406 |
| Carbon monoxide | 7,515 | 4,194 | 3,793 | 4,840 | 3,735 | 3,165 |
| Unburned hydrocarbons | 832 | 465 | 420 | 536 | 414 | 351 |
| Particulate matter | 567 | 316 | 286 | 365 | 282 | 239 |
| Sulfur dioxide | 6,114 | 3,412 | 3,086 | 3,937 | 3,039 | 2,575 |
| Nitrogen oxides | 67,055 | 37,426 | 33,841 | 43,184 | 33,331 | 28,245 |

## 8. SENSITIVITY ANALYSIS OF THE HRES

This paper examined three different sensitivity variables: average wind speed, solar radiation, and diesel price. The variables of the sensitivity analysis are determined to be in a suitable range to tolerate the variation of the inputs in the future. Table 4 shows the range of three sensitivity variables including velocity of wind, sunlight radiation, and diesel cost.

**Table 4.** Different wind speed and diesel prices values considered in the sensitivity analysis

| Wind speeds (m/s) | Solar radiation (kWh/m²/d) | Diesel prices ($/l) |
|---|---|---|
| 2 | 2 | 0.75 |
| 3 | 3 | 1 |
| 4 | 4 | 1.5 |
| 5.61 | 5.63 | 2 |
| 6 | 6 | 2.5 |

There are totally 125 sensitivity situations, estimated by the multiplication of wind speed (5), solar radiation (5), and diesel price (5). Different sensitivity situations and the optimum configured system with the present conditions are shown in Figure 9.

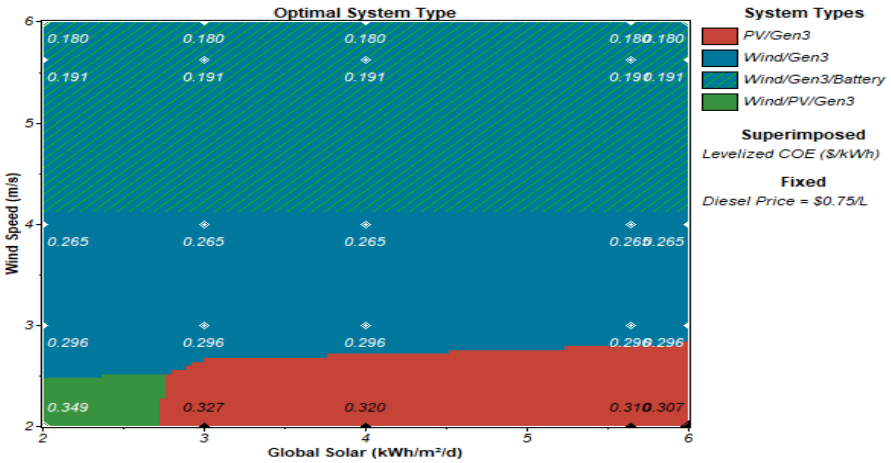


**(a)** Diesel price=0.75 $/l

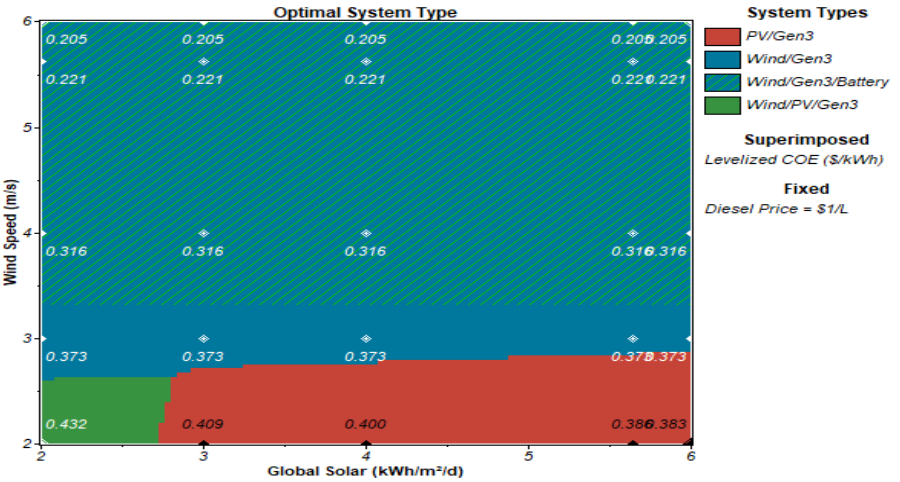


**(b)** Diesel price=1.0 $/l

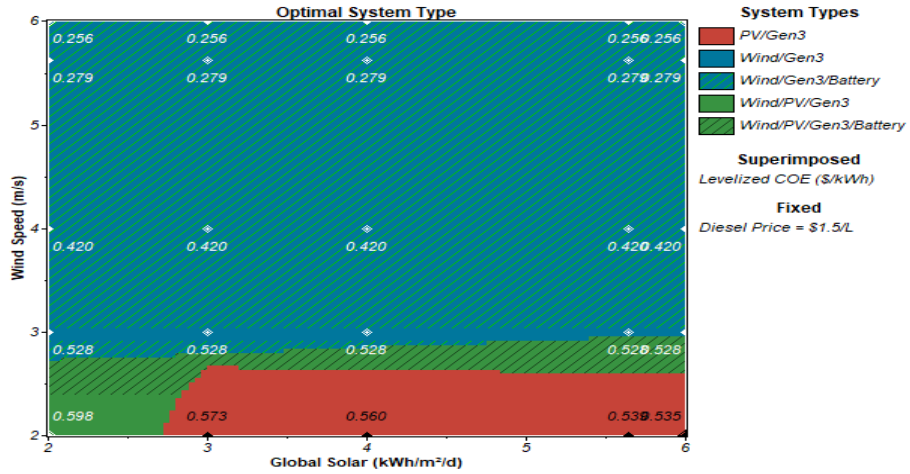


**(c)** Diesel price=$1.50/l

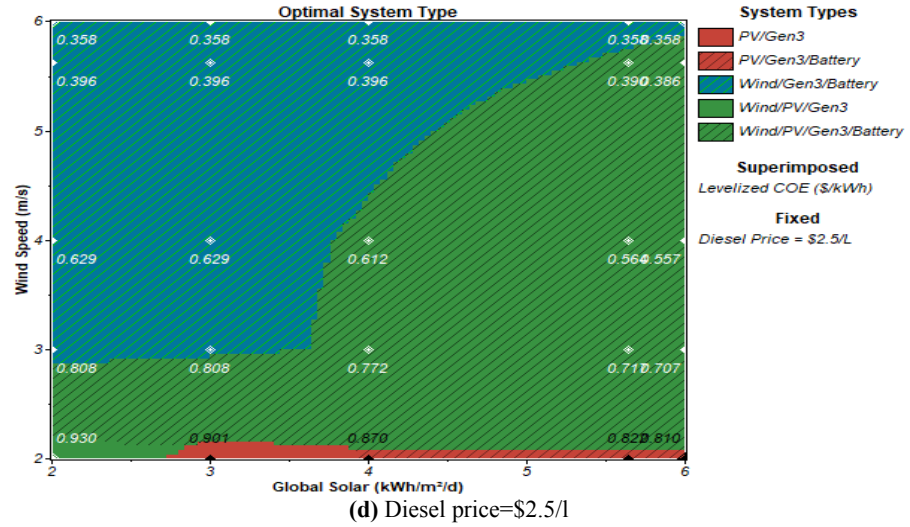


**(d)** Diesel price=$2.5/l

**Figure 9.** Different sensitivity situations and optimum configured system with the present conditions

Concerning the effects of changing sensitivity variables on the hybrid renewable power-generating systems configuration, detailed results of every feasible situation are given in Figure 7, which can be elaborated below comprehensively:

- For the least diesel fuel cost of 0.75 $/l, while both wind speed values vary from 2 m/s to 3.4 m/s and solar radiation value is lower than 2.8 kWh/m$^2$/d, the optimum hybrid system is wind/PV/diesel HRES. Moreover, in case the wind velocity value varies from 2.4 m/s to 3.4 m/s and sunlight radiation value is greater than 3 kWh/m$^2$/d, the optimum hybrid system with wind/PV/diesel HRES. Furthermore, if wind speed value is lower than 2.4 m/s and solar radiation value is higher than 2.8 kWh/m$^2$/d, then the optimum hybrid system is PV/diesel HRES. Similarly, in the situation that wind

speed value ranges between 3.3 m/s and 3.5 m/s and solar radiation value is greater than 4.6 kWh/m$^2$/d, the optimum hybrid system is wind/PV/diesel/battery HRES. While wind speed value is between 3.6 m/s and 4.9 m/s and for all solar radiation values, the optimum hybrid system is wind/diesel HRES. Lastly, in case wind speed is higher than 5 m/s and for all solar radiation values, the optimal hybrid system is wind/diesel/battery HRES.

- For the lowest diesel value of 1.50 $/l, in a situation where wind speed value varies from 2 m/s to 2.6 m/s and solar radiation value is above 2 kWh/m$^2$/d, the optimum hybrid system is wind/PV/diesel HRES. Similarly, in case where both wind speed value varies from 2.6 m/s to 3.2 m/s and solar radiation value is above 2 kWh/m$^2$/d, the optimum hybrid system is wind/PV/diesel HRES. In addition, if the wind speed value is between 2 m/s and 2.6 m/s and solar radiation value is greater than 2 kWh/m$^2$/d, then the wind speed value is between 3.2 m/s and 3.7 m/s and solar radiation value is greater than 2 kWh/m$^2$/d. Or, wind speed value is between 3.7 m/s and 4.0 m/s and solar radiation value is greater than 2.0 kWh/m$^2$/d; or, wind speed value is greater than 4.5 m/s and solar radiation value is higher than 5.3 kWh/m$^2$/d. Under these conditions, the optimum hybrid system is wind/PV/diesel/battery HRES. Moreover, the optimal hybrid system is wind/diesel/battery HRES in a condition where (a) wind speed value is between 3.7 m/s and 4 m/s and all solar radiation values, (b) wind speed value is between 4 m/s and 4.5 m/s and all solar radiation values, and (c) wind speed value is higher than 4.5 m/s and solar radiation value varies from 2.0 kWh/m$^2$/d to 6.0 kWh/m$^2$/d.

- For the lowest diesel value of 2.50 $/l, the optimum hybrid system is wind/diesel/battery HRES in a condition where (a) wind speed value varies from 3.8 m/s to 6.0 m/s and solar radiation value is lower than 3.2 kWh/m$^2$/d and (b) the wind speed value varies from 3.8 m/s to 6.0 m/s and solar radiation value is between 3.2 kWh/m$^2$/d and 3.8 kWh/m$^2$/d. In addition, the optimum hybrid system is wind/PV/diesel/battery HRES in a condition where (a) wind speed value varies from 3.8 m/s to 6.0 m/s and solar radiation value is between 3.1 kWh/m$^2$/d and 6.0 kWh/m$^2$/d, (b) wind speed value is between 2.8 m/s and 3.8 m/s and all solar radiation values, and (c) wind speed value varies from 2.0 m/s to 2.8 m/s and solar radiation value is higher than 4.0 kWh/m$^2$/d. Lastly, the optimum hybrid system is wind/PV/diesel HRES in a condition where wind speed value is between 2 m/s and 2.8 m/s and solar radiation value is greater than 2.0 kWh/m$^2$/d, or where wind speed value is between 3.2 m/s and 3.7 m/s and solar radiation value is lower than 5.0 kWh/m$^2$/d.

## 9. CONCLUSIONS

The following remarks or conclusions can be drawn from the study after examining and analyzing all the results obtained from the figures and tables which were received from the HOMER software.

- Renewable fraction rates of the hybrid renewable power generating systems range between 0 % and 75 %.
- Diesel generator used in the proposed HRES operates between 6,712-8,760 hours according to the case. In this sense, it can be said that in a situation with stand-alone diesel system, the diesel generator operates 8,760 hours per year and consumes 1,156,127 liter of diesel fuel.
- Due to the contribution of PV panels and wind turbines, the use of diesel generator and the consumed diesel fuel will be lowered. This will also lead to a great decrease in emissions between 42 % and 100 %.
- Wind/diesel/battery HRES is the most environmentally friendly system among the studied systems. PV/wind/diesel/battery HRES has the least emission value which is 42 %.
- The systems, except stand-alone diesel generator, have a CoE between 0.208 $/kWh and 0.359 $/kWh.
- For the current average wind speed, current diesel price and solar irradiation values for the hospital located in Mogadishu–Somalia, the optimum hybrid system is wind/diesel/battery HRES with the optimal hybrid configuration system that includes a 350 kW diesel generator, a 330 kW wind turbine, a 200 kW inverter, and 300 batteries. In addition, the net present cost and the CoE of this system are about $6,302,950 and 0.238 $/kWh, respectively. Furthermore, renewable fraction is about 49 %.
- Optimal HRESs fulfill the energy demand of the hospital completely. AC primary load of the hospital is approximately 2,436,836 kWh/year which comprises 464,481 kWh/year of PV, 1,016,096 kWh/year of wind turbine, 1,171,352 kWh/year of diesel generator, and the rest of the batteries. The diesel generator has operated 6,934 hours throughout the year. The excess energy of the standalone PV/wind/diesel/battery storage HRES is 101,958 kWh/year.
- Using diesel generator as the only power supplier, the CoE of the system is 0.360 $/kWh. Furthermore, this system produces high amounts of hazardous emission gases, as mentioned in Table 2.
- Converting the system into a complete or nearly complete renewable hybrid power generating system, the CoE of the hybrid systems is fairly lower (more than 50 % lower) than the diesel generator system. Moreover, the new hybrid systems never produce harmful emissions or partial emissions according to the renewable fraction values of the system. Hybrid systems are not only more economical but also more environmentally friendly.
- Examining the effects of minor or major changes in the sensitivity variables such as average wind speed, current diesel price and solar radiation value, for the numerous combinations of sensitivity variables, the most suitable hybrid systems are in order of wind/diesel/battery, PV/wind/diesel/battery, wind/PV/diesel, wind/diesel, PV/diesel/battery, and PV/diesel.
- Compared with the study of Olatomiwa which is entitled “Optimal configuration assessments of hybrid renewable power supply for rural healthcare facilities”, made for the similar region, Nigeria, the results showed that optimal renewable hybrid system determined by HOMER could be far more preferable than the standalone diesel generator by means of energy cost and gas emissions.
- The payback period is calculated to be about 5 years.
- For high diesel prices,

(i) it is the wind/diesel/battery hybrid system at low wind speed values.
(ii) it is the PV/wind/diesel/battery hybrid system at moderate wind speed values.
(iii) it is the PV/wind/diesel/battery hybrid system at high wind speed values.

## 10. ACKNOWLEDGEMENT

We thank the Director of Somalia–Turkish Training and Research Hospital in Mogadishu and are grateful to Dr. Ali Karakoc and his colleagues at the Somalia–Mogadishu Recep Tayyip Erdogan Vocational School of Health Sciences of the University of Health Sciences, Turkey.

## NOMENCLATURE

| | |
|---|---|
| $C_{a,t}$ | Total annualized cost |
| CoE | Cost of Energy |
| CRF | Capital Recovery Factor |
| CP | Capacity Factor |
| $E_{p,AC}$ | Ac primary load served |
| $E_{p,DC}$ | Dc primary load served |
| $E_{g,s}$ | Total grid sales |
| F | The annual inflation rate |
| $f_i$ | Frequency |
| HRES | Hybrid Renewable Energy System |
| i | The real interest rate |
| $i_0$ | The nominal interest rate |
| N | Number of years |
| NPC | Net Present Cost |
| $P_e$ | Electrical output power of a wind turbine |
| $P_{eR}$ | Rated electrical power |
| $R_p$ | Project lifetime |
| $v_i$ | Mean wind speed |
| $v_c$ | Cut–in wind speed |
| $v_f$ | Cut-out wind speed |
| $\%_L$ | The percentage of hourly load |
| $\%_{PV}$ | The percentage of solar power output |
| $\%_{WT}$ | The percentage of wind turbine power output |

## REFERENCES

1. Habbane, A.Y. and McVeigh, J.C., "An energy policy for Somalia", ***Solar & Wind Technology***, Vol. 2, (1985), 53-58. (https://doi.org/10.1016/0741-983X(85)90026-8).
2. AFDB, "Somalia energy sector needs assessment and investment programme", Somalia, (2015). (https://www.afdb.org/fileadmin/uploads/afdb/Documents/Generic-Documents/Final_Somalia_Energy_Sector_Needs_Assessment_FGS__AfDB_November_2015.pdf).
3. Dursun, B. and Aykut, E., "An investigation on wind/PV/fuel cell/battery hybrid renewable energy system for nursing home in Istanbul", ***Proceedings of the Institution of Mechanical Engineers, Part A: Journal of Power and Energy***, Vol. 233, (2019), 616-625. (https://doi.org/10.1177/0957650919840519).
4. Altay, A. and Dursun, B., "Determination of hybrid renewable energy systems for project type public library building", ***International Journal of Renewable Energy Research***, Vol. 9, No. 1, (2019), 24-31. (https://www.researchgate.net/publication/332142551_Determination_of_Hybrid_Renewable_Energy_Systems_for_Project_Type_Public_Library_Building).
5. Aykut, E. and Terzi, Ü.K., "Techno-economic and environmental analysis of grid connected hybrid wind/photovoltaic/biomass system for Marmara University Goztepe campus", ***International Journal of Green Energy***, Vol. 17, No. 15, (2020), 1036-1043. (https://doi.org/10.1080/15435075.2020.1821691).
6. Dursun, B. and Altay, A., "A green university library based on hybrid PV/wind/battery system", ***International Journal of Energy and Environment***, Vol. 9, (2019), 549-562. (https://acikerisim.bartin.edu.tr/handle/11772/991).
7. Pemndje, J., Ilinca, A., Tene Fongang, T.R. and Tchinda, R., "Impact of using renewable energy on the cost of electricity and environment in Northern Cameroon", ***Journal of Renewable Energy and Environment (JREE)***, Vol. 3, No. 4, (2016), 34-43. (https://doi.org/10.30501/jree.2016.70098).
8. Orosz, M.S., Quoilin, S. and Hemond, H., "Technologies for heating, cooling and powering rural health facilities in Sub-Saharan Africa", ***Proceedings of the Institution of Mechanical Engineers, Part A: Journal of Power and Energy***, Vol. 227, (2013), 717-726. (https://doi.org/10.1177/0957650913490300).
9. Malik, A.Q., "Assessment of the potential of renewables for Brunei Darussalam", ***Renewable and. Sustainable. Energy Reviews***, Vol. 15, (2011), 427-437. (https://doi.org/10.1016/J.RSER.2010.08.014).
10. Ajao, K.R., Oladosu, O.A. and Popoola, O.T., "Using HOMER power optimization software for cost benefit analysis of hybrid-solar power generation relative to utility cost in Nigeria", ***International Journal of Research and Reviews in Applied Sciences***, Vol. 7, No. 7, (2011). (https://www.semanticscholar.org/paper/USING-HOMER-POWER-OPTIMIZATION-SOFTWARE-FOR-COST-OF-Ajao-Oladosu/02ae78780ee9e69c325fe7086b9d270baebf89ce).
11. Himri, Y., Boudghene Stambouli, A., Draoui, B. and Himri, S., "Techno-economical study of hybrid power system for a remote village in Algeria", ***Energy***, Vol. 33, (2008), 1128-1136. (https://doi.org/10.1016/J.ENERGY.2008.01.016).
12. Gholami, A., Tajik, A., Eslami, S. and Zandi, M., "Feasibility study of renewable energy generation opportunities for a dairy farm", ***Journal of Renewable Energy and Environment (JREE)***, Vol. 6, (2019), 8-14. (https://doi.org/10.30501/jree.2019.95943).
13. Nfah, E.M., "Evaluation of optimal photovoltaic hybrid systems for remote villages in Far North Cameroon", ***Renewable. Energy***, Vol. 51, (2013), 482-488. (https://doi.org/10.1016/J.RENENE.2012.09.035).
14. Nfah, E.M., Ngundam, J.M. and Tchinda, R., "Modelling of solar/diesel/battery hybrid power systems for Far North Cameroon", ***Renewable Energy***, Vol. 32, (2007), 832-844. (https://doi.org/10.1016/J.RENENE.2006.03.010).
15. Olatomiwa, L. Mekhilef, S., Huda, A.S.N. and Ohunakin, O.S., "Economic evaluation of hybrid energy systems for rural electrification in six geo-political zones of Nigeria", ***Renewable. Energy***, Vol. 83, (2015), 435-446. (https://doi.org/10.1016/J.RENENE.2015.04.057).
16. Olatomiwa, L., "Optimal configuration assessments of hybrid renewable power supply for rural healthcare facilities", ***Energy Reports***. Vol. 2, (2016), 141-146. (https://doi.org/10.1016/J.EGYR.2016.06.001).
17. STH, Some information about Mogadishu, Somalia-Turkey training and research hospital, (2019). (https://somaliturkishhospital.saglik.gov.tr/?_Dil=2), (Accessed February 11, 2019).
18. World Factbook, "The map of Somalia". (https://www.cia.gov/library/publications/the-world-factbook/geos/so.html), (Accessed October 10, 2020).
19. Stackhouse P.W., "NASA surface meteorology and solar energy", (2018). (https://eosweb.larc.nasa.gov/cgi-bin/sse/grid.cgi?&num=226093&lat=2.03&submit=Submit&hgt=100&veg=17&sitelev=&email=skip@larc.nasa.gov&p=grid_id&p=wspd50m&step=2&lon=45), (Accessed June 12, 2018).
20. "Solar energy potential of Somalia", (2019). (https://solargis.com/maps-and-gis-data/download/somalia), (Accessed June 1, 2019).
21. HOMER, "HOMER (Hybrid Optimization of Multiple Energy Resources) microgrid software", (2018). (https://www.homerenergy.com/products/index.html), (Accessed March 3, 2019).
22. CBS, "Annual rate of inflation in Somalia, Central Bank of Somalia", (2020). (https://centralbank.gov.so/research-and-statistic), (Accessed October 10, 2020).
23. Dursun, B., "Determination of the optimum hybrid renewable power generating systems for Kavakli campus of Kirklareli University, Turkey", ***Renewable & Sustainable. Energy Reviews***, Vol. 16, (2012). (https://doi.org/10.1016/j.rser.2012.07.017).
24. Demiroren, A. and Yilmaz, U., "Analysis of change in electric energy cost with using renewable energy sources in Gökceada, Turkey: An island example", ***Renewable & Sustainable. Energy Reviews***, Vol. 14, (2010), 323-333. (https://doi.org/10.1016/J.RSER.2009.06.030).
25. Sonali Solar, "Sonali solar S-300W PV panel", (2019). (http://www.sonalisolar.com/pdf/280-320Series.pdf), (Accessed January 18, 2019).

26. Energy, A., "AKSA AC 350 diesel generator technical specifications", (2019). (http://www.aksajenerator.com.tr/tr-tr/FrontProduct/CreatePDF/66), (Accessed February 27, 2019).
27. Solectria Solar, "Solectria SGI 250 kW inverter specifications", (2019). (https://solectria.com/site/assets/files/2340/sgi_225-500pe_datasheet_rev_j_obsoletepe.pdf), (Accessed March 17, 2019).
28. Surette Rolls, "Rolls Surrette 6CS25P (6-CS-25P) battery specifications", (2019). (https://www.dcbattery.com/rollssurrette_6cs25p.pdf), (Accessed March 10, 2019).
29. Candelise, C., Gross, R. and Leach, M., "Conditions for photovoltaics deployment in the UK: The role of policy and technical developments", ***Proceedings of the Institution of Mechanical Engineers, Part A: Journal of Power and Energy***, Vol. 224, (2016), 153-166. (https://doi.org/10.1243/09576509JPE768).
30. WES-250 kW, "Technical specifications of WES 250 kW wind turbine". (http://www.vicometal.pt/ES/energia/WESHybrid_0209_optimized.pdf) , (Accessed May 4, 2019).
31. SRC31-250 kW, "Technical specifications of SRC31-250 kW wind turbine". (http://www.greenenergywind.co.uk/pdf/NEPC-250KW-WIND-TURBINE-TECH-SPEC.pdf), (Accessed April 4, 2019).
32. GEV MPC 250 kW, "Technical specifications of GEV MPC 250 kW wind turbine". (http://www.vergnet.com/wp-content/uploads/2016/01/DC-11-00-01-EN_GEV_MP-C_275_kW.pdf), (Accessed April 23, 2019).
33. Fuhrlander 250 kW, "Technical specification of Fuhrlander 250 kW wind turbine". (https://www.thewindpower.net/turbine_en_161_fuhrlander_fl-250-30.php), (Accessed April 2, 2019).
34. WES30-250 kW, "Technical specifications of WES30-250 kW wind turbine". (http://www.vicometal.pt/ES/energia/Complete Description WES30.pdf), (Accessed April 24, 2019).
35. Dursun, B. and Alboyaci, B., "An evaluation of wind energy characteristics for four different locations in Balikesir", ***Energy Sources Part A: Recovery, Utilization, and Environmental Effects***, Vol. 33, (2011). (https://doi.org/10.1080/15567030903330850).
36. Sohoni, V., Gupta, S.C. and Nema, R.K., "A critical review on wind turbine power curve modelling techniques and their applications in wind based energy systems", ***Journal of Energy***, (2016), 1-18. (https://doi.org/10.1155/2016/8519785).
37. Rohani, G. and Nour, M., "Techno-economical analysis of stand-alone hybrid renewable power system for Ras Musherib in United Arab Emirates" ***Energy***, Vol. 64, (2014), 828-841. (https://doi.org/10.1016/J.ENERGY.2013.10.065).
38. Dalton, G.J., Lockington, D.A. and Baldock, T.E., "Feasibility analysis of renewable energy supply options for a grid-connected large hotel", ***Renewable Energy***, Vol. 34, (2009), 955-964. (https://doi.org/10.1016/j.renene.2008.08.012).
39. Ngan, M.S. and Tan, C.W., "Assessment of economic viability for PV/wind/diesel hybrid energy system in southern Peninsular Malaysia", ***Renewable & Sustainable. Energy Reviews***, Vol. 16, (2012), 634-647. (https://doi.org/10.1016/j.rser.2011.08.028).
40. Lau, K.Y., Yousof, M.F.M., Arshad, S.N.M., Anwari, M. and Yatim, A.H.M., "Performance analysis of hybrid photovoltaic/diesel energy system under Malaysian conditions", ***Energy***, Vol. 35, (2010), 3245-3255. (https://doi.org/10.1016/J.ENERGY.2010.04.008).
41. Abnavi, M.D., Mohammadshafie, N., Rosen, M.A., Dabbaghian, A. and Fazelpour, F., "Techno-economic feasibility analysis of stand-alone hybrid wind/photovoltaic/diesel/battery system for the electrification of remote rural areas: Case study Persian Gulf Coast-Iran", ***Environmental Progress & Sustainable Energy***, Vol. 38, No. 5, (2019), 1-15. (https://doi.org/10.1002/ep.13172).
42. Al-Ghussain, L. and Taylan, O., "Sizing methodology of a PV/wind hybrid system: Case study in Cyprus", ***Environmental Progress & Sustainable Energy***, Vol. 38, No. 3, (2018), 1-7. (https://doi.org/10.1002/ep.13052).

Journal of Renewable Energy and Environment

Research Article

Journal Homepage: www.jree.ir

# Optimization of Pyrolysis Temperature and Particle Size on the Phenols and Hemicellulose Fast Pyrolysis Products in a Tandem Micro-Pyrolyzer

Payam Ghorbannezhad [a], Maryam Abbasi [b*]

[a] *Department of Biorefinery Engineering, Faculty of New Technologies Engineering, Shahid Beheshti University, Tehran, Tehran, Iran.*
[b] *Faculty of Civil, Water & Environmental Engineering, Shahid Beheshti University, Tehran, Tehran, Iran.*

*PAPER INFO*

*Paper history:*
Received 03 November 2020
Accepted in revised form 10 July 2021

*Keywords*:
Sugarcane Bagasse,
Fast Pyrolysis,
Phenolic Compounds,
Furfural

*ABSTRACT*

Fast pyrolysis of sugarcane bagasse was investigated in a tandem micro-pyrolyzer. The effects of temperature and particle size on the phenolic compounds and hemicellulose products distribution were examined during fast pyrolysis process. For this, changes in the micro-reactor parameters were made (particle size between 0.1 and 0.5 mm and reactor temperature between 450 and 600 °C). Response Surface Methodology (RSM) was used to optimize pyrolysis parameters. The results indicated that the temperature had the highest effect on phenolic and furfural-type compounds, whereas the particle size did not exhibit significant effects on carboxylic acid products. The largest number of phenolic compounds were achieved upon decreasing the temperature and increasing particle size. The ANOVA analysis revealed that the full quadratic model was more adequate for phenolic and furfural compounds, whereas the linear square model was accurate for carboxylic acids. In general, a tandem micro-pyrolyzer interfacing with a GC-MS analysis facilitated a better understanding of a chemical composition of biomass and therefore, could remarkably improve the valorising of sugarcane bagasse application in biorefinery processes.

https://doi.org/10.30501/jree.2021.255248.1155

## 1. INTRODUCTION

In recent years, many studies have been conducted to enhance the efficiency of processes for renewable energy. Biomass can be used for a partial or full replacement of fossil fuels given that it is a carbon-based energy resource with such benefits as potential for zero to net negative emission of carbon dioxide. Thermochemical and biological processes can transform biomass into high-energy fuels [1]. Thermochemical processes provide complex and multiple products in a short reaction time span; however, biological processes are more selective but require long processing times [2]. One of the commercially relevant thermochemical technologies for processing lignocellulosic materials into fuel and chemical products is fast pyrolysis [3, 4]. Using fast pyrolysis, the pyrolysis vapor is rapidly cooled to produce a liquid product (bio-oil), which is up to 75 wt % of the biomass feedstock and has a higher caloric value than the biomass [5]. While there are more than 300 oxygenated compounds in fast pyrolysis bio-oil, three classes of compounds can be typically identified in bio-oils [6] including sugars, small carbonyl compounds (e.g. furfurals and cyclopentanones), carboxylic acids and phenols, arguably derived from the three polymeric components of biomass, namely cellulose, hemicellulose, and lignin, respectively [7]. Recently, there is growing attention to producing added-value chemicals from fast biomass pyrolysis. Furfural derived from hemicellulose is an effective organic chemical extensively applied to production of fibres, synthetic rubbers, resins, flavors, food additives, dyes and paintings, and liquid hydrocarbon fuels [8]. Cellulose is hydrolyzed and dehydrated to form the furfural on an industrial scale from biomass feedstocks such as bagasse and corncob in aqueous acid solutions. Moreover, enhanced furfural production was reported using catalytic pyrolysis of biomass with $MgCl_2$, $ZnCl_2$, $H_2SO_4$, and solid superacid as catalysts [9].

Lignin is a promising natural resource for aromatic compound productions compared to hemicellulose and cellulose due to its hydroxyphenyl, syringyl, guaicyl, monomeric units [10]. The remarkable aromatic and highly functionalized nature of lignin make it appropriate for value-added aromatic products such as benzene, toluene, and xylenes [11]. However, recent research has also shown that these aromatic hydrocarbons can also be formed from intermediates compounds arising from cellulose and hemicellulose [12, 13]. For example, toluene can be produced from the Diels-Alder cycloaddition reactions of methyl furan and ethylene, followed by dehydration [14].

The yields and detailed compositions of fast pyrolysis products from the three main polymers of biomass have been mainly investigated by reacting each polymer separately [15, 16]. Except where the concept of fractionation is adopted in a biorefinery, fast pyrolysis of raw biomass feedstock involves co-processing of the component polymers under the same

*Corresponding Author's Email: mary_abbasi@sbu.ac.ir (M. Abbasi)
URL: https://www.jree.ir/article_133314.html

Please cite this article as: Ghorbannezhad, P. and Abbasi, M., "Optimization of pyrolysis temperature and particle size on the phenols and hemicellulose fast pyrolysis products in a tandem micro-pyrolyzer", ***Journal of Renewable Energy and Environment (JREE)***, Vol. 8, No. 3, (2021), 68-74. (https://doi.org/10.30501/jree.2021.255248.1155).

process conditions, which may lead to both beneficial and abortive interactions of intermediate reaction products. Such interactions may lead to enhanced yields of some reaction products in the bio-oil, while they could also decrease the yields of others. Processing parameters such as fast pyrolysis temperature, vapor residence times, biomass particle size, biomass type, biomass feeding rate, and reactor type are known to influence the yields and compositions of products in bio-oils [17-19]. Among these parameters, pyrolysis temperature, biomass type, and biomass particle size have been highlighted to have the predominant influence on bio-oil yield and composition [13, 20, 21]. Joubert et al. [22] studied the effects of the type of reactor and temperature on the fast pyrolysis of biomass. Using biomass particle size of >2 mm, they found that the ideal temperature for the production of the highest bio-oil yield (60 wt %) was 500 °C [23]. In addition, Park et al [24] and Amutio et al. [25] found that the yields of phenolic compounds depended mostly on the type of biomass, the amount of biomass feed, and pyrolysis temperature.

Karagoz et al [26] investigated online conversion of beech wood and microalgae on a laboratory reactor connected with GC-MS by using a catalyst. They reported that the relative yield of aromatic hydrocarbons such as Benzene, Toluene, and Xylenes (BTX) changed considerably depending on the biomass type. Wang et al. [27] compared the conversion of continuous and sequential pyrolyses of wood biomass using in-situ and ex-situ catalyses. The authors indicated that in-situ catalytic pyrolysis generated higher aromatic compounds than ex-situ under the same situations.

Fast pyrolysis of sugarcane bagasse, a vastly available biomass feedstock, has been studied by a number of researchers [1, 12, 28-30]. Sugarcane bagasse is obtained after the extraction of sugarcane juice (mostly hexose sugars) and therefore, is mostly composed of lignin and hemicellulose. The weight percentage of hemicellulose and lignin components in sugarcane bagasse is around 25 % and 23 %, respectively, with the elemental composition of about 42 % carbon, 5 % hydrogen, 52 % oxygen, and trace amounts of several metal ions [12]. This feedstock is therefore suitable to study the influence of processing parameters in a real biomass that will improve the understanding of the interactions among intermediate products of fast pyrolysis by following the yields of phenolic compounds, furfurals, and carboxylic acids. In this present study, the effects of temperature and particle size on these classes of bio-oil compounds have been investigated during ex-situ fast pyrolysis using Pyrolysis-Gas Chromatography/Mass Spectrometry (Py-GC-MS), an analytical micro-pyrolyzer instrument. Response Surface Methodology (RSM) was employed to reveal the role of particle size and temperature in hemicellulose and lignin compounds in fast pyrolysis process. This is a novel approach to determining the contributions of effective parameters in the stepwise conversion process of hemicellulose and lignin (in sugarcane bagasse) into a selection of bio-oil compounds and the performance of value-added chemicals recovery from hemicellulose and lignin.

## 2. MATERIALS AND METHODS

### 2.1. Biomass collection and preparation

The sugarcane bagasse fiber feedstock was collected from an agro-based pulp and paper industry in the southwest of Iran, used as paper mill raw material. The average fiber size was 3-5 cm in length with approximate moisture content 50 % (w/w). The biomass was dried in the open using solar energy for two days; then, it was put in the oven at 105 °C to reach a moisture content below 10 % (w/w). Dried materials were ground by a mill and, then, sieved to particle sizes of diameters 100, 212, 300, 425, and 500 µm. The small size of sugarcane bagasse (300 g, dry weight) was subjected to soxhlet extraction with ethanol/Toluene solvent (2:1, v/v) for 5 h. In order to remove the toluene, the sample was dewatered for 3 h followed by vacuum drying at 105 °C over a day. Table 1 shows the result of proximate and ultimate analysis, adapted by the ASTM protocols established for biomass. Hemicellulose fraction was measured by precipitation of pre-hyrolysis followed by acid hydrolysis. The acid hydrolysis based on the Technical Association of the Pulp and Paper (TAPPI) standard methods (T264 om-88, T211 om-85) was carried out for acid-soluble lignin. Soluble lignin was calculated by UV spectrophometry. To ensure the reproducibility of results, the chemical analysis procedures were conducted in triplicate. FTIR analysis was performed to characterize the hemicellulose and lignin from 4000 to 500 $cm^{-1}$ by platinum ATR Alpha instrument.

**Table 1.** The proximate and ultimate alanysis of sugarcane bagasse

| Component | Weight % | Standard method |
|---|---|---|
| **Proximate analysis (wt %, ar*)** | | |
| Moisture | 8 | ASTM D 3173 |
| Volatile | 77 | ASTM 3174 |
| Fixed carbon | 12.4 | ASTM 3175 |
| Ash | 2.6 | ASTM 3172 |
| **Ultimate analysis (wt %, db*)** | | |
| C | 43.5 | ASTM D 4239 |
| H | 6.4 | ASTM D 4239 |
| N | 0.1 | ASTM D 4239 |
| S | 0.01 | ASTM D 4239 |
| O | 49.9 | By difference |
| * ar = as received, db = dry base | | |

### 2.2. Fast pyrolysis experiment

A tandem micro-pyrolyzer system, Rx-300 TR, Frontier Laboratories, Japan was utilized for fast pyrolysis of the milled samples. The detailed schematic of the system can be found in another study (Wang et al. 2014). According to Figure 1, the micro-pylolyzer consisted of two individual parts: first, pyrolysis reactor and second, the *ex-situ* catalyst bed reactor. Microgram quantities of biomass sample were weighed (around 1-2 µg) and placed into a stainless steel cup, which was then dropped into the pyrolysis reactor fitted with programmable temperature control. Rapid thermal degradation and devolatilisation of the biomass produced vapor streams, carried by helium gas at a rate of 1 ml/min through the catalyst bed reactor. At a temperature of 500 °C, the retention time of hot vapor at micro-pyrolyzer occurred in less than 2 seconds. Vapor products leaving the catalyst bed were detected by GC-MS interfacing with the pyrolysis system. The yield of each compound was estimated individually using their percentage peak areas.

### 2.3. Experimental design

Statistical and mathematical techniques such as response surface methodology are helpful in developing, optimizing,

and improving chemical processes. Moreover, these techniques can be employed for developing, designing, and formulating new products and enhancing the designs of existing products. The RSM is widely used for industrial purposes, especially in case of determining the effects of several input variables on quality characteristics of the products or performance measure or process [31]. Two-variable Central Composite Design (CCD) was used to optimize and study the influence of process conditions on the chemical compounds of fast pyrolysis. The CCD is an effective method for estimation of combined value and quadratic polynomials to optimize the response through a three-dimensional observation space regarding the reaction variables including the temperature and particle size. Design Expert 7 was employed for analyzing the results including phenolic compounds, furfural, and carboxylic acids.

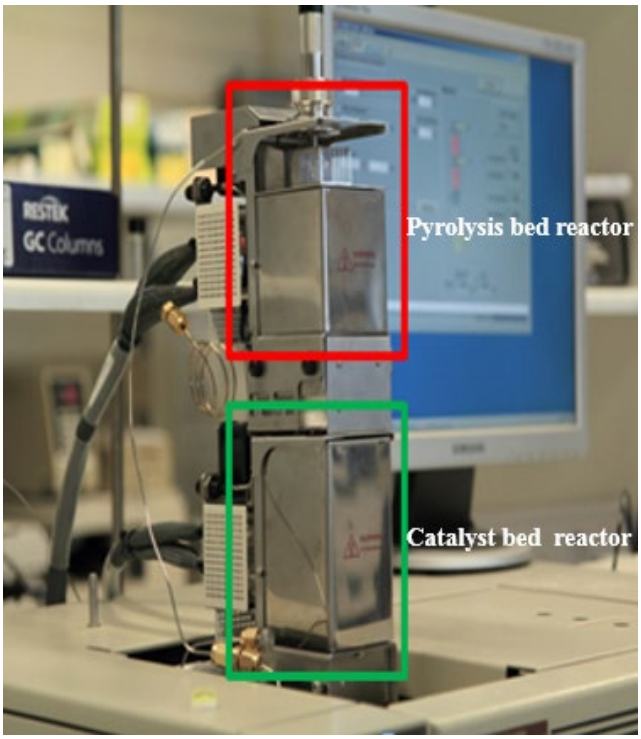


**Figure 1.** The tandem micro-reactor connected with GC-MS

## 3. RESULTS AND DISCUSSION

### 3.1. Characterization of hemicellulose and lignin

The FTIR analysis showed that the broad peak of 3500 $cm^{-1}$ resulted from O-H stretching vibration, while 2900 $cm^{-1}$ was attributed to C-H starching of methyl compounds. The region between 3200 and 3600 $cm^{-1}$ corresponds to hydrogen stretches in several compounds and amines and amides in amino acids. This band is broad because of the high number and large density of hydrogen bands, mainly hydroxyl radicals in the polysaccharide pyronose rings. At 2888 $cm^{-1}$, the observed absorbtion band is related to the axial deformation of C–H group. The peak at 1721 $cm^{-1}$ is characteristic of the carbonyl group (C=O) of the hemicellulose in the sugarcane bagasse. The aromatic ring bond from phenol is determined between 1650 and 1500 $cm^{-1}$. In fact, C=O bonds at 1650 $cm^{-1}$ increase conjugated groups qualitatively with aromatic rings in lignin. The region between 1250 and 1000 $cm^{-1}$ showed that the assignments mainly attributed to oxygenated group (C–O bonds) in alcohols, ethers, and carboxylic acids in sugar which were not affected by metal binding.

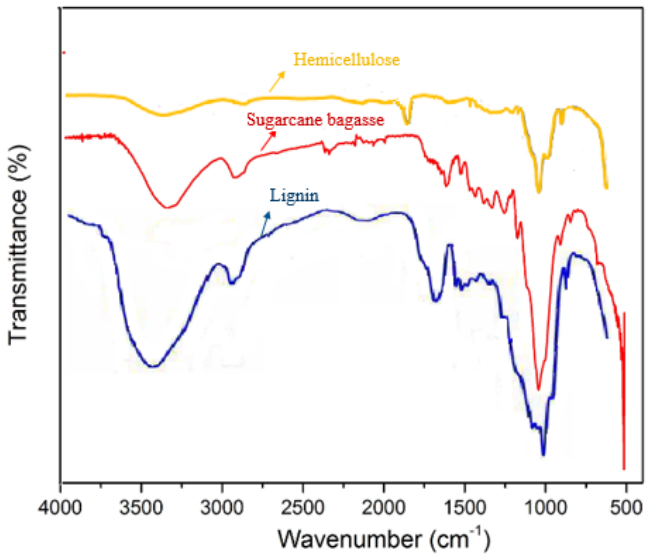


**Figure 2.** FTIR analysis of lignin, sugarcane bagasse, and hemicellulose

### 3.2. Hemicellulose and lignin production distribution from fast pyrolysis

In this study, the sugarcane bagasse product compositions and distribution were evaluated at different temperatures (450-600 °C) and particle size (100-500 µm). The results showed that different compounds could be produced by changing the pyrolysis conditions. In addition, each biomass component generates a wide range of chemical compounds. For example, acetic acid, propionic acid, furfural, 5-hydroxymethey furfural (HMF), and levoglocusan are generated from sugars, while lignin is a significant source of phenol, alkylphenols, and guaiacol. Figure 3 illustrates the main chemical compounds from the pyrolysis of sugarcane bagasse. In this study, the pyrolytic products were divided into three groups including carboxylic acids (sum of acids), furfural (furfural and HMF), and phenolic compounds (sum of lignin products). Among the carboxylic acids, the acetic acid, formic acid, and propionic acid were the main products of pyrolysis of sugarcane bagasse. All pyrolysis products were detected at temperatures above 450 °C.

Figure 4 presents the fast pyrolysis of hemicellulose and lignin compounds with different temperatures and particle sizes. The peak area % of carboxylic acids, furfural, and lignin compounds decreased as the temperature increased. Ben et al. [32] found that the yield of acetic acid dropped at higher temperatures. In this present work, at a temperature above 600 °C, the yield of lignin products declined from 5.9 % to 2.8 %. Lou et al. [33] reported that the amount of phenols slightly decreased at 550 °C. The results implied that the concentration of phenolic macromolecular compounds was enhanced when the temperature increased from 450 °C to 500 °C due to effective primary thermal reactions occurring in this temperature range. At higher temperatures, the secondary reaction decomposes the macromolecular to form the mono-molecular compounds [34].

The effect of particle size showed that the contents of phenolic compounds increased with the increase of particle size, whereas there were no strong effects on carboxylic acids. Montoya et al. [30] showed that the yield of pyrolysis products increased by increasing the particle size of sugarcane bagasse between 0.425 and 0.600 mm. The average particle heating rates were enhanced by decreasing biomass particle

sizes, which favored the release of larger fragments by destroying cell structure. Therefore, selecting an appropriate particle size can improve biomass devolatilization timing and increase the formation of vapor rather than char during fast pyrolysis. The particle size higher than 0.5 mm significantly decreased the contact time of volatiles with silica which led to a decrease in the yield of heavy compounds [35].

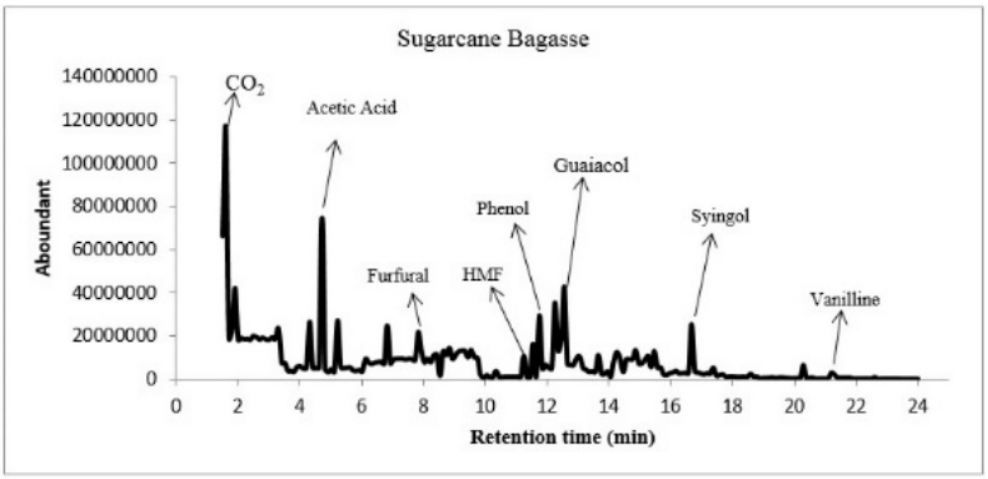


**Figure 3.** Py-GC-MS of sugarcane bagasse at 450 °C (Particle size 300 µm)

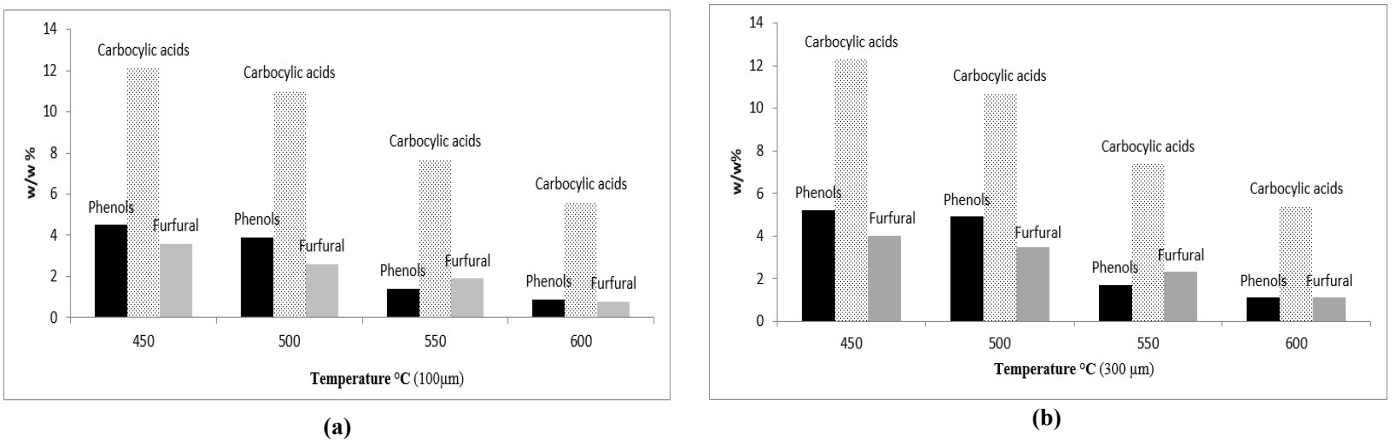


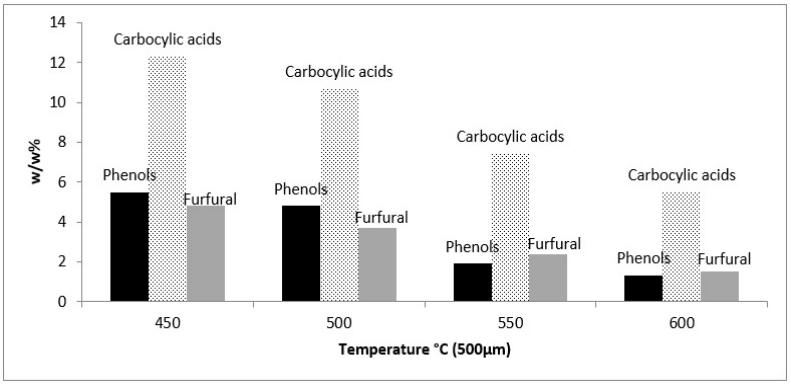


**Figure 4.** The effects of pyrolysis temperature and particle size on the w/w % of sugarcane bagasse: (a) particle size 100 µm, (b) particle size 300 µm, and (c) particle size 500 µm

### 3.3. Fitting the Response Surface Models

Initial comparison of statistical models indicated that the phenolic compounds and furfural were more desired with full quadratic models, while the carboxylic acids corresponded to the linear form (Table 2). The stepwise elimination of insignificant coefficients was deduced for the models based on each response at different temperatures, where $X_1$ and $X_2$ represent the temperature and particle size, respectively.

Phenolic compounds model (%): $+5.11 - 0.4X_1 + 0.95X_2 - 0.15X_{12} - 0.55X_{22}$

Furfural model (%): $+1.62 - 1.63\ X_1 + 0.48X_1X_2 + 0.45X_{12} - 0.4X_{22}$

Carboxylic acids model (%): $+8.45 - 2.55\ X_1 + 0.39\ X_2 - 1.22X_{12}\ X_2$

The significance of temperature and particle size was evaluated by analysis of variance (ANOVA). The highly

effective parameters were validated by a large F-value and a small P-value. Therefore, the comparison between temperature (A) and particle size (B) found that the temperature had more influence on the yields of phenolic compounds, furfural, and carboxylic acids during the process of fast pyrolysis (Table 3).

**Table 2.** The statistics of models

| Models | Statistics | Response | | |
|---|---|---|---|---|
| | | Phenolic compounds | Furfural | Carboxylic acids |
| Linear | $R^2$ | 0.79 | 0.83 | 0.92 |
| | $R^2$-adj. | 0.75 | 0.79 | 0.9 |
| | $R^2$-pred. | 0.63 | 0.63 | 0.83 |
| | Sdv. | 2.35 | 0.3 | 0.66 |
| Linear square | $R^2$ | 0.79 | 0.86 | 0.92 |
| | $R^2$-adj. | 0.72 | 0.82 | 0.90 |
| | $R^2$-pred. | 0.56 | 0.66 | 0.70 |
| | Sdv. | 2.4 | 0.3 | 0.69 |
| Full quadratic | $R^2$ | 0.99 | 0.97 | 0.93 |
| | $R^2$-adj. | 0.98 | 0.94 | 0.88 |
| | $R^2$-pred. | 0.95 | 0.80 | 0.5 |
| | Sdv. | 0.5 | 0.1 | 0.7 |
| Cubic | $R^2$ | 0.99 | 0.98 | 0.98 |
| | $R^2$-adj. | 0.99 | 0.97 | 0.96 |
| | $R^2$-pred. | 0.95 | 0.49 | 0.07 |
| | Sdv. | 0.4 | 0.1 | 0.4 |

**Table 3.** ANOVA for the models for phenolic compounds, furfural, and carboxylic acids

| Response | Factors | DF | Mean of square | F-value | P-value |
|---|---|---|---|---|---|
| Phenolic compounds | A | 1 | 1.26 | 112 | 0.0001 |
| | B | 1 | 7.21 | 641 | 0.0001 |
| | $A^2$ | 1 | 0.16 | 13.97 | 0.0057 |
| | $B^2$ | 1 | 2.07 | 184 | 0.0001 |
| | AB | - | - | - | - |
| | Residual | 8 | 0.01 | - | - |
| | Lack of fit | 4 | 0.017 | 3.23 | 0.14 |
| | Pure error | 4 | 0.13 | - | - |
| | Total | 12 | - | - | - |
| Furfural | A | 1 | 21.33 | 161 | 0.0001 |
| | B | - | - | - | - |
| | $A^2$ | 1 | 1.39 | 10.45 | 0.01 |
| | $B^2$ | 1 | 1.13 | 8.55 | 0.01 |
| | AB | 1 | 0.9 | 6.8 | 0.03 |
| | Residual | 8 | 0.029 | 0.13 | - |
| | Lack of fit | 3 | 0.25 | 14.6 | 0.013 |
| | Pure error | 4 | 0.017 | - | - |
| | Total | 12 | - | - | - |
| Carboxylic acids | A | 1 | 52.17 | 119 | 0.0001 |
| | B | 1 | 0.39 | 0.9 | 0.365 |
| | $A^2$ | - | - | - | - |
| | $B^2$ | - | - | - | - |
| | AB | 1 | 2.77 | 13.85 | 0.0045 |
| | Residual | 10 | 0.2 | - | - |
| | Lack of fit | 6 | 0.33 | 66 | 0.0006 |
| | Pure error | 4 | - | - | - |
| | Total | 12 | - | - | - |

### 3.4. Influence of the temperature and particle size on pyrolysis products

Figure 5(a) presents the interaction between the temperature and particle size on the phenolic compounds. As shown in the figure, yields of phenolic compounds gradually decreased with increasing temperature. On the other hand, more phenolic compounds were generated at a larger particle size at a given temperature. It is illustrated in Figure 5(a) that yields of phenolic compounds considerably decreased at a temperature

above 550 °C. At high temperatures, the more single ring lignin compounds could be produced by cleavage of β–O–4, α–O–4, C–C bond [36]. Chu et al. [37] reported that the β–O–4 ether bond as the most abundant linkage from lignin structure was easily broken at low temperatures because of the lowest dissociation energy (90.9 kcal/mole). Jung et al. [10] found that the lignin began to decompose at a temperature around 170 °C while increasing the temperature led to the generation of more single-ring products from phenolic compound by demethoxylation during secondary reactions [9, 38].

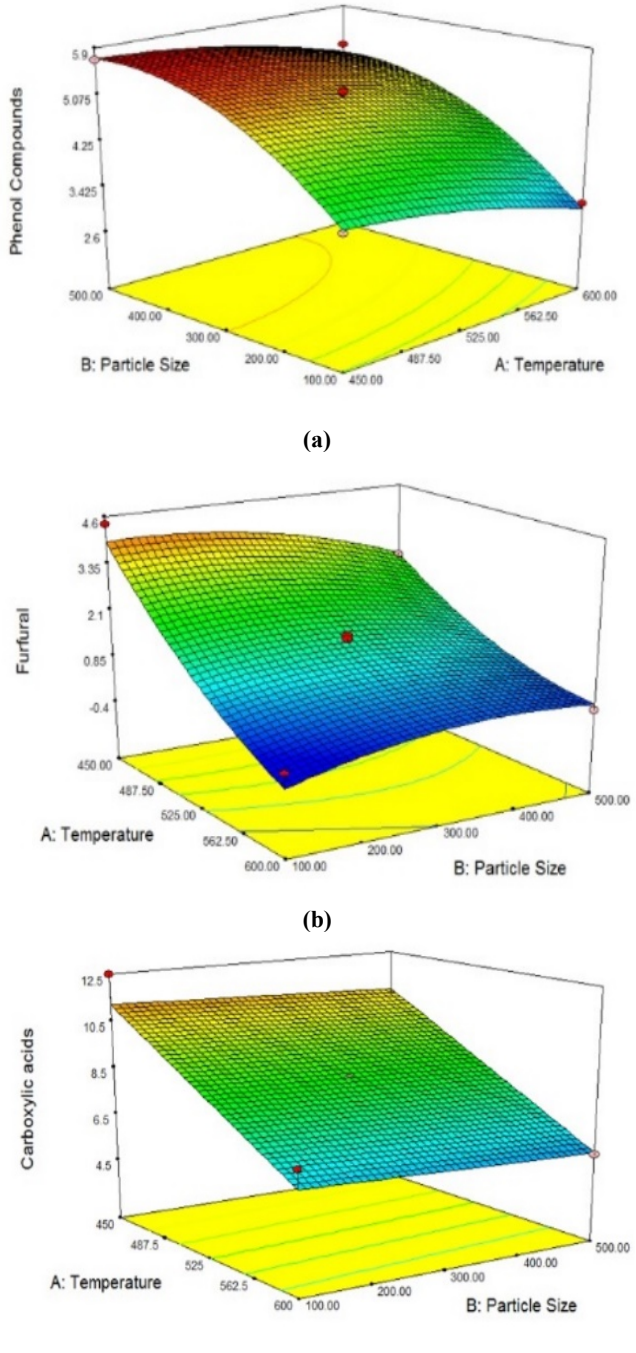


**Figure 5.** Three-dimensional surface of (a) phenolic compounds, (b) furfural and (c) carboxylic acids against temperature and particle size

Figure 5 (b) displays the interaction between temperature and particle size on the furfural. The furfural decreased by increasing the particle size, but it finally increased so that the maximum furfural was achieved at a particle size of 300 μm and at a temperature of 450 °C. It is noteworthy that the maximum furfural was obtained by decreasing the temperature of fast pyrolysis. The cleavage of C-H and C-OH bonding occurred during secondary reaction to break down the HMF from furfural at a temperature of 500 °C. Removal of hydroxymethyl group through dehydration of furanose generated the HMF and then, formed formaldehyde and furfural [33] (Lu et al., (2011)). The authors indicated that HMF and furfural were significantly promoted before reaching 550 °C, while the furans considerably increased after 600 °C, which is in agreement with this present work.

Figure 5 (c) exhibits that yields of carboxylic acids which were primarily decreased by elevating the pyrolysis temperature; however, this effect was not observed by increasing the particle size. Finally, this study shows that the maximum co-production yields of 5.8 % phenolic compounds, 3 % furfural, and 10.3 % carboxylic acids from sugarcane bagasse were found to be optimal conditions of temperature of 450 °C and particle size of 500 μm, respectively.

## 4. CONCLUSIONS

In this study, the yields of hemicellulose and lignin products from fast pyrolysis of sugarcane bagasse were investigated. The fast pyrolysis yields of phenols, furfural, and carboxylic acid compounds in a tandem micro-pyrolyzer were influenced by the variables studied (temperature and particle size). Variation in temperature was determined as the most important variable using RSM analysis. As the temperature raised from 450 °C to 600 °C, the yields of furfural, carboxylic acids, and phenolic compounds decreased. In addition, the yields of phenolic and furfural compounds were clearly enhanced by increasing the particle size, whereas it was not shown to be a critical factor that could influence the yields of carboxylic acids. However, it was found that the maximum content of target compounds of sugarcane bagasse fast pyrolysis occurred below 450 °C and at a particle size of nearly 500 μm.

## 5. ACKNOWLEDGEMENT

The authors would like to thank Aachen University, Germany for providing the pyrolysis data used in this study.

## REFERENCES

1. Leibbrandt, N., Knoetze, J. and Görgens, J., "Comparing biological and thermochemical processing of sugarcane bagasse: An energy balance perspective", ***Biomass and Bioenergy***, Vol. 35, No. 5, (2011), 2117-2126. (https://doi.org/10.1016/j.biombioe.2011.02.017).
2. Bridgwater, A.V., Czernik, S., Diebold, J., Meier, D., Oasmaa, A., Peacocke, G., Piskorz, J. and Radlein, D., Fast pyrolysis of biomass, A handbook, Vol. 1, CPL Press, Newbury Berkshire, (1999). (https://cris.vtt.fi/en/publications/fast-pyrolysis-of-biomass-a-handbook).
3. Venderbosch, R. and Prins, W., "Fast pyrolysis technology development", ***Biofuels, Bioproducts and Biorefining***, Vol. 4, No. 2, (2010), 178-208. (https://doi.org/10.1002/bbb.205).
4. Corton, J., Donnison, I., Patel, M., Bühle, L., Hodgson, E., Wachendorf, M., Bridgwater, A., Allison, G. and Fraser, M., "Expanding the biomass resource: Sustainable oil production via fast pyrolysis of low input high diversity biomass and the potential integration of thermochemical and biological conversion routes", ***Applied Energy***, Vol. 177, (2016), 852-862. (https://doi.org/10.1016/j.apenergy.2016.05.088).
5. Bridgwater, A.V., "Review of fast pyrolysis of biomass and product upgrading", ***Biomass and Bioenergy***, Vol. 38, (2012), 68-94. (https://doi.org/10.1016/j.biombioe.2011.01.048).

6. Mortensen, P.M., Grunwaldt, J.-D., Jensen, P.A., Knudsen, K. and Jensen, A.D., "A review of catalytic upgrading of bio-oil to engine fuels", ***Applied Catalysis A: General***, Vol. 407, No. 1-2, (2011), 1-19. (https://doi.org/10.1016/j.biombioe.2011.01.048).
7. Czernik, S. and Bridgwater, A., "Overview of applications of biomass fast pyrolysis oil", ***Energy & Fuels***, Vol. 18, No. 2, (2004), 590-598. (https://doi.org/10.1021/ef034067u).
8. Luo, Y., Li, Z., Li, X., Liu, X., Fan, J., Clark, J.H. and Hu, C., "The production of furfural directly from hemicellulose in lignocellulosic biomass: A review", ***Catalysis Today***, Vol. 319, (2019), 14-24. (https://doi.org/10.1016/j.cattod.2018.06.042).
9. Lu, Q., Dong, C.-Q., Zhang, X.-M., Tian, H.-Y., Yang, Y.-P. and Zhu, X.-F., "Selective fast pyrolysis of biomass impregnated with $ZnCl_2$ to produce furfural: Analytical Py-GC/MS study", ***Journal of Analytical and Applied Pyrolysis***, Vol. 90, No. 2, (2011), 204-212. (https://doi.org/10.1016/j.jaap.2010.12.007).
10. Jung, K.A., Woo, S.H., Lim, S.-R. and Park, J.M., "Pyrolytic production of phenolic compounds from the lignin residues of bioethanol processes", ***Chemical Engineering Journal***, Vol. 259, (2015), 107-116. (https://doi.org/10.1016/j.cej.2014.07.126).
11. Rinaldi, R., Jastrzebski, R., Clough, M.T., Ralph, J., Kennema, M., Bruijnincx, P.C. and Weckhuysen, B.M., "Paving the way for lignin valorisation: Recent advances in bioengineering, biorefining and catalysis", ***Angewandte Chemie International Edition***, Vol. 55, No. 29, (2016), 8164-8215. (https://doi.org/10.1002/chin.201636254).
12. Ghorbannezhad, P., Firouzabadi, M.D., Ghasemian, A., de Wild, P.J. and Heeres, H., "Sugarcane bagasse ex-situ catalytic fast pyrolysis for the production of Benzene, Toluene and Xylenes (BTX)", ***Journal of Analytical and Applied Pyrolysis***, Vol. 131, (2018), 1-8. (https://doi.org/10.1016/j.jaap.2018.02.019).
13. Ghorbannezhad, P., Kool, F., Rudi, H. and Ceylan, S., "Sustainable production of value-added products from fast pyrolysis of palm shell residue in tandem micro-reactor and pilot plant", ***Renewable Energy***, Vol. 145, (2020), 663-670. (https://doi.org/10.1016/j.renene.2019.06.063).
14. Ghorbannezhad, P., Park, S. and Onwudili, J.A., "Co-pyrolysis of biomass and plastic waste over zeolite-and sodium-based catalysts for enhanced yields of hydrocarbon products", ***Waste Management***, Vol. 102, (2020), 909-918. (https://doi.org/10.1016/j.wasman.2019.12.006).
15. Ansari, K.B., Arora, J.S., Chew, J.W., Dauenhauer, P.J. and Mushrif, S.H., "Fast pyrolysis of cellulose, hemicellulose, and lignin: Effect of operating temperature on bio-oil yield and composition and insights into the intrinsic pyrolysis chemistry", ***Industrial & Engineering Chemistry Research***, Vol. 58, No. 35, (2019), 15838-15852. (https://doi.org/10.1021/acs.iecr.9b00920).
16. Zhang, J., Choi, Y.S., Yoo, C.G., Kim, T.H., Brown, R.C. and Shanks, B.H., "Cellulose–hemicellulose and cellulose–lignin interactions during fast pyrolysis", ***ACS Sustainable Chemistry & Engineering***, Vol. 3, No. 2, (2015), 293-301. (https://doi.org/10.1021/sc500664h).
17. Ghorbannezhad, P., Dehghani Firouzabadi, M. and Ghasemian, A., "Catalytic fast pyrolysis of sugarcane bagasse pith with HZSM-5 catalyst using tandem micro-reactor-GC-MS", ***Energy Sources, Part A: Recovery, Utilization, and Environmental Effects***, Vol. 40, No. 1, (2018), 15-21. (https://doi.org/10.1080/15567036.2017.1381785).
18. Ghorbannezhad, P., Ghasemian, A., de Wild, P.J. and Heeres, H.J., "Biorefinery of bagasse and it's pith by fast pyrolysis", ***Journal of Wood and Forest Science and Technology***, Vol. 24, No. 4, (2018), 27-40. (https://doi.org/10.22069/jwfst.2017.13845.1703).
19. Makkawi, Y., Yu, X. and Ocone, R., "Parametric analysis of biomass fast pyrolysis in a downer fluidized bed reactor", ***Renewable Energy***, Vol. 143, (2019), 1225-1234. (https://doi.org/10.1016/j.renene.2019.05.077).
20. Heidari, A., Stahl, R., Younesi, H., Rashidi, A., Troeger, N. and Ghoreyshi, A.A., "Effect of process conditions on product yield and composition of fast pyrolysis of Eucalyptus grandis in fluidized bed reactor", ***Journal of Industrial and Engineering Chemistry***, Vol. 20, No. 4, (2014), 2594-2602. (https://doi.org/10.1016/j.jiec.2013.10.046).
21. Septien, S., Valin, S., Dupont, C., Peyrot, M. and Salvador, S., "Effect of particle size and temperature on woody biomass fast pyrolysis at high temperature (1000–1400 ºC)", ***Fuel***, Vol. 97, (2012), 202-210. (https://doi.org/10.1016/j.fuel.2012.01.049).
22. Joubert, J.-E., Carrier, M., Stahl, R. and Knoetze, J.H., "Fast pyrolysis of Eucalyptus grandis", ***Centre for Renewable and Sustainable Energy Studies, Stellenbosch***, (2011). (https://doi.org/10.1016/j.fuproc.2014.12.012).
23. Lira, C.S., Berruti, F.M., Palmisano, P., Berruti, F., Briens, C. and Pécora, A.A., "Fast pyrolysis of Amazon *tucumã* (*Astrocaryum aculeatum*) seeds in a bubbling fluidized bed reactor", ***Journal of Analytical and Applied Pyrolysis***, Vol. 99, (2013), 23-31. (https://doi.org/10.1016/j.jaap.2012.11.005).
24. Park, H.J., Park, Y.-K., Dong, J.-I., Kim, J.-S., Jeon, J.-K., Kim, S.-S., Kim, J., Song, B., Park, J. and Lee, K.-J., "Pyrolysis characteristics of oriental white oak: Kinetic study and fast pyrolysis in a fluidized bed with an improved reaction system", ***Fuel Processing Technology***, Vol. 90, No. 2, (2009), 186-195. (https://doi.org/10.1016/j.fuproc.2008.08.017).
25. Amutio, M., Lopez, G., Artetxe, M., Elordi, G., Olazar, M. and Bilbao, J., "Influence of temperature on biomass pyrolysis in a conical spouted bed reactor", ***Resources, Conservation and Recycling***, Vol. 59, (2012), 23-31. (https://doi.org/10.1016/j.resconrec.2011.04.002).
26. Karagöz, S., Kawakami, T., Kako, A., Iiguni, Y. and Ohtani, H., "Single shot pyrolysis and on-line conversion of lignocellulosic biomass with HZSM-5 catalyst using tandem micro-reactor-GC-MS", ***RSC Advances***, Vol. 6, No. 52, (2016), 46108-46115. (https://doi.org/10.1039/c6ra04225b).
27. Wang, K., Zhang, J., Shanks, B.H. and Brown, R.C., "Catalytic conversion of carbohydrate-derived oxygenates over HZSM-5 in a tandem micro-reactor system", ***Green Chemistry***, Vol. 17, No. 1, (2015), 557-564. (https://doi.org/10.1039/c4gc01784f).
28. Tsai, W., Lee, M. and Chang, D.Y., "Fast pyrolysis of rice straw, sugarcane bagasse and coconut shell in an induction-heating reactor", ***Journal of Analytical and Applied Pyrolysis***, Vol. 76, No. 1-2, (2006), 230-237. (https://doi.org/10.1016/j.jaap.2005.11.007).
29. David, G.F., Justo, O.R., Perez, V.H. and Garcia-Perez, M., "Thermochemical conversion of sugarcane bagasse by fast pyrolysis: High yield of levoglucosan production", ***Journal of Analytical and Applied Pyrolysis***, Vol. 133, (2018), 246-253. (https://doi.org/10.1016/j.jaap.2018.03.004).
30. Montoya, J., Valdés, C., Chejne, F., Gómez, C., Blanco, A., Marrugo, G., Osorio, J., Castillo, E., Aristóbulo, J. and Acero, J., "Bio-oil production from Colombian bagasse by fast pyrolysis in a fluidized bed: An experimental study", ***Journal of Analytical and Applied Pyrolysis***, Vol. 112, (2015), 379-387. (https://doi.org/10.1016/j.jaap.2014.11.007).
31. Myers, R.H., Montgomery, D.C. and Anderson-Cook, C.M., Response surface methodology: Process and product optimization using designed experiments, John Wiley & Sons, (2016). (https://doi.org/10.1080/00401706.1996.10484509).
32. Ben, H. and Ragauskas, A.J., "NMR characterization of pyrolysis oils from kraft lignin", ***Energy & Fuels***, Vol. 25, No. 5, (2011), 2322-2332. (https://doi.org/10.1021/ef2001162).
33. Lou, R., Wu, S.-B. and Lv, G.-J., "Effect of conditions on fast pyrolysis of bamboo lignin", ***Journal of Analytical and Applied Pyrolysis***, Vol. 89, No. 2, (2010), 191-196. (https://doi.org/10.1016/j.jaap.2010.08.007).
34. Garcia-Perez, M., Wang, S., Shen, J., Rhodes, M., Lee, W.J. and Li, C.-Z., "Effects of temperature on the formation of lignin-derived oligomers during the fast pyrolysis of mallee woody biomass", ***Energy & Fuels***, Vol. 22, No. 3, (2008), 2022-2032. (https://doi.org/10.1021/ef7007634).
35. Shen, J., Wang, X.-S., Garcia-Perez, M., Mourant, D., Rhodes, M.J. and Li, C.-Z., "Effects of particle size on the fast pyrolysis of oil mallee woody biomass", ***Fuel***, Vol. 88, No. 10, (2009), 1810-1817. (https://doi.org/10.1016/j.fuel.2009.05.001).
36. Rodrigues, J., Graca, J. and Pereira, H., "Influence of tree eccentric growth on syringyl/guaiacyl ratio in Eucalyptus globulus wood lignin assessed by analytical pyrolysis", ***Journal of Analytical and Applied Pyrolysis***, Vol. 58, (2001), 481-489. (https://doi.org/10.1016/s0165-2370(00)00121-2).
37. Chu, S., Subrahmanyam, A.V. and Huber, G.W., "The pyrolysis chemistry of a β-O-4 type oligomeric lignin model compound", ***Green Chemistry***, Vol. 15, No. 1, (2013), 125-136. (https://doi.org/10.1039/c2gc36332a).
38. Jiang, G., Nowakowski, D.J., and Bridgwater, A.V., "Effect of the temperature on the composition of lignin pyrolysis products", ***Energy & Fuels***, Vol. 24, No. 8, (2010), 4470-4475. (https://doi.org/10.1021/ef100363c).

Journal of Renewable Energy and Environment

Research Article

Journal Homepage: www.jree.ir

# Prediction of Discharge Using Artificial Neural Network and IHACRES Models Due to Climate Change

Maryam Hafezparast *, Seiran Marabi

*Department of Water Engineering, Faculty of Agriculture and Natural Sciences, Razi University, P. O. Box: 09914412984, Kermanshah, Kermanshah, Iran.*

*PAPER INFO*

*Paper history:*
Received 21 November 2020
Accepted in revised form 10 July 2021

*Keywords*:
RCP8.5,
Runoff Prediction,
IHACRES,
MLP,
Kermanshah

*ABSTRACT*

Understanding of climate change and its impacts on river discharge has affected the quality and quantity of water and also supplying water requirements for drinking, agriculture and industry. Therefore, prediction of precipitation and temperature by climate models as well as simulation and optimization of their runoff with suitable models are very important. In this study, four climate models of the Fifth Coupled Model Inter comparison Project (CMIP5) and RCP8.5 scenario were used to forecast future precipitation and temperature for the next two periods including 2020-2052 and 2053-2085. Mean Observed Temperature-Precipitation (MOTP) method was used to reduce the uncertainty of climate models and the change factor method was used to downscale the climate data. Then, the Lumped-conceptual Identification of unit Hydrographs and Component flows from Rainfall, Evaporation and Stream flow data (IHACRES) model and multi-layer Artificial Neural Network (ANN) model were employed to estimate the effects of these parameters on the Khorramrood River runoff. The neural network model is written and implemented using Scikit-Learn library and the Python programming language. The comparison of performance of ANN models with different input variables like monthly precipitation, monthly precipitation of previous months, monthly discharge, monthly discharge of previous months, monthly temperature was made to find the best and most efficient network structure. The results showed that the precipitation in Khorramrood River basin based on the weighted combination model decreased by 8.18 % and 9.75 % in the first and the second periods, respectively, while the temperature increased by 1.85 and 4.22 °C, respectively. The discharge parameter in the calibration and validation period in the IHACRES model based on criteria to evaluate the parameters of Root Mean Square Error (RMSE), Mean Absolute Error (MAE), The Coefficient of Determination (R), and the Nash-Sutcliffe Efficiency (NSE) performed better than the artificial neural network model. However, due to the small differences of these changes, the predictions were performed for both periods and using both models and the results indicated that future discharge in the IHACRES model decreased by 12.72 % during the first period and by 20.3 % in the second period, while the model of artificial neural network showed decrease rates of 2.12 % and 6.97 %, respectively.

https://doi.org/10.30501/jree.2021.257941.1162

## 1. INTRODUCTION

Human activities are one of the most important factors affecting water resources planning and regional hydrology [1, 2, 3]. Therefore, improving hydrological and regional climate simulation, especially precipitation and flow, is an important goal for meteorological and water professionals. Such improvements will increase the effectiveness of regional water resources planning and management and reduce flood and drought losses. Previous studies have shown that the slightest fluctuation in the probability or severity of precipitation has significant effects on runoff [4, 5]. There are three groups of hydrologic forecasting that have been used more than three decades: lumped conceptual models, models based on physical distributions, and empirical black box models [6]. There is a complex nonlinear relationship among discharge, precipitation, and temperature which affects the assessment climate change impacts on runoff [7]. Therefore, climate change scenarios in the future are very important for water resources planning and management, agriculture and water users [8, 1]. Climate change as one of the major challenges of the twenty-first century has affected human society. Rapid population growth and industrial development as well as deforestation and environmental degradation have led to an increase in greenhouse gas emitted from Earth's surface in recent decades. The increasing trend of warming has caused the Earth's surface temperature to rise in the current century. The rate of temperature increase is predicted between 0.3 and 4.8 °C under the four trends of greenhouse gas concentrations by 2100 [9]. The Fifth Assessment Report (AR5) of the Intergovernmental Panel on Climate Change (IPCC) in 2013 showed that global warming caused a change in the water cycle due to increased greenhouse gas concentrations. The consequences of this phenomenon have different effects on water resources systems and various aspects of human life the most important of which can be the changes in the spatial and temporal distribution of precipitation and its type, surface runoff, evaporation, groundwater recharge, and sea level rise

*Corresponding Author's Email: m.hafezparast@razi.ac.ir (M. Hafezparast)
URL: https://www.jree.ir/article_133315.html

Please cite this article as: Hafezparast, M. and Marabi, S., "Prediction of discharge using artificial neural network and IHACRES models due to climate change", ***Journal of Renewable Energy and Environment (JREE)***, Vol. 8, No. 3, (2021), 75-85. (https://doi.org/10.30501/jree.2021.257941.1162).

which ultimately affect human settlements and agricultural production. It, therefore, requires that the impacts and consequences of climate change on water resources be seriously considered. In recent years, the effect of this phenomenon on different catchments on the surface of the earth has been investigated. Most researchers around the world have used the Fifth Assessment Report to study climate change under new emission scenarios in different regions [10, 11, 12, 13, 3]. Some of them are listed below.

## 2. LITRATURE REVIEW OF EXSISTING METHODS

Tan studied the impacts of climate change on the Kalantan River in northeastern Malaysia. 36 Climate Change Downscaling Projects from five Atmospheric General Circulation Models (AGCMs) under three RCP Scenarios of 2.6, 4.5 and 8.5 for two future periods from 2015-2044 and 2045-2074 were studied with respect to the base period (1975-2004) [13]. The results of the five atmospheric general circulation models show the increase of 1.2 to 8.8 % in annual precipitation and 0.6 to 2.2 °C at maximum temperature. Decision making on water management and construction and operation of hydraulic structures requires reliable information about the flow discharge in the river basin to facilitate decision-making according to design flood discharge. IHACRES model is one of the semi-conceptual rainfall-runoff models that could generate effective rainfall and runoff simulation with inadequate information. Water resources management is a key issue for sustainable development in the future in arid and semi-arid regions like Western Australia. In a study conducted in this area, IHACRES rainfall-runoff model based on problem physics and artificial neural network models was used to simulate the runoff of the Marillana Basin in the Pilbara region [14]. Sadeghi Loyeh simulated the rainfall-runoff process using two conceptual models including HEC-HMS and IHACRES, and three experimental artificial neural network models, namely Multivariate Regression (MLR), and Simple Linear Regression (SLR), and monthly runoff time series and meteorological data of Lighvan river in Iran during 1972-2004 were used [15]. Ghanbarpour simulated and estimated runoff of Kasilian Basin using ANN, ARMA, SWRRB, and IHACRES despite lack of sufficient meteorological information, and the results of the study showed the proper performance of IHACRES and artificial neural network [16]. Karamouz developed IHACRES and ANNs models for long-term runoff simulation in Southeastern Iran and then, the two models were compared. At first, the rainfall was predicted using climatic signals and then converted to runoff. Therefore, daily precipitation was downscaled using SDSM and LARS-WG methods and the outputs of these two models were selected as inputs of the rainfall-runoff IHACRES model to simulate runoff. In the neural network model, Sea Level Pressure (SLP), Sea Surface Temperature (SST), and Sea Level Pressure Changes (ΔSLP) and runoff were introduced as input parameters and two MLP and ELMAN networks were investigated. The results pointed to the better performance of MLP network than ELMAN in artificial neural network model [17]. Pourkheirolah used hydrological modeling to assess the impact of climate change on the hydrological conditions of Dehloran Station. In this study, Csirok3-5-0 model output under RCP8.5 scenario was used. Precipitation and temperature values for future period (2016-2044) were calculated using the downscaled change factor method and IHACRES model was used to simulate basin runoff. The results showed that the average runoff decreased from 6.27 $m^3/s$ in the base period to 5.78 $m^3/s$ in the future period. Also, simulation of monthly basin runoff in the future period and comparison of its values with the observed period shows average decline of long-term annual runoff in the future period in the desired scenario [15]. Sayahi first calibrated IHACRES hydrological model using APHRODITE precipitation network data and CHCN-CAMS temperature dataset for the basin. Then, by introducing the temperature and precipitation scenario 2.6 of the fifth report to the mentioned hydrological model, discharge variations in the basin are predicted for the future periods. The results showed the rise of 0.17 to 2 degrees Celsius and a 3 to 75 percent of rainfall variation during 2011-2035 period compared to the 1983-2007 observation period. Runoff simulation results for the future period show the average annual runoff of 9.7 % compared to the observed period [18]. Hydrological models are vital and exigent tools for water resources and environmental planning and management. Three models of SWAT, IHACRES, and ANN were studied on daily, monthly, and annual bases in the Kan watershed, which were located in the west part of Tehran, Iran. ANN model showed a better performance for daily, monthly, and annual flow simulations compared with other two models (NSE=0.86, $R^2$=0.87, RMSE=2.2, MBE=0.08) and particularly for the simulation of maximum and minimum flow values. In addition, the performance of SWAT model (NSE=0.65, $R^2$=0.68, RMSE=3.3, MBE=-0.168) was better than that of the IHACRES model (NSE=0.57, $R^2$=0.58, RMSE=3.7, MBE=0.049). However, the results of the IHACRES model were still acceptable [19].

According to this review, the first goal of this work is to use IHACRES and ANNs to build a hydrologic model in basin under climatic conditions to simulate stream flow. These models are assessed on a basin scale and at monthly time intervals. To study climate change in the Kangavar region and its effects on the flow of the Khorramrood River, first, the suitable CMIP5 climate models for the region were selected. Then, these data were downscaled at the Aran station, and then the MLP neural network and the lumped-conceptual IHACRES models were compared to predict future discharge. A comparison of performance of ANN models with different input variables (e.g., monthly precipitation, monthly precipitation of previous months, and total precipitation of previous months, monthly temperature) has been made to find the best and most efficient network structure. In addition, their efficiency in the estimation of different ranges of flow (from very high to very low flow) is determined based on the Flow Duration Curve (FDC). To ensure the validity of the results, Aran station is in natural regime. Selecting an appropriate model to simulate the stream flow in a watershed is a key challenge, and analyzing the performance of these models in different climate scenarios could help researchers to apply the suitable model to each case.

## 3. STEPS OF THE PROPOSED METHODOLOGY

In this study, the rainfall and temperature data were first obtained from climate models and, then, downscaled for the target area to evaluate the discharge changes of Khorramrood River, which is a tributary of the Gamasiab River and, also, the Anahita Dam was built on it. Next, the discharge variations due to climate change in the Khorramrood River were estimated using artificial neural network and semi-

conceptual IHACRES model (Fig. 1). Neural network modeling was done in the Python programming language and the Scikit-Learn Library.

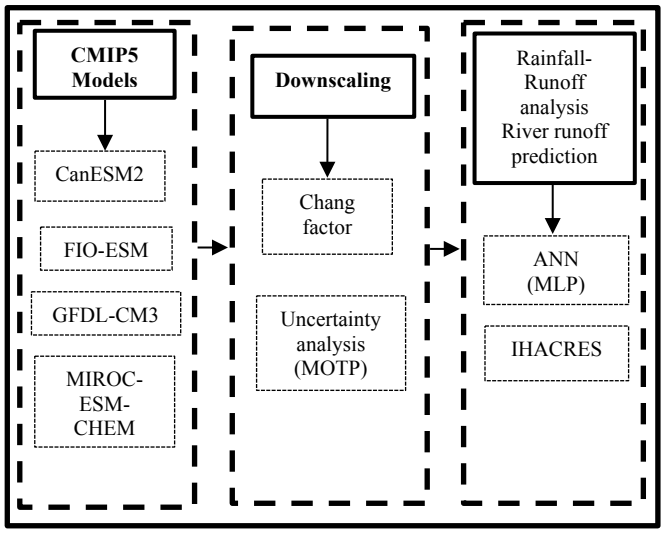


**Figure 1.** Flowchart of research

### 3.1. Climatic and hydrometric data

In order to study climate changes in the study area using RCP scenarios, monthly information of historical temperature and rainfall is required. Therefore, the Kangavar Synoptic Station information obtained over the course of 1983-2015 period, which is measured by Kermanshah Regional Meteorological Office, is used, as shown in Table 1. The measured quantitative monthly data including the flow discharge of Khorramrood River at Aran base station were obtained from Kermanshah Regional Water Authority, as shown in Table 2.

### 3.2. Study area

Kangavar County with an area of about 674 square kilometers is located in the east of Kermanshah province in West of Iran. Most western parts of Iran are composed of Zagros interconnected mountains and the fertile plain of Kangavar to the west of these highlands, which is located at an elevation of 1457 meters above sea level. The Central Zagros Highlands has covered the northern and northwestern parts of this vast plain. Aran base station is located at 47.925 °E longitude and 34.41 °N latitude. Much of precipitation occurs in December and January. The water in this region is supplied by rainfall stored in aquifers or from the many mirages of the area flowing into the rivers of Khorramrood, Asadabad, and Kangavar and the confluence of these rivers forms the water-filled Gamasiab River. Khoramrood River originates from southeast of Malayer highlands and joins Gamasiab River after irrigating agricultural land on its way to Hamadan and Kermanshah provinces (Fig. 2).


**Figure 2.** Geographical location of the Khorramrood watershed in Kermanshah Province and Iran

**Table 1.** Weather data of Kangavar synoptic station (1983-2015)

| Month | | Jan. | Feb. | Mar. | Apr. | May | Jun. | Jul. | Aug. | Sep. | Oct. | Nov. | Dec. |
|---|---|---|---|---|---|---|---|---|---|---|---|---|---|
| Mean | precipitation (mm) | 58 | 65 | 69 | 53 | 36 | 4 | 1 | 1 | 3 | 28 | 67 | 63 |
| Max | | 283 | 305 | 339 | 108 | 211 | 21 | 8 | 13 | 19 | 83 | 347 | 176 |
| Min | | 13 | 27 | 22 | 0 | 5 | 0 | 0 | 0 | 0 | 0 | 11 | 0 |
| Mean | Temperature (°C) | -0.06 | 2.32 | 6.97 | 2.96 | 16.85 | 22.53 | 26.5 | 25.8 | 20.76 | 14.8 | 12.08 | 7.78 |
| Max | | 4.47 | 6.87 | 11.0 | 7.28 | 20.06 | 25.87 | 29.8 | 28.3 | 23.89 | 17.6 | 15.41 | 10.87 |
| Min | | -8.65 | -8.30 | 1.46 | -1.22 | 13.70 | 18.61 | 23.36 | 22.21 | 17.97 | 12.80 | 9.94 | 5.54 |

**Table 2.** Khorramrood River flow in 1983-2015 ($m^3/s$)

| Month | Jan. | Feb. | Mar. | Apr. | May | Jun. | Jul. | Aug. | Sep. | Oct. | Nov. | Dec. |
|---|---|---|---|---|---|---|---|---|---|---|---|---|
| Mean flow ($m^3/s$) | 5.23 | 6.53 | 8.16 | 8.15 | 5.31 | 1.81 | 0.30 | 0.06 | 0.05 | 0.51 | 2.92 | 5.00 |

### 3.3. Climate scenarios (RCP)

At present, the most valid tool to generate climate scenarios is the Atmospheric-Ocean General Circulation Models (AOGCM) [20, 21]. The Intergovernmental Panel on Climate Change has used New RCP (Representative Concentration Pathways) scenarios as the trajectory of greenhouse gas concentrations to compile the Fifth Assessment Report (AR5). The new emission scenarios have four key trajectories called RCP2.6, RCP4.5, RCP6, and RCP8.5 that are named based on

Radiative Forcing in 2100 and can yield different levels of greenhouse gas emissions in any situation according to different characteristics of the technology level, socio-economic status, and future policies of a region. The variables in this scenario are:

- Emissions of gases such as $SF_6$, CFCs, PFCs, HFCs, $N_2O$, $CH_4$, $CO_2$.
- Emissions of chemically active gases and aerosols, Black Carbon (BC), $SO_2$, $NH_3$, organic carbon, VOCs, $NO_x$, $CO_2$, $NH_3$.
- The concentration of greenhouse gases including HFCs, PFCs, CFCs.
- The concentrations of aerosols & chemically active gases ($O_3$, aerosol).
- Land use and land cover data.

These scenarios were formulated in 2014 by the Scientific Committee under the auspices of the Intergovernmental Panel on Climate Change to provide a set of information whose results can track the main factors in climate change [9]. The present study was conducted based on downscaling of CMIP5 climate model data at Kangavar weather station and Aran Hydrometric station located in the Khorramrood River basin during the 33-year base period of 1983 to 2015. In order to create climate scenarios for the future 2020-2052 and 2053-2085 periods, the results of four models of the IPCC Fifth Assessment Report (AR5) under RCP8.5 scenario are used which have different resolutions, as shown in Table 3.

**Table 3.** AR5 models and their resolution

| Model | (m × m) |
|---|---|
| CanESM2 | 128 × 64 |
| FIO-ESM | 128 × 64 |
| GFDL-CM3 | 144 × 90 |
| MIROC-ESM-CHEM | 128 × 64 |

### 3.4. Uncertainty analysis with (MOTP)

In this method, the AR5 models are weighted based on the standard deviation of simulated mean temperature and precipitation in the base period of the average observational data.

$$W_i = \frac{(\frac{1}{\Delta P_i})}{\sum_{i=1}^{N}(\frac{1}{\Delta P_i})} \quad (1)$$

where $W_i$ is weight of each model in the desired month and $\Delta P_i$ is the Long-term mean deviation of the simulated rainfall by each model in the base period from the mean observational data. By assigning rainfall values instead of high temperatures, weights corresponding to rainfall variables are also obtained [22].

### 3.5. Downscaling

The outputs of climatic models do not have the required accuracy of spatial and temporal analysis; therefore, the outputs of climate models need to be downscaled to the target area. Existing conventional downscaling methods including LARS-WG have not yet been updated for the new RCP scenarios and a number of primary variables of the SDSM method have not yet been prepared for AR5 models [23]. Therefore, the change factor method is considered for this study. In order to downscale the data locally, the proportional method was used whose climate variables simulated by AOGCM were extracted from the cellular information where the target area was located. The change factor method (Equations 2 to 5) was also used for temporal downscaling of the data [22].

$$\Delta Ti = \overline{T}_{AOGCM,Fut,i} - \overline{T}_{AOGCM,Base,i} \quad (2)$$

$$\Delta P_i = (\frac{\overline{P}_{AOGCM,Fut,i}}{\overline{P}_{AOGCM,Base,i}}) \quad (3)$$

$$T = T_{Obs} + \Delta T \quad (4)$$

$$P = P_{Obs} \times \Delta P \quad (5)$$

In Equation 2, $\Delta Ti$ is the temperature variation for the long-term average of 33 years in each month, $\overline{T}_{AOGCM,Fut,i}$ is the simulated average temperature by each AOGCM in the future period for each month, $\overline{T}_{AOGCM,Base,i}$ is the simulated average temperature by each AOGCM in the observed period for each month, and the above items are considered for rainfall in Equation 3. In Equation 4, T is the time series derived from the climate temperature scenario for the future period, while Tobs is time series of the observed temperature in the base period (1983-2015). Equation 5 is time series of rainfall due to precipitation changes in Equation 3.

### 3.6. Rainfall-runoff simulation

Analysis of climate parameters variation on river discharge of the basin is possible using Rainfall-Runoff models. The changes in river discharge are important to satisfy water demands for agriculture, drinking, and industry demands. In this study, the IHACRES rainfall-runoff model and the artificial neural network model were employed to produce monthly runoff, and the results of both models were compared and the variations of climatic parameters on runoff were extracted.

### 3.7. IHACRES model

In IHACRES model, two nonlinear modulus reduction (loss) and linear unit hydrograph are used for runoff production. IHACRES model has two parts: (a) a part that converts rainfall at time k (rk) to effective rainfall (uk) (part of the rainfall that eventually enters the river) and the excess rainfall that is eventually removed by evapotranspiration (assuming the basin is impenetrable); (b) A linear conversion function (or UH unit hydrograph) that converts effective rainfall into the modeled flow (Xk). Here, these sections are called the loss section and the conversion function (unit hydrograph), respectively. The loss section is considered for all nonlinear rainfall-runoff processes on a watershed scale, while the conversion function is based on linear system theory. The IHACRES model has six parameters of which three parameters are related to the nonlinear loss section including (1/C), ($w\tau$), and f, which are the watershed storage capacity, the time constant at which the watershed wetness decreases, and the basin temperature modulation factor, respectively. Meanwhile, the other three parameters corresponding to the

linear conversion function include $\tau$ (q) and $\tau$ (s), which are the times required for the fast and slow stream flows, and the V (S) represents the volume of the slow stream involved in the creation of the river. Examples of studies that have used IHACRES model can be found in the studies of [24], [25] and [26].

In this research, observational data of temperature, precipitation, and monthly discharge in the base period were used for calibration purpose. First, the IHACRES model should be calibrated for the study area and after model calibration, the monthly runoff in the basin is predicted by introducing downscaled temperature and rainfall data of the climate models for the next two periods and finally, the results of the model performance are discussed.

### 3.8. Artificial neural network (ANN)

Artificial neural networks are one of the most widely used structures in artificial intelligence that can even be considered as the basis of branches of artificial intelligence. Artificial neural networks are the intersection of biology, psychology, mathematics, and computers. Today, these structures are used in various engineering and basic sciences to automate, classify, and estimate complex functions. Although the age of neural networks has not exceeded 80 years, its application has now expanded to such an extent that its role in the advancement of various scientific fields cannot be ignored [27]. The use of Python programming language libraries in the neural network facilitates very good prediction of parameters based on appropriate predictors.

### 3.9. Multi-layer perceptron

Two or more neurons can be combined into a single layer. A particular network itself can consist of multilayers in which each layer in the grid has its own weight matrix, bias vector, and output. Relation 6 shows the multi-layer perceptron formula where f is the nonlinear activation function; $w_j$ represents the weights of each layer; b is the bias, $x_j$ represents the inputs, and y is the target [28].

$$y = f(\sum_j w_j x_j + b) \quad (6)$$

Python language now provides the best and most convenient algorithms for data analysis and artificial intelligence. The MLP method of scikit-learn library was used for this purpose. The codes are available on: https://github.com/maryamhafezparast.

Using following formula (Equation 7) helps determine the total number of hidden layers needed.

$$N_h = N_s/(\alpha * (N_i + N_o)) \quad (7)$$

where $N_i$ is the number of input neurons, $N_o$ the number of output neurons, $N_s$ the number of samples in the training data set, and α an arbitrary scaling factor measured between 2-10.

In this study, the MLP multilayer perceptron networks with different hidden layers (Equation 7) and the number of neurons have been calibrated to model the runoff of Khorramrood River using artificial neural networks, which are widely used in hydrological modeling [29, 30]. 70 % of the data were considered for network training and 30 % for network testing period. Relation 8 was used to normalize the data [31].

$$X_{normal} = \left(\left(\frac{X_t - X_{min}}{X_{max} - X_{min}}\right) \times 2\right) + 1 \quad (8)$$

### 3.10. Performance criteria

In order to compare and evaluate the performance of the studied models, Root Mean Square Error (RMSE), Mean Absolute Error (MAE), the coefficient of determination (R), and the Nash Sutcliffe coefficient (NSE) were used.

$$RMSE = \left(\frac{1}{N}\sum_{i=1}^{n}(P_i - O_i)^2\right)^{0.5} \quad (9)$$

$$MAE = \frac{1}{N}\sum_{i=1}^{N}|P_i - O_i| \quad (10)$$

$$R = \sqrt{\frac{(\sum_{i=1}^{n}(P_i - \overline{P})(O_i - \overline{O}))^2}{\sum_{i=1}^{n}(P_i - \overline{P})^2 (O_i - \overline{O})^2}} \quad (11)$$

$$NSE = 1 - \frac{\sum_{i=1}^{N}|O_i - P_i|}{\sum_{i=1}^{N}|O_i - \overline{O}_i|} \quad (12)$$

where n is the number of data, $O_i$ is the observed values, $P_i$ is the computational values by the model, and $\overline{O}_i$ and $\overline{P}$ are the average observational and computational values by the model.

## 4. RESULTS AND DISCUSSION

The results of this study include downscaling results of 5 CMIP5 climate change models that show rainfall and temperature values in the first and second future periods and then, the role of these input variables in producing Khoramrood River discharge is estimated using artificial neural network and IHACRES models. Next, the results of both models are compared and the advantages and disadvantages of these methods are compared with the results reported by other researchers.

### 4.1. Reduction of uncertainty with MOTP

As mentioned, the uncertainty of each model can be reduced using the MOTP method and a weighted combination model is obtained by considering the weight of different climatic models. In this case, the results of this model can be used to predict the parameters in the future as an average of all the models used in the research. Meanwhile, in this method, weights of rainfall and temperature parameters of each climate model were determined separately for each month, as presented in Tables 4 and 5.

### 4.2. Comparing performance of climate models with observed data

In this section, the error criterion for evaluating the performance of climate models was used in this study. These criteria include coefficient of determination ($R^2$), the Nash Sutcliffe coefficient (NSE), Root Mean Square Error (RMSE), and Mean Absolute Error (MAE). The historical long-term averages of each climate model and the combined model were compared to observational data during the base period (1983-2015), as shown in Tables 6 and 7. It is observed that the performance of the combined model and the climate models of the fifth report used in this study to simulate rainfall and temperature for the studied station shows a high correlation

coefficient with relatively low error indicators. Therefore, it can be concluded that all models have a good ability to simulate the climate variables of Khorramrood River basin and one can trust the output of models for the studied basin. It should be noted that the weighted combination model had better performance than the other models, but all models have generally good predictability in this basin.

**Table 4.** Weight of each climate model for rainfall separated by months

| Models | Jan. | Feb. | Mar. | Apr. | May | Jun. | Jul. | Aug. | Sep. | Oct. | Nov. | Dec. |
|---|---|---|---|---|---|---|---|---|---|---|---|---|
| MIROC | 0.35 | 0.11 | 0.34 | 0.29 | 0.12 | 0.14 | 0.21 | 0.28 | 0.20 | 0.16 | 0.51 | 0.39 |
| CANSM2 | 0.21 | 0.11 | 0.21 | 0.21 | 0.17 | 0.27 | 0.17 | 0.17 | 0.20 | 0.43 | 0.15 | 0.30 |
| FIO | 0.14 | 0.39 | 0.22 | 0.18 | 0.47 | 0.43 | 0.41 | 0.23 | 0.19 | 0.29 | 0.14 | 0.16 |
| GFDL | 0.30 | 0.39 | 0.23 | 0.31 | 0.24 | 0.16 | 0.21 | 0.32 | 0.41 | 0.11 | 0.20 | 0.15 |

**Table 5.** Weight of each climate model for the temprature separated by months

| Models | Jan. | Feb. | Mar. | Apr. | May | Jun. | Jul. | Aug. | Sep. | Oct. | Nov. | Dec. |
|---|---|---|---|---|---|---|---|---|---|---|---|---|
| MIROC | 0.34 | 0.22 | 0.23 | 0.28 | 0.23 | 0.22 | 0.20 | 0.24 | 0.18 | 0.20 | 0.20 | 0.19 |
| CANSM2 | 0.17 | 0.25 | 0.27 | 0.26 | 0.25 | 0.32 | 0.28 | 0.28 | 0.40 | 0.48 | 0.45 | 0.33 |
| FIO | 0.24 | 0.20 | 0.18 | 0.21 | 0.26 | 0.24 | 0.23 | 0.19 | 0.19 | 0.15 | 0.15 | 0.21 |
| GFDL | 0.25 | 0.33 | 0.31 | 0.25 | 0.27 | 0.22 | 0.28 | 0.29 | 0.23 | 0.17 | 0.20 | 0.27 |

**Table 6.** Comparing performance criteria of climate models using the observed precipitation

| | Precipitation | | | |
|---|---|---|---|---|
| Models | NSE | MAE | RMSE | R |
| Weighted Model | 0.91 | 5.22 | 6.90 | 0.97 |
| MIROC-ESM-CHEM | 0.86 | 7.41 | 8.96 | 0.97 |
| FIO-ESM | 0.73 | 9.03 | 12.34 | 0.92 |
| GFDL-CM3 | 0.82 | 8.02 | 9.93 | 0.95 |
| CanESM2 | 0.75 | 9.52 | 12.03 | 0.92 |

**Table 7.** Comparing performance criteria of climate models by the observed temperature

| | Temperature | | | |
|---|---|---|---|---|
| Models | NSE | MAE | RMSE | R |
| Weighted Model | 0.97 | 1.23 | 1.3 | 0.99 |
| MIROC-ESM-CHEM | 0.97 | 1.37 | 1.45 | 0.99 |
| FIO-ESM | 0.97 | 1.49 | 1.54 | 0.99 |
| GFDL-CM3 | 0.97 | 1.1 | 1.27 | 0.99 |
| CanESM2 | 0.98 | 1.106 | 1.21 | 0.995 |

### 4.3. Prediction of temperature and precipitation with climate models

After downscaling the data for each climate model, the rainfall and temperature of each model and also the number of changes in these parameters (during the first and second future periods) with observational value could be observed. In Figs. (3, 4), rainfall and temperature variations for each model are specified as column chart and the observational value and weighted combination model for periods (2020-2052) and (2053-2085) are linear chart.

The results of the rainfall parameter under RCP 8.5 scenario showed that some models such as CanESM2, FIO-ESM, GFDL-CM3, and weighted combination model have predicted decreases of 13.86 %, 2.65 %, 23.47 %, 8.18 % in the first period compared to the base period. In the second period, this trend continues: CanESM2 model (6.61 %), FIO-ESM model (9.25 %), GFDL-CM3 model (26.33 %), and weighted combination model were reduced by 9.75 % compared to the base period. However, the MIROC-ESM-CHEM model showed an increase of 6.66 % for both first and second durations.

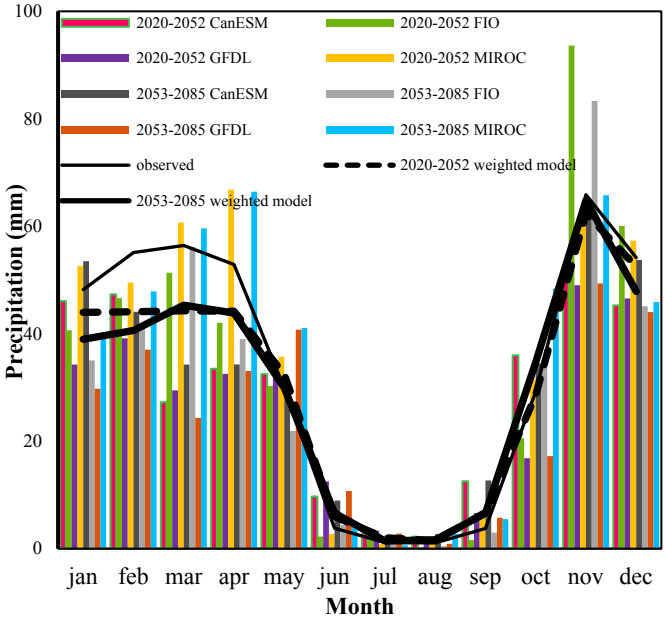


**Figure 3.** Rainfall changes in climate models under Scenario 8.5

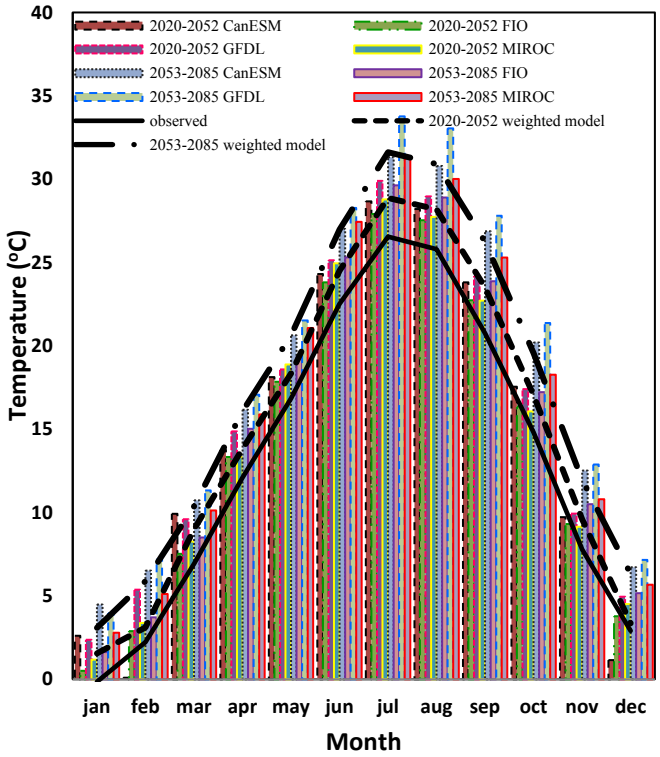


**Figure 4.** Temprature changes in climate models under Scenario 8.5

In the spring, the longest difference in long-term rainfall is observed in March using GFDL-CM3 model during 2053-2085 period. The results of the temperature predicted by climate models used for Khorramrood river basin have generally predicted an increasing temperature trend in which the increasing changes in the second future period are much more than the first period. In the first period, CanESM2, FIO-ESM, GFDL-CM3, MIROC-ESM-CHEM, and weight combination model increased 1.5, 1.21, 2.69, 1.66 and 1.85 °C, respectively, compared to the base period. In the second period, CanESM2 of 4.58 °C, FIO-ESM of 2.48 °C, GFDL-CM3 of 5.54 °C, MIROC-ESM-CHEM of 3.73 °C, and weight combination model increased by 4.22 °C compared to the base period.

### 4.4. Calibration and verification of IHACRES

In order to calibrate and validate the IHACRES rainfall-runoff model, it was tested for model calibration for several years. The results indicated that the period 1988, 2006 to 7, 12 correlated well with the observation period. After calibrating the model and parameters of the rainfall-runoff model, the rest of the data were employed to validate the model. The calibration parameters of the IHACRES model are shown in Table 8.

The simulation results of the IHACRES model for calibration and validation periods are presented in Figures 5 and 6. Comparative results of the simulated and observed runoff hydrographs pointed to a good compatibility between hydrographs. Meanwhile, the IHACRES model has simulated the occurrence time of peak discharge well. Validation of model results is essential to increasing user confidence for model simulation capability. Therefore, without changing the values of the input parameters, the calibrated model was used for the validation period.

**Table 8.** The calibration coefficients of IHACRES model

| Parameter | Description | Optimum value |
|---|---|---|
| C | Humidity storage capacity | 0.0024 |
| T(W) | Drying time | 1 |
| F | Watershed temperature coefficient | 2.4 |
| I | Humidity threshold coefficient | 0 |
| P | Soil humidity intensity | 1 |
| a(s) | Drought index | -0.198 |
| B(s) | Peak index | 2.25 |
| T(s) | Slow-down flow | 0.617 |
| V(s) | Volume ratio | 2.8 |
| $T_{ref}$ | Reference temperature | 20 |

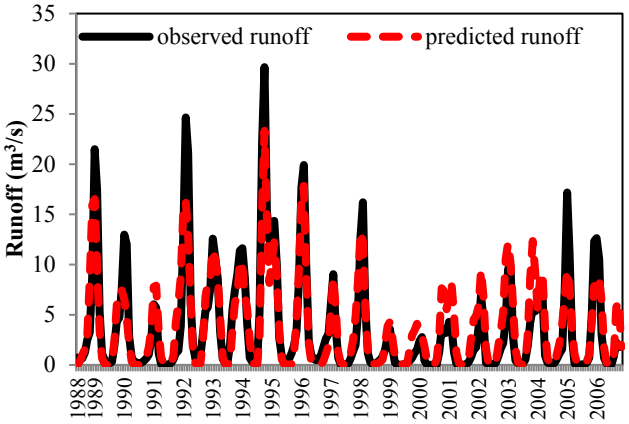


**Figure 5.** The simulated and observed runoffs during the calibration period for the IHACRES model

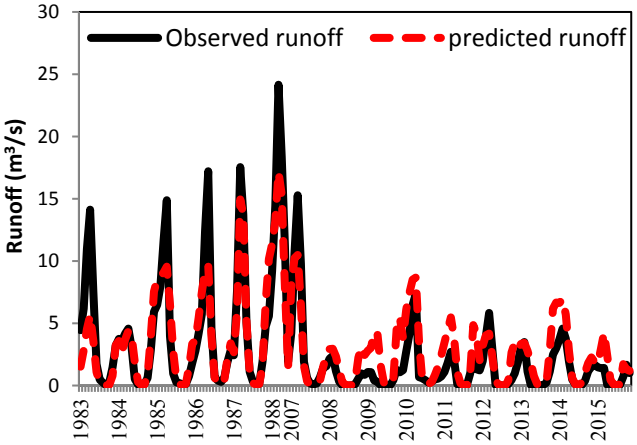


**Figure 6.** The simulated and observed runoffs during the validation period for the IHACRES model

### 4.5. Calibration and verification of ANN

The number of neurons in the input and output layers is determined by the nature of the problem under investigation. In this study, the number of neurons in the hidden layer was determined through trial and error in order to reduce the error. The process began with a small number of neurons and additional neurons were added until increase in the number of neurons had no effect on error recovery. The characteristics of the chosen network to simulate runoff using artificial neural network are listed in Table 9. The results showed that having only one hidden layer was better than more hidden layers and this could be due to the lack of direct correlation between the

middle layers with the network output and the minor impact of the middle layer changes on weight adjustment. Finally, the outputs of the selected models were compared with the observed values and the optimal model was selected.

**Table 9.** Properties of the selected ANN model

| Model characteristic | |
|---|---|
| Input variable | P(t) , P(t-1) ,Q(t-1),Q(t-2) |
| Target | Q(t) |
| Network | MLP |
| Percentage of verification | 70 |
| Percentage of calibration | 30 |
| Number of hidden layers | 1 |
| Number of neurons in the hidden layer | 13 |
| Number of iterations | 2000 |

Figures 7 and 8 show the observed and simulated hydrographs during the calibration and validation periods in the selected ANN model. The simulated discharge at the peak points overlapped well with the observed data, but the monthly patterns of discharge variations are weaker during the calibration and validation periods.

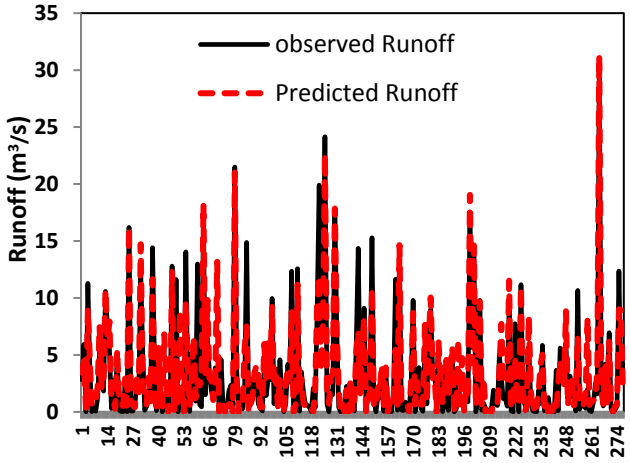


**Figure 7.** Observed and simulated runoffs for duration of calibration for the ANN model

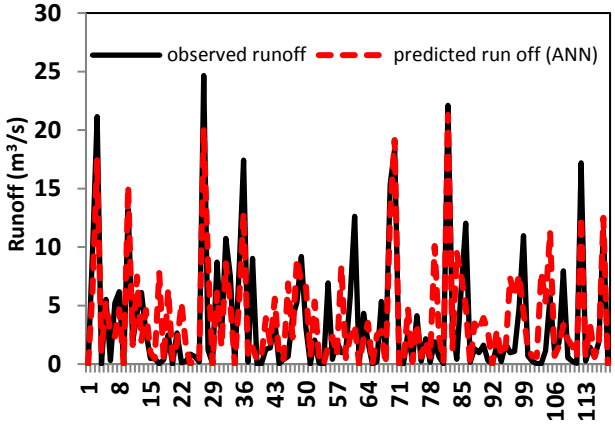


**Figure 8.** Observed and simulated runoffs for validation duration for ANN model

According to [32, 33] studies, model simulation can be recognized satisfactorily when the $R^2$ statistical index is more than 0.6 and the Nash-Sutcliffe efficiency (NSE) is greater than 0.5, which was used as a criterion for evaluating hydrological models in the studies conducted by [34], [35], [36], and [37]. After calibrating the artificial neural network models and IHACRES, the results of the models were compared. In both models, acceptable results were obtained in the calibration phase; however, the artificial neural network model in the validation phase reportedly achieved weaker values than the IHACRES model, as shown in Table 10.

**Table 10.** Comparing performance criteria in ANN and IHACRES

| Performance criteria | | $R^2$ | RMSE | MAE | NSE |
|---|---|---|---|---|---|
| ANN | Calibration | 0.82 | 2.33 | 1.46 | 0.6 |
| | Verification | 0.64 | 3.01 | 2.18 | 0.51 |
| IHACRES | Calibration | 0.9 | 2.08 | 1.29 | 0.71 |
| | Verification | 0.84 | 2.24 | 1.39 | 0.61 |

### 4.6. Prediction of runoff with IHACRES model

Following the calibration and validation of artificial neural network and IHACRES models, without changing the model parameters and only by changing the model inputs including rainfall and temperature of climate models, the river discharge during the first and second periods was predicted. For the forecast period, only the downscaled output of the weight combination model as a selected climate scenario was used. Figures 9 and 10 show the predicted rainfall against the predicted discharge for the RCP8.5 scenario.

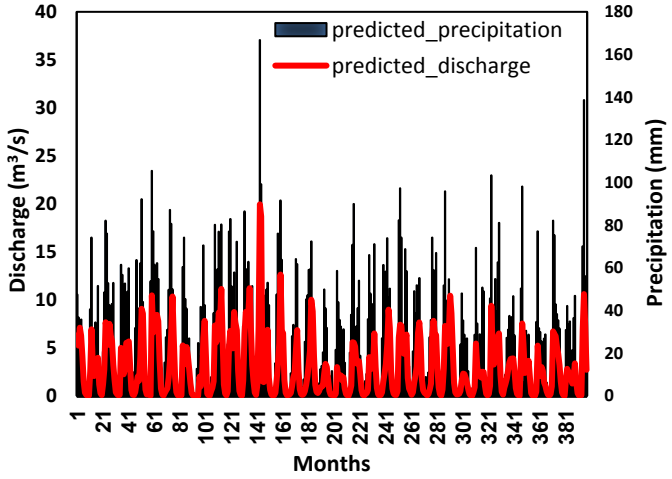


**Figure 9.** Predicted discharge of IHACRES model against precipitation in (2020-2053)

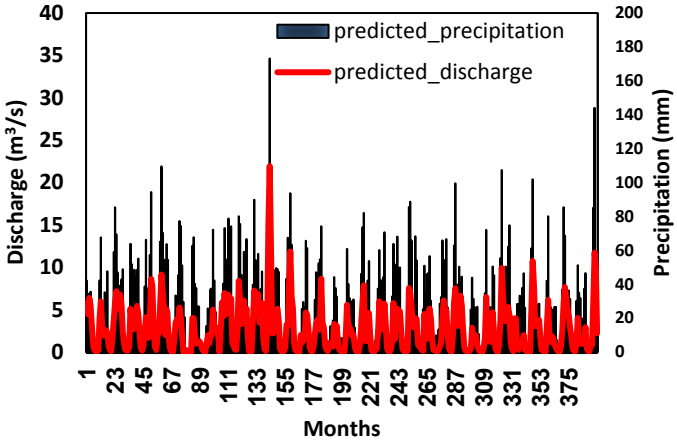


**Figure 10.** Predicted discharge of IHACRES model against precipitation in (2053-2085)

### 4.7. Prediction of runoff with ANN model

The prediction of discharge during the first and second periods for the weighted combination model was also done using the artificial neural network model. Figures 11 and 12 show the amount of rainfall predicted by Scenario 8.5 for the first and second periods against the predicted discharge. The results indicate that the neural network model has predicted more discharge than the IHACRES. Therefore, the long-term average discharge in the neural network model during the first period is 0.35, while during the second period is 0.44 cubic meters per second.

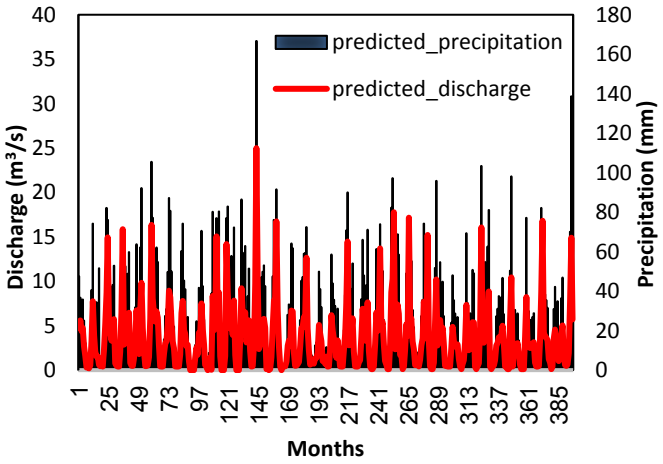


**Figure 11.** Predicted discharge of ANN model against precipitation in (2020-2052)

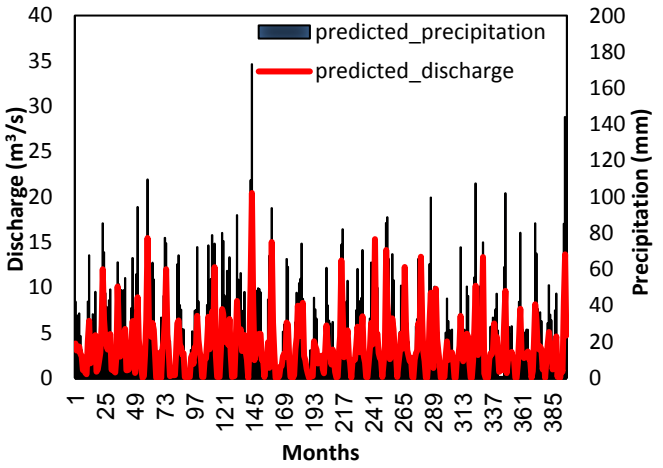


**Figure 12.** Predicted discharge of ANN model against precipitation in (2053-2085)

The results of the statistical characteristics of the discharge prediction in these models show decrease in discharge compared to the observation period in both models and both periods. The IHACRES model predicts a decrease of 12.72 % in the first period and 20.3 % in the second period, while the ANN model predicts a decrease of 2.12 % during the first period and 6.97 % during the second period.

### 4.8. Comparison of long-term monthly averages

In order to better analyze the output results of hydrological models, the monthly long-term average of the river flow was extracted. In both models and in both periods, a sharp decrease in peak discharge in March, April, and May of about five cubic meters per second is evident. While the peak flow in October and November shows a sharp increase of about three cubic meters per second in Figure 13.

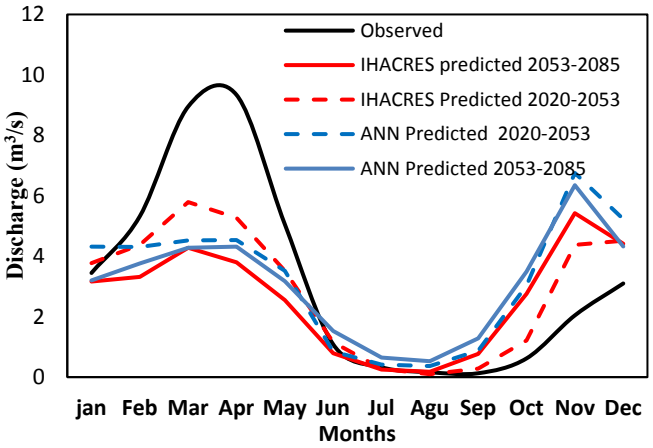


**Figure 13.** Comparison of long-term monthly averages of discharg

### 4.9. Comparison of models with duration curves

Flow Duration Curve (FDC) is a classic method used to graphically represent the relationship between frequency and flow rate. Various factors are involved in the shape (FDC) including climatic parameters and basin physiology. Figure 14 presents the flow duration curve for each category of flow range based on the quantile-domain model comparison. The results show that both the semi-conceptual and data-driven models underestimate the peak discharge of the catchments under climate change, which is related to the decrease in rainfall and increase in temperature in the context of climate change in the region. The FDC diagram shows that in the observed discharge mode, 10 % of the time, the flow is more than 90 cubic meters per second, while in the predicted discharge, it is more than 6 cubic meters per second. In general, the river is dry 25 % of the time. The results of this investigation of a specific study basin with monthly flow comparisons may not be applicable for the selection of robust rainfall-runoff models for climate change assessment studies. Therefore, climate change impact in the study basin should be assessed with more conceptual, distributed, and data-driven models together.

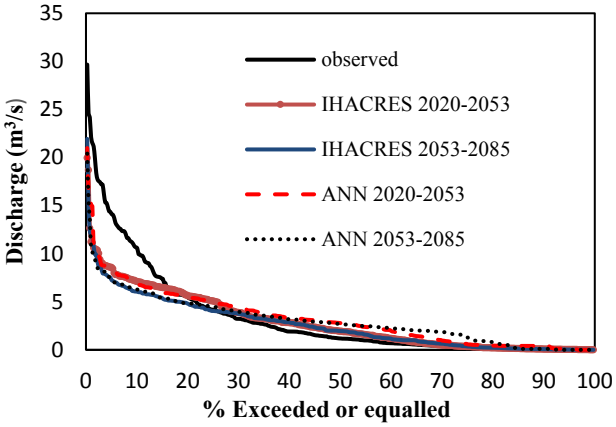


**Figure 14.** Flow duration curves of the observed and predicted flows

## 5. CONCLUSIONS AND REMARKS

The need for river discharge variations in the present and future periods is very important to satisfy the demands for

drinking, industry, and agriculture and studying these variations for future periods using CMIP5 climate models is a good option. The output of these models often includes meteorological variables and hydrological models play an important role in applying the effects of these climate variables to river runoff. Therefore, in this study, the results of a semi-conceptual hydrological and MLP artificial neural network models were evaluated and predicting future discharge was performed with both models. The results also showed a decrease runoff in the future for both models, but Artificial neural network model predicts generally more discharge in the future than IHACRES model and since the IHACRES model in this study shows more accurate quantitative evaluation criteria during the calibration and validation period, it is more acceptable to predict the future period.

Since the simulation and prediction of river discharge with IHACRES and ANN models has been done in some parts of the world, the present research attempts to compare the results of researchers who used these models with the results obtained from this study. In this way, a study by [16] predicted stream flow in Kasilian watershed in northern Iran and demonstrated that neural network and IHACRES models outperformed autoregressive integrated moving average and deseasonalized autoregressive moving average models which is in line with the results of the present study. The results of comparison of hydrological models for evaluating water resources in a low-data area by [38] showed that the selected simple conceptual models (GR4J and IHACRES) had a better daily performance than the more complex model (SWAT). The results of the present study also indicate that the IHACRES model has a good ability to simulate monthly runoff.

However, the use of climate models of the fifth scenario in hydrology has been evaluated since 2013 at the same time with their release [9]. Zulkarnain [39] showed that the performance of the multilayer neural network model was better than the IHACRES model, and this model could simulate runoff using the rainfall inputs and rainfall of previous months as well as runoff that occurred in previous months, which is not in line with the present study. In another study [40] found that the ANN model could simulate observed runoff and evaluated the comparison of IHACRES and neural network models for daily river discharge, but cannot keep the trends in daily and annual series. The present study also mentions this point about the artificial neural network model which failed to simulate the behavioral pattern of the observed time series. Ahooghalandari evaluated that the ANN was introduced as a good option for complex hydrological systems. Also, data derived from two adjacent stations were employed to improve the results of artificial neural networks compared to the IHACRES model, which is in line with the present study [14]. The results of the present study are also in line with the research of [17] who found that IHACRES performance was better than the ANN model, even though it was a more data intensive model than the ANN model. In doing so, three models of SWAT, IHACRES, and ANN on daily, monthly, and annual bases in the Kan watershed are used by [19]. According to the results, the performance of the three considered models is generally suitable for rainfall-runoff process simulation; however, ANN model exhibits a better performance for daily, monthly, and annual flow simulations than other two models.

## 6. ACKNOWLEDGEMENT

The authors would like to thank Kermanshah Regional Water Company and Kermanshah Province Meteorological Administration. The authors received no financial support for the research, authorship, and publication of this article. This manuscript is the result of the research of S. Marabi under the supervision of M. Hafezparast. Authors designed the study, developed the methodology, discussed the results and wrote the paper. (https://github.com/maryamhafezparast).

## REFERENCES

1. Fu, G., Charles, S.P., Chiew, F.H., Teng, J., Zheng, H., Frost, A.J., Liu, W. and Kirshner, S., "Modelling runoff with statistically downscaled daily site, gridded and catchment rainfall series", ***Journal of Hydrology***, Vol. 429, No. 7, (2013), 254-265. (https://doi.org/10.1016/j.jhydrol.2013.03.041).
2. Hao, X., Chen, Y., Xu, C. and Li, W., "Impacts of climate change and human activities on the surface runoff in the Tarim River Basin over the last fifty years", ***Water Resources Management***, Vol. 22, (2008), 1159-1171. (https://doi.org/10.1007/s11269-007-9218-4).
3. Zhang, D., Chen, X., Yao, H. and Lin, B., "Improved calibration scheme of swat by separating wet and dry seasons", ***Ecological Modelling***, Vol. 301, (2015), 54-61. (https://doi.org/10.1016/j.ecolmodel.2015.01.018).
4. Risbey, J.S. and Entekhabi, D., "Observed Sacramento Basin stream flow response to precipitation and temperature changes and its relevance to climate impact studies", ***Journal of Hydrology***, Vol. 184, No. 3-4, (1996), 209-223. (https://doi.org/10.1016/0022-1694(95)02984-2).
5. Ouyang, F., Zhu, Y., Fu, G., Lü, H., Yu, Zh. and Chen, X., "Impacts of climate change under CMIP5 RCP scenarios on streamflow in the Huangnizhuang catchment", ***Stochastic Environmental Research and Risk Assessment***, Vol. 29, (2015), 1781-1795. (https://doi.org/10.1007/s00477-014-1018-9).
6. Hafezparast, M., Araghinejad, S., Fatemi, S.E. and Bressers, H., "A conceptual rainfall-runoff model using the auto calibrated NAM models in the Sarisoo River", ***Hydrology Current Research***, Vol. 4, No. 1, (2013), 1-6. (https://doi.org/10.4172/2157-7587.1000148).
7. Fu, G., Charles, S.P. and Chiew, F.H.S., "A two-parameter climate elasticity of streamflow index to assess climate change effects on annual streamflow", ***Water Resources Research***, Vol. 43, No. 11, (2007), 1-12. (https://doi.org/10.1029/2007WR005890).
8. Liu, Z., Xu, Z., Charles, S.P., Fu, G. and Liu, L., "Evaluation of two statistical downscaling models for daily precipitation over an arid basin in China", ***International Journal of Climatology***, Vol. 31, No. 13, (2011), 6006-6060. (https://doi.org/10.1002/joc.2211).
9. Stocker, T.F., Qin, D., Plattner, G.-K., Tignor, M., Allen, S.K., Boschung, J., Nauels, A., Xia, Y., Bex, V. and Midgley, P.M., IPCC, Summary for policymakers, Climate change: The physical science basis, contribution of working group I to the fifth assessment report of the intergovernmental panel on climate change, Cambridge University Press, Cambridge, United Kingdom and New York, NY, USA, (2013). (https://www.cambridge.org/core/books/climate-change-2013-the-physical-science-basis/summary-for-policymakers/356E277FD1FBC887845FB9E8CBC90CCD).
10. Ma, C., Pan, S., Wang, G., Liao, Y. and Xu, Y.P., "Changes in precipitation and temperature in Xingjian River Basin, China", ***Theoretical and Applied Climatology***, Vol. 123, No. 3-4, (2016), 859-871. (https://doi.org/10.1007/s00704-015-1386-1).
11. Kharin, V.V., Zwiers, F.W., Zhang, X. and Wehner, M., "Changes in temperature and precipitation extremes in the CMIP5 ensemble", ***Journal of Climate Change***, Vol. 116, (2013), 345-357. (https://doi.org/10.1029/2005JD006290).
12. Chadwick, R., Boutle, I. and Martin, G., "Spatial patterns of precipitation change in a CMIP5: Why the rich do not get richer in the tropics", ***Journal of Climate***, Vol. 26, No. 11, (2013), 3503-3566. (https://doi.org/10.1175/JCLI-D-12-00543.1).
13. Tan, M.L., Ficklin, D.L., Ibrahim, A.L. and Yusop, Z., "Impacts and uncertainties of climate change on stream flow of the Johor River Basin, Malaysia using a CMIP5 general circulation model ensemble", ***Journal of Water and Climate Change***, Vol. 5, No. 4, (2014), 676-695. (https://doi.org/10.2166/wcc.2014.020).

14. Ahooghalandari, M., Khiadani, M. and Kothapalli, G., "Assessment of artificial neural networks and IHACRES models for simulating stream flow in Marillana catchment in the Pilbara, Western Australia", ***Australasian Journal of Water Resources***, Vol. 19, No. 2, (2015), 116-126. (https://doi.org/10.1080/13241583.2015.1116183).
15. Sadeghi Loyeh, N. and Jamnani, M.R., "Comparison of different rainfall-runoff models performance: A case study of Liqvan catchment, Iran", ***European Water***, Vol. 57, (2017), 315-322. (http://www.ewra.net/ew/pdf/EW_2017_57_44.pdf).
16. Ghanbarpour, M.R., Amiri, M., Zarei, M. and Darvari, Z., "Comparison of stream flow predicted in a forest watershed using different modelling procedures: ARMA, ANN, SWRRB, and IHACRES models", ***International Journal of River Basin Management***, Vol. 10, No. 3, (2012), 281-292. (http://dx.doi.org/10.1080/15715124.2012.699893).
17. Karamouz, M., Fallahi, M., Nazif, S. and Farahani, M.R., "Long lead runoff simulation using data-driven models", ***International Journal of Civil Engineering***, Vol. 10, No. 4, (2012), 328-336. (http://ijce.iust.ac.ir/article-1-414-en.html).
18. Sayahi, S., Shahbazi, A. and Khademi, Kh., "Simulation of the climate change impact on monthly runoff of Dez watershed using IHACRES model", ***Journal of Water Science Engineering***, Vol. 7, No. 15, (2017), 7-18. (In Farsi with English Abstract). (http://wsej.iauahvaz.ac.ir/article_531584.html).
19. Ahmadi, M., Moeini, A., Ahmadi, H., Motamedvaziri, B. and Zehtabiyan, Gh.R., "Comparison of the performance of SWAT, IHACRES and artificial neural networks models in rainfall-runoff simulation (Case study: Kan watershed, Iran)", ***Physics and Chemistry of the Earth***, Vol. 111, (2019), 65-77. (https://doi.org/10.1016/j.pce.2019.05.002).
20. Mitchell, T.D., "Pattern scaling: An examination of accuracy of the technique for describing future climates", ***Climatic Change***, Vol. 60, (2003), 217-242. (https://doi.org/10.1023/A:1026035305597).
21. Wilby, R.L. and Harris, I., "A framework for assessing uncertainties in climate change impacts: Low flow scenarios for the River Thames, UK", ***Water Resources Research***, Vol. 42, No. 2, (2006), 1-10. (https://doi.org/10.1029/2005WR004065).
22. Massah Bavani, A. and Morid, A.R., "The impacts of climate change on water resources and agricultural production", ***Journal of Water Resources Research***, Vol. 1, No. 1, (2005), 40-47. (In Farsi with English Abstract). (http://iwrr.sinaweb.net/article_32831.html?lang=en).
23. Moazami Goudarz, F., Sarraf, A. and Ahmadi, H., "Prediction of runoff within Maharlu basin for future 60 years using RCP scenarios", ***Arabian Journal of Geosciences***, Vol. 13, No. 605, (2020). (https://doi.org/10.1007/s12517-020-05634-x).
24. Hansen, D.P., Ye, W., Jakeman, A.J., Cooke, R. and Sharma, P., "Analysis of the effect of rainfall and streamflow data quality and catchment dynamics on streamflow prediction using the rainfall-runoff model IHACRES", ***Environmental Software***, Vol. 11, (1996), 193-202. (https://doi.org/10.1016/S0266-9838(96)00048-2).
25. Post, D.A. and Jakeman, A.J., "Predicting the daily stream flow of ungauged catchments in S.E. Australia by regionalizing the parameters of a lumped conceptual rainfall-runoff model", ***Ecological Modelling***, Vol. 123, (1999), 91-104. (https://doi.org/10.1016/S0304-3800(99)00125-8).
26. Schreider, S.Y., Jakeman, A.J. and Pittock, A.B., "Modelling rainfall-runoff from large catchment to basin scale: The Goulburn Valley, Victoria", ***Hydrological Processes***, Vol. 10, (1996), 863-876. (https://doi.org/10.1002/(SICI)1099-1085(199606)10:6<863::AID-HYP376>3.0.CO;2-8).
27. Haykin, S., Neural networks: A comprehensive foundation, 2nd Edition, Prentice Hall, Englewood Cliffs, New Jersey, USA, (1999), 1-696. (https://www.amazon.com/Neural-Networks-Comprehensive-Foundation-2nd/dp/0132733501).
28. Bhattacharyya, B., Price, R.K. and Solomatine, D.P., "Machine learning approach to modelling sediment transport", ***Journal of Hydraulic Engineering***, Vol. 133, No. 4, (2007), 440-450. (https://doi.org/10.1061/(ASCE)0733-9429(2007)133:4(440)).
29. Dawson, C.W. and Wilby, R.L., "Hydrological modelling using artificial neural networks", ***Progress in Physical Geography***, Vol. 25, No. 1, (2001), 80-108. (https://doi.org/ 10.1177/030913330102500104. 2001).
30. Kamruzzaman, J. and Aziz, M.A., "Note on activation function in multilayer feed forward learning", ***Proceedings of the 2002 International Joint Conference on Neural Networks. IJCNN'02 (Cat. No.02CH37290)***, Honolulu, HI, USA, (2002). (https://doi.org/10.1109/IJCNN.2002.1005526).
31. Asadollahfardi, G., Taklify, A. and Ghanbari, A., "Application of artificial neural network to predict TDS in Talkheh Rud River", ***Journal of Irrigation and Drainage Engineering***, Vol. 138, No. 4, (2011), 363-370. (https://doi.org/10.1061/(ASCE)IR.1943-4774.0000402).
32. Bannem, J. and Shoemaker, C.A., "An analysis of high-flow sediment event data for evaluating model performance", ***Journal of Hydrological Processes***, Vol. 19, (2005), 605-620. (https://doi.org/10.1002/hyp.5608).
33. Santhi, C., Arnold, J.G., Williams, J.R., Dugas, W.A., Srinivasan, R. and. Hauck, L.M., "Validation of the SWAT model on a large river basin with point and nonpoint sources", ***Journal of American Water Resources Assocciation***, Vol. 37, No. 5, (2001), 1169-1188. (https://doi.org/10.1111/j.1752-1688.2001.tb03630.x).
34. Sevat, E. and Dezetter, A., "Selection of calibration objective functions in the context of rainfall-runoff modeling in a Sudanese savannah area", ***Hydrological Science Journal***, Vol. 36, No. 4, (1991), 307-330. (https://doi.org/10.1080/02626669109492517).
35. Boyle, D.P., Gupta, H.V. and Sorooshian, S., "Toward improved calibration of hydrologic models: Combining the strengths of manual and automatic methods", ***Water Resources Research***, Vol. 36, No. 12, (2000), 3663-3674. (https://doi.org/1029/2000WR900207).
36. Legates, D.R. and McCabe, G.J., "Evaluating the use of "goodness-of-fit" measures in hydrologic and hydro climatic model validation", ***Water Resources Research***, Vol. 35, No. 1, (1999), 233-241. (https://doi.org/10.1029/1998WR900018).
37. Pourkheirollah, Z., Hafezparast, M. and Fatemi, S.E., "Changes in precipitation, temperature and discharge under RCP scenarios case study: Dehloran city", ***Proceedings of the Second Iran National Conference***, Shahrekord University, (2017). (In Farsi with English Abstract). (https://civilica.com/papers/l-8405/).
38. Tegegne, G., Kwan Park, D. and Kim, Y., "Comparison of hydrological models for the assessment of water resources in a data-scarce region, the Upper Blue Nile River Basin", ***Journal of Hydrology: Regional Studies***, Vol. 14, (2017), 49-66. (https://doi.org/10.1016/j.ejrh.2017.10.002).
39. Zulkarnain, H., Shamsudin, S. and Harun, S., "Minimum input variance for modelling rainfall-runoff using ANN", ***Jurnal Teknologi***, Vol. 69, No. 3, (2014), 113-118. (https://doi.org/10.11113/jt.v69.3154).
40. Zulkarnain, H., Shamsudin, S., Harun, S., Marlinda, A. and Hamidon, N., "Suitability of ANN applied as a hydrological model coupled with statistical downscaling model: A case study in the northern area of Peninsular Malaysia", ***Environmental Earth Sciences***, Vol. 74, No. 1, (2015), 463-477. (https://doi.org/10.1007/s12665-015-4054-y).

JREE: Vol. 8, No. 3, (Summer 2021) 86-93

Journal of Renewable Energy and Environment

Research Article

Journal Homepage: www.jree.ir

# Bioethanol Production from Wastes: An Experimental Evaluating Study for Iran

Abolfazl Taherzadeh Fini, Abolfazl Fattahi *

*Department of Mechanical Engineering, University of Kashan, P. O. Box: 8731753153, Kashan, Isfahan, Iran.*

*PAPER INFO*

*Paper history:*
Received 01 November 2020
Accepted in revised form 11 July 2021

*Keywords*:
Biofuel Production,
Pretreatment and Hydrolysis,
Agricultural Wastes,
Renewable Energy,
Gas Chromatography

*ABSTRACT*

Energy crisis in the world motivates countries to hire new and renewable energies. One of the main and valuable renewable sources of energy is agricultural waste. This is widely disposed of through the world during the harvest, packing, and transportation. In many countries, agricultural waste is considerably weighty. Nonetheless, most of that is used for animal feed or herbal fertilizer and no useful value is added. Despite its location in an arid region, Iran produces various citrus, cereals, and vegetables in high tonnage. The waste of the agricultural product, especially those disposed of by the food processing industries, such as fruit juice factories, remains also useless. The potential of the residues to extract biofuel is investigated in the current experimental study. Six samples of abundant agricultural products in Iran are chosen: sugarcane, grape, potato, orange peel, date, and mulberry. The processes of pretreatment, hydrolysis, and fermentation are performed and the extracted juice is directed to the distiller to gather bioethanol. To evaluate the distilled juice purity, a gas chromatography test is carried out. It is shown that date and mulberry can produce a maximum of 29.5 and 23 ml (ethanol)/100 g (dry waste) as the most efficient agricultural products.

https://doi.org/10.30501/jree.2021.255487.1156

## 1. INTRODUCTION

Drastic increment in energy demand in the current century motivates humans to extract fuel from new sources. Renewable energies such as biofuels are the most prominent targets to subside fossil fuel dependency for countries. Utilizing biofuels takes countries to the safe side regarding oil price fluctuating, air pollutions, and fossil fuel depletion [1]. Among the threats of applying fossil fuels, outdoor pollution, causing more than 4.2 million deaths annually [2], motivates the idea of finding alternative fuels. Extracting fuels from crop wastes or as a by-product during the food processing of agricultural products is so promising to achieve sustainable energy development. Among different types of biofuels, bioethanol is more common due to source variety and its ability to blend with fossil fuels in commercial vehicles [3,4]. Although it has a lower energy content than gasoline, its octane number is higher, which preserves the motor from knocking in the condition of high pressure [5]. Further, higher oxygen content and non-toxic combustion products lower air pollution.

Bioethanol production in Iran is far behind some other countries, owing to the high resources of crude oil and natural gas [6]. However, during pandemic Covid-19, there emerges a high demand for disinfection liquids, especially ethanol, which can be supplied through bioprocessing. Switching from fossil fuels to biofuels and enhancing the economic value of agricultural products by considering the waste is potentially a promising step to develop a country. It is estimated that more than 21.5 million tons of agro-food waste are annually disposed of in Iran, which can produce more than 5.5 billion liters of bioethanol [7]. The lignocellulosic feedstock and sugar or sucrose ingredient in the gardening products, which can be found most abundantly in Iran's crops, are two main sources of producing bioethanol that can be investigated in the current experimental study. Bioethanol, which is the most produced biofuel by up to 95 % of the global production, can be replaced by 32 % of the global gasoline consumption [8]. This means the creation of economic interest from something with no profit. The reduction of emission in dirty cities can be another indirect economical key that should be considered as an achievement. However, the economic chain of biofuel production in Iran should be planned and the policies should be accurately passed, as well. Although this study focuses on Iran as its case study, the goal of this study is inclusive of the case in other countries where bioethanol by-producing has been developed and, therefore, some published works have been found in the literature.

Sritrakul et al. [9] investigated bioethanol formation from sugarcane pith using two processes of simultaneous saccharification and fermentation as well as separate hydrolysis and fermentation. Their case study was Thailand. The former was found more efficient than the latter. Maximum bioethanol extraction was achieved by 3.7 g/L. Zakir et al. [10] compared ethanol production from sugarcane bagasse in terms of various variables affecting enzymatic hydrolysis and yeast fermentation process. Their study showed the optimum value of temperature and PH for the process of production. The fermentation process remained unchanged after a certain time, as the concentration of ethanol

*Corresponding Author's Email: afattahi@kashanu.ac.ir (A. Fattahi)
URL: https://www.jree.ir/article_133346.html

Please cite this article as: Taherzadeh Fini, A. and Fattahi, A., "Bioethanol production from wastes: An experimental evaluating study for Iran", ***Journal of Renewable Energy and Environment (JREE)***, Vol. 8, No. 3, (2021), 86-93. (https://doi.org/10.30501/jree.2021.255487.1156).

in water was kept constant. Moodley and Kana [11] evaluated the bioethanol production from sugarcane leaf and optimized the involved variables in the hydrolysis process. There was no difference between enzyme filtration and infiltration on the production rate.

Noufal et al. [12] extracted bioethanol from the flour of the potato waste. After fermentation of hydrolysate with Saccharomyces cerevisiae, the maximum ethanol rate of 33 g/L was given. The best temperature of the fermentation process was at 35 °C with the optimum pH between 5 and 6. Hashem and Darwish [13] showed that bioethanol production from potato wastes could be obtained without adding organic additives, while some minerals such as Zn were required in a small concentration. The maximum ethanol production rate of 5.8 g/L was achieved. Yamada et al. [14] found that ethanol production by enzyme hydrolyses of potato peel could be improved by a factor of 2.5 if the potato mash with an equal weight ratio was added.

In a case study for Bangladesh, Swaraz et al. [15] investigated bioethanol production from the wild date palm. They reached 0.278 g/g bioethanol after a batch fermentation of *Saccharomyces cerevisiae*. They emphasized the importance of dates as a promising sugary feedstock for ensuring enough food and energy. Using a low-cost and direct bioethanol production from the date palm, Ben Atitallah et al. [16] introduced Wickerhamomyces anomalus X19 yeast and extracted a maximum of 61.5 g/L ethanol by a batch mode fermentation. Corbin et al. [17] utilized white and red grape marcs to evaluate the ethanol product. Using sulfuric acid pretreatment, about 10 percent of glucose liberation after saccharification was reported. Then, 270 L/tone bioethanol extraction was achieved. Bioethanol production from grape pomace was evaluated by Rodriguez et al. [18] using solid-state fermentation. The optimum time to fulfill the fermentation process was detected. Oberio et al. [19] optimized the parameters involved in hydrolysis and fermentation of orange peel. Two steps of hydrolysis were taken. They showed that the hydrolysis could be managed such that the fermentation process would become unimportant. Joshi et al. [20] reported bioethanol and biobutanol production from orange peel using Saccharomyces cerevisiae and Clostridium acetobutylicum. A maximum value of 4.1 g/100mL bioethanol was extracted after hydrolysis and fermentation, while 19.5 g/L bioethanol was given without adding nutritional supplements. Although the berries can be an appreciated source of bioethanol production, bioethanol extraction from mulberries has been rarely reported. This is, however, one of the goals of the current study. The work of Wang et al. [21], as the only publication on this issue up to now, presented Fed-nonisothermal-simultaneous saccharification to achieve the goal of higher bioethanol production from mulberry. Ethanol was extracted by about 63.9 g/L, improving more than 30 % in comparison with those traditional processes. Pretreatment using $H_3PO_4/H_2O_2$ was introduced as the most effective method.

The current work to evaluate bioethanol extraction from some abundant agricultural production in Iran. Pretreatment, hydrolysis, and fermentation are followed to prepare the juice added to the distiller. Gas Chromatography (GC) test is carried out to measure the purity of the obtained ethanol. This study shows the potential of crop waste in Iran to add economic value and produce cleaner fuels.

## 2. MATERIALS AND METHODS

### 2.1. Raw materials

The raw materials are chosen from the most seeded crops in Iran. According to the FAO (Food and Agriculture Organization of the United Nations) report [22], Iran is one of the most important countries to produce some kind of agricultural products relating to human food. Iran can compete with many countries in production date, grape, orange, sugarcane, potato, and mulberry, which are considered as the sources of bioethanol extraction in this study. Due to the poor and traditional harvest as well as non-advanced food industries, the waste of these crops is considerable. Table 1 shows the details of the chemical compositions of the raw materials applied. The presented values may contain ±1 % deviation, in maximum.

It should be noted that in this table, Dates 1 to 3 belong to Jiroft, Bushehr, and Hajiabad (located near Bandarabbas city) cities, correspondingly. The sugarcane was supplied from Haft Tappeh of Shush city. Other crops were provided from Kashan and its countryside. Dried mulberries (Morus alba) were used for the tests.

**Table 1.** the composition weight percentage of the raw materials used in this study

| Material | Raw material | | | | | Moisture |
|---|---|---|---|---|---|---|
| | Carbohydrates | Cellulose | Hemicellulose | Lignin | Ash | |
| Date 1 | 80.45 | 5.70 | 3.9 | 1.6 | 1.78 | 20 |
| Date 2 | 82.43 | 6.50 | 2.3 | 1.3 | 1.89 | 12 |
| Date 3 | 76.47 | 5.25 | 2.9 | 1.0 | 1.55 | 14 |
| Sugarcane | 95.03 | 21.3 | 18.4 | 5.4 | 2.84 | 13 |
| Orange peel | 38 | 13.61 | 6.10 | 2.10 | 1.5 | 75.4 |
| mulberry | 75.30 | 9.68 | 4.22 | 2.88 | 3.99 | 11 |
| grapes | 79.20 | 17.87 | 7.0 | 10.23 | 4.65 | 3.3 |
| Potato | 17.88 | 0.55 | 0.045 | 0.20 | 0.29 | 70.5 |

### 2.2. Pretreatment, hydrolysis, and fermentation

Figure 1 shows a schematic view of bioethanol extraction from target agricultural products. The process is presented in Figure 2 with more details using the block box diagram. The wastes are collected and washed without adding any chemical substance. The raw pomaces can be found in the farms or residue of the food processing industrial units. Then, all of the wastes are crushed and chopped up on a similar 5-2 mm scale, depending on the initial size of the materials [12-14]. The pretreatment is followed by stirring the mixture at a temperature of 100 °C for about 25 minutes [23]. The

obtained juice is injected into a fermentation container where the liquid is kept for 48-72 hours depending on the product type. Saccharomyces cerevisiae, made by Iran Malas Company [24], is used as the yeast. The used yeast has a lower protein rate than 45 % and lower phosphor and ash rates than 6 % and 3 %, respectively, according to its brochure. The number of 2×1010 living cells is found per gram. The concertation of the yeast should be 5 g per 1 kg of the substrate [23]. By achieving better performance, the yeast is grown by solving problems in a mixture of distilled water and sugar at a temperature of 50 °C. The fermentation process is kept at a nearly constant temperature of 30 °C in anaerobic conditions [25-27]. Therefore, the batch container should be sealed and only a scape way for carbon dioxide, called an airlock (see Figure 2a), is implemented. Figure 2b shows the carbon dioxide produced in the fermentation process, as the calcium carbonate-water mixture became darker. The extracted liquid at the end of the fermentation process is filtered and collected. The filter should be used on a fine scale to remove all the solid particles. It is worth noting that all the processes were performed in the city located at about 940 meters over the sea level at the room temperature of 19±1 °C.

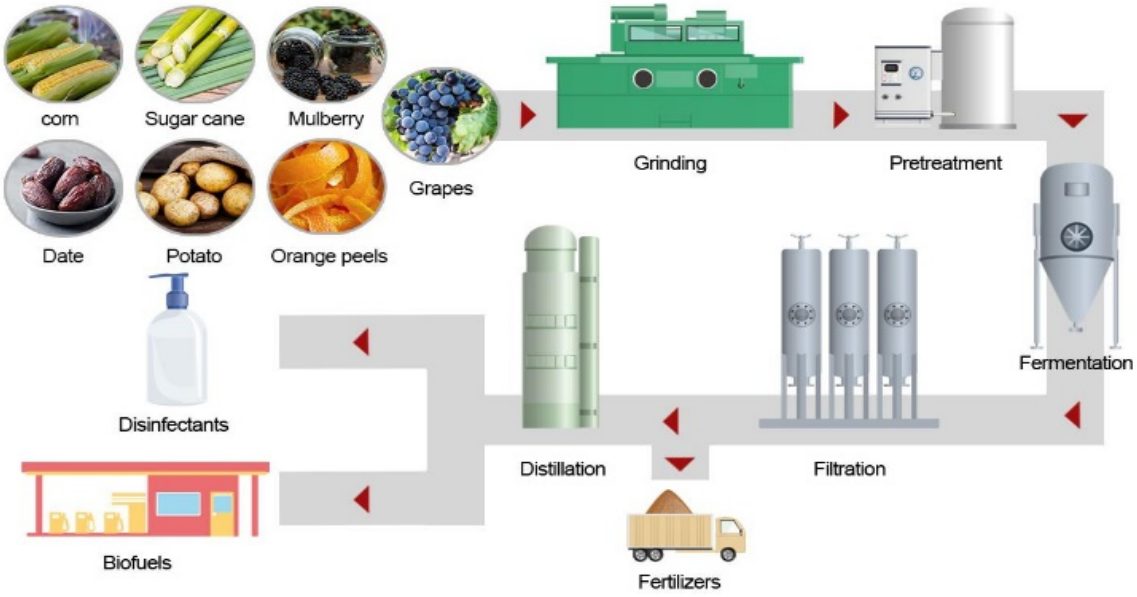


**Figure 1.** Schematic bioethanol production process

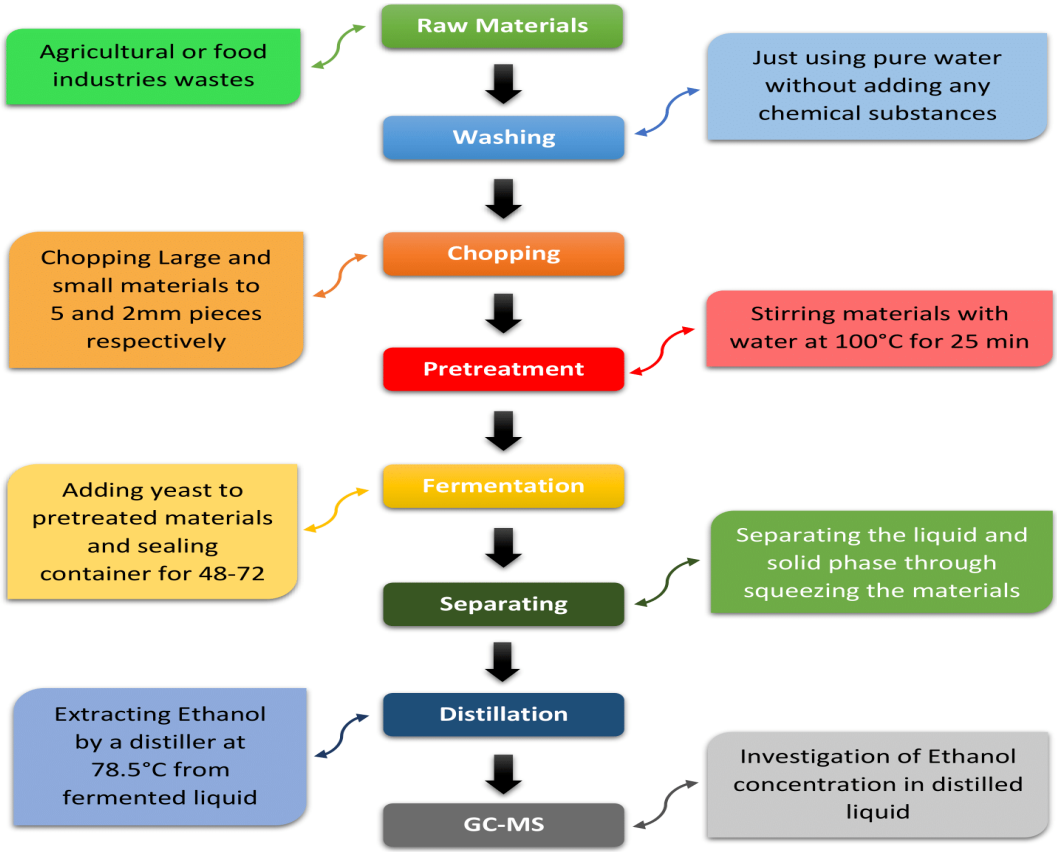


**Figure 2.** Block diagram of the production process

### 2.3. Distillation and gas chromatography

The filtered juice is subsequently added to the distiller (see Figure 4) and the ethanol is extracted at a temperature of 78.5 °C. The temperature is set at a certain value by a digital thermometer made by OMEGA Company. To verify the purity of the alcohol, a sample is tested in a GC machine (Agilent 6890: Mass selective detector 5973N) made in the USA. It contains a non-polar column (HP-5MS) with a length of 30 m and an inside diameter of 0.25 mm. Helium is used as the carrying gas. The GC machine injection volume is 0.5 µl with a split ratio of 50. For a test process, the Column temperature was initially maintained at 40 °C for 5 minutes. It was then heated to the temperature of 60 °C with a rate of 2 °C/min and finally, it was allowed to become hot at a temperature of 150 °C at a rate of 4 °C/min. The lab temperature during the tests was kept at 20±1 °C. The outputs are displayed in the next main section. The produced ethanol can be utilized as the biofuel source or disinfector.

### 2.4. Uncertainty and statistical analysis

Any experiments include bias and random errors [28]. Bias or systematic error is related to the measurement machines and can be found from the catalogs. GC machine is the main unit in the current study, having the bias error, called $b_1$, lower than 0.1 %, depending on what type of material is used. However, the upper limit is chosen to calculate the total uncertainty, here. The thermometer of the distiller could be another source, which was the precise one made by OMEGA company with the disparity rate lower than 0.2 °C, meaning lower 0.2 % error, as $b_2$. The error of weight measurement with the scales was about 1 %, denoted by $b_3$.

Random error, as the other source, derives from any unsteadiness or chance occurrence that may be unavoidable during the tests. To subside this source of error, we repeated each test five times and reported the arithmetic average of the data obtained as the result. Standard deviation, SD, for each test case was fallen in the range of 1-2 % of the arithmetic average value. Total uncertainty, TU, which reads [28]:

$$TU = \sqrt{b_1^2 + b_2^2 + b_3^2 + SD^2} \quad (1)$$

is provided as the error bars in the final absolute value of the ethanol extracted (See Figure 8). This is calculated by about ±2.3 %, in maximum. It should be noted that following variance analysis using ANOVA, null hypothesis was refused at a significance level of $P<0.05$.

**(a)** **(b)**

**Figure 3.** (a) The airlock and (b) the carbon dioxide produced

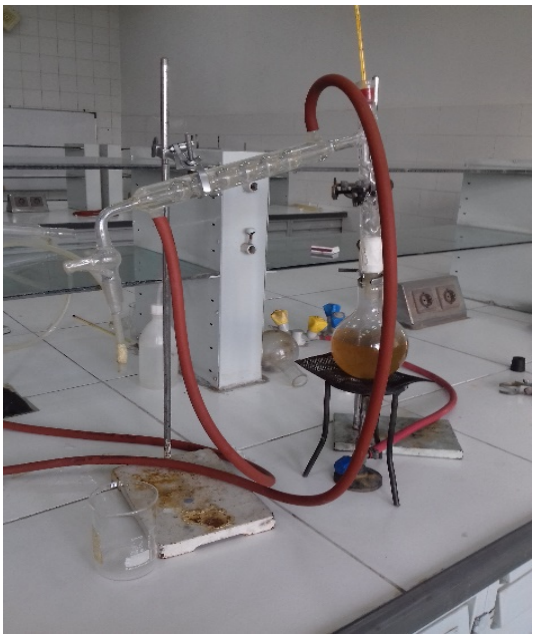

**Figure 4.** The distiller unit in the lab

## 3. RESULTS AND DISCUSSION

The GC results for sugarcane and potato are presented in Figure 5. This indicates that ethanol is the dominant species found in the sample. The value of ethanol for these two samples is nearly equal. However, the potato includes more undesirable chemical substances with a higher boiling point than the ethanol that may affect the engine performance, which requires to be purified. However, the higher flash points of 2-Methyle 1-Propanol and 3-Methyle 1-Buthanol are 29 °C and 42 °C compared to those of ethanol, as 12 °C, which can contribute to greater safety of the combustive system. Acetic acid is also reported for the potato sample, which causes a weak aqua-acidic environment after solving in the water of the combustion products.

Figure 6 depicts the pie charts of the GC test for three types of Iranian dates. The main species of the distilling process is ethanol and Date 2 contains a higher ethanol concentration. This is followed by Dates 3 and 1. The second dominant species for three samples is 3-Methyle 1-Buthanol, similar to previous results for sugarcane and potato. The high sugar content of the data can be converted into ethanol during the fermentation process. However, the optimization for temperature and other conditions for the batch container is substantially beneficial.

The results for grape, orange peel, and mulberry are presented in Figure 7. They can be sorted for ethanol production by ordering as stated earlier. The side products following the fermentation of mulberries are more significant. It can be implied that a longer period of hydrolysis is required with alternative methods. Further, the importance of purification is highlighted. Similar to the other cases, this figure shows that 3-Methyle 1-Buthanol is the second-highest concentration in the mixture.

The mass of ethanol extracted by each sample is given in Figure 8. To determine the value of concentration in terms of a milliliter bioethanol produced for 100 g of dry material, the following relation can be used.

$$C = \frac{L_D(g) \times S_E}{100 \times M_t(g) \times \rho_E(\frac{g}{ml})}, \quad (2)$$

where C is the concentration, $L_D$ the mass of distilled liquid, $\rho_E$ the ethanol density, $M_t$ the total solid weight, and $S_E$ the mass fraction of the ethanol. $L_D$ and $M_t$ can be easily weighted and $S_E$ is provided by the GC machine.

Figure 8 shows that Date 2 can produce 29.5 ml ethanol for 100 g dry material, more than another agricultural residue, indicating that Bushehr date contains the higher value of ethanol among the date types examined. Date 1, i.e., the crop of Jiroft, is set in the next step by assigning 27 and 23 ml ethanol to 100 g dry material, respectively. Despite high sugar content, sugarcane falls in the last position. It is shown that the sugarcane samples should be processed by optimizing the pretreatment, hydrolysis, and fermentation conditions. It can be concluded that the waste of dates largely disposed of in Iran is a substantial source of bioethanol production, deserving greater attention to exploitation and extensive development.

The current study aims to accentuate the high potential of biofuel production in Iran. Therefore, the absolute value of the bioethanol production may be higher [18, 21, 29] or lower [9, 15, 30] than other similar attempts found in the literature, perhaps, in part, due to the different pretreatment and fermentation processes. If the involved variables such as time, temperature, and pH of the pre-test process become optimized, higher production may be attained. Further, the raw material of the tests is one of the other sources of probable disparity of the results compared to those earlier published. The compositions of the crops are different, depending on the soil, weather, and plant breeding conditions [31, 32].

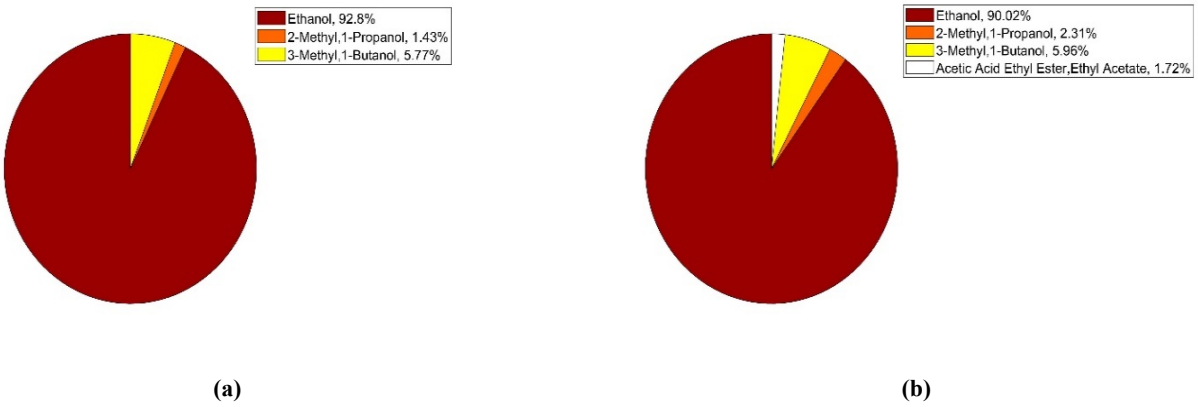


**Figure 5.** The results of the GC test for (a) sugarcane and (b) potato

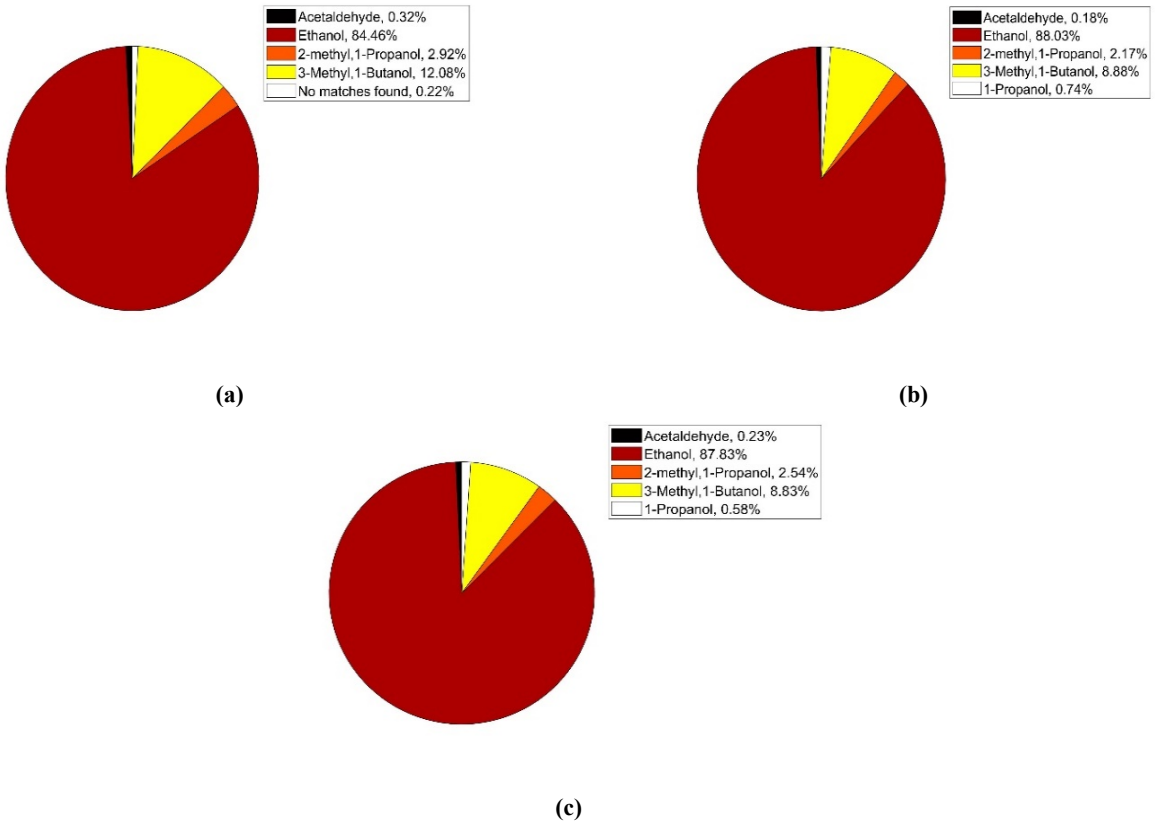


**Figure 6.** The results of GC test for (a) Date 1, (b) Date 2, and (c) Date 3

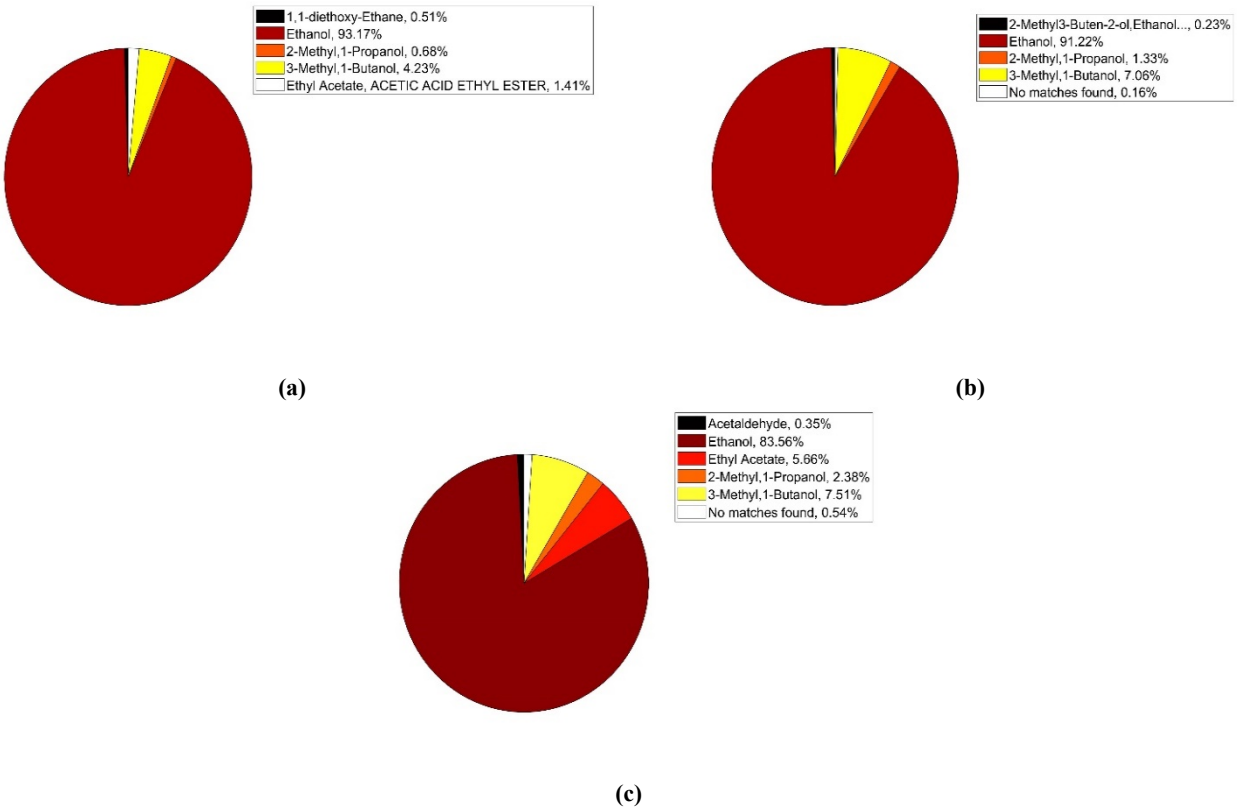


**Figure 7.** The results of GC test for (a) grape, (b) orange peel, and (c) mulberry

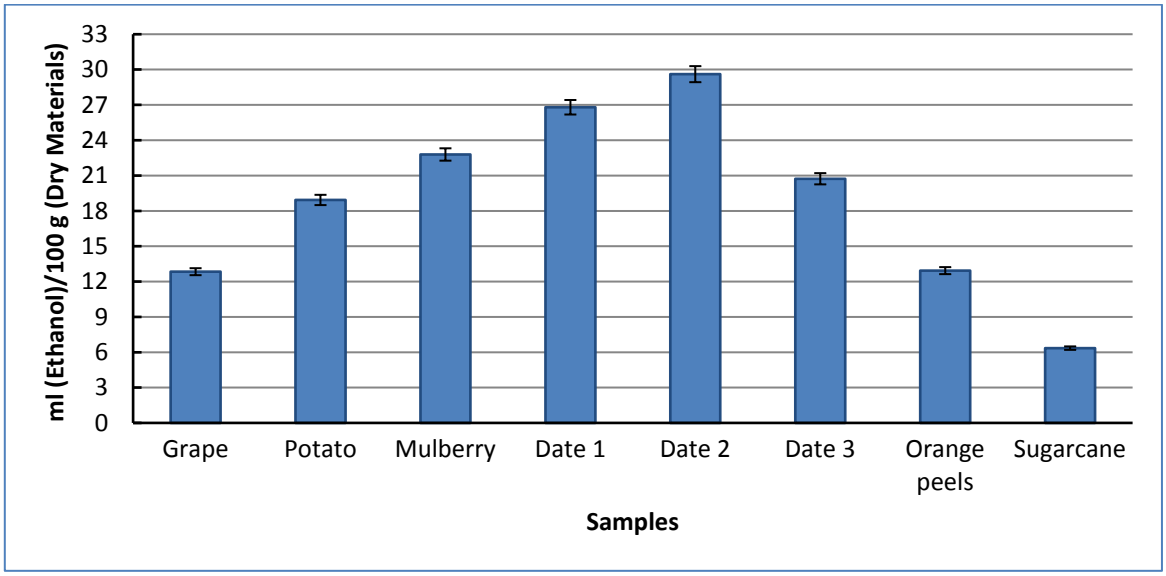


**Figure 8.** The volume concentration of ethanol extracted by each sample

## 4. CONCLUSIONS

The significance of biofuel in the current energy situation of the world cannot be neglected. Many countries seek new sources of energy, which are secure and independent of economical fluctuations. The waste of agricultural products, which is heavy in many countries due to wide food processing industries, can be considered as a promising energy source. Bioethanol is an applicable fuel in cars, in absolute or blended form. This can be produced by the agricultural residues, as studied experimentally in this work for Iran. The samples of many products in Iran, including sugarcane, potato, date, grape, orange peel, and mulberry, were gathered and the processes of pretreatment, hydrolysis, and fermentation were applied to them. The extracted juice was evaporated and condensed in the distiller to obtain the bioethanol. All samples showed an acceptable continent of ethanol. Bushehr date (29.5 ml (ethanol)/100 g (dry waste)), Jiroft date (27 ml (ethanol)/100 g (dry waste)), and mulberry (23 ml (ethanol)/100 g (dry waste)) were shown to be the most efficient products. The bioethanol production should be improved by optimizing the parameters involving the pretreatment and fermentation processes, which can be the subject of future study. Another type of fermentation process which can be more effective such as applying organic acids like formic, acetic, maleic, citric, and tartaric acid can be also considered as another development on the current work for future works. Further, many other agricultural wastes such as

cereals stalk can be examined as the source of bioethanol production in Iran. The current study showed that the biofuel industries should be set up and developed in Iran, ensuring energy saving and alleviating air pollution. This scheme could be potentially lucrative and beneficial for everybody who invests in this industry.

## 5. ACKNOWLEDGEMENT

The authors would like to thank the University of Kashan to support this work under Grant No. 1038274.

## NOMENCLATURE

| | |
|---|---|
| b1 | GC machine bias error |
| b2 | Thermometer bias error |
| b3 | Weight measurement error |
| C | Concentration |
| $L_D$ | Mass of distilled liquid |
| $\rho_E$ | Ethanol density |
| $M_t$ | Total solid weight |
| $S_E$ | Mass fraction of the ethanol |
| **Abbreviation** | |
| GC | Gas Chromatography |
| SD | Standard Deviation |
| TU | Total Uncertainty |

## REFERENCES

1. Saravanan, A.P., Pugazhendhi, A. and Mathimani, T., "A comprehensive assessment of biofuel policies in the BRICS nations: Implementation, blending target and gaps", ***Fuel***, Vol. 272, (2020), 117635. (https://doi.org/10.1016/j.fuel.2020.117635).
2. Fedacko, J., Singh, R.B., Mojto, V., Elkilany, G., Hristova, K., Pella, D. and Chaves, H., "Air pollution and the global heart health: A view point of the International College of Cardiology", ***World Heart Journal***, Vol. 9, No. 4, (2017), 269-272. (https://www.researchgate.net/publication/330161859_Air_pollution_and_the_global_heart_health_A_view_point_of_the_international_college_of_cardiology).
3. Muradov, N., "Low to near-zero $CO_2$ production of hydrogen from fossil fuels: Status and perspectives", ***International Journal of Hydrogen Energy***, Vol. 42, No. 20, (2017), 14058-14088. (https://doi.org/10.1016/j.ijhydene.2017.04.101).
4. Shuba, E.S. and Kifle, D., "Microalgae to biofuels:'Promising' alternative and renewable energy, review", ***Renewable and Sustainable Energy Reviews***, Vol. 81, No. 1, (2018), 743-755. (https://doi.org/10.1016/j.rser.2017.08.042).
5. Saravanan, P., Kumar, N.M., Ettappan, M., Dhanagopal, R. and Vishnupriyan, J., "Effect of exhaust gas re-circulation on performance, emission and combustion characteristics of ethanol-fueled diesel engine", ***Case Studies in Thermal Engineering***, Vol. 20, (2020), 100643. (https://doi.org/10.1016/j.csite.2020.100643).
6. Panahi, H.K.S., Dehhaghi, M., Aghbashlo, M., Karimi, K. and Tabatabaei, M., "Shifting fuel feedstock from oil wells to sea: Iran outlook and potential for biofuel production from brown macroalgae (ochrophyta; phaeophyceae)", ***Renewable and Sustainable Energy Reviews***, Vol. 112, (2019), 626-642. (https://doi.org/10.1016/j.rser.2019.06.023).
7. Panahi, H.K.S., Dehhaghi, M., Aghbashlo, M., Karimi, K. and Tabatabaei, M., "Conversion of residues from agro-food industry into bioethanol in Iran: An under-valued biofuel additive to phase out MTBE in gasoline", ***Renewable Energy***, Vol. 145, (2020), 699-710. (https://doi.org/10.1016/j.renene.2019.06.081).
8. Balat, M., Balat, H. and Öz, C., "Progress in bioethanol processing", ***Progress in Energy and Combustion Science***, Vol. 34, No. 5, (2008), 551-573. (https://doi.org/10.1016/j.pecs.2007.11.001).
9. Sritrakul, N., Nitisinprasert, S. and Keawsompong, S., "Evaluation of dilute acid pretreatment for bioethanol fermentation from sugarcane bagasse pith", ***Agriculture and Natural Resources***, Vol. 51, No. 6, (2017), 512-519. (https://doi.org/10.1016/j.anres.2017.12.006).
10. Zakir, H.M., Hasan, M., Shahriar, S.M.S., Ara, T. and Hossain, M., "Production of biofuel from agricultural plant wastes: Corn stover and sugarcane bagasse", ***Chemical Engineering and Science***, Vol. 4, No. 1, (2016), 5-11. (https://doi.org/10.12691/ces-5-1-1).
11. Moodley, P. and Kana, E.G., "Bioethanol production from sugarcane leaf waste: Effect of various optimized pretreatments and fermentation conditions on process kinetics" ***Biotechnology Reports***, Vol. 22, (2019), e00329. (https://doi.org/10.1016/j.btre.2019.e00329).
12. Memon, A.A., Shah, F.A. and Kumar, N., "Bioethanol Production from waste potatoes as a sustainable waste-to-energy resource via enzymatic hydrolysis", ***Proceedings of IOP Conference Series: Earth and Environmental Science: International Conference on Sustainable Energy Engineering***, Perth (Australia), (2017), 012003. (https://doi.org/10.1088/1755-1315/73/1/012003).
13. Hisham, M. and Darwish, S.M., "Production of bio-ethanol and associated by-products from potato starch residue stream by Saccharomyces cerevisiae", ***Journal of Food and Dairy Sciences***, Vol. 34, No. 8, (2009), 8835-8848. (https://doi.org/10.21608/jfds.2009.115800).
14. Yamada, S., Shinomiya, N., Ohba, K., Sekikawa, M. and Oda, Y., "Enzymatic hydrolysis and ethanol fermentation of by-products from potato processing plants", ***Food Science and Technology Research***, Vol. 15, No. 6, (2009), 653-658. (https://doi.org/10.3136/fstr.15.653).
15. Swaraz, A.M., Satter, M.A., Rahman, M.M., Asad, M.A., Khan, I. and Amin, M.Z., "Bioethanol production potential in Bangladesh from wild date palm (Phoenix sylvestris Roxb.): An experimental proof", ***Industrial Crops and Products***, Vol. 139, (2019), 111507. (https://doi.org/10.1016/j.indcrop.2019.111507).
16. Ben Atitallah, I., Ntaikou, I., Antonopoulou, G., Alexandropoulou, M., Brysch-Herzberg, M., Nasri, M., Lyberatos, G. and Mechichi, T., "Evaluation of the non-conventional yeast strain *Wickerhamomyces anomalus* (*Pichia anomala*) X19 for enhanced bioethanol production using date palm sap as renewable feedstock", ***Renewable Energy***, Vol. 154, (2020), 71-81. (https://doi.org/10.1016/j.renene.2020.03.010).
17. Corbin, K.R., Hsieh, Y.S., Betts, N.S., Byrt, C.S., Henderson, M., Stork, J., DeBolt, S., Fincher, G.B. and Burton, R.A., "Grape marc as a source of carbohydrates for bioethanol: Chemical composition, pre-treatment and saccharification", ***Bioresource Technology***, Vol. 193, (2015), 76-83. (https://doi.org/10.1016/j.biortech.2015.06.030).
18. Rodríguez, L.A., Toro, M.E., Vazquez, F., Correa-Daneri, M.L., Gouiric, S.C. and Vallejo, M.D., "Bioethanol production from grape and sugar beet pomaces by solid-state fermentation", ***International Journal of Hydrogen Energy***, Vol. 35, No. 11, (2010), 5914-5917. (https://doi.org/10.1016/j.ijhydene.2009.12.112).
19. Oberoi, H.S., Vadlani, P.V., Madl, R.L., Saida, L. and Abeykoon, J.P., "Ethanol production from orange peels: Two-stage hydrolysis and fermentation studies using optimized parameters through experimental design", ***Journal of Agricultural and Food Chemistry***, Vol. 58, No. 6, (2010), 3422-3429. (https://doi.org/10.1021/jf903163t).
20. Joshi, S.M., Waghmare, J.S., Sonawane, K.D. and Waghmare, S.R., "Bio-ethanol and bio-butanol production from orange peel waste", ***Biofuels***, Vol. 6, No. 1-2, (2015), 55-61. (https://doi.org/10.1080/17597269.2015.1045276).
21. Wang, Z., Ning, P., Hu, L., Nie, Q., Liu, Y., Zhou, Y. and Yang, J., "Efficient ethanol production from paper mulberry pretreated at high solid loading in Fed-nonisothermal-simultaneous saccharification and fermentation", ***Renewable Energy***, Vol. 160, (2020), 211-219. (https://doi.org/10.1016/j.renene.2020.06.128).
22. Food and Agriculture Organization of the United Nations (FAO), Statistics Division (ESS), (2021). (Available at: http://www.fao.org/faostat/en/#data/QC/visualize), (Accessed: 6 July 2021).
23. Mosier, N., Hendrickson, R., Ho, N., Sedlak, M. and Ladisch, M.R., "Optimization of pH controlled liquid hot water pretreatment of corn stover", ***Bioresource Technology***, Vol. 96, No. 18, (2005), 1986-1993. (https://doi.org/10.1016/j.biortech.2005.01.013).
24. Iran Mellas Company, (2021). (Available at: http://fariman.com/products/instant-yeast-breads-and-pastries/), (Accessed: 6 July 2021).
25. He, Q., Hemme, C.L., Jiang, H., He, Z. and Zhou, J., "Mechanisms of enhanced cellulosic bioethanol fermentation by co-cultivation of *Clostridium* and *Thermoanaerobacter* spp", ***Bioresource Technology***, Vol. 102. No. 20, (2011), 9586-9592. (https://doi.org/10.1016/j.biortech.2011.07.098).

26. Cerveró, J.M., Skovgaard, P.A., Felby, C., Sørensen, H.R. and Jørgensen, H., "Enzymatic hydrolysis and fermentation of palm kernel press cake for production of bioethanol", ***Enzyme and Microbial Technology***, Vol. 46, No. 3-4, (2010), 177-184. (https://doi.org/10.1016/j.enzmictec.2009.10.012).

27. Raina, N., Slathia, P.S. and Sharma, P., "Experimental optimization of thermochemical pretreatment of sal (*Shorea robusta*) sawdust by Central Composite Design study for bioethanol production by co-fermentation using *Saccharomyces cerevisiae* (MTCC-36) and *Pichia stipitis* (NCIM-3498)", ***Biomass and Bioenergy***, Vol. 143, (2020), 105819. (https://doi.org/10.1016/j.biombioe.2020.105819).

28. Figliola, R.S. and Beasley, D.E., Theory and design for mechanical measurements, John Wiley & Sons, (1995), 386-387. (https://doi.org/10.1080/03043799508928292).

29. Manmai, N., Unpaprom, Y., Ponnusamy, V.K. and Ramaraj, R., "Bioethanol production from the comparison between optimization of sorghum stalk and sugarcane leaf for sugar production by chemical pretreatment and enzymatic degradation", ***Fuel***, Vol. 278, (2020), 118262. (https://doi.org/10.1016/j.fuel.2020.118262).

30. Nouri, H., Ahi, M., Azin, M. and Gargari, S.L.M., "Detoxification vs. adaptation to inhibitory substances in the production of bioethanol from sugarcane bagasse hydrolysate: A case study", ***Biomass and Bioenergy***, Vol. 139, (2020), 105629. (https://doi.org/10.1016/j.biombioe.2020.105629).

31. Guo, Y., Zhao, H., Zhang, S., Wang, Y. and Chow, D., "Modeling and optimization of environment in agricultural greenhouses for improving cleaner and sustainable crop production", ***Journal of Cleaner Production***, Vol. 285, (2021), 124843. (https://doi.org/10.1016/j.jclepro.2020.124843).

32. Wowra, K., Zeller, V. and Schebek, L., "Nitrogen in life cycle assessment (LCA) of agricultural crop production systems: Comparative analysis of regionalization approaches", ***Science of The Total Environment***, Vol. 763, (2021), 143009. (https://doi.org/10.1016/j.scitotenv.2020.143009).

# *ABSTRACTS*

# Energy Consumption Management of Commercial Buildings by Optimizing the Angle of Solar Panels

Nima Amani *, Abdul Amir Reza Soroush

*Department of Civil Engineering, Chalous Branch, Islamic Azad University, P. O. Box: 46615-397, Chalous, Mazandaran, Iran.*

*PAPER INFO*

*Paper history:*
Received 30 July 2020
Accepted in revised form 24 January 2021

*Keywords*:
Optimal Angle,
Renewable Energy,
Photovoltaic Modules,
Energy Efficiency,
Energy Consumption Management

*ABSTRACT*

One of the main reasons of environmental pollution is energy consumption in buildings. Today, the use of renewable energy sources is increasing dramatically. Among these sources, solar energy has favorable costs for various applications. This study examined a commercial building in a hot and humid climate. The findings showed that choosing the optimal angle of solar panels with the goal of optimized energy consumption would yield reduced costs and less environmental pollutants with the least cost and maximum energy absorption. In this study, to calculate the energy requirements of the building, DesignBuilder software was used. To study the solar angles and estimate the energy produced by the solar panels, Polysun software was used after simulating the building energy. Energy simulation results showed that the whole building energy consumption was 26604 kWh/year. Finally, the evaluation results of solar panels showed that the energy produced by photovoltaic modules at an optimal angle of 31° would be equal to 26978 kWh/year, which is more than the energy required by the building. This system can prevent 14471 kg of carbon dioxide emissions annually. Sustainable energy criteria showed that for the studied building, photovoltaic modules could be used in energy production to reach a zero-energy system connected to the grid with an annual energy balance.

https://doi.org/10.30501/jree.2020.241836.1134



**چکیده**

یکی از دلایل اصلی آلودگی محیطزیست، مصرف انرژی در ساختمان‌ها می‌باشد. امروزه، استفاده از منابع انرژی تجدید پذیر بـه طـور چشـمگیری در حال افزایش است. در بین این منابع، انرژی خورشیدی هزینه‌های مطلوبی برای کاربردهای مختلف دارد. این مطالعه به بررسی یک ساختمان تجـاری در آب و هوای گرم و مرطوب پرداخت و نشان داد که انتخاب زاویه بهینه پانل‌های خورشیدی با هدف مصرف بهینه انرژی باعث کـاهش هزینـه‌هـا و آلاینده‌های محیطزیست با کمترین هزینه و حداکثر جذب انرژی خواهد شد. در این مطالعه برای محاسبه انـرژی مـورد نیـاز سـاختمان از نـرم‌افـزار دیزاین بیلدر استفاده شد. پس از شبیه‌سازی انرژی ساختمان، جهت بررسی زوایای خورشید و برآورد انرژی تولید شده توسط پنل‌های خورشـیدی از نرم افزار پلی سان استفاده شد. نتایج شبیه‌سازی انرژی نشان داد که کل انرژی مصرفی ساختمان ۲۶۶۰۴ کیلووات سـاعت در سـال اسـت. سـرانجام، نتایج ارزیابی پنل‌های خورشیدی نشان داد که انرژی تولید شده توسط ماژول‌های فتوولتائیک تحت زاویه بهینه ۳۱ درجه برابـر بـا ۲۶۹۷۸ کیلـووات ساعت در سال خواهد بود، که بیش از انرژی مورد نیاز ساختمان می‌باشد. این سیستم می‌تواند سـالانه از انتشـار ۱۴۴۷۱ کیلـوگرم دی‌اکسـیدکـربن جلوگیری کند. معیارهای انرژی پایدار نشان می‌دهد که ساختمان مورد مطالعه می‌تواند با استفاده از ماژول‌های فتوولتائیک در تولید انـرژی بـه یـک سیستم انرژی صفر متصل به شبکه با تعادل انرژی سالانه برسد.

# Simplex Centroid Mixture Design for Optimizing and Promoting the Anaerobic Co-Digestion Performance of Sheep Blood and Cheese Whey

Rasoul Aydram, Hossein Haj Agha Alizade*, Majid Rasouli, Behdad Shadidi

*Department of Biosystems Engineering, Faculty of Agriculture, Bu-Ali Sina University, Hamedan, Hamedan, Iran.*

*PAPER INFO*

*Paper history:*
Received 10 November 2020
Accepted in revised form 06 April 2021

*Keywords*:
Slaughterhouse Waste,
Biogas,
Biochemical Methane Potential Test,
Optimization,
Response Surface Methodology

*ABSTRACT*

Reduced emissions of greenhouse gases and global warming can be made possible by discovering alternative energies and reduced dependence on fossil fuels. Biogas is considered as one of the alternatives to fossil fuels. This study investigates anaerobic co-digestion for the development of biogas with sheep blood and cheese whey. Digested cow manure was used as inoculum. Using the Design Expert 10 program and within the context of mixture design, the experiments were designed. Then, 22 experimental digesters with a volume of 500 mL were considered for doing the experiments considering the design output provided by the software. Each one was filled with 300 mL of different compositions of three matters. The digesters were kept in the mesophilic temperature range (37 °C ) for 21 days. Biogas was measured using the BMP test on a daily basis. According to the experimental findings, the best composition included 35 % sheep blood, 35 % cheese whey, and 30 % inoculum. This biogas composition produced a biogas yield of 146.66 mL/g vs. The amount of methane production in this compound was 73.33 mL/g vs. After modeling, the Design Expert software predicted an optimal composition including 44 % sheep blood, 24 % cheese whey, and 32 % inoculum. Biogas yield of this prediction was 143 mL/g vs. The findings show that in order to overcome acidification in digestion of matters such as cheese whey, a composition of matters with higher pH stability can be used to increase the amount of biogas and methane produced in a particular period. Furthermore, using inoculum accelerates the digestion operations due to existence of many microorganisms and saves time and energy.

https://doi.org/10.30501/jree.2021.251583.1151



**چکیده**

آلودگی‌های زیست‌محیطی و امنیت انرژی از جمله بزرگترین چالش‌های انسان در قرن ۲۱ است. کاهش انتشار گازهای گلخانه‌ای و گرمایش جهانی با اکتشاف انرژی‌های جایگزین و کاهش وابستگی به سوخت‌های فسیلی امکان‌پذیر است. بیوگاز به عنوان یکی از جایگزین های سوخت های فسیلی به‌شمار می‌رود. بیوگاز از گازهای در اثر تخمیر فضولات گیاهی و جانوری دور از اکسیژن و در اثر فعالیت باکتریهای بی هوازی تولید می‌گردد. در این پژوهش، به بررسی هضم بی‌هوازی خون گوسفند و آب پنیر برای تولید بیوگاز پرداخته شد. همچنین از کود گاوی هضم شده به‌عنوان ماده تلقیح استفاده گردید. طراحی آزمایش‌ها به وسیله نرم‌افزار دیزاین اکسپرت و در قالب طرح مخلوط انجام شد. ۲۲ هاضم آزمایشگاهی هرکدام با حجم ۵۰۰ میلی‌لیتر برای انجام آزمایشات، با توجه به خروجی طراحی آزمایش‌ها توسط نرم‌افزار در نظر گرفته شد که هرکدام به میزان ۳۰۰ میلی‌لیتر از ترکیبات مختلفی از سه ماده پر شدند. هاضم‌ها در محدوده دمایی مزوفیلیک (۳۷ درجه سانتی‌گراد) در یک زمان ماند ۲۱ روزه نگهداری شدند و اندازه‌گیری بیوگاز با روش BMP test به صورت روزانه انجام شد. طبق نتایج به دست آمده از آزمایش‌ها، بهترین ترکیب شامل ۳۵ ٪ خون گوسفند، ۳۵ ٪ آب پنیر و ۳۰ ٪ ماده تلقیح بود که این ترکیب بیوگازی معادل ۱۴۶/۶۶ mL/g vs تولید کرد. میزان تولید متان در این ترکیب معادل ۷۳/۳۳ mL/g vs بود. پس از مدل‌سازی، نرم‌افزار دیزاین اکسپرت ترکیب بهینه‌ای را پیش‌بینی کرد که شامل ۴۴ ٪ خون گوسفند، ۲۴ ٪ آب پنیر و ۳۲ ٪ ماده تلقیح بود. میزان تولید بیوگاز در این پیش‌بینی برابر با ۱۴۳ mL/g vs بود. از نتایج به دست آمده از این پژوهش می‌توان دریافت که به‌منظور غلبه بر شرایط اسیدی شدن در هضم موادی مانند آب پنیر، می‌توان از ترکیب موادی با ثبات pH بالاتر استفاده کرد و حجم بیوگاز و متان تولیدی را در یک دوره مشخص افزایش داد. همچنین استفاده از ماده تلقیح به دلیل وفور میکروارگانیسم‌ها به عملیات هضم سرعت می‌دهد و باعث صرفه‌جویی در زمان و انرژی می‌گردد.

# Evaluation of the Effective Factors in Locating a Photovoltaic Solar Power Plant Using Fuzzy Multi-Criteria Decision-Making Method

Aychar Khajavi Pour [a], Mohammad Reza Shahraki [a*], Faranak Hosseinzadeh Saljooghi [b]

[a] *Department of Industrial Engineering, School of Engineering, University of Sistan and Baluchestan, Zahedan, Sistan and Baluchestan, Iran.*
[b] *Department of Mathematics, School of Mathematics, University of Sistan and Baluchestan, Zahedan, Sistan and Baluchestan, Iran.*

*PAPER INFO*

*Paper history:*
Received 21 September 2020
Accepted in revised form 25 April 2021

*Keywords*:
Locating,
Photovoltaic Solar Power Plant,
Fuzzy Hierarchical Method

*ABSTRACT*

The energy of processes is mainly supplied by fossil fuels. Short life of fossil energy sources and increasing environmental pollution caused by fossil fuels and increasing demand have made researchers introduce new solutions for supply of energy. Energy production in a photovoltaic solar power plant is cost-effective due to being clean and renewable. The power generation of these plants is affected by their site due to climate conditions, effective radiation periods, and the rate of solar radiation absorption. Therefore, finding the optimal location to establish a solar power plant is important. Identifying effective location criteria and the importance of these criteria is effective in choosing the optimal location.In this research, in the first phase, the effective criteria in locating a photovoltaic solar power plant were investigated based on the Delphi method. Then, in the second phase, based on the criteria identified in the first phase, fuzzy hierarchy method was used to compare the criteria with each other and determine the importance of each of them. The results of the study showed that the rate of solar radiation and average temperature were the most important criteria in locating photovoltaic solar power plant. Moreover, the criteria of slope, distance to main roads, distance to power lines, and land use were of highest importance in locating a photovoltaic solar power plant.

https://doi.org/10.30501/jree.2020.247756.1145



**چکیده**

تأمین انرژی عمدتاً توسط سوخت‌های فسیلی انجام می‌گیرد. عواملی مانند رو به اتمام بودن سوخت‌های فسیلی، آلودگی‌های زیست‌محیطی، افزایش جمعیت و افزایش تقاضا منجر به ارائه راهکارهای جدید برای تأمین انرژی شد. تولید انرژی در نیروگاه خورشیدی فتوولتائیک به دلیل پاک بودن و تجدیدپذیر بودن، مقرون به صرفه می‌باشد. میزان انرژی تولیدی این نیروگاه‌ها به شرایط آب و هوایی، زمان‌های تابش مؤثر و میزان جذب نور خورشید وابسته می‌باشد. بنابراین یافتن مکان بهینه برای تأسیس نیروگاه خورشیدی حائز اهمیت می‌باشد. شناسایی معیارهای مؤثر مکان‌یابی و میزان اهمیت این معیارها، در انتخاب مکان بهینه تأثیرگذار می‌باشد. در این تحقیق، در فاز اول به شناسایی معیارهای مؤثر در مکان‌یابی نیروگاه خورشیدی براساس روش دلفی پرداخته شده است. سپس در فاز دوم، با توجه به معیارهای شناسایی شده در فاز اول، با استفاده از روش سلسله مراتبی فازی، معیارها با یکدیگر مقایسه و میزان اهمیت هر یک از معیارها تعیین شده است. نتایج تحقیق نشان داد که میزان تابش خورشید و میانگین دما در مکان‌یابی نیروگاه خورشیدی بیشترین اهمیت را دارند. هم چنین معیارهای شیب، فاصله از راه‌های اصلی، فاصله از خطوط برق و کاربری اراضی، به ترتیب بیشترین اهمیت را در مکان‌یابی نیروگاه خورشیدی دارا هستند.

# The Assessment of Effect of Fatty Acid Profile on the Physical Properties and Emission Characteristics of New Feedstocks Used for Biodiesel

Farid Jafarihaghighi [a], Hassanali Bahrami [b], Mehdi Ardjmand [a*], Mehrdad Mirzajanzadeh [a]

[a] *Department of Chemical Engineering, South Tehran Branch, Islamic Azad University, Tehran, Tehran, Iran.*
[b] *Department of Mechatronics, Arak University, Arak, Markazi, Iran.*

*PAPER INFO*

*Paper history:*
Received 15 November 2020
Accepted in revised form 26 April 2021

*Keywords*:
Physical Properties,
Chemical Properties,
Three Different Biodiesel Generation,
Emissions

*ABSTRACT*

The present study uses three generations of biodiesels and studies their effects on physical properties and exhaust gases. They are comprised of *Palmaria palmate* oil (third generation), *Eucheuma spinosum* oil (third generation), *Eucheuma cottonii* oil (third generation), *Common wormwood* oil (second generation), *Marjoram* oil (second generation), *Peganum harmala* oil (second generation), *Zingiber officinale* oil (first generation), *Anethum graveolens* oil (first generation), and *Cacao bean* oil (first generation). Results show that first-generation oils gain a higher level of Calorific value around 41.16 MJ/kg than other generations. The longest carbon chain is observed by the first generation with higher unsaturated fatty acids than other generations (94.11 %). The first generation gains a higher level of density around 882 kg/m$^3$ than other generations. Also, the first generation gains a higher level of flash point around 193 ˚C than other generations. The third generation gains a high level of cetane number at about 69, compared to other generations. The first generation gains a minimum level of cloud and pour point around -3 ˚C and -2 ˚C compared to other generations. Moreover, the third generation gains the lowest level of viscosity about 2.51 CSt compared to the first generation. The third generation gains the lowest level of $NO_x$ around 371 ppm compared to other generations. Finally, the third generation gains the lowest level of soot, CO, and HC around 0.47 Vol. %, 0.018 Vol. %, and 4.82 ppm, compared to other generations.

https://doi.org/10.30501/jree.2021.257527.1161



**چکیده**

سه نسل از بیودیزل و تأثیرات آن بر خصوصیات فیزیکی و گازهای خروجی، مورد استفاده و بررسی قرار گرفته است. روغن‌های مورد مطالعه شامل روغن پوسته‌های کاهو دریایی (نسل سوم)، جلبک دریایی *Eucheuma spinosum* (نسل سوم)، جلبک دریایی *Eucheuma cottonii* (نسل سوم)، افسنطین معمولی (نسل دوم)، مرزنجوش (نسل دوم)، *Peganum harmala* (نسل دوم)، زنجبیل (نسل اول)، شوید (نسل اول) و لوبیا کاکائو (نسل اول) می‌باشد. نتایج نشان داد که نسل اول در مقایسه با تمام نسل‌ها، مقدار بالاتری از ارزش گرمایی را بدست آورد (حدود ۴۱/۱۶ MJ/kg). طولانی ترین زنجیره کربن توسط نسل اول با اسیدهای چرب اشباع نشده بالا در مقایسه با همه نسل‌ها مشاهده شد (۹۴/۱۱ ٪). نسل اول در مقایسه با همه نسل‌ها، دانسیته بالاتری در حدود ۸۸۲ kg/m$^3$ به دست آورد. نسل اول در مقایسه با همه نسل‌ها، نقطه اشتعال بالاتری در حدود ۱۹۳ ˚C به دست آورد. بالاترین میزان عدد ستان توسط نسل سوم نشان داده شد که مقدار آن در حدود ۶۹ می‌باشد. کمترین مقدار نقطه ریزش و نقطه ابری شدن توسط نسل اول بدست آمد که مقدار آن ها در حدود ۳- ˚C و ۲- ˚C می‌باشد. حداقل میزان ویسکوزیته به وسیله نسل سوم نشان داده شد که مقدار آن در حدود ۲/۵۱ CSt بوده است .نسل سوم نشان داد که میزان $NO_x$ تولید شده در مقایسه با نسل‌های دیگر حداقل بوده است و مقدار آن در حدود ۳۷۱ ppm بوده است. در واقع نسل سوم از بیودیزل ها نشان داد که میزان soot، CO و HC را در حدود ۰/۴۷ درصد حجمی، ۰/۰۱۸ درصد حجمی و ۴/۸۲ ppm کاهش داد که بیشترین میزان کاهش بین تمامی نسل‌ها می‌باشد.

# Determining Optimal Locations for Biogas Plants: Case Study of Tehran Province for Utilization of Bovine and Aviculture Wastes

Maryam Nosratinia [a], Ali Asghar Tofigh [b], Mehrdad Adl [a*]

[a] *Department of Energy, Materials and Energy Research Center (MERC), P. O. Box: 3177983634, MeshkinDasht, Alborz, Iran.*
[b] *Department of Industrial Engineering, Amirkabir University of Technology, P. O. Box: 159163-4311, Tehran, Tehran, Iran.*

*PAPER INFO*

*Paper history:*
Received 13 October 2020
Accepted in revised form 17 May 2021

*Keywords*:
Location,
Biogas,
Geographical Information System (GIS),
Fuzzy Logic

*ABSTRACT*

Given the world's growing population and energy demand, modern methods are developed to contribute to generating alternative energies. They aim to maintain the renewability of the supplied energy and decrease environmental contaminations. Biogas is a renewable energy carrier that has recently been under consideration in Iran. One objective of such plans is to find proper locations for installing and running the existing potentials and infrastructures. In this paper, Tehran, Iran is selected as the study area which is ranked the 1st in population density and proper infrastructures available here are accessible. According to the widespread poultry and cow-breading farms in this province, bovine and aviculture excreta are considered as raw materials in producing biogas. An inference network was established in this research for evaluating the process taking into account the infrastructural parameters, geomorphological constraints, resource availability factors, and limiting parameters such as protected/prohibited areas.In this paper, the fuzzy method was used to standardize the data and the fuzzy-analytical hierarchy process method was employed to weight the locating criteria in the geographical information system. The evaluation outcomes suggested certain zones in southern parts of the province in which the industrial livestock farms become frequently widespread and the suburb areas of smaller cities on the eastern part of the province are the most proper areas for this purpose.

https://doi.org/10.30501/jree.2021.251191.1149



**چکیده**

با نگرش به روند فزاینده جمعیت و نیاز به انرژی در جهان، روش‌های نوینی برای پاسخ به این نیاز همراه با حفظ تجدیدپذیر بودن و کاهش آلایندگی محیط‌زیست گسترش یافته اند. انرژی بیوگاز نوعی انرژی تجدیدپذیر است که اخیراً در ایران مورد توجه قرار گرفته است. یکی از الزامات در برنامه گسترش فناوری بیوگاز، یافتن مکان‌های مناسب برای نصب و اجرای تأسیسات برپایه قابلیت‌های بالقوه و زیرساخت‌های مورد نیاز می‌باشد. در این مقاله، استان تهران که حدود ۱۹ ٪ جمعیت ایران را در خود جای داده و از زیرساخت‌های لازم برخوردار است، بعنوان مطالعه موردی برگزیده شده است. فضولات گاوی و مرغداری بعنوان خوراک خام برای تولید بیوگاز درنظر گرفته شده و شبکه‌های برق‌رسانی، گازرسانی، جاده ها، منابع آب و کانون‌های جمعیتی بعنوان زیرساخت‌های مؤثر بشمار آورده شده اند و همچنین شیب زمین، مناطق حفاظت‌شده و نواحی ممنوعه بعنوان عوامل محدودکننده در فرایند مکان‌یابی احداث تأسیسات بیوگاز مورد ارزیابی قرار گرفته اند. روش فازی برای استانداردسازی داده‌ها و روش ترکیبی فازی-اولویت بندی تحلیلی، برای وزن‌دهی به معیارها در سامانه اطلاعات جغرافیایی (GIS) در این مقاله بکار گرفته شده‌اند.

# Effects of PCM Mass on Heat Dynamics and Thermal Performance of Solar Air Heaters: A Numerical and Analytical Study

Ehsan Hasan Zaim [a], Hadi Farzan [b*]

[a] *Department of Mechanical Engineering, School of Engineering, Sirjan University of Technology, P. O. Box: 78137-33385, Sirjan, Kerman, Iran.*
[b] *Department of Mechanical Engineering, School of Engineering, Higher Education Complex of Bam, P. O. Box: 76615-314, Bam, Kerman, Iran.*

*PAPER INFO*

*Paper history:*
Received 04 December 2020
Accepted in revised form 18 May 2021

*Keywords*:
Solar Air Heater,
Phase Change Material,
Analytical Study,
Thermal Performance,
Heat Dynamics

*ABSTRACT*

Utilizing thermal storage units such as Phase Change Materials (PCMs) is a suitable approach to improving Solar Air Heaters (SAHs). The present study tries to assess the effects of PCM mass values on the heat dynamics and thermal performance of SAHs. To this aim, an analytical thermodynamic model was developed and validated by available experimental data. This model provides a robust numerical framework to model the phase change phenomenon and analyze the heat dynamics and thermal performance of SAH using various PCM masses. Four scenarios were considered using the developed analytical model including SAHs using 0, 30, 60, 90 kg PCM. The obtained results illustrated that the maximum outlet temperature was reduced, approximately near 20 %, by increasing the PCM mass between 0 and 90 kg; however, heating time was extended to periods when solar energy availability was inadequate. The thermal performance improved by nearly 14.5 % in the SAH using 90 kg PCM mass compared to the SAH without using PCM. The thermal performance of the SAH with 90 kg PCM was slightly higher than the SAH using 30 kg of PCM; hence, a significant portion of stored thermal energy was lost during nighttime through heat exchange with ambient surroundings. The obtained results also showed that despite available latent thermal energy, the outlet air temperature profiles for the SAHs using different PCM mass were close after sunset due to the low thermal conductivity of paraffin.

https://doi.org/10.30501/jree.2021.259570.1169



**چکیده**

استفاده از واحدهای ذخیره‌ساز حرارت مانند مواد تغییر فاز دهنده یکی از راهکارهای مؤثر در افزایش راندمان گرم‌کننده‌های خورشیدی است. مطالعه حاضر به بررسی اثر مقدار جرم مواد تغییر فاز دهنده بر روی دینامیک حرارتی و راندمان کلکتورهای هوایی می‌پردازد. برای این منظور، یک مدل تحلیلی توسعه یافته و با نتایج تجربی اعتبارسنجی شده است. این مدل یک زیرساخت مناسب برای ارزیابی دینامیک حرارتی کلکتورهای هوایی حاوی مقادیر متفاوت مواد تغییر فاز دهنده ایجاد کرده است. چهار رویکرد متفاوت شامل کلکتور هوایی حاوی ۰، ۳۰، ۶۰ و ۹۰ kg مواد تغییر فاز دهنده در نظر گرفته شده است. نتایج بررسی تحلیلی نشان می‌دهد، بیشینه‌ی دمای خروجی در صورت استفاده از ۹۰ kg مواد تغییر فاز دهنده نسبت به رویکرد کلکتور بدون مواد تغییر فاز دهنده نزدیک به ۲۰ ٪ کاهش می‌یابد، اگرچه فرآیند گرمایش به زمان‌هایی که تابش خورشید وجود ندارد، گسترش می‌یابد. با استفاد از مواد تغییر فاز دهنده، راندمان حرارتی به میزان ۱۴/۵ ٪ در کلکتور حاوی ۹۰ kg مواد تغییر فاز دهنده نسبت به کلکتور بدون مواد تغییر فاز دهنده افزایش می‌یابد. راندمان حرارتی به مقدار نسبتاً کمی در کلکتور حاوی ۹۰ kg مواد تغییر فاز دهنده نسبت به کلکتور حاوی ۳۰ kg مواد تغییر فاز دهنده افزایش داشته است. این امر نشان می‌دهد که بخش قابل ملاحظه‌ای از حرارت ذخیره شده در مواد تغییر فاز دهنده در طول شب از طریق تابش و جابجایی با محیط بیرون تلف می‌شود. نتایج همچنین نشان داد که علی‌رغم حرارت نهان ذخیره شده در مواد تغییر فاز دهنده، بدلیل ضریب هدایت پایین پارافین، دمای هوای خروجی از کلکتور بعد از غروب آفتاب با تغییر جرم مواد تغییر فاز دهنده تغییر ناچیزی می‌کند.

# Assessment of Optimum Renewable Energy System for the Somalia–Turkish Training and Research Hospital in Mogadishu

Sibel Dursun [a], Ercan Aykut [b], Bahtiyar Dursun [c*]

[a] *Branch of Physics, Capa Final Anatolian High School, P. O. Box: 34093, Istanbul, Turkey.*
[b] *Department of Electrics, Gelisim Vocational School, Istanbul Gelisim University, P. O. Box: 34310, Istanbul, Turkey.*
[c] *Department of Electrical-Electronics Engineering, Fatih Sultan Mehmet Vakif University, P. O. Box: 34421, Istanbul, Turkey.*

*PAPER INFO*

*Paper history:*
Received 20 October 2020
Accepted in revised form 19 May 2021

*Keywords*:
Somalia,
Renewable Power Generating System,
Hospital,
Environmental Assessment,
Hybrid Systems,
Renewable Energy

*ABSTRACT*

Somalia–Turkish Training and Research Hospital in Mogadishu, is only powered by diesel generator currently. In this paper, the energy demand of this hospital is utilized by determining the optimum hybrid renewable energy generating system. By HOMER, a sensitivity analysis has been made with emphasis on three significant variables such as average wind speed, present diesel price, and solar radiation. From the results, it can be said that an optimum system is the standalone wind-diesel-battery storage Hybrid Renewable Energy System (HRES) with the configuration of 1,000 kW wind turbine, 350 kW diesel generator, 250 kW power converters, and 300 batteries. Additionally, the net present cost of the optimum system is calculated to be $5,056,700 and its cost of energy is estimated to be 0.191 $/kWh. The present cost of energy for Somalia is 0.5 $/kWh. This shows that the energy cost for the proposed HRES is cheaper than the conventional one. Lastly, according to the results, it is clear that the wind–diesel–battery storage HRES seems more environment friendly than other HRESs.

https://doi.org/10.30501/jree.2021.245232.1140



**چکیده**

بیمارستان آموزشی و تحقیقاتی ترکیه ای – سومالی در موگادیشو، در حال حاضر فقط توسط دیزل ژنراتور تأمین برق می‌شود. در این مقاله، برای تأمین انرژی این بیمارستان از سیستم انرژی تجدیدپذیر ترکیبی بهینه‌شده استفاده می‌شود. تجزیه و تحلیل بسیار دقیقی توسط نرم‌افزار HOMER با تأکید بر روی سه متغیر قابل توجه مانند سرعت متوسط باد، قیمت فعلی دیزل و تابش خورشید انجام شده است. از نتایج بدست آمده می‌توان گفت که یک سیستم مطلوب، سیستم مستقل ذخیره انرژی باد – دیزل –باتری به شکل سیستم انرژی تجدیدپذیر ترکیبی (HRES) است، با پیکربندی توربین بادی ۱۰۰۰ کیلووات، دیزل ژنراتور ۳۵۰ کیلووات، مبدل برق ۲۵۰ کیلووات و ۳۰۰ باتری. علاوه براین، هزینه فعلی خالص سیستم مطلوب ۵،۰۵۶،۷۰۰ دلار و هزینه انرژی آن ۰/۱۹۱ دلار بر کیلووات ساعت برآورد شده است. هزینه کنونی انرژی برای سومالی ۰/۵ دلار بر کیلووات ساعت است. این نشان می‌دهد که هزینه انرژی برای HRES پیشنهادی ارزان‌تر از هزینه معمولی است. سرانجام، با توجه به نتایج، مشخص است که سیستم ذخیره انرژی باد – دیزل –باتری HRES نسبت به سایر سیستم‌های HRES با محیط‌زیست سازگارتر به نظر می‌رسد.

# Optimization of Pyrolysis Temperature and Particle Size on the Phenols and Hemicellulose Fast Pyrolysis Products in a Tandem Micro-Pyrolyzer

Payam Ghorbannezhad [a], Maryam Abbasi [b*]

[a] *Department of Biorefinery Engineering, Faculty of New Technologies Engineering, Shahid Beheshti University, Tehran, Tehran, Iran.*
[b] *Faculty of Civil, Water & Environmental Engineering, Shahid Beheshti University, Tehran, Tehran, Iran.*

*PAPER INFO*

*Paper history:*
Received 03 November 2020
Accepted in revised form 10 July 2021

*Keywords*:
Sugarcane Bagasse,
Fast Pyrolysis,
Phenolic Compounds,
Furfural

*ABSTRACT*

Fast pyrolysis of sugarcane bagasse was investigated in a tandem micro-pyrolyzer. The effects of temperature and particle size on the phenolic compounds and hemicellulose products distribution were examined during fast pyrolysis process. For this, changes in the micro-reactor parameters were made (particle size between 0.1 and 0.5 mm and reactor temperature between 450 and 600 °C). Response Surface Methodology (RSM) was used to optimize pyrolysis parameters. The results indicated that the temperature had the highest effect on phenolic and furfural-type compounds, whereas the particle size did not exhibit significant effects on carboxylic acid products. The largest number of phenolic compounds were achieved upon decreasing the temperature and increasing particle size. The ANOVA analysis revealed that the full quadratic model was more adequate for phenolic and furfural compounds, whereas the linear square model was accurate for carboxylic acids. In general, a tandem micro-pyrolyzer interfacing with a GC-MS analysis facilitated a better understanding of a chemical composition of biomass and therefore, could remarkably improve the valorising of sugarcane bagasse application in biorefinery processes.

https://doi.org/10.30501/jree.2021.255248.1155



**چکیده**

در مطالعه حاضر، پیرولیز سریع باگاس نیشکر در یک میکروپیرولیزر پیوسته مورد بررسی قرار گرفت. آزمایشهایی برای بررسی اثر دمای پیرولیز و اندازه ذرات بر روی ترکیبات فنلی و توزیع محصولات همی‌سلولز انجام شد. بدین منظور، پارامترهای میکروراکتور (اندازه ذرات بین ۰/۱ تا ۰/۵ میلی‌متر و دمای راکتور بین ۴۵۰ تا ۶۰۰ درجه سانتیگراد) تغییر داده شد. برای بهینه‌سازی پارامترهای پیرولیز از روش سطح پاسخ استفاده شد. نتایج نشان داد که دما بیشترین تأثیر را بر روی ترکیبات فنلی و فورفورال دارد در حالی که اندازه ذرات تأثیر قابل توجهی بر روی محصولات اسید کربوکسیلیک نداشت. بیشترین مقدار ترکیبات فنلی با کاهش دما و افزایش اندازه ذرات بدست آمد. تجزیه و تحلیل ANOVA نشان می‌دهد که مدل درجه دوم، جهت تعیین ترکیبات فنلی و فورفورال مناسب است، درحالی‌که مدل مربع خطی برای اسیدهای کربوکسیلیک دقت بیشتری دارد. بطور کلی، یک میکروپیرولایزر پیوسته با تجزیه و تحلیل GC-MS امکان درک بهتر ترکیب شیمیایی زیست‌توده را فراهم می‌آورد و در نتیجه، می‌تواند کاربرد باگاس نیشکر را در فرایندهای پالایش زیستی بطور چشمگیری بهبود بخشد.

# Prediction of Discharge Using Artificial Neural Network and IHACRES Models Due to Climate Change

Maryam Hafezparast *, Seiran Marabi

*Department of Water Engineering, Faculty of Agriculture and Natural Sciences, Razi University, P. O. Box: 09914412984, Kermanshah, Kermanshah, Iran.*

*PAPER INFO*

*Paper history:*
Received 21 November 2020
Accepted in revised form 10 July 2021

*Keywords*:
RCP8.5,
Runoff Prediction,
IHACRES,
MLP,
Kermanshah

*ABSTRACT*

Understanding of climate change and its impacts on river discharge has affected the quality and quantity of water and also supplying water requirements for drinking, agriculture and industry. Therefore, prediction of precipitation and temperature by climate models as well as simulation and optimization of their runoff with suitable models are very important. In this study, four climate models of the Fifth Coupled Model Inter comparison Project (CMIP5) and RCP8.5 scenario were used to forecast future precipitation and temperature for the next two periods including 2020-2052 and 2053-2085. Mean Observed Temperature-Precipitation (MOTP) method was used to reduce the uncertainty of climate models and the change factor method was used to downscale the climate data. Then, the Lumped-conceptual Identification of unit Hydrographs and Component flows from Rainfall, Evaporation and Stream flow data (IHACRES) model and multi-layer Artificial Neural Network (ANN) model were employed to estimate the effects of these parameters on the Khorramrood River runoff. The neural network model is written and implemented using Scikit-Learn library and the Python programming language. The comparison of performance of ANN models with different input variables like monthly precipitation, monthly precipitation of previous months, monthly discharge, monthly discharge of previous months, monthly temperature was made to find the best and most efficient network structure. The results showed that the precipitation in Khorramrood River basin based on the weighted combination model decreased by 8.18 % and 9.75 % in the first and the second periods, respectively, while the temperature increased by 1.85 and 4.22 °C, respectively. The discharge parameter in the calibration and validation period in the IHACRES model based on criteria to evaluate the parameters of Root Mean Square Error (RMSE), Mean Absolute Error (MAE), The Coefficient of Determination (R), and the Nash-Sutcliffe Efficiency (NSE) performed better than the artificial neural network model. However, due to the small differences of these changes, the predictions were performed for both periods and using both models and the results indicated that future discharge in the IHACRES model decreased by 12.72 % during the first period and by 20.3 % in the second period, while the model of artificial neural network showed decrease rates of 2.12 % and 6.97 %, respectively.

https://doi.org/10.30501/jree.2021.257941.1162



**چکیده**

شناخت تغییرات اقلیمی و اثرات آنها بر آبدهی رودخانه‌ها بر کیفیت و کمّیت آب تأثیر گذاشته و تأمین تقاضاهای شرب، کشاورزی و صنعت را تحت تأثیر قرار می‌دهد. از این رو پیش بینی بارش و دما با مدلهای اقلیمی و شبیه‌سازی و بهینه‌سازی رواناب ناشی از آنها با مدلهای مناسب از اهمیت ویژه ای برخوردار است. در این پژوهش برای پیش بینی بارش و دمای آینده، از ۴ مدل اقلیمی گزارش پنجم CMIP5 و سناریوی RCP8.5 برای دو دوره آتی شامل ۲۰۵۲-۲۰۲۰ و ۲۰۸۵-۲۰۵۳ استفاده گردید و برای کاهش عدم قطعیت مدلهای اقلیمی از روش MOTP و برای ریزمقیاس سازی داده‌ها از روش عامل تغییر استفاده شد. سپس به منظور برآورد اثرات این پارامترها بر میزان رواناب رودخانه خرم‌رود، از مدلهای نیمه مفهومی ایهکرس (IHACRES) و مدل داده محور شبکه عصبی مصنوعی چندلایه استفاده گردید. مدل شبکه عصبی با استفاده از کتابخانه سایکیت لرن (Scikit-Learn) و زبان برنامه نویسی پایتون نوشته و اجرا شده است. نتایج نشان داد بارش در حوضه رودخانه خرم‌رود در مدل ترکیب وزنی در دوره اول ۸/۱۸ درصد و در دوره دوم ۹/۷۵ درصد کاهش و دما به ترتیب ۱/۸۵ و ۴/۲۲ درجه سانتی گراد افزایش را نشان می‌دهد. پارامتر آبدهی در دوره واسنجی و صحت‌سنجی در مدل ایهکرس از لحاظ معیارهای ارزیابی پارامترهای میانگین‌مربعات‌خطا (RMSE)، خطای‌مطلق‌میانگین (MAE)، ضریب‌تعیین (R) و ضریب نش-ساتکلیف (NSE) نسبت به مدل شبکه عصبی مصنوعی عملکرد بهتری داشته است، ولی به دلیل اختلاف کم این تغییرات، پیش بینی برای هر دو دوره با هر دو مدل انجام شده و نتایج حاکی از آن است که آبدهی در آینده در مدل ایهکرس در دوره آتی اول ۱۲/۷۲ درصد و در دوره دوم ۲۰/۳ درصد نسبت به وضعیت موجود کاهش و در مدل شبکه عصبی مصنوعی به ترتیب ۲/۱۲ درصد و ۶/۹۷ درصد کاهش را نشان می‌دهد.

# Bioethanol Production from Wastes: An Experimental Evaluating Study for Iran

Abolfazl Taherzadeh Fini, Abolfazl Fattahi *

*Department of Mechanical Engineering, University of Kashan, P. O. Box: 8731753153, Kashan, Isfahan, Iran.*

*P A P E R  I N F O*

*Paper history:*
Received 01 November 2020
Accepted in revised form 11 July 2021

*Keywords*:
Biofuel Production,
Pretreatment and Hydrolysis,
Agricultural Wastes,
Renewable Energy,
Gas Chromatography

*A B S T R A C T*

Energy crisis in the world motivates countries to hire new and renewable energies. One of the main and valuable renewable sources of energy is agricultural waste. This is widely disposed of through the world during the harvest, packing, and transportation. In many countries, agricultural waste is considerably weighty. Nonetheless, most of that is used for animal feed or herbal fertilizer and no useful value is added. Despite its location in an arid region, Iran produces various citrus, cereals, and vegetables in high tonnage. The waste of the agricultural product, especially those disposed of by the food processing industries, such as fruit juice factories, remains also useless. The potential of the residues to extract biofuel is investigated in the current experimental study. Six samples of abundant agricultural products in Iran are chosen: sugarcane, grape, potato, orange peel, date, and mulberry. The processes of pretreatment, hydrolysis, and fermentation are performed and the extracted juice is directed to the distiller to gather bioethanol. To evaluate the distilled juice purity, a gas chromatography test is carried out. It is shown that date and mulberry can produce a maximum of 29.5 and 23 ml (ethanol)/100 g (dry waste) as the most efficient agricultural products.

https://doi.org/10.30501/jree.2021.255487.1156



**چکیده**

بحران انرژی در جهان باعث شده است که کشورها تمایل بیشتری به استفاده از منابع جدید و تجدیدپذیر انرژی نشان دهند. پسماندهای کشاورزی را می‌توان به عنوان یکی از منابع اصلی و ارزشمند انرژی‌های تجدیدپذیر معرفی نمود. این پسماندها در حین برداشت، بسته‌بندی و حمل‌ونقل محصولات کشاورزی، به طور گسترده در سرتاسر جهان دفع می‌شوند. در بسیاری از کشورها، پسماندهای کشاورزی به مقدار قابل توجهی تولید می‌شوند و عموماً بدون ایجاد هرگونه ارزش افزوده‌ای، به عنوان غذای دام یا کودهای گیاهی مورد استفاده قرار می‌گیرند. علیرغم این‌که کشور ایران در منطقه‌ای خشک قرار گرفته است، سالانه میزان قابل‌توجهی از محصولات کشاورزی مانند مرکبات، غلات و سبزیجات را تولید می‌نماید. حجم قابل توجهی از پسماندهای این محصولات، مخصوصاً پسماند شرکت‌های فرآوری مواد غذایی، مانند کارخانه‌جات تولید آب میوه‌های طبیعی، به صورت بلااستفاده دور ریخته می‌شوند. در این مطالعه‌ی تجربی، پتانسیل استخراج زیست‌سوخت‌ها، از این قبیل پسماندها بررسی شده است. به این منظور، شش نمونه از محصولات کشاورزی که در ایران به وفور کشت می‌شوند جمع آوری شده است: نی‌شکر، انگور، سیب‌زمینی، پوست پرتقال، خرما و توت. در این مطالعه، فرآیندهای پیش فرآوری، آب‌کافت و تخمیر بر روی پسماندها صورت گرفته است و محصولات آن‌ها پس از گذراندن فرآیند تقطیر، مستقیماً به اتانول تبدیل شده‌اند. به منظور ارزیابی خلوص مایع تقطیر شده، از آزمایش کروماتوگرافی گازی استفاده شده است. همچنین در این مطالعه نشان داده شده است که خرما و توت به عنوان پربازده‌ترین پسماندها توانسته‌اند به ترتیب ۲۹/۵ و ۲۳ میلی‌لیتر اتانول به ازای هر صد گرم از پسماند خشک تولید کنند.

## CONTENTS




**Journal Homepage: www.jree.ir**